

**Crustal structure modelling and interpretation
of the East Greenland continental margin
between 72°N and 77°N**

DISSERTATION

zur Erlangung des Grades Dr. rer.nat.
vorgelegt dem Fachbereich Geowissenschaften
der Universität Bremen
von

MAX VOSS

Alfred-Wegener-Institut für Polar- und Meeresforschung
Bremerhaven

Hamburg, 19. December 2007

Name: Max Voß

Datum: 19.12.2007

Anschrift: Fraenkelstr. 6
22307 Hamburg

ERKLÄRUNG

Hiermit versichere ich, dass ich

1. die Arbeit ohne unerlaubte fremde Hilfe angefertigt habe,
2. keine anderen als die von mir angegebenen Quellen und Hilfsmittel benutzt habe und
3. die den benutzten Werken wörtlich oder inhaltlich entnommenen Stellen als solche kenntlich gemacht habe.

Bremen, den

Max Voß

DIE TRAGÖDIE DER WISSENSCHAFT –
DAS ERSCHLAGEN EINER SCHÖNEN
HYPOTHESE DURCH EINE HÄSSLICHE
TATSACHE.

THERE IS NO SADDER SIGHT IN THE
WORLD THAN TO SEE A BEAUTIFUL
THEORY KILLED BY A BRUTAL FACT.

BERTRAND RUSSELL, 1872-1970

CONTENTS

KURZFASSUNG	IV
ABSTRACT.....	VI
1 INTRODUCTION.....	- 1 -
1.1 GREENLAND – A UNIQUE LANDSCAPE	- 1 -
1.2 GEOPHYSICAL INVESTIGATIONS OFF EAST GREENLAND	- 3 -
1.3 AIM OF THE THESIS	- 5 -
1.4 STRUCTURE OF THE THESIS	- 6 -
2 CLASSIFICATION OF CONTINENTAL RIFTED MARGINS	- 8 -
2.1 NON-VOLCANIC RIFTED MARGINS.....	- 8 -
2.2 VOLCANIC RIFTED MARGINS	- 10 -
3 DATA ACQUISITION AND PROCESSING METHODS.....	- 12 -
3.1 SEISMIC REFRACTION.....	- 12 -
3.1.1 <i>Seismic data acquisition</i>	- 12 -
3.1.2 <i>Data processing</i>	- 14 -
3.1.3 <i>Phase identifications</i>	- 16 -
3.1.4 <i>P-wave velocity models through ray-tracing</i>	- 17 -
3.2 GRAVITY DATA.....	- 19 -
3.2.1 <i>Gravity data acquisition</i>	- 19 -
3.2.2 <i>Latitude correction</i>	- 20 -
3.2.3 <i>Eötvös correction</i>	- 20 -
3.2.4 <i>Free-air (FA) and Bouguer (BA) correction</i>	- 20 -
3.2.5 <i>2D gravity modelling</i>	- 20 -
3.3 MAGNETIC DATA	- 23 -
3.3.1 <i>Magnetic data acquisition</i>	- 23 -
3.3.2 <i>Magnetic line data editing</i>	- 23 -
3.3.3 <i>IGRF correction</i>	- 23 -
3.3.4 <i>Diurnal correction</i>	- 25 -
3.3.5 <i>Levelling</i>	- 25 -
4 CONTRIBUTION TO SCIENTIFIC JOURNAL PUBLICATIONS	- 27 -
4.1 CONTINENT-OCEAN TRANSITION AND VOLUMINOUS MAGMATIC UNDERPLATING DERIVED FROM P-WAVE VELOCITY MODELLING OF THE EAST GREENLAND CONTINENTAL MARGIN	- 27 -
4.2 VARIATIONS IN MAGMATIC PROCESSES ALONG THE EAST GREENLAND VOLCANIC MARGIN.....	- 27 -
4.3 FROM DEVONIAN EXTENSIONAL COLLAPSE TO EARLY EOCENE CONTINENTAL BREAKUP: AN EXTENDED TRANSECT OF THE KEJSER FRANZ JOSEPH FJORD OF THE EAST GREENLAND MARGIN.....	- 28 -
5 CONTINENT – OCEAN TRANSITION AND VOLUMINOUS MAGMATIC UNDERPLATING DERIVED FROM P-WAVE VELOCITY MODELLING OF THE EAST GREENLAND CONTINENTAL MARGIN.....	- 29 -
5.1 SUMMARY	- 29 -
5.2 INTRODUCTION	- 29 -
5.3 DATA ACQUISITION AND PROCESSING	- 32 -
5.4 MODELLING.....	- 34 -
5.5 RESULTS	- 37 -
5.5.1 <i>The Godthåb Gulf profile (GG) AWI-20030400</i>	- 39 -
5.5.1.1 Continental crust (km 0 – 100).....	- 40 -
5.5.1.2 Continent – ocean transition zone (100 – 224 km)	- 41 -
5.5.1.3 Oceanic crust (224 – 320 km).....	- 42 -
5.5.2 <i>The Kejser Franz Joseph Fjord profile (KFJF) AWI-20030500</i>	- 43 -
5.5.2.1 Continental crust (0 – 130 km).....	- 43 -
5.5.2.2 Continent – ocean transition zone (130 – 260 km)	- 43 -
5.5.2.3 Oceanic crust (260 – 460 km).....	- 45 -
5.5.3 <i>Gravity models</i>	- 47 -
5.6 INTERPRETATION AND DISCUSSION	- 48 -
5.6.1 <i>Continental crust</i>	- 48 -
5.6.2 <i>The continent – ocean transition (COT)</i>	- 50 -

5.6.3	<i>The oceanic crust</i>	- 52 -
5.6.4	<i>The lower crustal body (LCB)</i>	- 54 -
5.6.5	<i>Rift propagation</i>	- 55 -
5.6.6	<i>Competitive interpretation of the conjugate margins</i>	- 56 -
5.7	CONCLUSION	- 59 -
5.8	ACKNOWLEDGEMENTS	- 59 -
5.9	REFERENCES	- 59 -
6	VARIATIONS IN MAGMATIC PROCESSES ALONG THE EAST GREENLAND VOLCANIC MARGIN	- 64 -
6.1	SUMMARY	- 64 -
6.2	INTRODUCTION	- 66 -
6.3	BRIEF REVIEW OF GEODYNAMIC MODELS FOR VOLCANIC RIFTED MARGIN	- 67 -
6.4	NEW TRANSECTS OF THE NORTHEAST GREENLAND MARGIN	- 68 -
6.4.1	<i>Processing and modelling</i>	- 68 -
6.4.2	<i>Profile AWI-20030200</i>	- 71 -
6.4.2.1	Continent – ocean transition	- 71 -
6.4.2.2	Oceanic section	- 72 -
6.4.2.3	Gravity modelling	- 73 -
6.4.2.4	Stratigraphic and structural interpretation of AWI-20030200	- 75 -
6.4.3	<i>Profile AWI-20030300</i>	- 78 -
6.4.3.1	Continental section	- 78 -
6.4.3.2	Oceanic section	- 79 -
6.4.3.3	Gravity modelling	- 79 -
6.4.3.4	Stratigraphic and structural interpretation of AWI-20030300	- 81 -
6.4.4	<i>Comparison of structural style with the conjugate Lofoten-Verstålen margin</i>	- 83 -
6.5	HALF SPREADING RATES AND TIME OF BREAK-UP	- 85 -
6.6	OFFSHORE CRUSTAL ARCHITECTURE OF THE EAST GREENLAND MARGIN	- 86 -
6.6.1	<i>Seismic profiles</i>	- 87 -
6.6.2	<i>Depth to crystalline basement</i>	- 89 -
6.6.3	<i>Depth to Moho</i>	- 91 -
6.6.4	<i>Crustal thickness</i>	- 91 -
6.6.5	<i>Thickness of high velocity lower crust</i>	- 91 -
6.7	DISCUSSION	- 97 -
6.7.1	<i>HVLC distribution at North Atlantic conjugate margins</i>	- 97 -
6.7.2	<i>Northeast Greenland melt distribution and margin formation models</i>	- 99 -
6.8	CONCLUSION	- 102 -
6.9	ACKNOWLEDGEMENTS	- 103 -
6.10	REFERENCES	- 104 -
7	FROM DEVONIAN EXTENSIONAL COLLAPSE TO EARLY EOCENE CONTINENTAL BREAK-UP: AN EXTENDED TRANSECT OF THE KEJSER FRANZ JOSEPH FJORD OF THE EAST GREENLAND MARGIN	- 112 -
7.1	SUMMARY	- 112 -
7.2	INTRODUCTION	- 112 -
7.3	GEOLOGICAL BACKGROUND	- 113 -
7.4	CRUSTAL SCALE CHARACTERISTICS OF RIFT EPISODES	- 114 -
7.4.1	<i>Precambrian Shield and Caledonian orogen</i>	- 116 -
7.4.2	<i>Post-Caledonian Basins</i>	- 117 -
7.5	RIFT GEOMETRIES	- 118 -
7.5.1	<i>Upper plate margin segment</i>	- 119 -
7.5.2	<i>Lower plate margin segment</i>	- 120 -
7.5.3	<i>Asymmetric rifting of conjugate margins</i>	- 120 -
7.6	DURATION AND PRODUCTION RATES OF NORTHEAST GREENLAND MAGMATISM	- 122 -
7.6.1	<i>Productivity</i>	- 122 -
7.6.2	<i>Duration</i>	- 123 -
7.6.3	<i>Poly-productivity model</i>	- 124 -
7.7	DISCUSSION	- 125 -
7.8	CONCLUSIONS	- 126 -
7.9	ACKNOWLEDGEMENTS	- 127 -
7.10	REFERENCES	- 127 -
8	SUBSIDENCE ANALYSIS	- 133 -

8.1	SUBSIDENCE MODELS	- 133 -
8.1.1	<i>McKenzie model – Thermal tectonic subsidence</i>	- 133 -
8.1.2	<i>Subsidence by sediment load</i>	- 136 -
8.1.3	<i>Uplift by magmatic underplating</i>	- 136 -
8.1.4	<i>Subsidence by intrusion</i>	- 136 -
8.1.5	<i>Parson and Sclater model – Thermal subsidence of oceanic basins</i>	- 137 -
8.2	OCEANIC BASIN AND COT	- 138 -
8.2.1	<i>Predicted depths of ocean basin</i>	- 138 -
8.2.2	<i>Discussion of predicted depths</i>	- 140 -
8.3	CONTINENTAL PARTS AND COT	- 143 -
8.3.1	<i>Predicted depth to basement of profile AWI-20030300</i>	- 144 -
8.3.2	<i>Predicted depth to basement of profile AWI-20030400</i>	- 145 -
8.3.3	<i>Predicted depth to basement of profile AWI-20030500</i>	- 146 -
8.3.4	<i>Interpretation and Discussion</i>	- 146 -
8.4	CONCLUSION OF THE SUBSIDENCE ANALYSIS.....	- 148 -
9	CONCLUSION AND OUTLOOK.....	- 154 -
9.1	CONCLUSION	- 154 -
9.1.1	<i>Crustal architecture of the continent - ocean transition zone</i>	- 154 -
9.1.2	<i>Constraints for magmatic underplating</i>	- 155 -
9.1.3	<i>Comparisons with the conjugate Norwegian and adjacent southeast Greenland margins</i>	- 156 -
9.1.4	<i>First utilization of the results</i>	- 156 -
9.2	OUTLOOK	- 156 -
	ACKNOWLEDGEMENTS.....	- 160 -
	REFERENCES.....	- 162 -
	CURRICULUM VITAE.....	- 170 -

Kurzfassung

Das wissenschaftliche Interesse an gedehnten Kontinentalrändern wird durch den stetigen Bedarf an verbesserten Rekonstruktionsmodellen lithosphärischer Plattenbewegungen angetrieben. Dabei liefern Untersuchungen gegenüberliegender Kontinentalränder wichtige Randbedingungen für die zeitliche und räumliche Zuordnung der dehnungsbegleitenden tektonischen und magmatischen Prozesse. Insbesondere werden dadurch die Anfangsbedingungen für die Entstehung ozeanischer Kruste, der thermische Einfluss und die Subsidenz sedimentärer Becken veranschaulicht. Letzteres gewinnt schließlich auch das wirtschaftliche Interesse an vulkanischen Kontinentalrändern, das sich auf ihr mögliches Kohlenwasserstoffpotential konzentriert.

Die vorliegende Arbeit befasst sich mit der geophysikalischen Ausarbeitung der bisher nur unzureichend untersuchten Region des nordostgrönländischen Kontinentalrandes. Der Fokus gilt dem strukturellen Aufbau innerhalb der Übergangszone von kontinentaler zur ozeanischen Kruste (COT). Entscheidend dabei ist die Lage der Kontinent – Ozean Grenze, die erstmalig durch ganzheitliche Krustenmodelle für die Region Nordostgrönlands näher beschrieben wird. Eine entscheidende Rolle für die Diskussion der Dehnungsprozesse spielt die Identifizierung magmatischer Einlagerungen und Unterplattung, die den Krustenaufbau der Übergangszone entscheidend prägen. Zu diesem Zweck akquirierte das Alfred- Wegener- Institut für Polar- und Meeresforschung im Jahr 2003 zwischen der Jan-Mayen- (JMFZ) und Grönlandbruchzone (GFZ) (72° N – 77° N) neue refraktionsseismische Daten über den ostgrönländischen Kontinentalrand. Zusätzlich werden helikoptergestützte Magnetik- und schiffs-gravimetrische Daten verwendet, die zeitgleich vom Forschungsschiff FS „Polarstern“ aus akquiriert wurden.

Profilschnitte, basierend auf seismischen Geschwindigkeitsmodellen, bieten für diese Region neue Erkenntnisse über die tiefen Krustenstrukturen der Übergangszone. Im Einklang mit den Potentialfelddaten offenbaren sie eine deutliche Segmentierung des nordostgrönländischen Kontinentalrandes. Dabei ist die Beobachtung eines bis zu 16 km mächtigen Hochgeschwindigkeitskörpers in der Unterkruste seewärts des Kaiser-Franz-Joseph Fjords (KFJF) und Godthåb Golfes (GG) von fundamentaler Bedeutung. Dieser zeichnet sich durch P-Wellen Geschwindigkeiten von 7.0 bis 7.4 km s⁻¹ und einer lateralen Ausdehnung von ~200 km bis zu Beginn der ozeanischen Kruste aus und ist damit größer als bisher angenommen. Eine Reduzierung nach Norden ist klar erkennbar. Die 120 – 130 km weiten Übergangszonen lassen sich aus den landseitigen Hochstrukturen, der Ausdehnung sedimentärer Dehnungsbecken und dem lateralen Geschwindigkeitsanstieg innerhalb der oberen und unteren Kruste ableiten. Die dargestellten Variationen der Krustenstrukturen entlang des Kontinentalrandes zeigen, dass lang anhaltende kontinentale Dehnung im südlichen Teil durch ertragsreichen Magmatismus begleitet wurde. Der nördliche Teil wird wegen seiner im Vergleich geringeren magmatischen Überprägung während der Dehnungsphase als „magmaarmer“ Kontinentalrand bezeichnet. Der kontinentale Aufbruch lässt sich auf eine Zeit zwischen ~54 Ma im nördlichen Teil (GFZ) und 50 Ma im südlichen Segment (KFJF) eingrenzen und stellt einen gegenläufigen Aufbruch des Nordatlantiks für diese Region dar. Diese Beobachtung basiert auf den Interpretationen der COT und den ersten zu beobachteten Spreizungsanomalien (C24 – C22). Weiterhin wird eine mächtige ozeanische Kruste (9 – 13 km) an allen vier Profilen zu Beginn der Ozeanbildung beobachtet. Ihre fortschreitende Reduzierung auf 5 – 7 km steht im Gegensatz zu anderen vulkanischen Kontinentalrändern mit verdickter ozeanischer Kruste. Im Vergleich mit den konjugierenden norwegischen und den benachbarten südostgrönländischen Kontinentalrändern zeigen sich deutliche Asymmetrien. Dabei werden die Eingrenzung der Übergangszone, die Zuordnung des Hochgeschwindigkeitskörpers und die Interpretation magnetischer Spreizungsanomalien kontrovers diskutiert. Variationen entlang des ostgrönländischen Kontinentalrandes zeigen

sich sowohl in Form von Tiefenkarten für die kristalline Kruste und der Krusten-Mantel Grenze, als auch in Mächtigkeitskarten für die gedehnte Kruste und des Hochgeschwindigkeitskörpers ($>7 \text{ km s}^{-1}$).

Drei mögliche Szenarien zur Entstehungsgeschichte des lokal ausgeprägten Hochgeschwindigkeitskörpers werden vorgestellt. Der erste Fall betrachtet eine massive magmatische Unterplattung, und erklärt dies mit sowohl bekannten als auch neu bestimmten Produktionsraten durch einem lang andauernden Prozess ($\sim 58 - 50 \text{ Ma}$) mit mehreren magmatischen Produktionsphasen. In diesem Zusammenhang kann eine Verbindung zum isländischen Mantelplume, der als Quelle heißen Mantelmaterials, das durch Konvektion aus dem unteren Mantel (Hotspot) zur Lithosphäre transportiert und zur Bildung der nordatlantischen vulkanischen Provinz verstanden wird, hergestellt werden. Eine zweite Möglichkeit betrachtet die Einlagerung vulkanischer Schmelzen in noch vorhandene gedehnte kontinentale Unterkruste. Diese könnte möglicherweise entlang einer nach westen abtauchenden Scherzone in flachere Regionen invertiert worden sein. Für diesen Fall bestünde der Hochgeschwindigkeitskörper aus schon existierender kontinentaler Kruste und reduziert somit die Dehnungsrate und die Menge magmatischer Schmelzen. Die Bildung des Kolbeinsey-Rückens südlich der Jan-Mayen-Bruchzone erlaubt eine dritte Betrachtung aufgrund eines jüngeren magmatischen Ereignisses. Der Hochgeschwindigkeitskörper in der Region des KFJF und GG kann demnach zum einen als Teil gedehnter kontinentaler Kruste mit Einlagerungen aus dem frühen Paläozän betrachtet werden. In einer zweiten Phase könnte sich im Oligozän/Miozän eine ergänzende magmatische Unterplattung zeitgleich mit der Abspaltung des Jan-Mayen-Kontinents und der beginnenden Ozeanbeckenbildung am Kolbeinsey-Rücken abgelagert haben. Aus den beiden letzteren Modellansätzen wird der mögliche Einfluss des isländischen Mantelplumes im frühen Paläozän auf den nordostgrönländischen Kontinentalrand in Frage gestellt. Im Vergleich zum ersten Fall ist ein geringerer magmatischer Einfluss nötig und eine Reduzierung nach Norden hin begründet.

Eine Analyse der Absenkungsgeschichte soll zu einer Favorisierung eines der drei Modelle führen. Dabei zeigt sich, dass die Anhebung einer reinen magmatischen Unterplattung (erstes Modell) der thermo-tektonischen Absenkung stark gedehnter kontinentaler Kruste nicht ausreichend entgegenwirkt und die modellierte tiefe der Kruste nicht erklären kann. Daher scheint es wahrscheinlich, dass primär mit magmatisch überprägter kontinentaler Kruste und mit nur einem geringen Teil magmatischer Unterplattung zu rechnen ist. Diese Annahme stützt sich jedoch weiterhin auf eine Anhebung der Übergangszone und des ozeanischen Beckens zur Übergangsgrenze. Neogene Hebungsprozesse und Erosion könnten dies erklären. Eine Unterteilung des Hochgeschwindigkeitskörpers kann jedoch aus den bestehenden tiefenseismischen Modellen nicht aufgelöst werden und bleibt damit ungeklärt.

Abschließend werden weitere Maßnahmen für eine vollständige Untersuchung des Hochgeschwindigkeitskörpers und einer Synthese der konjugierenden Kontinentalränder empfohlen.

Abstract

The scientific interest in rifted continental margins is driven by the demand for improved models of lithospheric plate reconstructions. Integrated studies of conjugate margins provide important constraints for the sequence of events of syn-rift tectonic and magmatic processes. In particular, initial conditions can be depicted for seafloor spreading, the influence on the thermal regime and subsidence of sedimentary basins. The latter meets at the end the economic interests for the assessment of the hydrocarbon-potential at volcanic margins.

The aim of this study is the geophysical investigation and evaluation of the weakly explored region of the northeast Greenland margin. The main objective is the crustal architecture of the continent-ocean transition zone (COT). Crucial is therefore the location of the continent-ocean boundary, which is depicted for the first time from integrated crustal models for the northeast Greenland region. The identification of magmatic intrusions and underplating contributes to the discussion about rifting processes due to their significant impact in the crustal architecture within the transition zone. New seismic refraction data were acquired for this purpose across the East Greenland margin between the Jan Mayen (JMFZ) and Greenland fracture (GFZ) zones (72° N – 77° N) by the Alfred Wegener Institute of Polar and Marine Research in 2003. Operating from the RV “Polarstern”, helicopter-borne magnetic data and ship-borne gravity data complete the comprehensive geophysical data-set used in this thesis.

Transects of seismic velocity models shed some new light into the deeper crustal structure of the transition zone in this regions. They reveal a significant segmentation of the northeast Greenland margins, which is compatible with the potential field data. A crucially important observation is an up to 16 km thick lower crustal body off the Kejser Franz Joseph Fjord (KFJF) and Godthåb Gulf (GG). It is associated with seismic P-wave velocities in the range between 7.0 and 7.4 km s⁻¹, which extends for over ~200 km to the onset of oceanic crust, and is therefore larger than supposed before. A northward decrease is clearly recognizable. The 120 – 130 km wide continent-ocean transition zones are inferred from the landward basement highs, from the extent of syn-rift sediment basins and the lateral increase of velocities in the upper and lower crust. Based on these comprehensive observations, excessive magmatism is inferred to have occurred in the southern domain during a long-lasting period of rifting. The northern part of the northeast Greenland margin is classified as a “magma-starved” volcanic margin, due to the reduced syn-rift intrusions compared to the region further south.

Break-up is proposed to have occurred at ~54 Ma in the northern region (GFZ), and at 50 Ma in the southern domain (KFJF), which draws up a counter-directional rift propagation of the North Atlantic break-up for this region. This observation is based on the definition of the COT, and the earliest identifiable ocean spreading magnetic anomalies (C24 – C22).

All four seismic profiles show initial oceanic crustal thicknesses that are increased (9 – 13 km), which decreases rapidly to a thickness of 5 – 7 km unlike other volcanic margins, which incorporates extended thicker oceanic crust.

Asymmetries and variations of the crustal architectures are inferred from a comparison of the conjugate northeast Greenland and Norwegian margins, and also with the adjacent southeast Greenland margin. Constraints of the COT, the origin of the high velocity lower crustal body and interpretation of magnetic spreading anomalies is controversially discussed. Regional variations along the East Greenland margins are illustrated in terms of depth to basement and Moho, crustal thickness and the thickness of the high velocity (>7 km s⁻¹) layer.

Three possible scenarios of the formation of the high velocity lower crustal body are presented. Pure magmatic underplating is explained in a first model by a history of multi-phase magmatism beginning at ~58 Ma and lasting until break-up at 50 Ma, based on previously published and newly derived magma production rates. Accordingly, the excess melt generation can be associated with the Iceland plume, which is understood as a localised

heat source generated in the lower mantle (hotspot) and transported to the lithosphere by convection in the mantle, forming the North Atlantic Volcanic Province. In a second model, the transition zone is suggested to consist of highly intruded pre-existing continental crust. It is discussed whether lower crustal material has been brought to shallower levels along a west-dipping shear zone during rifting. Reduced stretching factors and melt generation can be attributed to the thicker crust in the transition zone. The vicinity of the new spreading system of the Kolbeinsey Ridge south of the Jan Mayen Fracture Zone permits the third suggestion for a second major magmatic event. The high velocity lower crustal body off KFJF and GG is therefore assumed to consist of primary of intruded pre-existing continental crust according to magmatism in Early Paleocene. The accretion of Oligocene/Miocene magmatic underplating beneath the transition zone is related to the break-up of the Jan Mayen microcontinent and the onset of oceanization along the young Kolbeinsey Ridge in a second phase. The inferences for the latter two models query the influence of the Iceland mantle plume on the northeast Greenland margin in Early Paleocene as they require less melt production and explain a strong decrease in the melt distribution towards the north.

A comprehensive subsidence analysis is established in order to favour one of the models. It can be shown that magmatic underplating (model 1) is not sufficient to uplift the rifted and thermal-tectonically subsided crust to the observed depth to basement. It seems more likely, that the high velocity lower crust consists of primary intruded pre-existing lower crust and incorporates only minor magmatic underplating. This assumption needs to incorporate, however, a transient uplift of the continent-ocean boundary towards the transition zone and the oldest oceanic crust. Neogene uplift and erosion could explain this phenomenon. However, an internal segmentation of the high velocity lower crustal body can not be supported from the seismic data and remains debatable.

Suggestions for further research are finally outlined in order complete the investigation of the high velocity lower crustal body and synthesize the conjugate margins.

1 INTRODUCTION

1.1 Greenland – a unique landscape

Greenland, a Danish territory, is the largest Island of the world (2.175 Mio km²) and is located at the Arctic region between 60° N and 83° N. It is surrounded from the Labrador Sea and Baffin Bay in the west, the North Atlantic in the south and east and the ice-covered Arctic Sea in the north. About 80 per cent of Greenland is covered by an ice sheet of up to 3.4 km thickness. The ice-free coast line belt (up to 250 km wide) provides scenic outcrops of one of the oldest datable rocks on earth (Escher and Watt 1976). The north-eastern Greenland coastline (Figure 1.1) exhibits spectacular land-cutting fjords and the Caledonian mountains, which are up to 2000 m high.



Figure 1.1: Godthåb Gulf of the East Greenland margin (AWI, private photography).

The region of the northern North Atlantic borders has been the target area for many scientists for several decades. Outcrops of the mountains provide the only opportunity to find answers about the Caledonian orogen on the Greenland Island, the formation of the sedimentary basins, tectonic movements and volcanism. Many of those investigations contribute to a detailed knowledge of the stratigraphy, lithology and tectonic features along the shore (e.g. Escher and Pulvertaft 1995; Henriksen et al. 2000). Inland seismological surveys mapped the thicknesses of the Proterozoic and Archean cratons and depth to the Mohorovičić (Moho) discontinuity (Dahl-Jensen et al. 2003), which is the structural boundary between the lower crust and upper mantle.

Approaches from the seaside of the Greenland margin have been always the major challenge, and not only for the earliest expeditions more than 130 years ago. Karl Koldewey started the first German non-scientific polar vessel (*GRÖNLAND*) to the East Greenland coast in 1868 but didn't get closer than just in the range of vision. Pack ice in the land-cutting fjords and on the shelf region prevented a closer approach. His second scientific vessel (*GERMANIA*) started from Bremerhaven in 1869/70, and the crew arrived at the East Greenland coast near 74° 30'N.

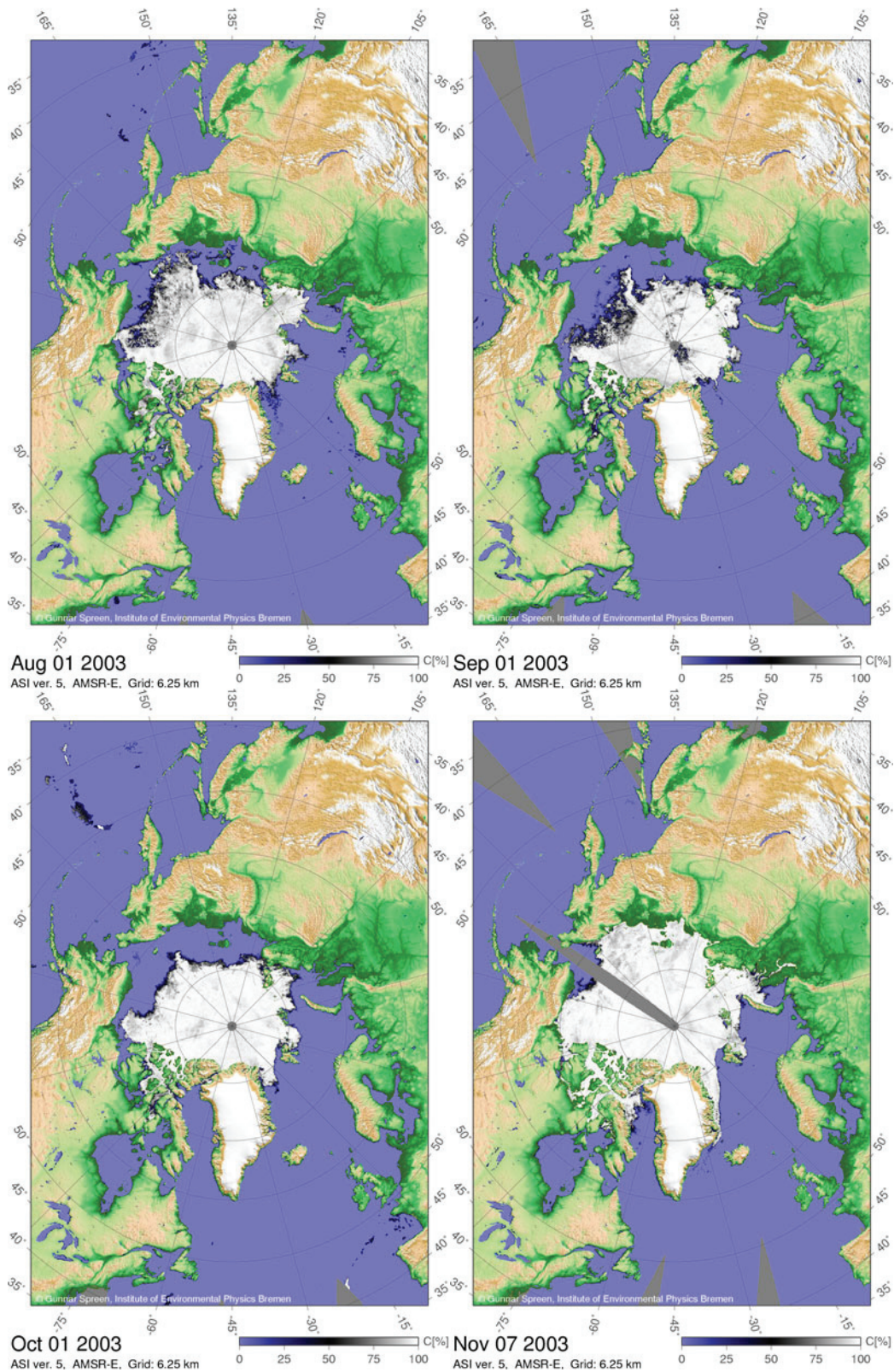


Figure 1.2: Satellite images of the arctic ice coverage for August to November 2003 (http://iup.physik.uni-bremen.de:8084/amsrdata/asi_daygrid_swath/11a/n6250). Note the sea ice coverage between 70 °N and 75 °N along the East Greenland coast.

Sea ice coverage is observed and recorded in our modern world by satellite images. The variation and coverage of pack ice is exemplarily shown for the months August to November 2003 in Figure 1.2. But, it is still the challenge to hit the tiny window of ice free fjords and

uncovered shelf regions, even for an ice-breaking vessel in the summer season due to the unpredictable sea ice formation.

1.2 Geophysical investigations off East Greenland

Continental rifting between Greenland and Scandinavia culminated in the opening of the northern North Atlantic in early Tertiary times, and is marked by the ocean spreading anomalies C24A/B at 56 – 53 Ma (Talwani and Eldholm 1977; Srivastava and Tapscott 1986). Larsen (1988) suggested a rapid propagation of the spreading along a fairly straight line from the south of Greenland and northward to the Greenland–Senja Fracture Zone, which is still an unresolved question (Saunders et al. 1998). Extensive geophysical research of the eastern Greenland shelf region started for this purpose at more than 25 years ago (Larsen 1990). Seismic reflection surveys have been carried out on the south-eastern Greenland shelf but only a sparse coverage has been obtained for the northern region. Short profiles focused on the shelf edge and on the investigation of so-called seaward dipping reflectors (Hinz et al. 1987; Mutter and Zehnder 1988, Figures 1.3 and 1.4) which gave hints for increased magmatism during continental break-up. The universities of Hamburg and Kiel in cooperation with the Alfred Wegener Institute for Polar and Marine Research (AWI) carried out first seismic refraction surveys on- and offshore in 1988 (Weigel et al. 1995, Figure 1.3). Further experiments of the AWI focused on the Scoresby Sund region and the East Greenland fjord region (Figure 1.3) which allowed combined land and sea experiments (Fechner and Jokat 1996; Mandler and Jokat 1998; Schlindwein and Jokat 1999; Schmidt-Aursch and Jokat 2005a). The geophysical observations gathered important insights from the Caledonian crustal root, the Devonian and Mesozoic sedimentary basins and the continental crustal structure (Figure 1.4). Evidences of increased magmatism north and south of the Jan Mayen Fracture Zone has been proposed from seismic velocity models, which revealed a positive lower crustal velocity anomaly, which has been interpreted as a magmatic underplate, and is a marker for volcanic rifted margins.

The limited seaward prolongation of the seismic profiles due to sea ice coverage left the full spatial extent of the magmatic body debatable. On the other hand, reinterpreted data from ocean bottom seismometers (OBS) within the Hall Bredning and landward of the Scoresby Sund has shown that such magmatic underplating is absent (Schmidt-Aursch and Jokat 2005a), although a large amount of flood basalts extend over the adjacent Geikie Plateau (Figure 1.3). Correlations between the magmatism and the magnetic anomalies along the northeast Greenland margin were also not fully understood. The oblique termination of the magnetic ocean spreading anomalies and the disordered anomaly pattern (Verhoef et al. 1996) on the shelf give reasons to debate the structural boundaries between continental and oceanic crust (COB). Scott (2000) inferred from magnetic lineaments a continuation of the spreading anomalies and a structural boundary close to the coastline, between Godthåb Gulf and Kejser Franz Joseph Fjord (Figure 1.3). Escher and Pulvertaft (1995), and Henriksen (2000), have marked the COB along the termination of the clearly visible ocean spreading anomalies. A different approach has come from Tsikalas et al. (2002), based on plate reconstructions and interpretation of high-pass filtered magnetic data. These authors located the COB about 60 – 85 km off Traill Ø and Hold with Hope (Figure 1.3), which is just between the two previous locations. Seismic investigations have been carried out for the same purpose at the southeast Greenland margin (Korenaga et al. 2000; Holbrook et al. 2001; Hopper et al. 2003, Figure 1.3) and the conjugate Norwegian margin (e.g. Raum et al. 2002; Mjelde et al. 2003) and revealed constraints on the extent of magmatism and the crustal structure of the margins. An equivalent database of crustal structural models does not exist for the northeast Greenland margin. Several other questions about the variations of the style of rifting and the total extent of magmatism along the East Greenland margin remained also unresolved.

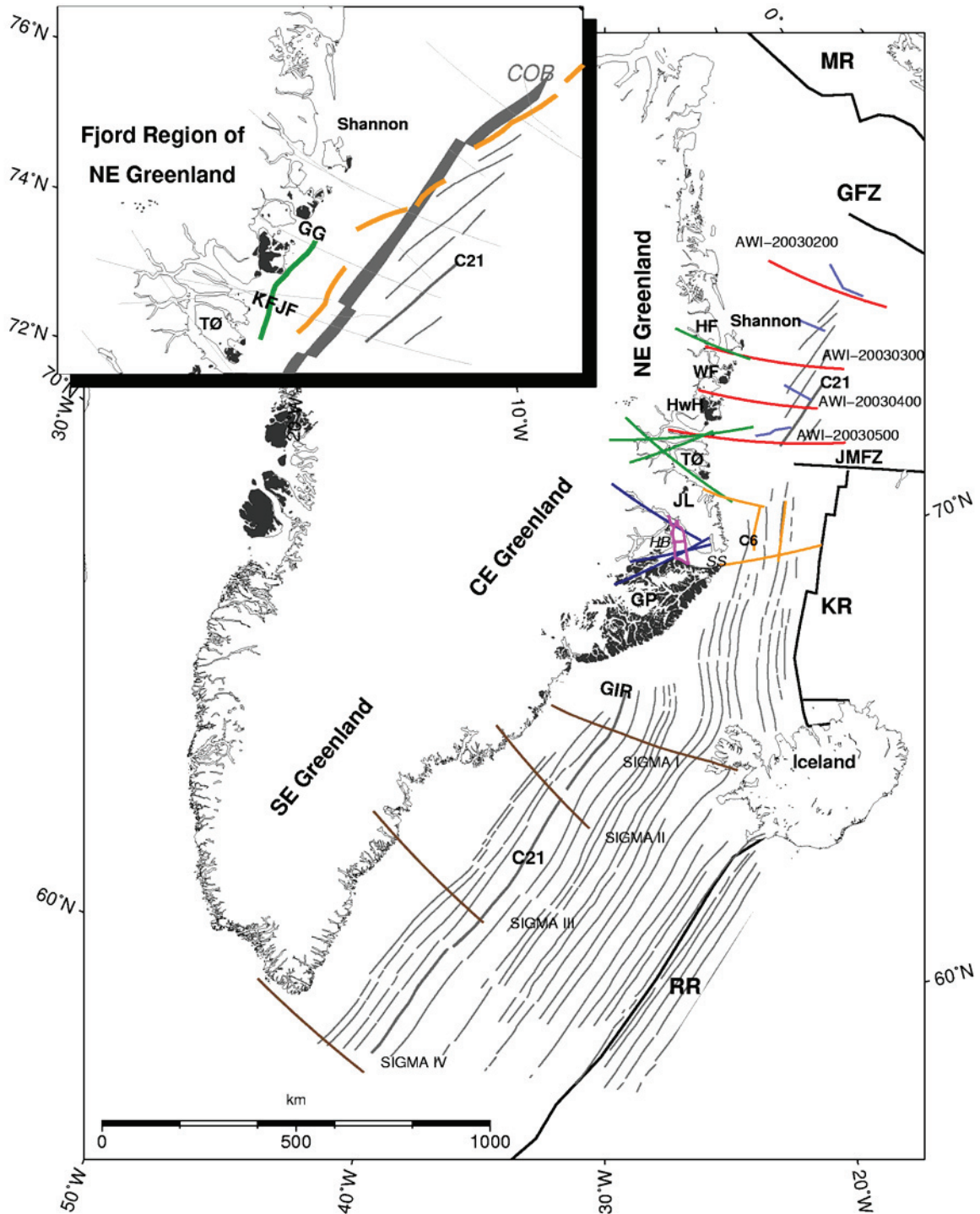


Figure 1.3: Overview of East Greenland margin. Grey stripes mark oceanic spreading anomalies. C21 is highlighted. Black regions are onshore basalts. Light blue profiles refer to Hinz et al. (1987) and Mutter and Zehnder (1988), green to Schlindwein and Jokat (1999), orange to Weigel et al. (1995), magenta to Fechner and Jokat (1996), dark blue to Mandler et al. (1998) and Schmidt-Aursch and Jokat (2005a), brown to Korenaga et al. (2000) and Hopper et al. (2003) and are labelled with SIGMA xx. Red lines are seismic lines of this study and are labelled with AWI-2003xxxx. Upper left box: Continent ocean boundaries off the East Greenland Fjord Region after Escher and Pulvertaft (1995) in grey, Tsikalas et al. (2002) (orange) and Scott (2000) (green). Abbreviations are: COB, Continent – ocean boundary; GFZ, Greenland Fracture Zone; GG, Godthåb Gulf; GIR, Greenland-Iceland Ridge; GP, Geikie Plateau; HB, Hall Bredning; HF, Hochstetter Foreland; HwH, Hold with Hope; JL, Jameson Land; JMFZ, Jan Mayen Fracture Zone; KKFJ, Kejser Franz Joseph Fjord; KR, Kolbeinsey Ridge; MR, Mohns Ridge; RR, Reykjanes Ridge; SS, Scoresby Sund; TØ, Traill Ø.

Possible asymmetries of the conjugate Norwegian and northeast Greenland margins remained unexplained due to the lack of information within the continent – oceanic transition zone (COT) of the northeast Greenland margin north of the Jan Mayen Fracture Zone (Figure 1.3). A successful approach to the crustal architecture of the continent ocean transition zone has been achieved in the late summer of 2003 (Jokat et al. 2004). The AWI acquired seismic refraction and reflection data, and potential field data, across the East Greenland shelf (Figure 1.4) and gathered a database for crustal structure modelling, and therefore an important contribution for the understanding of the tectono-magmatic processes evolved in the volcanic margin formation.

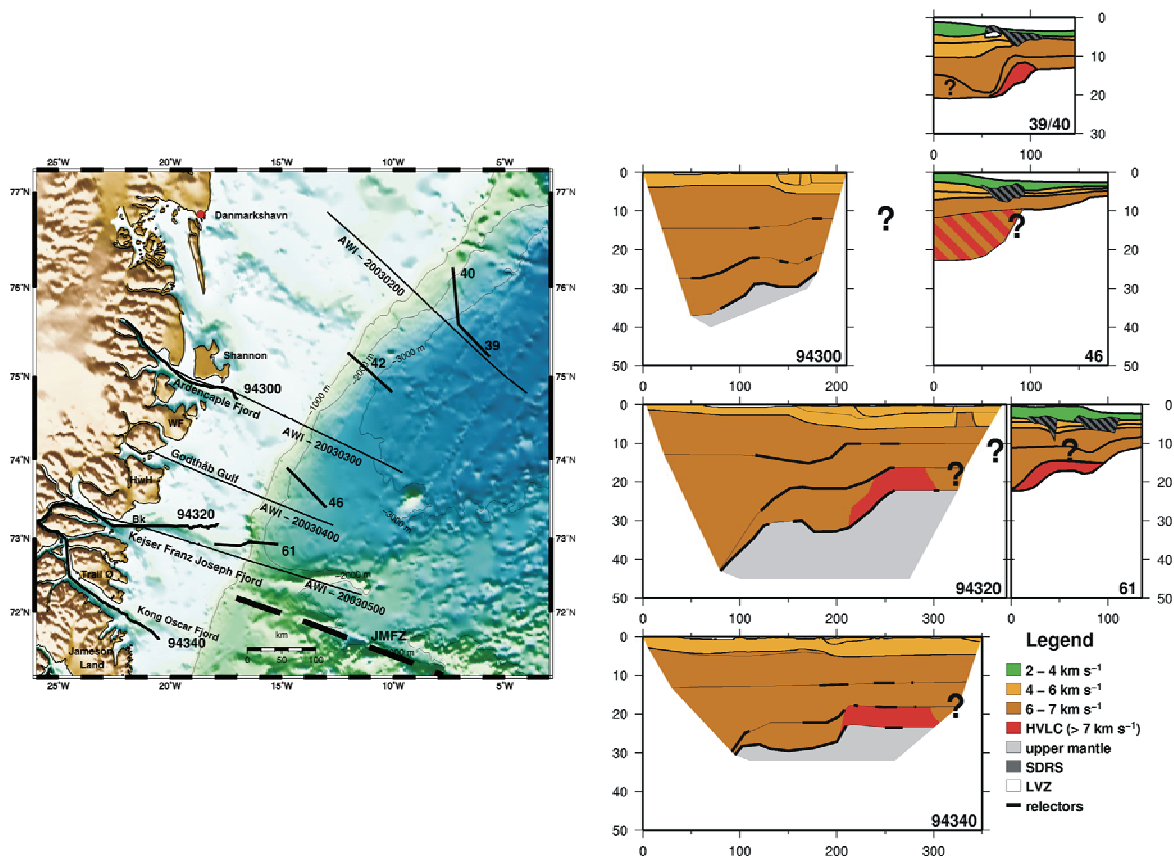


Figure 1.4: Location map of seismic transects with respect to former profiles and associated models. Models 39/40, 46, 61 after Eldholm and Grue (1994), 94300 after Schlindwein (1998) and 94320 and 94340 after Schlindwein and Jokat (Schlindwein and Jokat 1999). Lines AWI-20030200-500 are presented in this study. Abbreviations are HVLC, high velocity lower crust associated with magmatic underplating; JMFZ, Jan Mayen Fracture Zone; LVZ, low velocity zone; SDRS, seaward dipping reflectors.

1.3 Aim of the thesis

The geophysical work of this thesis was funded by the EUROMARGINS Project initiated in 2003 by the European Science Foundation (ESF). Support and scientific collaboration was provided by ten European countries (Belgium, France, Germany, Italy, the Netherlands, Norway, Portugal, Spain, Sweden, and the United Kingdom) and by the European Science Foundation under the EUROCORES Programmes, with support from the European Commission (<http://www.esf.org/euromargins>).

The aim of the thesis is to focus on the crustal architecture of the continent – ocean transition zone off the East Greenland fjord region between the Jan Mayen and Greenland fracture zones. The main objectives are:

What is the detailed crustal architecture of the continent – ocean transition zone off the northeast Greenland margin, and where is the continent – ocean boundary from the crustal structural point of view? Is there a segmentation of the northeast Greenland margin and are there correlations between the crustal structures and the magnetic and gravity anomalies? Can a formation model be established, which describes the formation of the northeast Greenland margin? If not, what are the possibilities?

Is the proposed magmatic underplating likely, and what is the extent of it in the seaward and northern directions, and its volume and source?

Are the conjugate northeast Greenland and Norwegian margins symmetric or asymmetric in their structural styles and/or interpretations? What can be deduced from the variations along-strike the East Greenland margins according to the sources and quantities of magmatism?

Seismic refraction data, recorded on- and offshore, as well as gravity data and magnetic data, will be used from the 2003 expedition (Jokat et al. 2004), in order to answer these questions. Crustal-scale models are constructed, addressing the variations of the crustal thicknesses, rift variations, distributions of outer syn-rift sedimentary basins and volcanic extrusives, intrusions and magmatic underplating. A compilation of former published seismic crustal models will be used to discuss along-strike margin variations and the possibility of asymmetries compared with the conjugate Norwegian margins.

P-wave velocity models are obtained for profile AWI-20030400 and AWI-20030500 (Figures 1.3 and 1.4). For this purpose 29 OBS/OBH and 4 Reftek land stations are processed, interpreted (identifications of long offset refracted and reflected arrivals) and modelled for profile AWI-20030400. An equivalent procedure is applied to profile AWI-20030500, which includes 30 OBS/OBH and 7 Reftek land stations. Previously processed data of 25 OBS/OBH, 6 land stations, and a starting model of the oceanic part of profile AWI-20030300 is incorporated into this study. Therefore, an improved P-wave velocity model of the full transect is developed. A starting P-wave velocity model based on processed 25 OBS/OBH data of profile AWI-20030200 is examined, and also finalised and integrated. 2D gravity models are obtained for all four seismic P-wave velocity models based on ship-borne gravity data recorded during the 2003 expedition. The geological interpretation on stratigraphy and lithology for all four profiles base on onshore geological observations (Escher and Pulvertaft 1995; Henriksen et al. 2000), interpretations of adjacent seismic models (Schlindwein 1998; Schlindwein and Jokat 1999), and on correlations of P-wave velocities and densities. A high resolution aeromagnetic dataset acquired also in 2003 is processed, interpreted and compared with the regional magnetic map (Verhoef et al. 1996) for additional constraints on volcanic features (dykes, intrusions and ocean spreading anomalies).

The large amount of ocean bottom seismometer and hydrophones (in total 126) and the processing and interpretation of the data, as well as magnetic and gravity data processing and interpretation requires stable, and comparable methods and techniques, in order to combine the findings with previous results. Therefore, common processing procedures, forward modelling using raytracing (Zelt and Smith 1992) is applied for the seismic data, followed by regional interpretations and comparisons with the conjugate and adjacent margins.

1.4 Structure of the thesis

The general classification and the significance of investigations of rifted margins are described by classical examples in Chapter 2. The geophysical data acquisition and processing methodology is described in Chapter 3. The reader is referred to appropriate literature and

software manuals for the mathematical background of the common techniques, which are used for processing and modelling.

Chapter 4 shows my contributions to scientific manuscripts, which are included in their original text and figures. The first manuscript (Voss and Jokat 2007) in Chapter 5 has been published in August 2007 by the professional journal *Geophysical Journal International*. The two other manuscripts, presented in Chapter 6 and 7, have been submitted to peer-reviewed in December 2007. Reviewer comments received in September 2007 have been incorporated.

Chapter 8 contains calculations on the subsidence and uplift history of the northeast Greenland margin. It demonstrates the likely uplifted status of the margin and provides constraints for the lithology of the high velocity lower crustal body.

All conclusions are summarized in Chapter 9. An outlook for further geophysical work is finally given, including suggestions for future seismic surveys at the northeast Greenland margin.

2 CLASSIFICATION OF CONTINENTAL RIFTED MARGINS

Continental rifted margins, which are one of the most distinctive morphological features of the world's ocean basins, mark the transition between continental and oceanic crust. They are also the sites of some of the world's largest accumulations of sediments and are one of the few remaining frontiers in the search for natural resources.

Rifted margins form when continental lithosphere ruptures and give birth to a new ocean basin (Menzies et al. 2002). Some authors used to call them passive margins, in view of the fact that no subduction occurs (Mutter et al. 1988; Mutter 1993). The main tectonic processes prior to, during and after break-up are extension, uplift and erosion while magmatism is understood to be a consequence of decompression and partial melting of the upwelling mantle beneath the lithosphere (White 1992).

Scientific and industrial researches share an interest in the geological processes and evolution of continental rifted margins. An increased knowledge of the physical, geological and petrological parameters of continental rifted margins, and insights into their crustal architecture and thermal regime yield improved plate reconstructions and models of rift mechanisms responsible for the margins' formation. Key questions concern the driving forces of rifting and continental break-up, dynamics of the lithosphere, the role of mantle plumes and hotspots, and the reasons for uplift, subsidence and the associated formation of sedimentary basins. As well as this, a large number of major hydrocarbon provinces are associated with continental rifted margins. The sedimentary basins at the outer margins, over the shelf and into the deeper sea, are considered as the most prospective areas for the oil and gas industry (Hinz et al. 1993). The resource potential is not yet fully assessed, especially in remote areas like the North Atlantic continental margins. Tectonic and magmatic events have major impacts on the development or destruction of hydrocarbon reservoirs, since uplift would unroof reservoirs and increased heat might crack hydrocarbons. Therefore, both academic and industrial research, sometimes in cooperation, has focused on determining the key constraints on the mechanisms and structural evolution of continental rifted margins.

Intensive investigations of the North Atlantic margins (e.g. Eldholm and Grue 1994; Holbrook et al. 1994a; Whitmarsh et al. 1996; Saunders et al. 1997) have shown that two distinct types of continental rifted margins can be distinguished by their thermal regime and the amount of magmatism involved in the rifting and break-up process, namely volcanic and non-volcanic rifted margins (Vink 1984; White 1987; Mutter et al. 1988). Constraints on initial rifting mechanisms are probably best preserved at non-volcanic margins, where the pre-existing continental crust has not been significantly altered by volcanic activity. Large amounts of emplaced lavas characterize volcanic margins and mostly prevent detailed structural investigations of the rifted regions.

2.1 Non-volcanic rifted margins

Non-volcanic margins are generally characterized by rotated fault blocks (the result of continental rifting) between unaffected continental and newly accreted oceanic crust over normal temperature mantle (White 1992). The contact between the stretched and thinned continental crust and the newly developed oceanic crust can be well imaged because it has not been modified by magmatism. Long duration stretching and rifting of the continent allows conductive cooling of the upwelling asthenosphere, which inhibits the development of melt and magmatism within the rift zones (Bown and White 1995). Another consequence of this

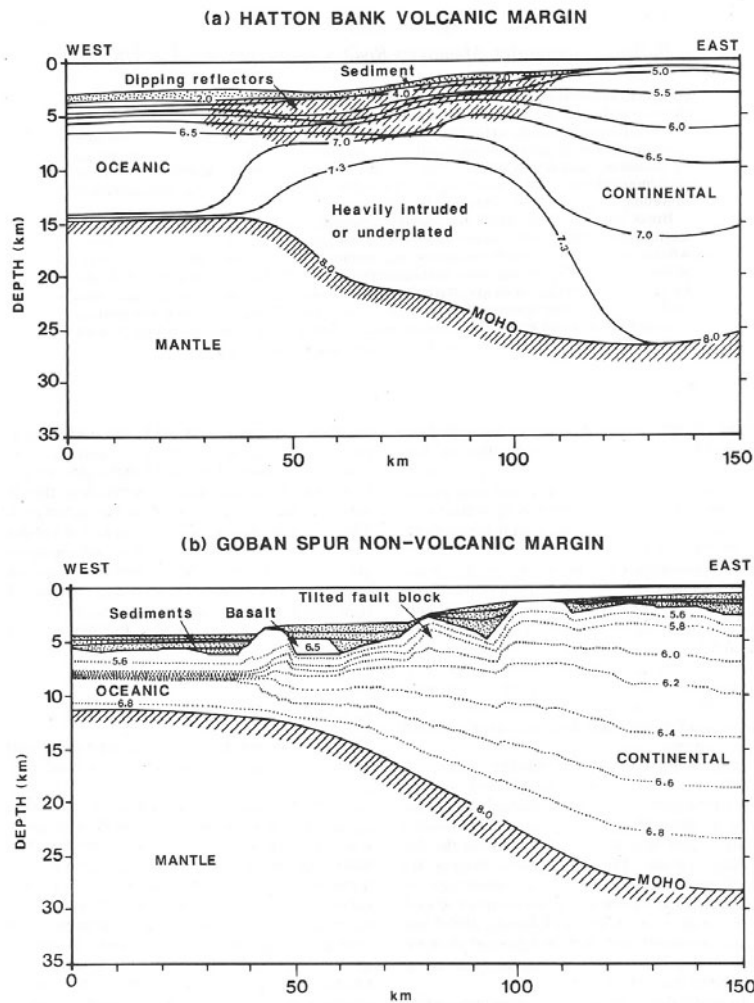


Fig. 1. Cross-sections at the same scales with velocity contours from wide-angle seismic profiles across (a) typical volcanic continental margin west of Hatton Bank (from White *et al.* 1987; Morgan *et al.* 1989), and (b) a typical non-volcanic margin on the Goban Spur (from Horsefield *et al.* in press). Vertical exaggeration is 2.3:1.

Figure 2.1: Classical examples of volcanic and non-volcanic types of margins from White (1992).

magma starvation is significantly thin oceanic crust immediately following break-up, although this adjusts to normal thicknesses (~ 7 km) (White *et al.* 1992) with further seafloor spreading. Thin oceanic crust also occurs on ultra-slow spreading ridges with full spreading rates of less than 2 cm a^{-1} , but such rates are not necessarily seen at non-volcanic margins (White *et al.* 1992).

A typical non-volcanic margin pair is the Goban Spur margin (Horsefield *et al.* 1994), Bay of Biscay, and Galicia Bank, off Iberia (Whitmarsh *et al.* 1996) and the conjugate southeast Flemish Cap margin east of Newfoundland (Reid 1994; Chian *et al.* 1995; Loudon and Chian 1999; Funck *et al.* 2003; Hopper *et al.* 2006). Investigations of non-volcanic rifted margins yield insights into the mechanical response of the crust and lithosphere to extensional stresses. Extreme thinning of the continental crust also allows exhumation of mantle material, which might to some degree undergo serpentinization when exposed to seawater, as seen on Galicia Bank (Boillot *et al.* 1988; Brun and Beslier 1996). Here, Whitmarsh *et al.* (1996) recorded continental crust that had thinned to 2 km, and initial oceanic crust of only 2.5 – 3.5 km thickness, increasing to normal thickness over a distance of 20 km. Both the continental and the oceanic crust are underlain by a lens-shaped body of serpentinized peridotite with seismic velocities of $7.2 - 7.6 \text{ km s}^{-1}$. A peridotite ridge was found in the outer part of the rift zone, marking the continent-ocean boundary. The region of extension is ~ 80 km wide, which is narrow compared to most non-volcanic margins. A similar narrow thinning zone was

proposed at Goban Spur (Horsefield et al. 1994) and contrasts with the 180 km wide region of thinning from the Nova Scotia margin (Funck et al. 2004), which is followed by ~150 km serpentinized mantle within the transition zone (Figure 2.2). Volcanism is not entirely absent at non-volcanic margins but is usually restricted to small amounts of extrusives and lower crustal sills formed at the time of break-up, as seen on Goban Spur (White 1992; Horsefield et al. 1994, Figure 1.2).

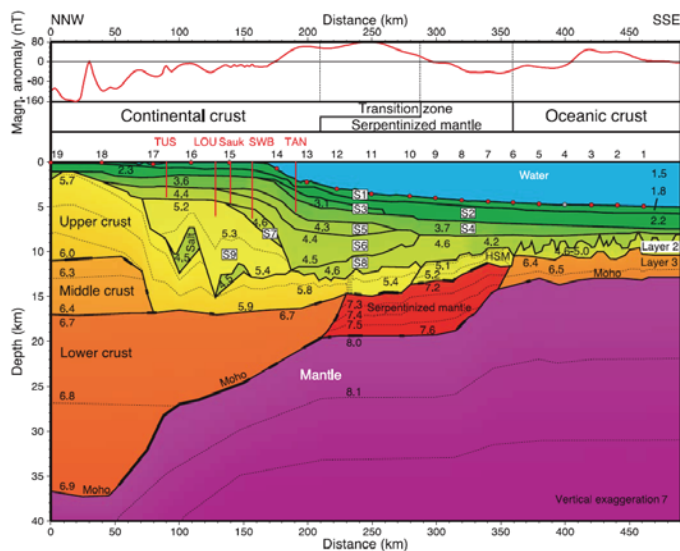


Figure 2.2: Example of a non-volcanic rifted margin from Funck et al. (2004), northern Nova Scotia, Canada. It clearly demonstrates the extent of serpentinized mantle beneath the highly thinned transitional crust. Red circles mark OBS locations, red lines exploration well sites. Note the highly serpentinized mantle (HSM) above the high velocity body. Magnetic anomalies plotted along the profile at the top, including the segmentation of the transect.

2.2 Volcanic rifted margins

Morgan (1971) was the first to propose a correlation between flood basalt volcanism and continental break-up. As much as 90 % of rifted margins world-wide are associated with excess volcanism (Menzies et al. 2002). The associated Large Igneous Provinces (LIPs) are characterised by the emplacement of mafic rocks, (i.e. magnesium and iron rich) at higher rates (Coffin and Eldholm 1994) than those required for the production of normal thickness oceanic crust (Menzies et al. 2002). The major characteristics of volcanic margins are:

- i. flood basalts observed as strong reflective seaward dipping reflector series (SDRS) (Hinz 1981; Eldholm et al. 1987)
- ii. sill intrusions in the continental crust and
- iii. a high velocity ($>7 \text{ km s}^{-1}$) lower crust (HVLC), interpreted mostly as mafic to ultra-mafic magmatic underplating/intrusions beneath continental and/or oceanic crust (Mutter et al. 1984; White et al. 1987).

Classic examples are those from Hatton Bank (Morgan et al. 1989, Figure 1.2) and the Norwegian margin (e.g. Eldholm and Grue 1994; Mjelde et al. 1997; Mjelde et al. 2005). Several models have been suggested to explain the formation of Large Igneous Provinces and the characteristics of volcanic rifted margins. Most of these models invoke the influence of mantle plumes (Morgan 1971; White and McKenzie 1989), which are localised heat sources generated in the lower mantle (hotspots) and transported to the surface (mantle diapir) by convection in the mantle. Persistent post-break-up mantle melting forming thicker-than-normal oceanic crust ($>7 \text{ km}$) (White et al. 1992) is often explained by the plume hypothesis. At the U.S. Atlantic margin (Holbrook et al. 1994a; Holbrook et al. 1994b) and the south-east Greenland margin (Korenaga et al. 2000; Holbrook et al. 2001; Hopper et al. 2003), 20 – 30 km thick igneous crust was observed. The Early Paleogene volcanism of the North Atlantic Igneous Province is widely related to the lithospheric impingement of the proto-Iceland mantle plume, first proposed by Morgan (1971). A wide variety of modifications to this basic

model have been discussed, e.g. to plume-size, origin and path and the possibility of pulsating plumes or multiple plume-heads (Lawver and Müller 1994; White et al. 1995; Nadin et al. 1997). Several alternative non-plume sources and origins of NAIP magmatism are reviewed by Meyer et al. (2007). Korenaga (2004) introduced the concept of recycled subducted oceanic crust of the former Iapetus Ocean. Foulger and Anderson (2005) used this model to explain magmatism during the tectonic extension of the lithosphere near Iceland. King and Anderson (1995; 1998) proposed an edge-driven convection scenario, which suggests inception of small scale convection cells at lithospheric discontinuities, i.e. thicker cratonic adjacent to thinner normal lithosphere.

One of the best routes to understanding the fundamental processes responsible for the break-up and separation of lithospheric plates is through the intense study of adjacent and conjugate rifted continental margins. The bounding continental margins of the North Atlantic, the East Greenland margin, the Norwegian margin and the margins west of the British Isles, therefore provide the working areas to study the evolution of volcanic rifted margins and the influence and extent of magmatism.

3 DATA ACQUISITION AND PROCESSING METHODS

Proceedings of data acquisition, processing, modelling and interpretation used in this study are described in this chapter. Details for each data-set along the individual profiles and error estimates are described within the manuscripts in chapters 5 - 7.

3.1 Seismic refraction

The main geophysical method used in this study is seismic refraction. Information of subsurface layers and crustal structures are obtained by recording the travel times of acoustic waves propagating through the earth's interior. The long offset configuration of a seismic transect allows the recording of refracted waves, and wide-angle reflections of subsurface boundaries. A layer boundary, in the geophysical sense, is understood as a seismic interface with contrasting impedance. The impedance of a media is defined by the product of the acoustic velocity and density. The advantage of wide-angle seismic surveying is the direct velocity information of lithospheric layers (sediments, crust, upper mantle), obtained from the slope of an associated phase in the time (two way travel time) versus offset seismogram. Wide-angle reflections from layer boundaries provide useful structural depth constraints. A common method for modelling is two dimensional (2D) ray-tracing, which can be operated as forward modelling or inversion of refraction and reflection travel times (Zelt and Smith 1992). I refer the reader to the appropriate literature for the mathematics of ray-tracing and focus instead on the data preparation and working-flow used for this study. An outstanding description of the ray-tracing method is summarized in Grobys (Grobys in press).

Figure 3.1 shows a flow-chart, which comprises five major categories; data acquisition, data processing, phase identification, modelling and interpretation.

3.1.1 Seismic data acquisition

An extensive data-set was acquired during the expedition ARK-XIV/4 in summer 2003 with the Research Vessel *Polarstern* (Jokat et al. 2004), which is used in this study. The setup of the East Greenland margin survey was designed as a combined land-sea seismic experiment. On- and offshore deployed registration units recorded seismic waves generated from a seismic airgun array towed behind the vessel. In total 126 recording units, Reftek land stations (REF), ocean bottom hydrophones (OBH) and three component ocean bottom seismometers (OBS) were deployed along four transects (Figure 3.2). The spacing of the recording units was set to ~10 km in order to cover the margin from the fjords into the East Greenland Basin. Exact positioning of the recording units along a line is necessary for modelling. Drifts of the ocean bottom equipments due to sub-sea currents are possible and need corrections in the following processing steps. An average shot point distance of 125 m results from a shot interval of 60 s at an average cruise speed of 4.5 kts. A brief summary of each seismic transect is listed in Table 3.1. The seismic source consisted of 5 x 9 litre and a 32 litre airgun array (Jokat et al. 2004).

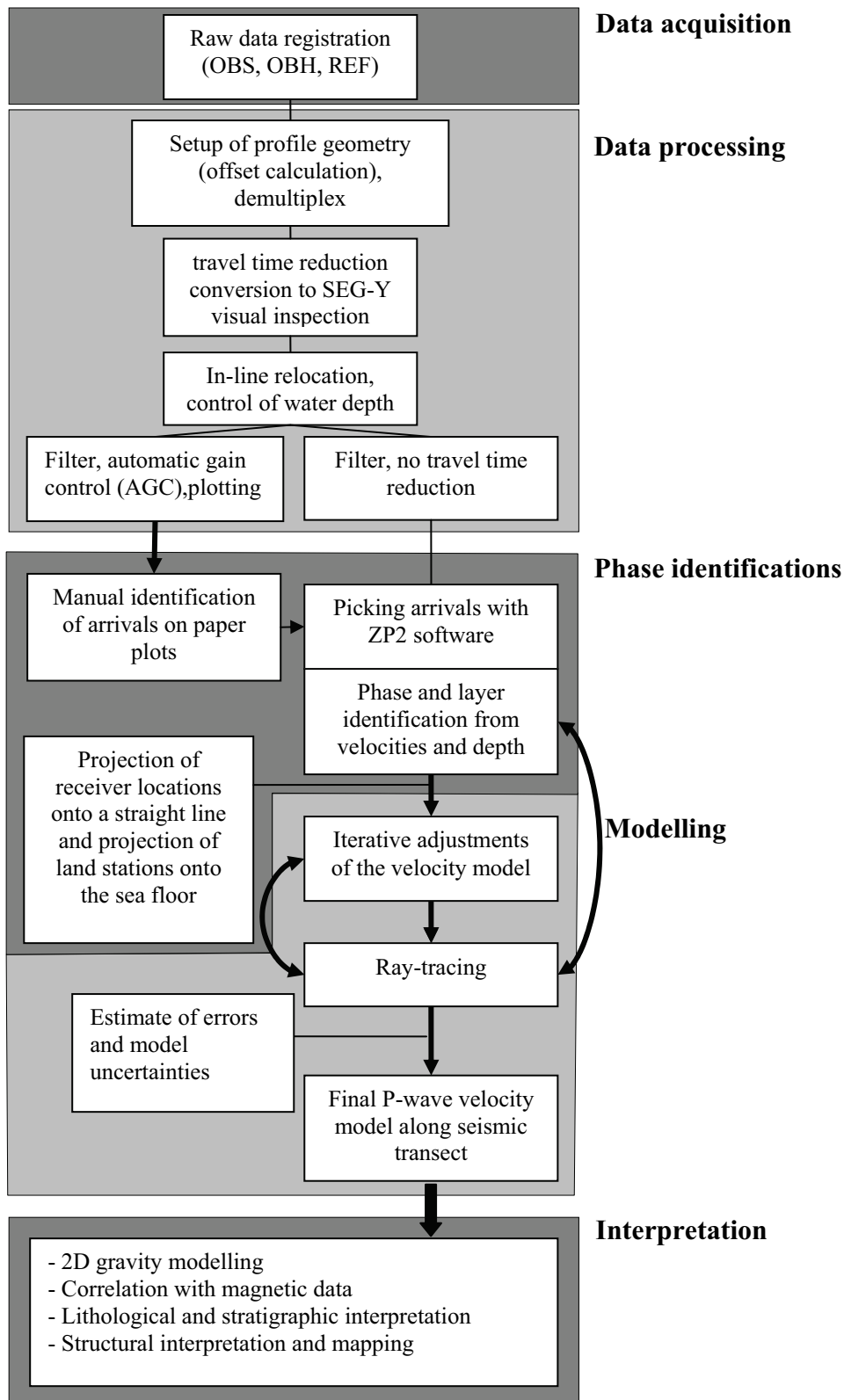


Figure 3.1: Principle flow-chart from seismic data acquisition to the interpretation of crustal structural styles.

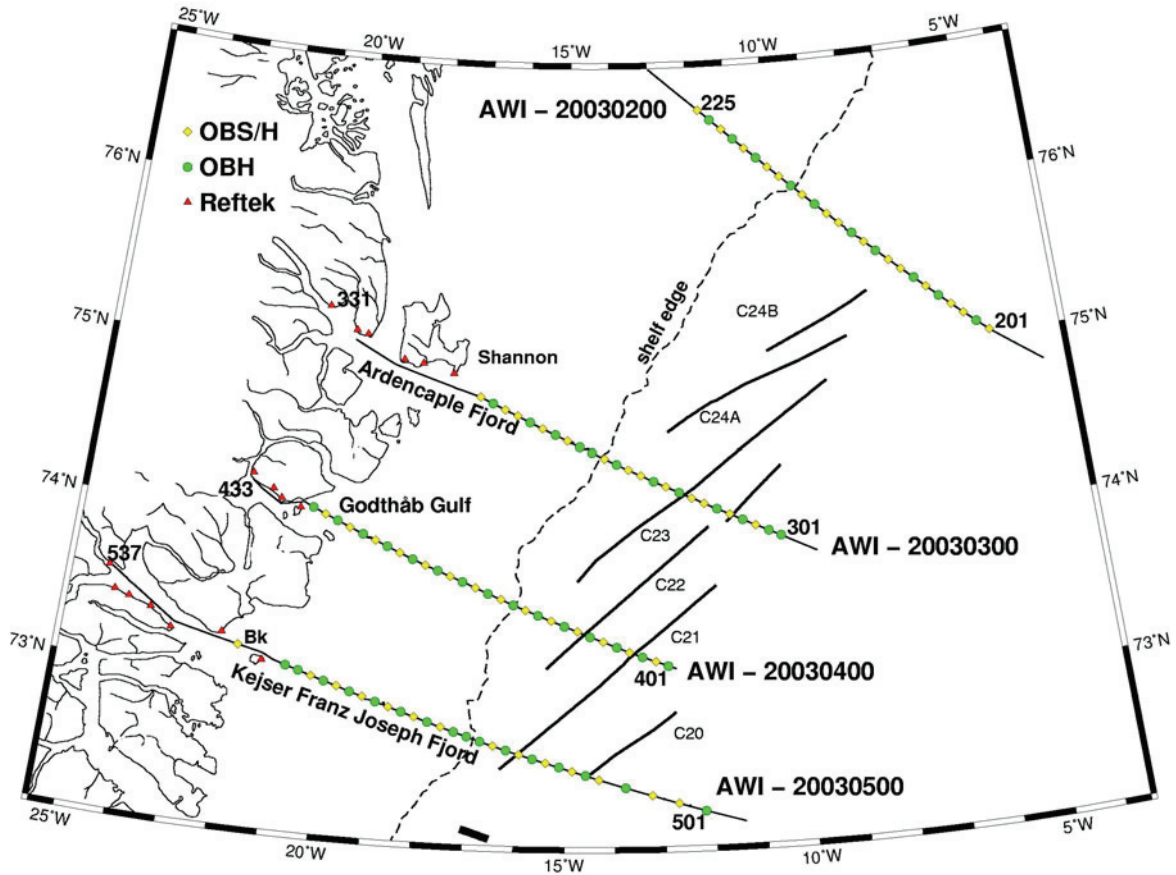


Figure 3.2: Experimental setup of seismic refraction profiles acquired during expedition ARK-XIX/4. First and last station of each profile is labelled. Yellow dots mark combined OBS/H units. Green dots mark units with only a hydrophone (OBH), and Reftek land stations are marked with red triangles. The profile line marks the ship track. Thick black lines are ocean spreading anomalies, marking the region of oceanic crust. Dashed line marks shelf edge. Abbreviations are Bk: Bontekoe Ø. OBS/H: ocean bottom seismometer/hydrophone.

Seismic profile	length	REF	OBS/H	OBH	total	used	shots
AWI-20030200	330/210* km	0	15	10	25	17	2204
AWI-20030300	365 km	6	14	11	31	27	2228
AWI-20030400	320 km	4	14	15	33	32	2057
AWI-20030500	465 km	7	14	16	37	32	3009

Table 3.1: Setup of the seismic refraction profiles (Jokat et al. 2004). Stations 218 – 225 were not used for the final modelling (see section 4.2). Therefore, the final profile length is only 210 km. Abbreviations: REF, Reftek land stations; OBS/H, ocean bottom seismometers with additional hydrophone channel; OBH, ocean bottom hydrophone.

3.1.2 Data processing

The used registration units, on- and offshore seismometers and hydrophones, recorded arrivals continuously during the entire period of surveying along a transect. Positions of each unit and shot point where determined with GPS and the water depth was obtained with the Hydrosweep system of RV *Polarstern* (Jokat et al. 2004). GPS time signals were used as reference. The first processing of the recorded data is usually performed on board after recovering the equipment. Data are stored in a time sequence and for each time stamp all available channels of a recording unit are written into its memory. In a first step, the geometry of a seismic line is setup, and the offsets between shots and receivers are calculated.

Registered water depths from the Hydrosweep are stored additionally for each receiver in the data header, which needs later be checked at the zero-offset phase. Further, the data of each receiver are sorted from a time series to a shot gather (demultiplexing). A common travel time reduction of 8 km s^{-1} is applied on the raw data in order to enhance the visibility of the deep (long travel time) mantle phases, which are expected to have this velocity and appear horizontally in the seismogram. The raw data are converted into the SEG-Y format, which is one of several tape standards developed by the Society of Exploration Geophysicists (SEG). It is the most common format used for seismic data in the exploration and production industry and was created in 1973. At this stage, the data are prepared for a first visual inspection, to check for the quality of the data at each shot, for the correct water depth from the first arrivals at zero offset, the amplitude spectra for additional filtering and variety of recorded arrivals.

An example of a shot gather $\pm 80 \text{ km}$ from the location of OBH 510 on profile AWI-20030500 is shown in Figure 3.3. Arrivals of sedimentary and crustal layers are associated refractions, and the crust-mantle boundary (Moho) is marked by a strong reflection. All arrivals are multiple reflected between sea-surface and seafloor at the receiver location. Note, that multiples arrive with a reversed phase compared to the associated first arrivals due to the inverse impedance contrast ($\rho_{air} V_{air} < \rho_{water} V_{water}$).

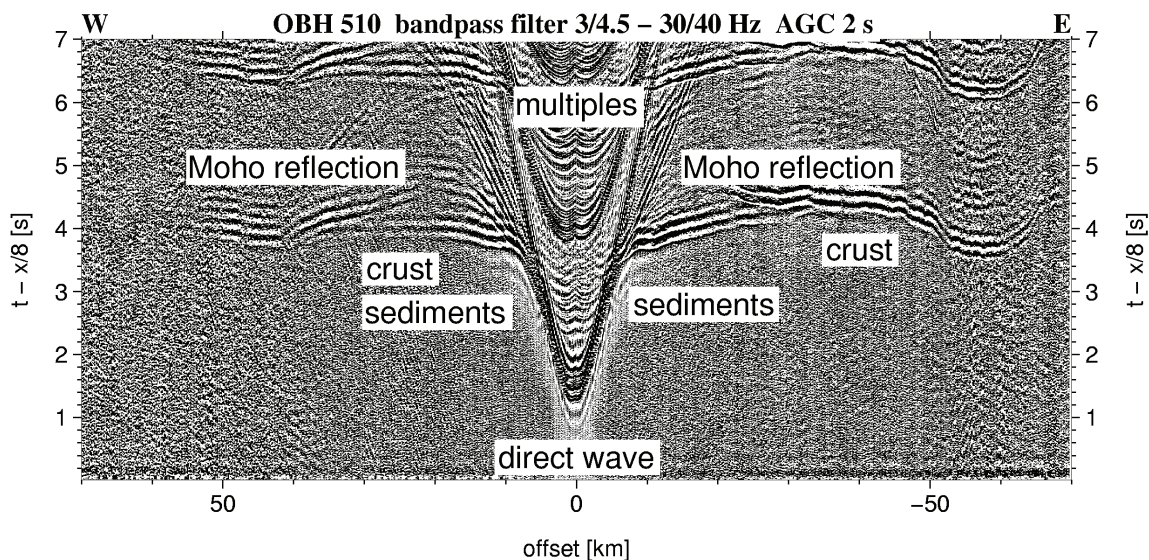


Figure 3.3: Seismic section of ocean bottom hydrophone 510 on line AWI-20030500. Origins of arrivals are labelled. Note the strong reverberations of all phases, which was unsuccessfully tried to suppress by a deconvolution filter (not shown).

The general quality of the demultiplexed data is very good. In some cases, ocean bottom seismometers and hydrophones need corrections of their in-line position (relocation) due to a drift during sinking and/or lifting in the water. The relocation was applied on the demultiplexed data by a static shift of the offset channel, thus this correction can only be applied in profile direction and not perpendicular. An example of station 407 of profile AWI-20030400 is shown in Figure 3.4 before and after a relocation of 200 m westwards. The shot closest to the receiver location is identified and the offset is shifted until the two hyperbolas in the reduced shot-gather are symmetric. This approach worked best for the deep sea stations because their direct wave and hyperbolas are clearest.

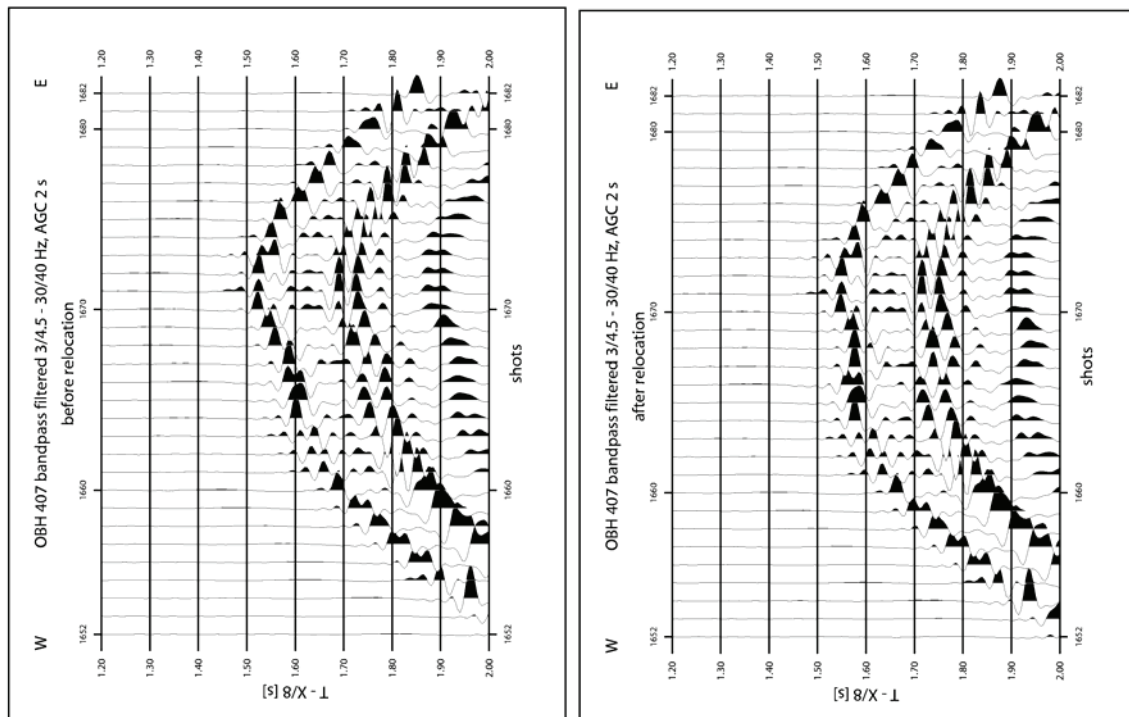


Figure 3.4: Shot gathers of OBH 407 (profile AWI-20030400) before and after relocation. A static offset shift of 200 m was applied westwards.

A band-pass filter has been applied prior to plotting in order to suppress high frequency noise. Peak-frequencies were obtained from an amplitude spectra analysis of several seismograms. The signal energy spectrum ranges between 4.5 and 30 Hz with a peak at 8 - 10 Hz. Thus a trapezoidal band-pass filter was applied with margins between 3 and 4.5 Hz, and 30 and 40 Hz. Finally, the signals were scaled for plotting with an automatic gain control (AGC) within a window of 1 s or 2 s, depending on the data quality. The travel time reduction is removed for the data used for further work, which allows determining the slope of the phases, i.e. the velocity of a layer, directly. Appropriate software is able to apply additional filtering and travel time reduction for a better display and have functions for velocity determinations.

3.1.3 Phase identifications

P-wave arrivals were picked using *ZP2* software from *B.C. Zelt* (available at <http://www.soest.hawaii.edu/~bzelt/zp/zp.html>). The data were used with a frequency range of between 3/4.5 Hz and 20/30 Hz and without any AGC and travel time reduction. Arrivals were picked from the seismic sections in intervals of 0.5 - 5 km, depending on the quality of signals. Deep crustal arrivals with weakly amplitudes did not appear clearly in the digital version but better on paper plots. Therefore picks were determined manually and later added to the digital seismogram. Here, minimum intervals of 5 km were chosen in order to mark the weakly resolved regions for ray-tracing and can later be distinguished from the better quality by its larger picking interval. The *ZP2* software determined errors for each pick in fix and discrete steps, which were set generally to 40, 55, 65, 85, 110, and 150 ms rather than determining manually error bars for entire phases or single picks. This yields varying error bars for adjacent picks even if the arrivals appear almost constantly clear on a plot. The uncertainty is calculated by the software internally, considering the variation within a window of 250 ms before and after the pick.

Velocities were determined for a band of arrivals within the picking procedure and were later associated with a model layer representing a lithological unit of the margin. For the case of increasing slopes, this method of velocity determination was used to reveal top and bottom velocities within a layer. Calculating the intercept time, which is the linear approximation and extension of a refracted phase to the zero offset, provides the opportunity to estimate the depth of the refracting layer. It has to be noted, it is slightly lower than t_0 of the reflection hyperbola. These methods assume homogenous and horizontally layered subsurfaces, which is generally highly simplified. However, it provides sufficient initial conditions for building a velocity-depth model to start with.

An extraordinary problem of the used seismic lines is that they are angled within the fjords, and shots and receivers should be in a single plane for ray-tracing. A projection of the receiver locations onto a straight line is necessary. A straight line fit through stations 201 and 225 was used for profile AWI-20030200 and revealed a maximum shift of 3.6 km for station 210. The maximum shift, for ocean bottom station 314 on profile AWI-20030300, is 4.3 km for a line through stations 301 and 325 and 14.1 km for the westernmost land station 331. A fit through stations 401 and 429 was used for profile AWI-20030400 and through stations 501 and 531 for AWI-20030500. The maximum perpendicular projections onto the lines were 5.3 km for OBH 413 and 22 km for REF 537. The true offsets of the shots and therefore of the observed P-wave arrivals, remained unchanged. The true offsets of the observed P-wave arrivals remained unchanged, which results in averaging of laterally inhomogeneous crustal structures due to the different ray paths between the real position and the projected location.

Land stations (not the last one) were projected onto the sea floor, using the depths, which was measured from Hydrosweep in the fjord. This is necessary because the ray-tracing software does not allow shots below a receiver location (Zelt and Smith 1992). A static correction was applied to account for the differences between rock and water sound velocities. The observed travel times of REF 432, 431 and 430 were corrected, assuming a vertical ray incidence, and a rock velocity of 5.2 km s^{-1} derived from the curvature of first arrivals. The same procedure was applied to REF 536, 533, 531 and 529. A slightly lower reduction velocity of 4.5 km s^{-1} was used for REF 330 - 326. The errors resulting from these approximations are estimated to be smaller than the pick uncertainties. Travel time arrivals for REFs 433 and 537 were located at the origin of the projection lines and no projection onto the seafloor was necessary.

3.1.4 P-wave velocity models through ray-tracing

A common and useful tool of crustal structure modelling for seismic refraction data is raytracing (*rayinvr*, from Zelt and Smith (1992)). Prior to ray-tracing, a two dimensional velocity model is build along a seismic transect. It consists of layers defined by seismic interfaces and velocities, which describe a lithological subsurface unit. Intercept times of arrivals associated to a layer unit provide constraints for an initial starting model. Seismic velocities (here P-wave velocities) are proposed layer-wise at the top and bottom of each defined layer. Landward boundary conditions were available for line AWI-20030300 and AWI-20030500. Previous acquired seismic transects in the Brede Fjord (94300) and Keiser Franz Joseph Fjord (94320) (Figure 1.3) were used for continental crustal constraints for the initial P-wave velocity models.

The ray-tracing technique allows modelling of wide angle reflections, diving waves, head waves and multiples at the shot points. The primary use of ray-tracing was forward modelling, although it is designed for travel time inversion. In particular, the program requires reversed receivers and shots, i.e. calculating the travel time of a ray for a given model from the station to the shot-point offset. Rays, representing the propagation of the acoustic wave through the model, are traced from each receiver to a shot point, where an associated arrival was picked. The refractions and reflections occur in a layer or at the interface denoted by the phase

number of the pick. An example is shown in Figure 3.5. Phases labelled with Pg are arrivals from sedimentary layers, Pc from crustal layers. P_w is generally the direct wave in the water column, PmP the reflection at the Moho and Pn the refractions of the upper mantle. Additional phases in Figure 3.5, PmP' and Pc2P', are significant multiples at the shot point locations.

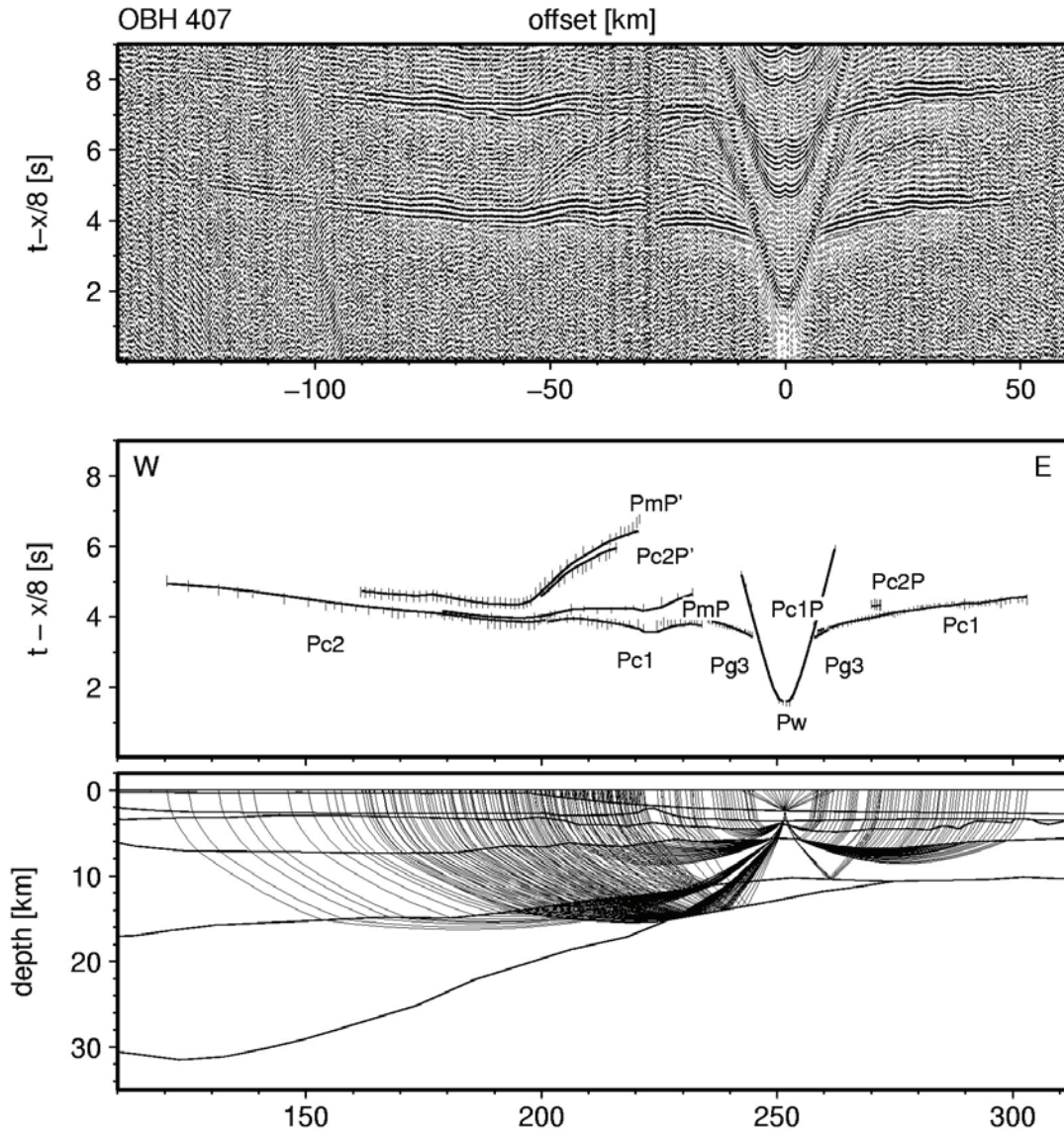


Figure 3.5: Example of ray-tracing of station OBH 407 of profile AWI-20030400. Top: Seismogram displayed in reduced travel time (8 km s^{-1}) versus offset of the receiver location. Middle: Picks and fits from forward modelling. Labels are: Pg, refractions in sedimentary layers; Pc, refractions in crustal layers; PcP, reflections on top of crustal layers; PmP, reflection at crust-mantle boundary. Numbers mark the layer of the 2D model. Quoted labels mark multiples at the shot point. Bottom: Rays traced through the model.

Forward modelling requires iterative adjustments of the velocity and layer nodes in the model, and adjustments of the picked phases and associated labels in order to achieve the best fits. This procedure was applied from top to bottom layers. Inversion was only performed in areas of small scale variations in order to gain enhanced model solutions especially for the geometry of seismic interfaces. Layer boundaries were used to fit the slope of arrivals and thus the velocity gradient within a lithological unit, where wide angle reflections did not reveal constraints of the base of the unit.

The uncertainties of the velocity models were estimated by varying single nodes until an unacceptable misfit occurred, which was used to constrain the reliability of the layer depths and velocities. The formal error analysis for the individual phases is calculated in order to determine the quality of the phase. The program (*rayinvr*) is based on a damped least squares inversion algorithm minimizing the root-mean-square (rms) travel time residual. For the inversion of travel times, the residual to the observed picks is expressed by the root-mean-square of the travel time misfit, t_{rms} . This is used to quantify the quality of the model. The length of the error bars of the picks depend solely on the noise of the data unless denoted else. The normalized χ^2 value describes the fit of the data within their assigned error. These parameters have to be considered carefully and individually, because a larger error bar causes a smaller χ^2 but a larger t_{rms} . In complex subsurface structures the misfits might be large and the statistic parameters give the impression of a weakly assessed velocity model. It is sometimes rather convenient to fit the slope of a phase and accept a misfit to the picks (larger χ^2), when a compromise is necessary between good fits for single phases or a larger number of the total traced picks.

Here, the focus during modelling was laid on achieving fits for almost all phases of all stations and picks rather than minimizing single station residuals. Thus, the best compromises revealed larger misfits within a single section, especially when the errors assigned for the picks are very small, but more picks and stations were included in determining layer parameters and modelling. However, in this work the focus was primary in the order of

- i) fitting the slope of travel time arrivals
- ii) modelling and matching most picks
- iii) simplicity of the solution without unnecessary details
- iv) test to minimize residuals by minor variations of depth and velocity nodes.

Further details concerning initial constraints for the starting models, and the quality of the final P-wave velocity models and uncertainties are discussed for each seismic transect individually within the manuscripts in section 4.

3.2 Gravity data

The structural analysis is complemented by gravity anomaly modelling in order to derive further physical properties of the model layers. The demands on the gravity modelling are that it should confirm or refine the finally obtained P-wave velocity models. Density contrasts reveal also additional constraints for the interpretation of the subsurface lithological units.

3.2.1 Gravity data acquisition

Gravity data were recorded continuously with a sampling rate of 1 Hz along the ship track for the entire cruise with an onboard fixed installed KSS31 Bodenseewerke gravimeter, which is a relative measuring instrument. The measure unit of gravity data is mGal (10^{-5} m s^{-2}). Before and after the cruise, onshore calibration values are obtained from fixed reference locations. Measurements at fixed points in Tromsø and Bremerhaven, and at the pier next to the ship, allowed the link of the onboard measurements. Doing so, the first correction of the data is applied by evaluating the drift of the gravimeter, which is basically the difference of the two absolute values minus the difference of the two ship values. For this cruise, the total drift was -3.64 mGal. Several other corrections have to be applied before using gravity data for modelling.

3.2.2 Latitude correction

Gravity varies with the latitude on the non-spherical Earth's surface due to the different angular velocity, the centripetal force and the different distance to the centre of the mass. A general formula for correction of this effect depending on the latitude is the International Gravity Formula (IGF)

$$g_{\Phi} = 978049 \cdot (1 + 0.0052884 \cdot \sin^2 \Phi - 0.0000059 \sin^2 2\Phi) \text{ in mGal}$$

and is subtracted from the measurements.

3.2.3 Eötvös correction

Measurements from a moving platform such as ships, requires an added correction for the acceleration due to the earth centripetal force, and the relative movement of the platform to it. Parameters of the cruise speed v_S in knots, the heading H and latitude Φ determine the Eötvös effect

$$g_E = 7.503v_S \cos\Phi \sin H + 0.004v^2 \text{ in mGal.}$$

It is obvious, that navigation data must be highly accurate, otherwise the Eötvös-correction yields large correction errors. The used data revealed a correction value of ± 10 mgal depending on the heading and was applied to the data.

3.2.4 Free-air (FA) and Bouguer (BA) correction

The free-air correction compensates for topographic elevations and projects them onto the datum (mean sea level) without removing them. Free-air corrected data are generally used in marine settings, where the gravimeter is near the datum level (with respect to the draft of the ship) and topographic heights are all below. Instead, a Bouguer correction is convenient in land and shallow marine areas, and corrects for the local effects associated with the local water depths (the water column with a density of $1.03 \times 10^3 \text{ kg m}^{-3}$ is replaced by a density of $2.67 \times 10^3 \text{ kg m}^{-3}$) (Kearey and Brooks 1999). Bouguer anomalies were used in this study in order to compare the results with the landward models and accepted the large anomaly in the deep water areas (Figure 3.6). The focus was, however, on the continent – ocean transition zone beneath the shelf region, which is a shallow marine environment (Figure 3.6). Details of the oceanic section might have been suppressed, but are not expected to reveal major difficulties in the modelling.

The used data were re-sampled to 10 s, which yields a data point distance of about 25 m with a cruise speed of 5 knots during seismic surveying. The remaining high frequency noise on the data is a result of ice-breaking and shipping manoeuvres and is filtered with a 100 s low-pass filter before modelling.

3.2.5 2D gravity modelling

The process of 2D gravity modelling starts with the conversion of the seismic velocity model to density. A variety of velocity-density relationships for sedimentary, igneous, magmatic and metamorphic rocks were proposed by many authors (e.g. Nafe and Drake 1957; Ludwig et al. 1970; Christensen and Mooney 1995). Funck et al. (2004) proposed a formula after Ludwig et al. (1970) which approximates the Nafe-Drake curve (Figure 3.7) by

$$\rho = -0.00283 v^4 + 0.0704 v^3 - 0.598 v^2 + 2.23 v - 0.7 \quad (\text{Eq. 3.1})$$

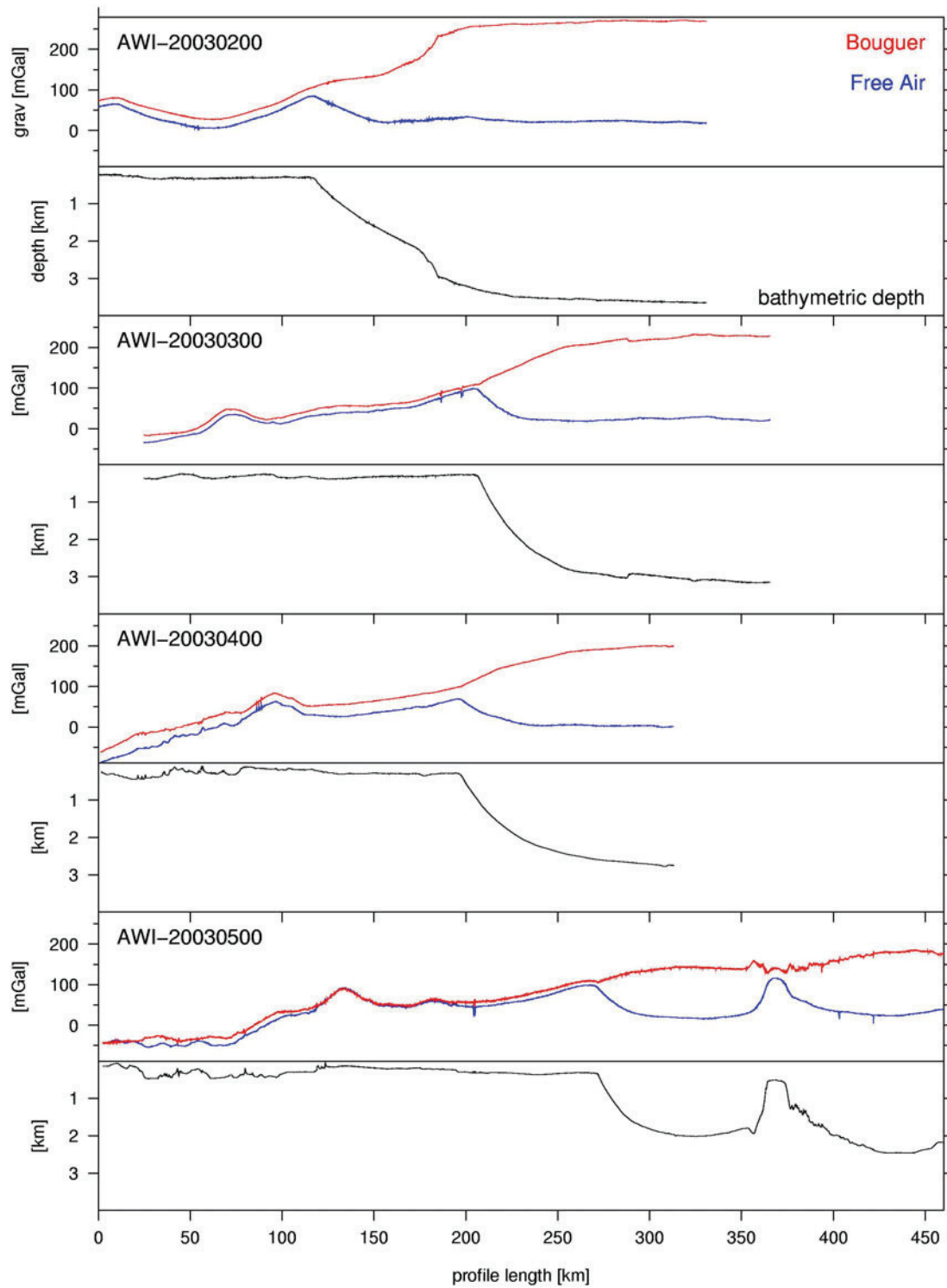


Figure 3.6: Free-air, Bouguer gravity anomalies and associated ocean bed topography of profile AWI-20030200, AWI-20030300, AWI-20030400 and AWI-20030500.

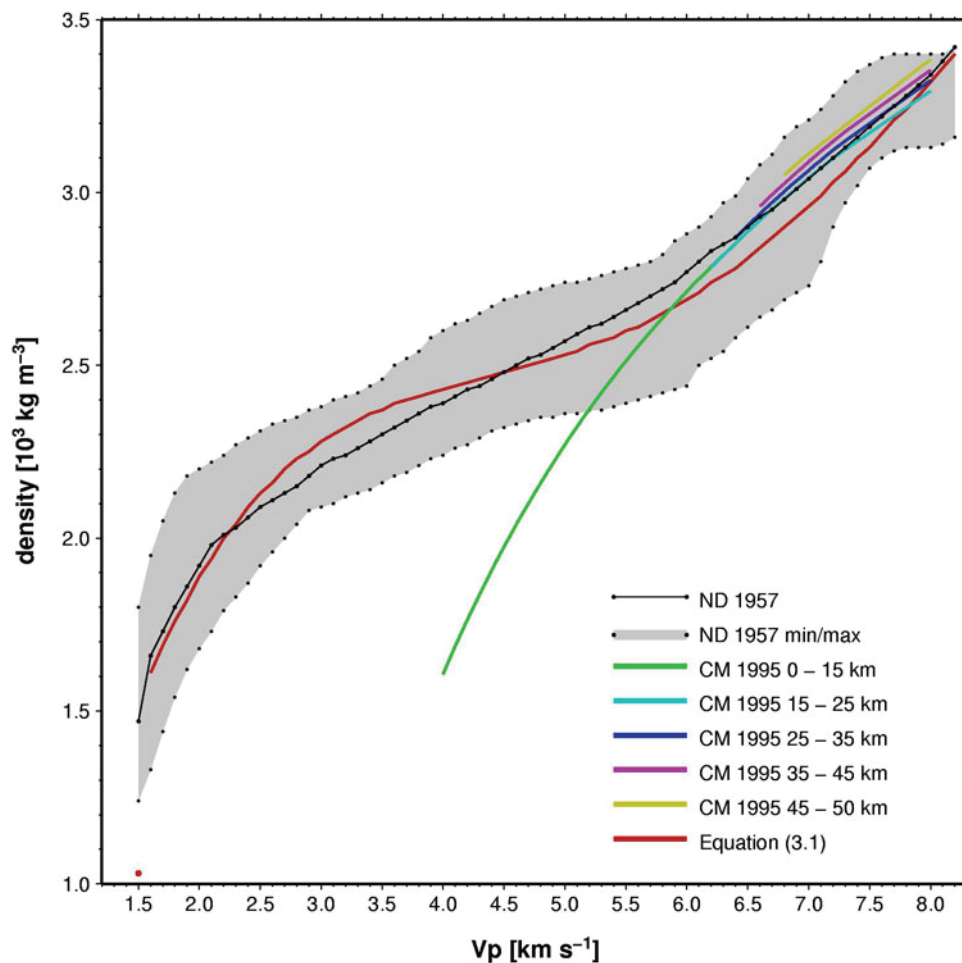


Figure 3.7: Density versus P-wave velocity (ρ/V_p) diagram. Shown are the different ranges after ND: Nafe and Drake (1957) centre values and minimum and maximum, CM: Christensen and Mooney (1995) for different depth ranges and the curve after the equation 3.1.

with the density ρ in 10^3 kg m^{-3} and the P-wave velocity v in km s^{-1} . Christensen and Mooney (1995) defined densities from seismic velocities of crustal and igneous rocks with respect to their depths. The variations are small for higher velocities but densities are rather low for shallow and lower velocities, e.g. for basalts (Figure 3.7).

The P-wave velocity models are gridded into $1 \times 0.1 \text{ km}$ blocks, transferred to densities using Equation 3.1. The obtained density grid is contoured in 0.2 mGal intervals (Figure 3.8). Modelling is performed using *LCT* (commercial software by Fugro Ltd.). The 2D gravity modelling procedure requires polygons of constant densities describing the crustal structure models. The initial density model was constructed of polygons along layer boundaries of the final velocity models and carefully chosen contour lines and assigned with an averaged constant density value. The initial density model was modified mainly in adjustments of the densities and only on freely chosen polygons without changing layers originated from the velocity model. Splitting a layer into further polygons represents a higher complexity than derived from the velocity modelling and is associated with lateral lithological inhomogeneities (Figure 3.8). Minor corrections were generally necessary for the sedimentary and crustal layers. Major modifications were necessary for the sub-oceanic mantle due to large misfits which could only related to mantle densities. Even variations of the background density defining the surrounding of the 2D structural model (*LCT* User Manual) could not account for

the large density differences between the continental and oceanic crustal parts. Thus, the background density was set for all models obtained for this study to $3.03 \times 10^3 \text{ kg m}^{-3}$. Density adjustments of the crustal structure polygons were applied until the approximation of the calculated to the observed Bouguer gravity anomalies deviated only within an acceptable misfit (Figure 3.8).

A reverse test of the final gravity model is to assign each velocity node of the P-wave velocity model with the value of the related modified density polygon and displaying it in a ρ/V_P – diagram. It can be shown (Figure 3.9) that the derived densities are still consistent with the seismic velocities within the range of the P-wave velocity – density relation after Nafe and Drake (1957) and Christensen and Mooney (Christensen and Mooney 1995).

3.3 Magnetic data

Magnetic data were used in this study in order to find correlations between structural variations and magnetic anomalies. Data were available along the two seismic lines AWI-20030400 and AWI-20030500.

3.3.1 Magnetic data acquisition

A helicopter-borne magnetic survey operated from board of *RV Polarstern* was designed to reveal more details of the area of investigation especially about the large negative magnetic anomaly extending along the margin (Figure 3.10). The area of the two southern seismic transects AWI-20030400 and AWI-20030500 (Figure 3.10) was planned to be covered with the high resolution and low altitude magnetic survey but gaps resulted due to the fast changing weather conditions (Jokat et al. 2004). The airborne survey operated in a flying altitude of 100 m and an average cruise speed of 40 m s^{-1} . The sensor, a Cs-vapour magnetometer, was towed 30 m beneath the helicopter and the total magnetic intensity was recorded with 10 Hz. The survey pattern was planned with a line spacing of 5 km and tie lines where flown whenever it was possible.

The magnetic data processing consisted of survey line and data editing, IGRF and diurnal variation corrections and levelling. A compensation of sensor moves was not necessary due to the erase of any helicopter turns at line ends.

3.3.2 Magnetic line data editing

Raw survey data were re-sampled to 1 Hz before inspection and further processing. Small spikes in the navigation and magnetic data were immediately interpolated. Larger spikes exceeding several tens of seconds, e.g. due to radio transmission were carefully check before interpolation. The data were removed when interpolation was not acceptable. Helicopter turns at the end of lines were consequently removed because large data disturbances occurred in most cases. If a change of lines yields a tie line across two or more survey lines, the partial line with undisturbed data was kept for final levelling.

3.3.3 IGRF correction

Magnetic anomalies were obtained by removing the International Geomagnetic Reference Field (IGRF) from the measured data. The IGRF for the epoch 2000-2005 (IAGA 2000) was used to determine the correction value for each date and location of a magnetic data point. An appropriate IGRF correction is necessary, since the earth magnetic field changes not only in space but also in the time continuum.

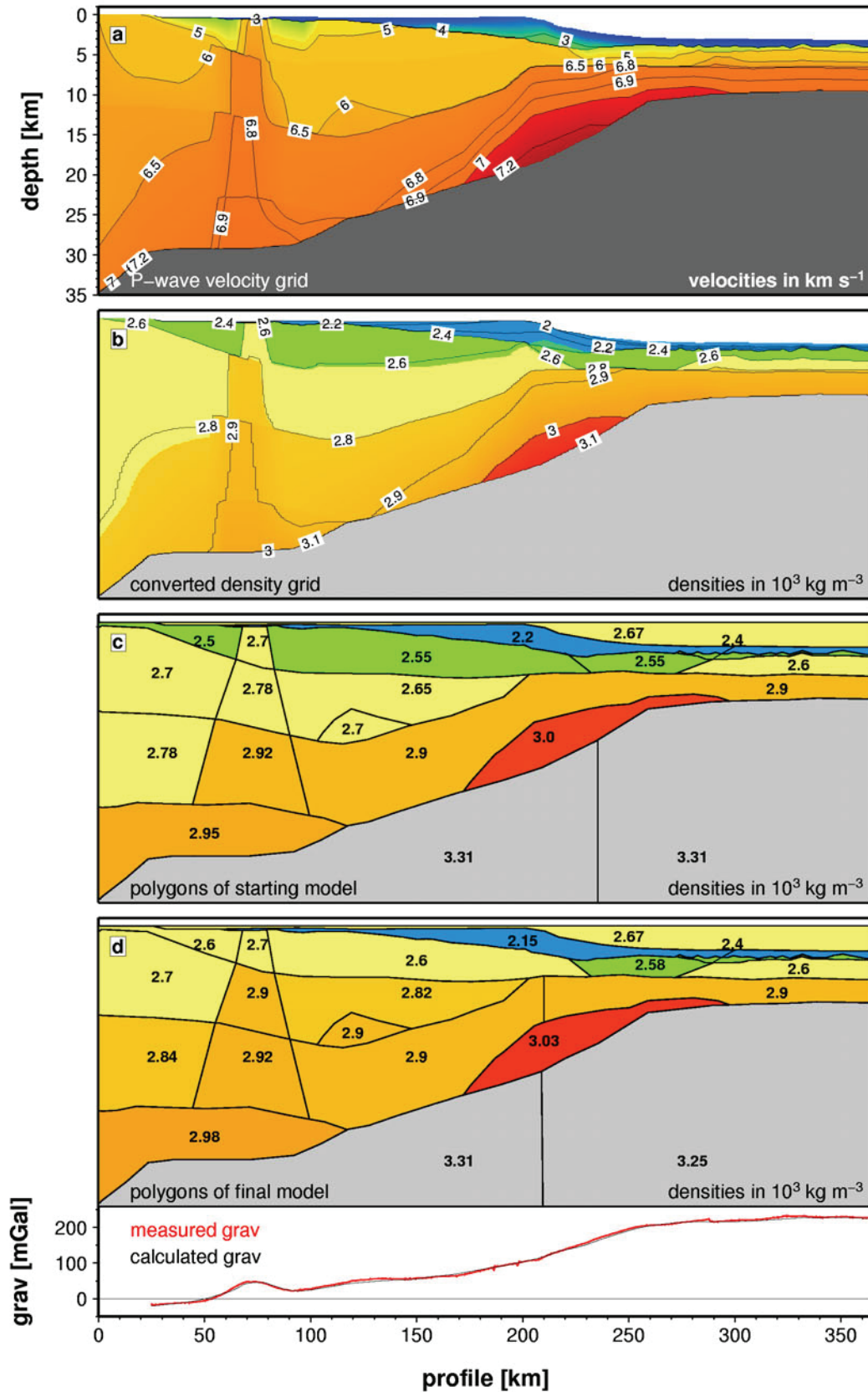


Figure 3.8: Scheme of gravity model construction for profile AWI-20030300. a) P-wave velocity grid in 1 x 0.1 km cell size. Selected contour lines are shown as reference. b) Converted density grid using equation (3.1) and contour lines of every 0.1 10^3 kg m^{-3} . c) Definition of starting polygons and initial average densities. d) Final polygons and modelled densities which fit the measured gravity anomalies. Note that a background density of $3.03 \text{ } 10^3 \text{ kg m}^{-3}$ was used. The vertical exaggeration of the models is 4.

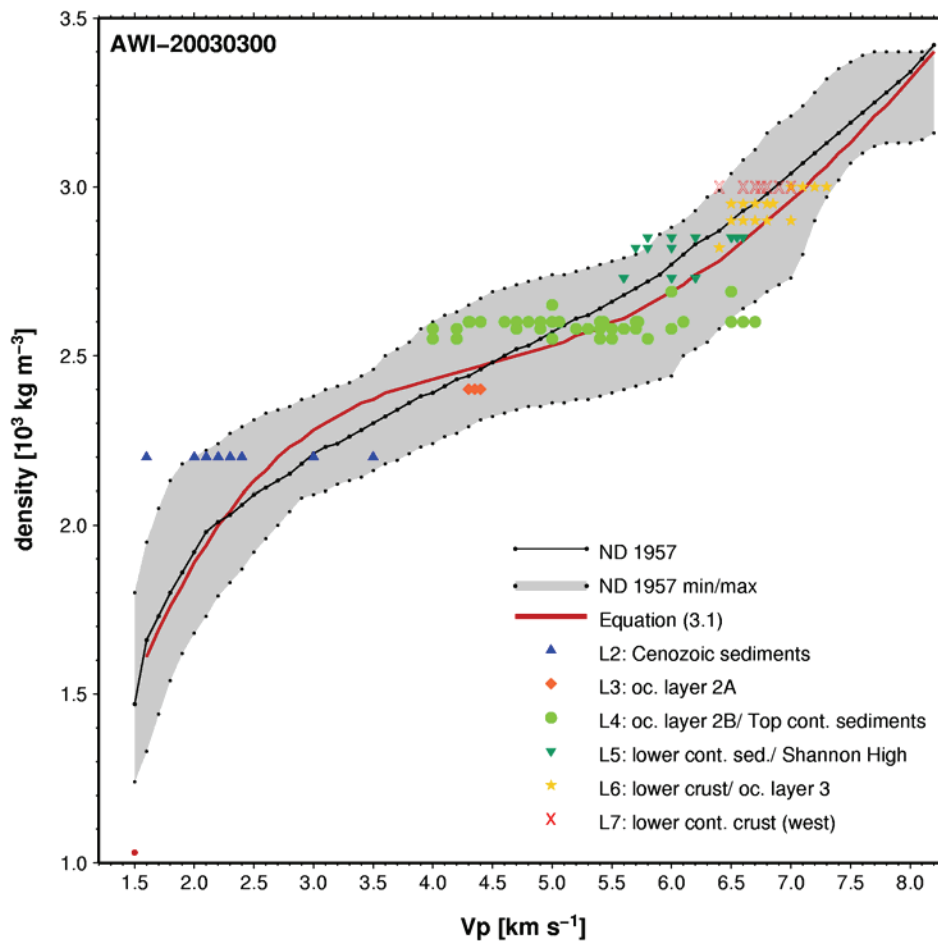


Figure 3.9: ρ/V_p – diagram for profile AWI-20030300. Each modelled velocity node of the seismic model was assigned with the density of the corresponding density polygon. A range of velocities reveal therefore a constant density. Colours of dots refer to the layer number of the model.

3.3.4 Diurnal correction

The transient variations of the Earth's external magnetic field have a large impact especially in polar regions. The magnetic field induced from the ionospheric current systems of an auroral electrojet (e.g. Kertz 1992) greatly influence ground magnetic recordings. The observatory in Danmarkshavn, operated from the *Danish Meteorological Institute* (data available at <http://web.dmi.dk/fsweb/projects/chain/#list>) provided relative measurements of the horizontal and vertical magnetic component. A comparison of all recorded data during the period of the revealed a static shift of the quite level of -150 nT of the vertical component. Thus, a constant shift of +150 nT was applied on the raw base station data. The horizontal components were neglected due to their minor influence. This ground station was the closest one to the survey area with continuously recorded data but with still a distance of 300 – 550 km. Lowpass filtering at 1800 s of the diurnal data allows the correction for the general trend of the external influence. Shorter wave-length variations were expected as local effect and are therefore suppressed. The diurnal correction was applied on the IGRF corrected data without any other modifications. Upward continuation of the diurnal data was not applied due to the low surveying altitude of 100 m only.

3.3.5 Levelling

All magnetic data were loaded into a database and line adjustments were performed using the *LCT* software (Fugro Ltd.). The aim was to minimize the misfits at line intersections. The

mean cross line misfit could be reduced to less than 10 nT and an absolute maximum misfit of 130 nT. The final product is a magnetic anomaly map (Figure 3.10) which supplements the interpretation of the two southern seismic profiles and reveals higher details than obtained from a regional magnetic grid (Verhoef et al. 1996; Schlindwein and Meyer 1999). Correlations with the seismic velocity models were made by obtaining magnetic data from the grid along the seismic transect, since the helicopter lines were not flown parallel to the profile directions. The high frequency variations of magnetic anomalies appear clear in Figure 3.10 where the magnetic data are traced along the flight lines.

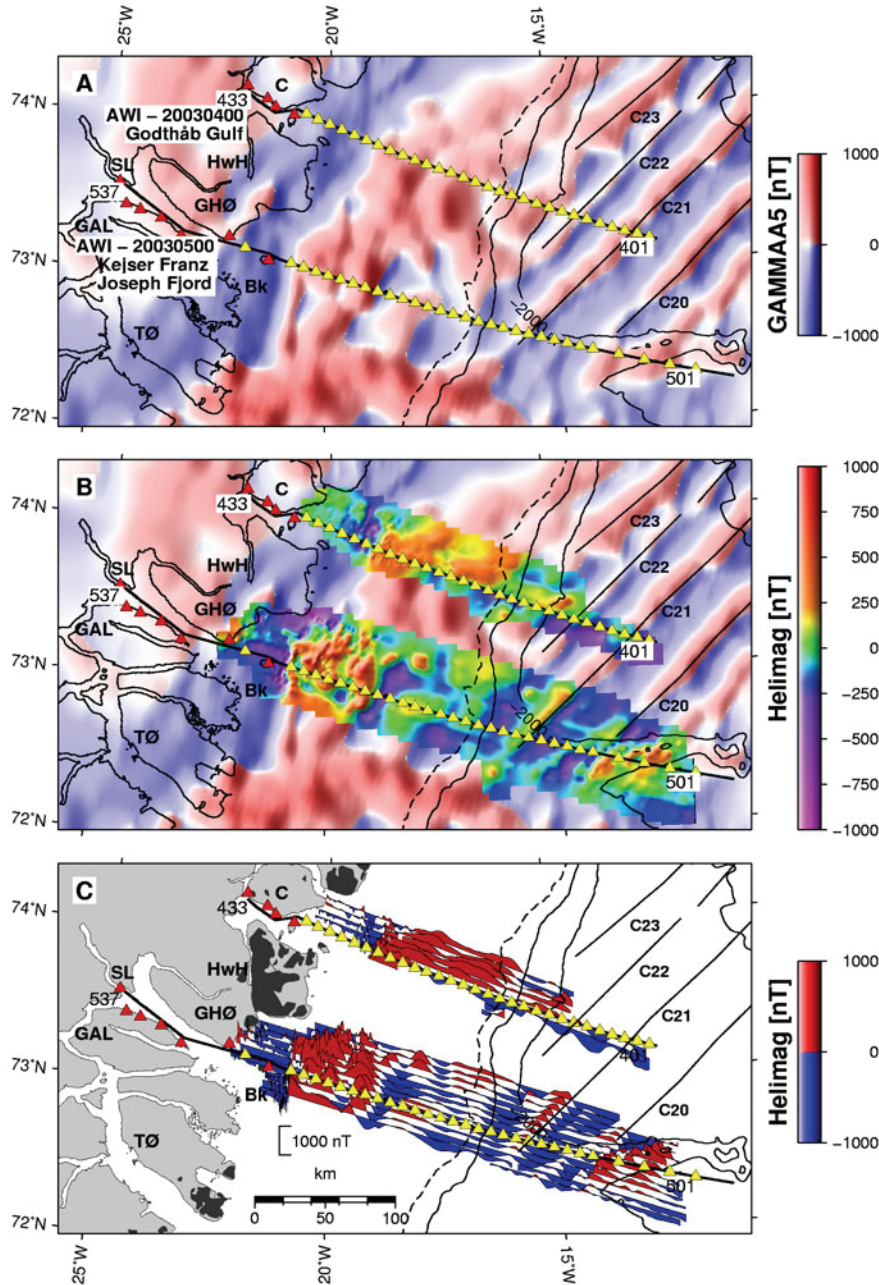


Figure 3.10: Magnetic data of the East Greenland margin. A) Regional magnetic grid after Verhoef et al. (1995). Seismic profiles AWI-20030400 and AWI-20030500 are shown as reference. B) High resolution aeromagnetic grid. C) Magnetic anomalies traced along the flight lines. Abbreviations are as in Figure 1.1.

4 CONTRIBUTION TO SCIENTIFIC JOURNAL PUBLICATIONS

This chapter summarizes my contributions and the main topics of the scientific articles presented in chapters 5 – 7 in their original form.

4.1 Continent-ocean transition and voluminous magmatic underplating derived from P-wave velocity modelling of the East Greenland continental margin

Max Voss and Wilfried Jokat
Geophysical Journal International (2007) **170**, 580-604
Doi: 10.1111/j.1365-246X.2007.03438.x

This paper presents results from wide-angle seismic modelling of two refraction seismic lines from the Greenland continental margin. The data are new and provide important insights into the deep structure of the margin. Additionally, new magnetic data are presented which show high resolution details of shallow dyke intrusions and constrain the positions of oceanic spreading anomalies. The comparison to a conjugate profile, located on the Vøring Plateau, shows major differences in the extent of the continent – ocean transition zone, the thickness of the continental crust and the position of the earliest oceanic spreading anomaly.

Max Voss has done all the seismic, magnetic and gravity data processing, modelling and interpretation. Wilfried Jokat supervised the research.

4.2 Variations in magmatic processes along the East Greenland volcanic margin

Max Voss, Mechita C. Schmidt-Aursch and Wilfried Jokat
Geophysical Journal International

Submitted on June, 30th 2007
Reviewed on September 6th 2007
Revision submitted on December 16th 2007

The paper presents new results of seismic velocity and gravity modelling along two profiles (AWI-20030200 and AWI-20030300) across the NE Greenland margin. The manuscript first describes the data and methods used for the modelling. A lithological interpretation is provided for each transect and compared with the conjugate Lofoten-Versterålen Margin. Furthermore, half spreading rates and estimates for the timing of break-up are determined. In the second part, the new crustal sections are combined with published results in order to generate regional maps of the basement and Moho depth, and the thickness of high velocity lower crust along and across the southeast to northeast Greenland margin. Important variations in crustal thickness and the geometry of high velocity lower crust are identified and discussed in relation to other North Atlantic margins. Different scenarios for the formation of the northeast Greenland margin are outlined.

Mechita Schmidt-Aursch visually inspected the data of both profiles and established starting models for their oceanic parts. Max Voss continued the raytracing modelling for the continental part of AWI-20030300 and also finalized the oceanic model of AWI-20030200, and did the gravity modelling, compilation and mapping, and all interpretation. Wilfried Jokat supervised the research.

4.3 From Devonian extensional collapse to Early Eocene continental breakup: an extended transect of the Kejsers Franz Joseph Fjord of the East Greenland margin

Max Voss and Wilfried Jokat
Geophysical Journal International

Submitted on June, 30th 2007
Reviewed on September 6th 2007
Revision submitted on December 16th 2007

A conceptual crustal cross-section from the Precambrian shield to the Greenland Sea through the Kejsers Franz Joseph Fjord is presented which was composed on the basis of existing and recently published studies using 2D seismic and 3D gravity data. The transect is more than 1000 km long and crosses the Precambrian shield, the Caledonian orogen, Post-Caledonian basins in the region of the Kejsers Franz Joseph Fjord, and the continent-ocean transition. The combination of the three segments forming the total transect allows a discussion of the long-term history of the margin from its Devonian extensional collapse to Early Eocene continental break-up. One important advantage of this approach is that major features, like deep crustal shear zones, are discussed in the wider context of geodynamic events that affected the evolution of the margin. The style and chronology of rifting, and rift-related magma production, are discussed. The rates and volumes of melt production between this transect and the classic Iceland plume-affected segments of the SE Greenland margin are compared. Max Voss did the compilation, review, and interpretation. Wilfried Jokat supervised the research.

5 Continent – ocean transition and voluminous magmatic underplating derived from P-wave velocity modelling of the East Greenland continental margin

Max Voss and Wilfried Jokat

*Alfred Wegener Institute for Polar and Marine Research, Columbusstrasse, 27568 Bremerhaven, Germany
E-mails: Max.Voss@awi.de (MV); Wilfried.Jokat@awi.de (WJ)*

5.1 Summary

Deep seismic refraction data were gathered across the entire East Greenland rifted margin north of the Jan Mayen Fracture Zone between 72°N and 75°N in 2003. Investigations of the deep crustal structure of this continental margin provide constraints on the formation of the margin and its structural evolution during and after Late Cretaceous - Early Tertiary rifting and continental break-up. We present here the results along two profiles located in the prolongation of the Godthåb Gulf and the Kejsers Franz Joseph Fjord. Regional P-wave velocity models were derived from forward travel-time modelling of land stations and ocean bottom hydrophone (OBH) recordings. For the first time, long deep seismic sounding transects off East Greenland provide a full insight into the crustal architecture of the transition from continental to oceanic crust. A mean result is the identification of voluminous magmatic underplating, which is wider and thicker than previously thought. P-wave velocities of the underplated material range between 7.1 and 7.4 km s⁻¹ and the horizontal extents on the profiles are 225 km and 190 km. The maximum thickness of the underplated material is 15 - 16 km. Furthermore, the P-wave velocity models reveal a 120 – 130 km wide continent – ocean transition zone (COT), based on an interpretation of the extent of Cretaceous syn-rift sediments mixed with basaltic intrusions and the lateral increase of velocities in the crustal layers. Excess magmatism must have been present during a long-term rifting process, accompanying the extension of the continental crust and giving rise to the voluminous magmatic underplating. A consequence of our interpretation of the seismic refraction data is a likely rift propagation in the Greenland Sea from north to south. Additionally a comparison of P-wave velocity models of the East Greenland Margin and Vøring Margin reveals significantly asymmetric crustal architectures. The voluminous magmatic underplating and asymmetrical conjugate margins formations are considered as a mirror of complex pre- and syn-rift processes.

Key words: crustal structure, East Greenland, ray tracing, rifted margin, underplating.

5.2 Introduction

The East Greenland continental margin is bounded landwards between the Jan Mayen and Greenland fracture zones by the Caledonian fold belt, formed in Silurian times (Escher and Pulvertaft 1995; Henriksen et al. 2000) and Devonian sedimentary basins developed during the ensuing extensional collapse (Figure 5.1). Subsequently, sedimentary basin formation took place during a long-term Mesozoic rifting process that terminated in Tertiary magmatism generally related to the Iceland hotspot and the break-up of the North Atlantic. Onshore outcrops of igneous rocks prove this on Hold with Hope, Wollaston Foreland and Shannon Island. Here, the lavas reach 800 m in thickness (Upton et al. 1980; Upton 1988). South of the Jan Mayen Fracture Zone, much larger amounts of flood basalts are found onshore on the Geikie Plateau, and there is evidence for the erosion and removal of a thick pile of basaltic lavas on Jameson Land (Larsen and Marcussen 1992; Saunders et al. 1997). Modelling of wide angle seismic data, from Shannon Island to the Scoresby Sund area, have also given evidence for varying intensities of Tertiary magmatic activity offshore from north to south. Crustal structure models

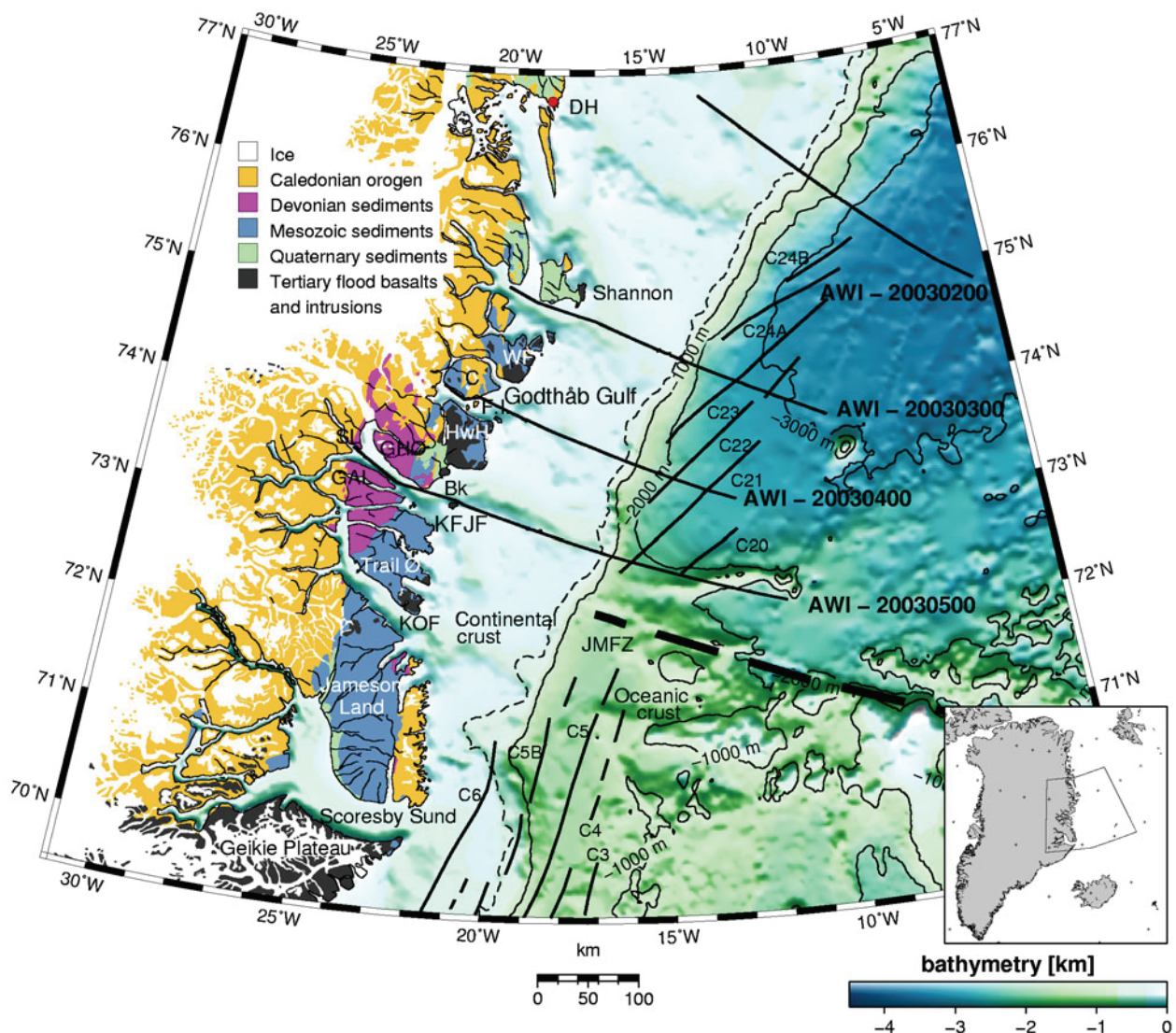


Figure 5.1. Simplified geological map of East Greenland Fjord Region after *Escher and Pulvertaft* (Escher and Pulvertaft 1995) (copyright Geological Survey of Denmark and Greenland) and *Henriksen et al.* (2000). IBCAO Bathymetry after *Jakobsson et al.* (2000). Bk: Bontekoe Ø. C: Clavering Ø. DH: Danmarkshavn (magnetic base station). F.I.: Finsch Island. GAL: Gunnar Anderson Land. GHØ: Gauss Halvø. HwH: Hold with Hope. JMFZ: Jan Mayen Fracture Zone. KFJF: Kejser Franz Joseph Fjord. KOF: Kong Oscar Fjord. SL: Strindberg Land. WF: Wolaston Foreland. All seismic profiles acquired in 2003 shown as thick solid black lines. Thin solid black lines mark ocean spreading anomalies. Thick dashed line represents the location of JMFZ as reference. Thin dashed line marks the smoothed shelf edge (330 m). Scale is valid for 73°N.

along the margin reveal variations in the Moho topography (Weigel et al. 1995; Fechner and Jokat 1996; Mandler and Jokat 1998; Schlindwein and Jokat 1999). Seaward dipping reflector sequences (SDRs) (Hinz et al. 1987) and high velocity bodies in the lower crust, with P-wave velocities of more than 7.0 km s^{-1} (Mutter and Zehnder 1988; White and McKenzie 1989; Schlindwein and Jokat 1999) are reported north of the Jan Mayen Fracture Zone. However, south of Kong Oscar Fjord, deep seismic data provide no evidence of such a high velocity lower crust (Schlindwein and Jokat 1999; Schmidt-Aursch and Jokat 2005a). The total melt production north of the Jan Mayen Fracture Zone remained unresolved from these studies, because sea ice cover prevented the transects from crossing the entire shelf and continental margin into the normal oceanic realm. Thus, the seaward and northward extent of magmatic underplating seen partly on seismic profiles of Kong Oscar Fjord and Kejser Franz Joseph Fjord are the subject of debate (Schlindwein and Jokat 1999; Schmidt-Aursch and Jokat 2005a). Seismic data from

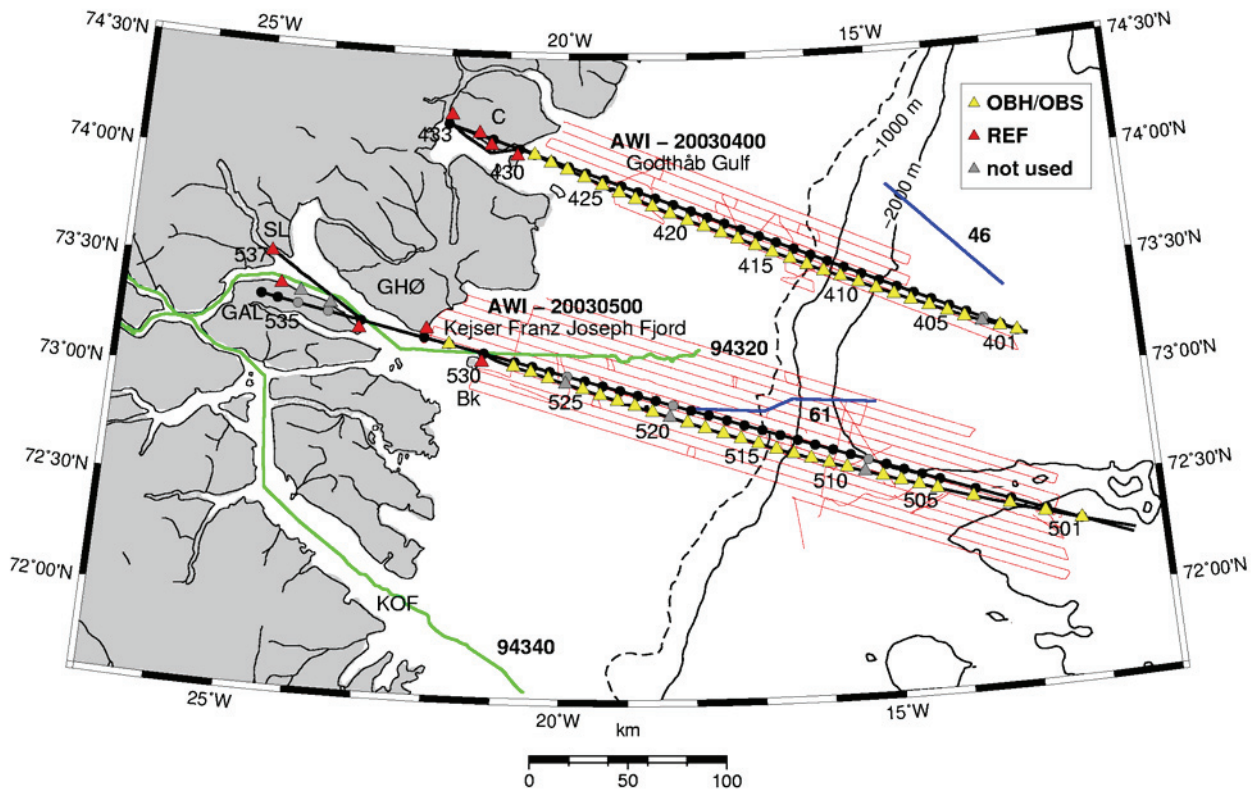


Figure 5.2: Location of the Godthåb Gulf and Keiser Franz Joseph Fjord seismic refraction profiles. Red lines show flight lines of the airborne magnetic survey. Yellow triangles show locations of the OBS/OBH, red triangles represent locations of REF land stations. Black dots show the locations of the receivers projected onto the straight line, as described in the text. Gray triangles and dots mark unused receiver stations. First, last and every fifth location are labelled. Green lines represent seismic refraction profiles after *Schindwein & Jokat* (1999); blue lines mark multi channel seismic profiles after *Hinz et al.* (1987). For additional labels see Fig. 1. Scale is valid for 73°N.

the conjugate Vøring Margin off Norway (Mjelde et al. 1997; Mjelde et al. 2001; Raum et al. 2002; Mjelde et al. 2005), on the other hand, revealed extensive magmatic underplating and thickened oceanic crust, which would support models of larger than known underplating for the East Greenland Margin. The location of the continent ocean boundary (COB) in this part of the East Greenland margin is the subject of further controversy. Until now, the deeper crustal structure of the continental margin off East Greenland was unknown, with suggestions based instead on short seismic transects and/or potential field data. No seismic profiles, imaging the deeper crustal structure, were available, which would provide constraints for an unambiguous continent – ocean transition. *Hinz et al.* (1987) showed seaward dipping reflector sequences on multi-channel seismic profiles, and argued for a coincidence of the COB and SDRs in consideration of the eruption of massive volcanic sequences over highly extended continental crust during the latest phases of rifting prior to seafloor spreading (*Hinz* 1981). *Escher & Pulvertaft* (1995) established the COB based on the coincidence of a gravity high with the bathymetric shelf margin, and using magnetic data. *Scott* (2000) suggested that anomaly C23 can be traced into the previously interpreted continental crust and placed the COB further west, about 10 km off the East Greenland coastline. He interpreted the ambiguous magnetic pattern between the old COB and the coast line as oceanic spreading anomalies. *Tsikalas et al.* (2002) based their location of the COB on reconstruction models and reinterpretation of the magnetic lineations. Those authors proposed C22 to be the oldest confidently identifiable magnetic anomaly and placed the COB 50 – 80 km east of that of *Scott* (2000).

To investigate the deeper crustal structure and the transition from continental to oceanic crust between the Jan Mayen and Greenland fracture zones (Jokat et al. 2004) new seismic refraction data across the East Greenland Margin were acquired by the Alfred Wegener Institute for Polar and Marine Research (AWI) using R/V *Polarstern* in 2003. This paper presents forward modelling of P-wave arrivals recorded by onshore receivers and ocean bottom seismometers on the two southernmost profiles, which are conjugate to the Vøring Plateau. The southern transect, AWI-20030500, extended an earlier profile (94320) along the Kejsler Franz Joseph Fjord (Schlindwein and Jokat 1999) (Figure 5.1 and 5.2). Profile AWI-20030400 was located further north, off the Godthåb Gulf, in order to gain insight into north-south trends in the crustal structure.

In this study we use the definition of a continent – ocean transition zone (COT) provided by *Whitmarsh and Miles* (1995): the COT is that part of the lithosphere, which includes the crust between the thinned continental crust characterized by tilted fault blocks, and the first oceanic crust formed by seafloor spreading. Because of this, the interpretation of magnetic anomalies as spreading products, or not, has strong implications for the location of the COT. We discuss the interpretation of P-wave velocity models in combination with magnetic data and present evidence for wide and voluminous magmatic underplating.

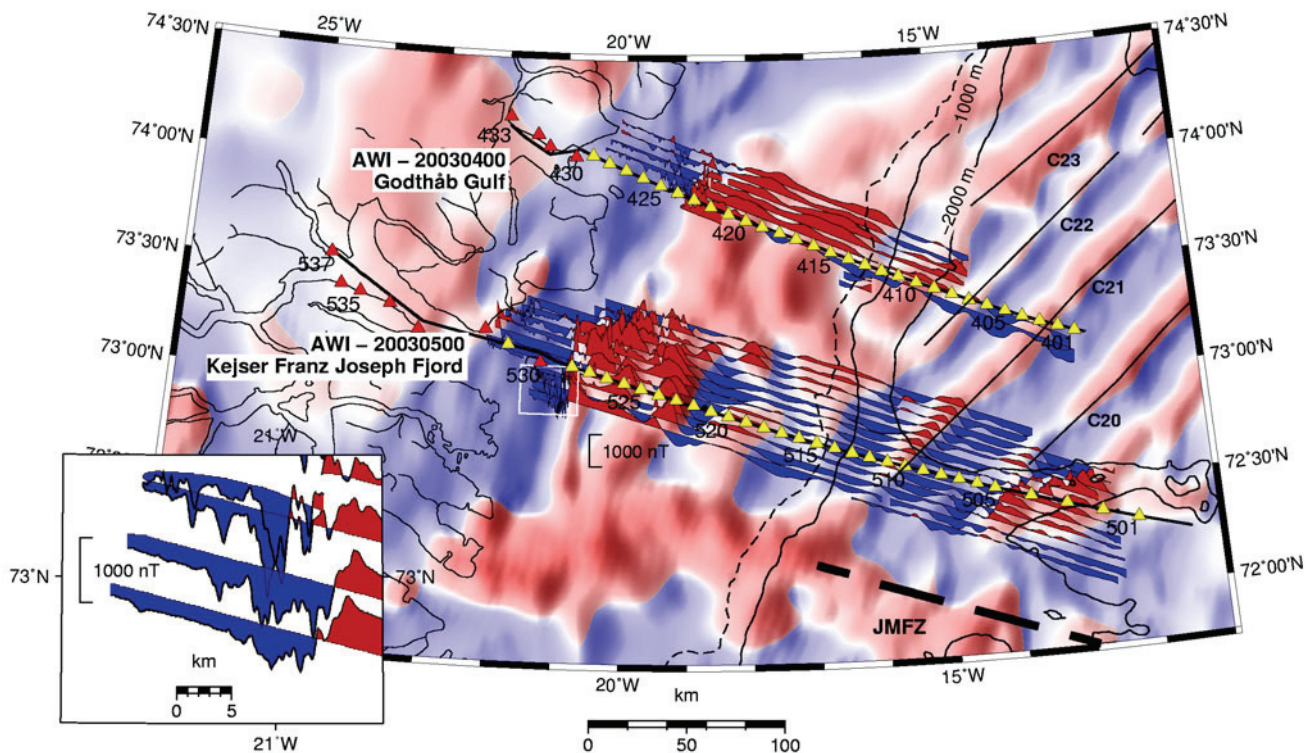


Figure 5.3: Wiggle plot along new magnetic survey traverse lines. See text for range of maximum values. Background shows regional magnetic grid (Verhoef et al. 1996). Positive values are red, negative values are blue. Seismic profiles are shown as in Figure 5.2. Spreading anomalies modified after *Escher & Pulvertaft* (1995). White box denotes portion of map depict in inset. Note the short wavelength magnetic variations within the pronounced negative magnetic anomaly. Scale is valid for 73°N.

5.3 Data acquisition and processing

Four seismic refraction profiles were shot in the area between 72°N and 76°N off East Greenland (Jokat et al. 2004) during cruise Arktis XIX/4 of R/V *Polarstern* in summer 2003 (Figure 5.1). Two profiles were located near the Greenland Fracture Zone and Shannon Island. The two profiles used for this study, are perfectly located for comparisons of the deep crustal structure with a former transects of this region and with the conjugate Vøring Margin. On profile AWI-20030400, seismic signals were

recorded by four 3-component REFTEK (REF) land stations and 29 ocean bottom instruments (15 ocean bottom hydrophones (OBH) and 14 3-component ocean bottom seismometers (OBS)). Along profile AWI-20030500, a total of seven land stations, 16 OBH and 14 OBS were used. Land stations recorded with 100 Hz sampling rate and OBH and OBS with 200/250 Hz, respectively. The locations of the receivers are displayed in Figure 5.2. The average receiver spacing was 10 km. The seismic source consisted of an array of five G-guns with a total volume of 42.5 L and an additional 32 L *Bolt* airgun fired every 60 s. The shot distance was about 125 m.

OBH 403 yielded no reliable data, while OBS 416 and REF 430 had a 1 s and 2 s time shift and were used for processing after an adequate travel-time correction. On the southern profile, REFs 535 and 534 and OBHs 526 and 520, and OBS 509 had recording problems and were not used for modelling. For P-wave modelling, we used hydrophone recordings of the appropriate ocean bottom instruments, as well as the recorded vertical z-component of the onshore receivers. Stacking the vertical component channels for each REF stations did not result in better data quality. A tapered bandpass filter of 4.5 – 30 Hz was used for the seismic data. All displayed seismic sections (Figures 5.7a-d and 5.8a-d) are filtered with 4.5 and 12 Hz to enhance the display quality and are scaled with an automatic gain control (AGC) window of 2s. The reduction velocity is 8 km s⁻¹. Deconvolution filters were tested, with the intension of enhancing secondary arrivals, but did not provide significant improvements for this data set.

Phase	20030400			20030500		
	n	t _{RMS} , s	χ ²	n	t _{RMS} , s	χ ²
Pw	560	0.208	8.687	255	0.186	8.294
Pg1*	-	-	-	10	0.057	1.21
P1P	-	-	-	19	0.257	3.096
Pg1	426	0.123	3.703	156	0.118	4.843
P2P	134	0.161	2.783	24	0.096	1.059
Pg2	190	0.092	2.709	373	0.105	3.363
P3P	-	-	-	25	0.05	0.232
Pg3	1194	0.082	1.672	877	0.119	2.48
Pc1P	36	0.098	1.538	11	0.168	3.227
Pc1P'	20	0.118	2.073	-	-	-
Pc1	1980	0.107	1.394	1940	0.13	2.003
Pc2P	569	0.145	2.466	611	0.183	2.896
Pc2P'	56	0.214	2.942	-	-	-
Pc2	768	0.181	4.903	85	0.316	14.112
PmP	658	0.153	2.049	169	0.25	6.714
PmP'	211	0.185	2.114	24	0.124	0.88
Pn	140	0.112	1.379	53	0.136	4.063
Pn'	-	-	-	230	0.97	0.957
All	6942	0.137	2.804	4862	0.147	3.049

Table 5.1: Number of used observations (n), RMS misfit between calculated and observed picked travel times (t_{RMS}) in seconds and normalized χ² for individual phases of each profile. See Table 1 for phase nomenclature.

An aeromagnetic survey was flown using a Scintrex Caesium-vapour magnetometer sensor towed 30 m under a helicopter. The survey was flown at 100 m altitude with a line spacing of 5 km (Figure 5.3). In total, 2000 km were flown in the northern part and 5500 km in the southern area. A data point spacing of 40 m results from the sampling rate of 1 Hz and an average cruising speed of 40 m s⁻¹. The magnetic data were reduced with IGRF and diurnal corrections from the *Danish Meteorological Institute* in Danmarkshavn (Figure 5.1) (data available at <http://web.dmi.dk/fsweb/projects/chain/#list>). Owing to local atmospheric variations and the 300 – 550 km distance between the survey area and the ground station, the diurnal data were lowpass filtered at 1800 s to avoid short wavelength miss-corrections. The resulting magnetic anomalies range between -1312 nT and 1064 nT in amplitude. After levelling, the mean cross line mistie is less than 10 nT and an absolute maximum value of 130 nT. Figure 5.3 shows

the new magnetic data as wiggles along the survey lines with the regional magnetic grid (Verhoef et al. 1996) in the background.

Gravity data were recorded continuously with a sampling rate of 10 s along the ship track for the entire cruise with an onboard fixed installed KSS 31 Bodenseewerke gravimeter. The data were converted to Bouguer anomalies and lowpass filtered at 100 s in order to reduce the high frequency noise of the ship movements. Only full circles in the ship track were cut out but other minor course variations remained and appear as small scale variations in the profile data. The full range of the Bouguer anomaly data along the profiles used for this study is between -50 mGal and 200 mGal.

5.4 Modelling

P-wave travel time arrivals were picked with the *zp* software from *B.C. Zelt* (available at <http://www.soest.hawaii.edu/~bzelt/zp/zp.html>). This programme calculated the signal to noise ratio within a 0.25 s time window before and after each pick time and associated it with an error value ranging between 0.04 s and 0.15 s.

Prior to ray tracing, shots and receivers have to be in a single plane. Thus, a projection of the receiver locations onto a straight line is necessary, due to the slightly curved geometry of the transects within the fjords. A straight line fit through stations 401 and 429 was used for profile AWI-20030400 and through stations 501 and 531 for AWI-20030500 (Figure 5.2). The maximum perpendicular projections onto the lines were 5.3 km for OBH 413 and 22 km for REF 537. The true offsets of the observed P-wave arrivals remained unchanged. This projection results in averaging of laterally inhomogeneous crustal structures due to the different ray paths between the real profile and the approximation.

Stations located onshore were projected onto the seafloor and a static correction was applied to account for the differences between rock and water sound velocities. The observed travel times of REF 432, 431 and 430 were corrected, assuming a vertical ray incidence, and a rock velocity of 5.2 km s⁻¹ derived from the curvature of first arrivals. The same procedure was applied to REF 536, 533, 531 and 529. The errors resulting from these approximations are estimated to be smaller than the pick uncertainties. Travel time arrivals for REFs 433 and 537 were located at the origin of the projection lines and no projection onto the seafloor was necessary.

The P-wave velocity models were obtained by forward modelling with two-dimensional (2-D) ray tracing software *RAYINV* (Zelt and Smith 1992). 2-D inversion was also used in questionable areas of the model, in order to obtain further modelling ideas. The formal error analysis for the individual phases is summarized in Table 1. The normalized χ^2 value is based on the assigned error value of each pick. Initial values for layer velocities were determined from the slopes of the travel time curves. After this, we focused on fitting the slope of the first arrivals rather than minimizing residuals (Figure 5.4 and Figure 5.5). This results in individual cases in large normalized χ^2 values. For profile AWI-20030500 largest deviations to the optimum normalized χ^2 value of 1.0 are caused by small error values for the Pw phases or larger misfits to Pc2 picks and yield values of 8.294 and 14.112, respectively (Table 1). Highest t_{RMS} values of profile AWI-20030400 occur at phases Pw and Pc1P' and of profile AWI-20030500 at Pg1*, Pc2 and Pc2P (see Table 2 for origin of phases). The total RMS misfits result in 0.137 s for profile AWI-20030400 and 0.147 s for profile AWI-20030500 and in normalized χ^2 values of 2.804 and 3.049, respectively. Fitting the curves of travel time arrivals for adjacent receiver stations often leads to a compromise of vertical and lateral velocity gradients. Ray paths bend more for larger velocity gradients within a layer. Therefore, in some cases, shorter maximum offsets could be modelled and rays did not reach observed picks (see Figure 5.4 for OBHs 404, 418 and Figure 5.5 for OBHs 504 and 506). In total, 7336 picks were used for AWI-20030400 and 5036 picks for AWI-20030500. Rays were traced for 88% and 93% of the observations on the two profiles. Layer boundaries were constrained where wide angle reflections were identified. In all other instances, the layer boundaries were shifted to adjust the velocity gradients within the layers.

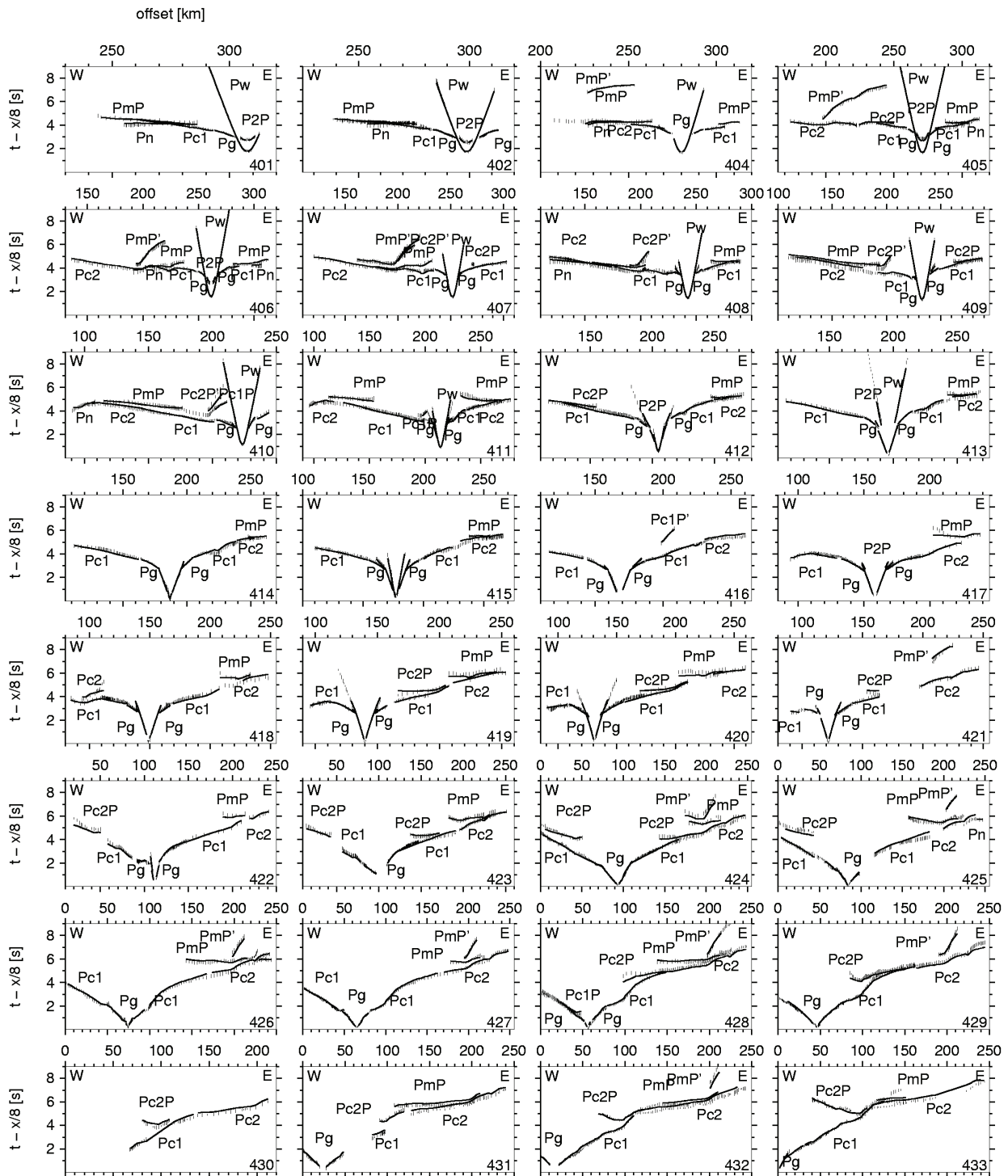


Figure 5.4: Observed and calculated P-wave arrivals for profile AWI-20030400. Observed arrivals are assigned with a vertical error bar. The picked arrival time is in the centre. Lines show the calculated arrivals. Note the variety of PmP' and Pc2P' phases. See Table 2 for nomenclature of phases. Short offset phases are not differentiated and labelled as Pg.

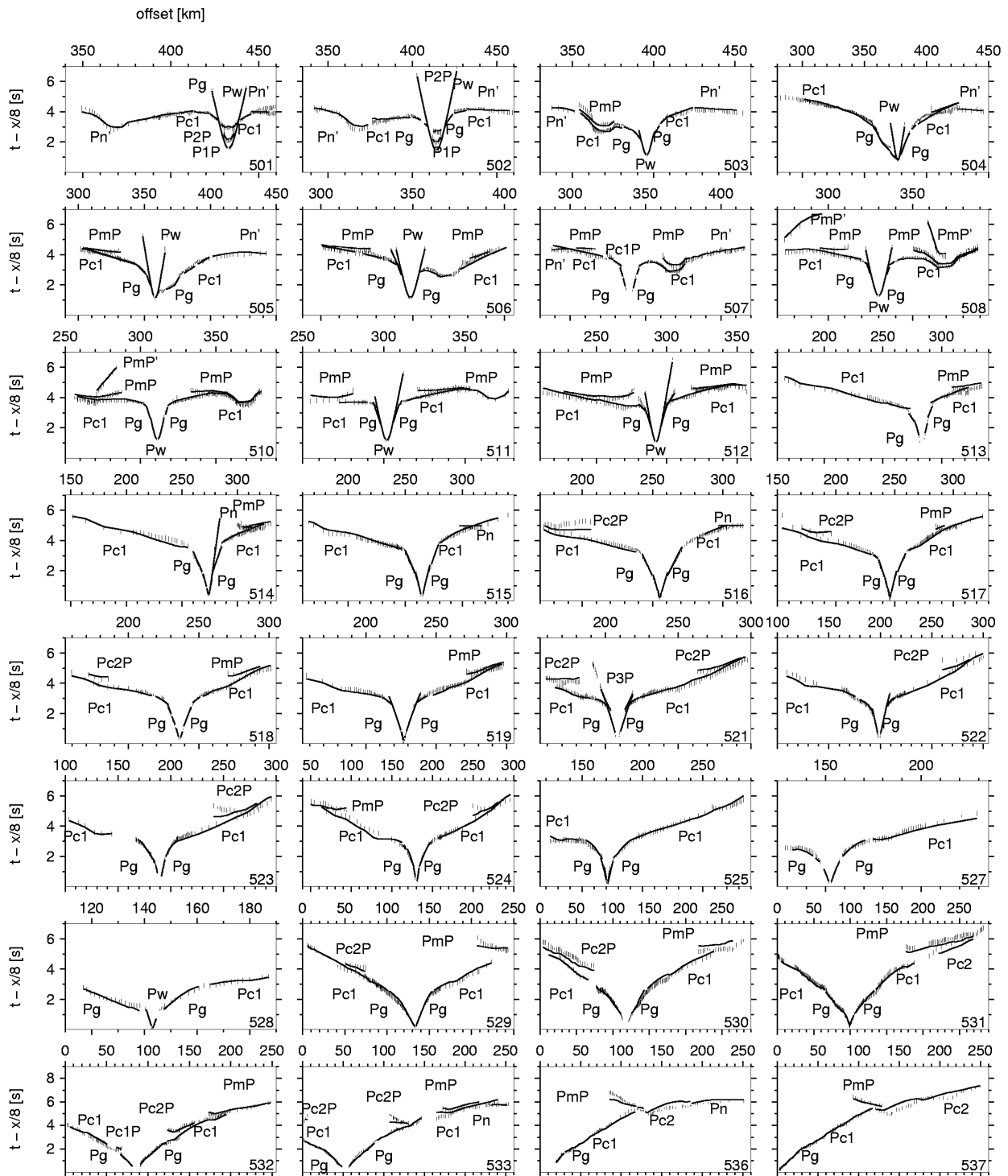


Figure 5.5: Observed and calculated P-wave arrivals for profile AWI-20030500. See Figure 5.4 and Table 5.2 for explanations.

Layer of velocity models	rfl on top of layer	rfr in layer
Layer 1 : upper sediments (1 & 1* of AWI-20030500)	Pw P1P	Pg1 Pg1, Pg1*
Layer 2: intermediate layer	P2P	Pg2
Layer 3: lower sediments	P3P	Pg3
Layer 4: upper crust	Pc1P, Pc1P'	Pc1
Layer 5: lower crust	Pc2P, Pc2P'	Pc2
Layer 6: upper mantle	PmP, PmP'	Pn, Pn'

Table 5.2: Nomenclature of seismic phases. rfl: reflection. rfr: refraction. Pw phase reflects at seafloor. An additional thin layer was inserted at the top for model AWI-20030500. Reflections on this layer are labelled with P1P, a refraction phase with Pg1*. Phase Pc1P', Pc2P', and PmP' have a multiple reflection between the water surface from below and the seafloor. Pn' represents head waves along the Moho.

Traveltime arrivals were assigned as listed in Table 2 and correspond to the model layers as in Figures 5.6a – d. P1P – P3P mark reflections on layers interpreted as sedimentary layers and/or upper oceanic layer 2; Pg1 – Pg3 correspond to refracted rays. Pc1P and Pc2P were used for reflections at the continental crust and lower oceanic crustal layers. PmP stands for Moho reflections. The corresponding refracted rays are labelled as Pc1, Pc2 and Pn for the mantle. An additional thin top sedimentary layer was obtained from MCS data (AWI unpublished data, see *Jokat et al. (2004)* as reference) in the oceanic part of profile AWI-20030500. Only two P1P reflections on OBH 501 and 502 and Pg1 refractions from OBH 507 (Figure 5.5) provided constraints on this layer. For the interpretation, the layer was not distinguished from the one beneath. Some travel time arrivals (Pc1P', Pc2P' and PmP') were identified with a multiple reflection within the water column. Examples are shown in Figures 5.7a and 5.8a. Pn' arrivals were modelled as head waves propagating along the Moho but with the P-wave velocity of the upper mantle (Figure 5.5, e.g. 501 - 505).

The coverage of refracted and reflected rays traced for each layer (Figures 5.6a – d) gives an impression of the reliability of the models. The calculation of the model resolution is strongly dependant on the parameterization of the velocity-depth model. Only a uniform spacing of nodes would be meaningful, which was not practicable in this case. Instead, the model uncertainties were estimated by the perturbation of single node parameters until the fit of calculated travel times was no longer acceptable. Errors for the seismic velocities are hereby estimated as ranging from $\pm 0.1 \text{ km s}^{-1}$ for upper sedimentary layers to $\pm 0.2 \text{ km s}^{-1}$ for the lower crustal layers. The resulting uncertainties in the modelled depths of layer boundaries vary between $\pm 0.2 - 0.5 \text{ km}$ for the upper layers and $\pm 2.0 \text{ km}$ for the lower ones, depending on the coverage of reflected rays. These uncertainties have to be considered as rough estimates since the perturbation could not be performed for all nodes.

5.5 Results

We present the results of P-wave velocity modelling across the East Greenland margin for the Godthåb Gulf profile AWI-20030400 and Kejser Franz Joseph Fjord profile AWI-20030500 separately. Figures 5.4 and 5.5 show the picked travel time arrivals of all stations and examples of data are shown in Figures 5.7a – d and 5.8a – d, which are representative for the data quality. Velocity models are shown in Figures 5.9 and 5.10.

A rough separation into three distinct crustal units simplifies the description of the velocity models; continental crust, transitional crust and oceanic crust. The structural interpretation will demonstrate that the transitional crustal unit correlates with the tectonic and magmatic definitions of a continent – ocean transition zone.

To distinguish the different oceanic crustal layers, we use the classification of *White et al. (1992)* for mean oceanic crustal structures. Oceanic layer 2 ($2.5 - 6.6 \text{ km s}^{-1}$) consists of extrusive basalts. Oceanic

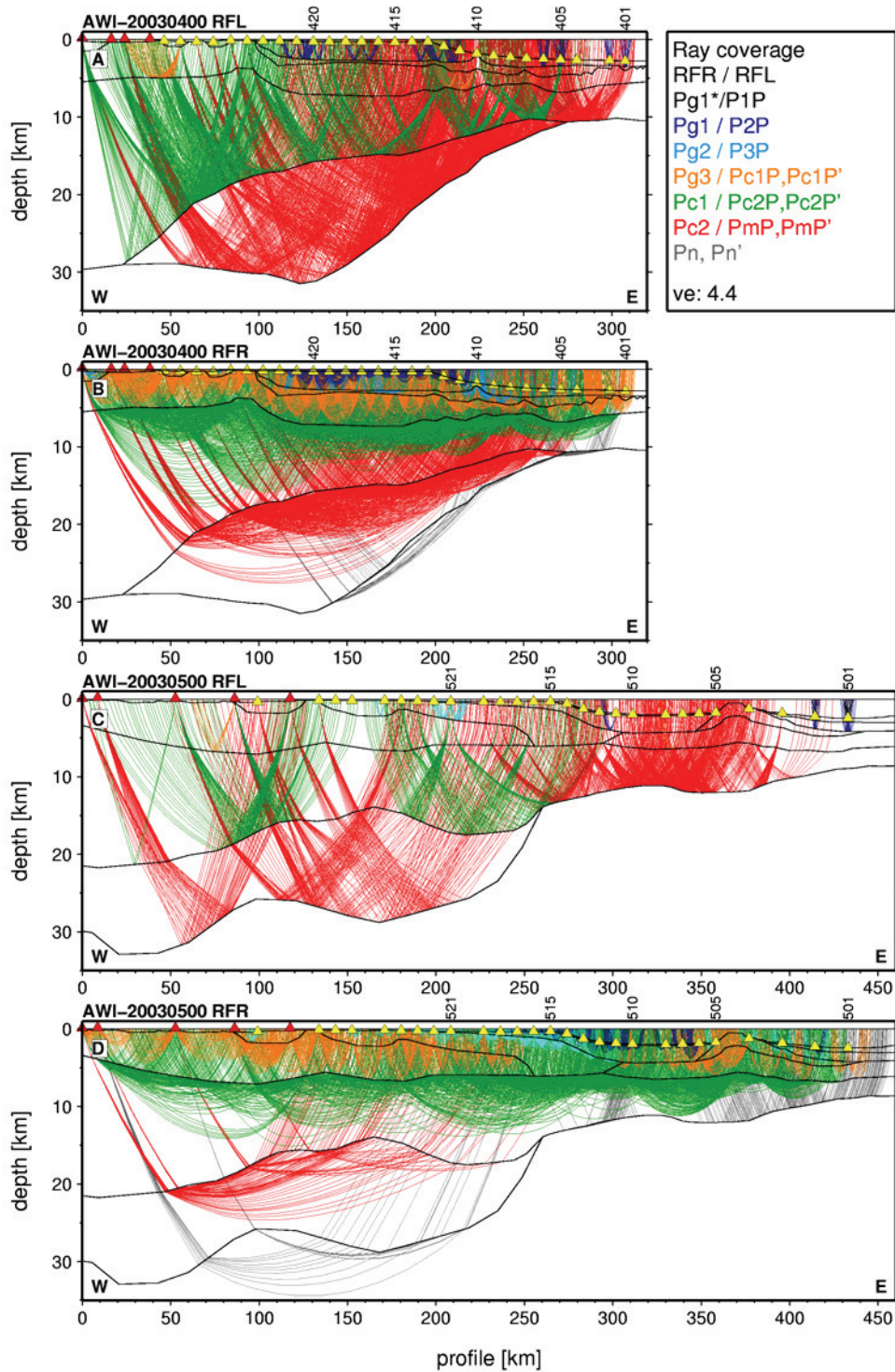


Figure 5.6: Ray tracing for both profiles. RFL: reflected rays. RFR: refracted rays. Vertical exaggeration is 4.4. Triangles represent receiver station locations as in Figure 5.2. The different colours symbolize the rays for the individual layers. See Table 2 for a further explanation of the phases. A) All reflected rays for profile AWI-20030400. Note the excellent coverage of the intra crustal reflector and the Moho by Pc2P and PmP phases. From km 270 on Pc2P phases equal PmP phases. B) All refracted rays for profile AWI-20030400. Only individual Pn phases traced the upper mantle. C) All reflected rays for profile AWI-20030500. From km 260 on Pc2P equal PmP phases. D) All refracted rays for AWI-20030500. See text for model parameters and velocities.

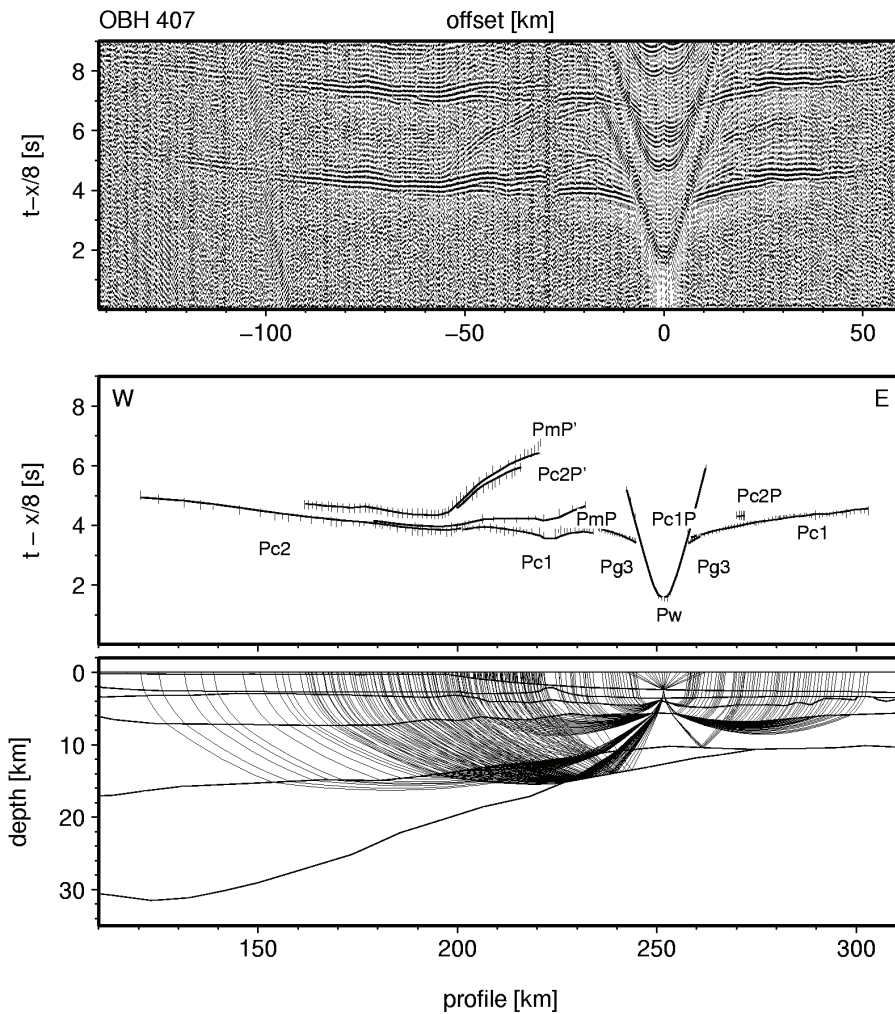


Figure 5.7: Examples of recorded seismic data from profile AWI-20030400. A 4.5 to 12 Hz band pass filter was applied. The signals are scaled by automatic gain control in windows of 2 s. The traveltimes are reduced by 8 km s^{-1} . Observed phases are labelled (see Table 1). The ray coverage of each station is marked in the lower model. a) Station 407 represents recordings of the oceanic crust and the eastern COT. Note the multiple reflected phase PmP' and $\text{Pc2P}'$. b) Station 415 is placed within the COT and shows typical shorter offsets. c) OBH 423 is located near the landward termination of the COT. d) Land station 431 shows typical long offsets. Note the poor quality of data between km 150 and 250. A filter of 4.5 to 21 Hz was here applied. The offset between the first arrivals and the location is due to the horizontal deviation of the station to the ship track.

layer 3 ($6.6 - 7.6 \text{ km s}^{-1}$) is generally presumed to be of gabbroic material. Some authors use more subdivisions of the oceanic layers (Fowler 2005; Mjelde et al. 2005) and distinguish between layers 2A and 2B of pillow lavas and sheeted dikes. Divisions into layers 3A and 3B distinguish between gabbros ($6.6 - 6.9 \text{ km s}^{-1}$) and more cumulate-rich gabbros ($7.2 - 7.7 \text{ km s}^{-1}$).

5.5.1 The Godthåb Gulf profile (GG) AWI-20030400

Profile AWI-20030400 (Figure 5.2) has a total length of 320 km. Four stations were deployed onshore and recorded seismic signals up to 220 km distance. OBH/OBS instruments recorded diving and reflection waves at a maximum offset of 180 km, and a mean of 115 km. The corresponding P-wave velocity model is shown in Figure 5.9.

5.5.1.1 Continental crust (km 0 – 100)

The western part of the seismic profile between km 0 and 100 shows an almost 30 km thick continental crust. The westernmost land stations, REF 433 – 430, are located on Carboniferous sediments on Clavinging Ø (Escher and Pulvertaft 1995). Signals from a 1 km deep sedimentary basin with a velocity of 4 km s^{-1} can be detected on the first 15 km of the profile. Two additional basins, each with a width of 10 km and velocities between 3.4 and 3.7 km s^{-1} , can be modelled from stations 429, 428, 426 and 425. The depths of the basins are assumed to be less than 1 km. Velocities in the continental sediments increase rapidly from $4.8 - 5.2 \text{ km s}^{-1}$ near the surface to $5.9 - 6.1 \text{ km s}^{-1}$ at 5 km depth ($0.13 - 0.25 \text{ km s}^{-1} \text{ km}^{-1}$). A single reflection at the bottom of this layer is modelled from station 428 (Figures 5.4 and 5.6a). A low gradient ($0.03 - 0.05 \text{ km s}^{-1} \text{ km}^{-1}$) crystalline continental crust is well constrained by Pc1

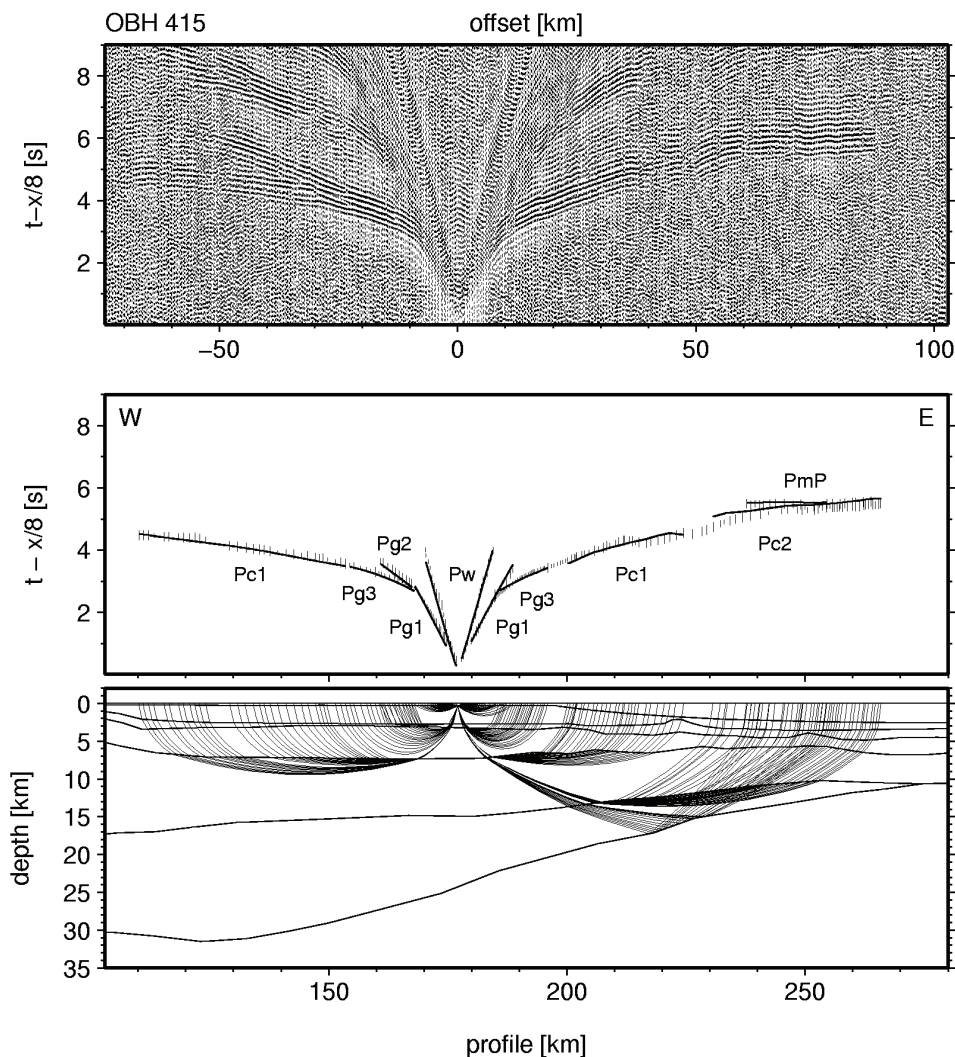


Figure 5.7: b) (Continued.)

phases with P-wave velocities of $6.0 - 6.1 \text{ km s}^{-1}$ at 5 km depth and $6.9 - 7.0 \text{ km s}^{-1}$ at the bottom. These latter values are slightly higher than the global average for continental crust (Christensen and Mooney 1995). The layer boundary at 5 km depth represents a change in seismic gradient and is not connected with an impedance contrast. A basement high at km 100 is clearly resolved from several stations (Figure 5.4). A significant delay of Pc1 travel time arrivals is observed eastward of the escarpment. The different Pg3 slopes of OBH 424 east and 423 west confirm the modelled basement high at this part of the profile. Pc2P phases infer a reflector in the lower continental crust, rising up from km 20 in 29 km depths to 18 km depth at km 100 (Figure 5.6a), which represents a significant velocity contrast. Beneath

this lower crustal reflector, a clear and almost continuously resolved reflector was modelled from PmP arrivals. The lower crust is modelled with velocities of $7.2 - 7.4 \text{ km s}^{-1}$ between the two prominent reflections.

5.5.1.2 Continent – ocean transition zone (100 – 224 km)

The transitional crustal unit extends from km 100 to 224. Landwards, it is bounded by the continental basement high. A shallow, most probably volcanic, basement high and the first clearly identifiable magnetic spreading anomaly, C22, marks the transition into oceanic crust in the east (Figure 5.9). The upper sediment layer on the shelf has a thickness of $\sim 2.5 \text{ km}$ ($2.0 - 2.8 \text{ km s}^{-1}$). Secondary Pg2 arrivals at OBH 422 and 419 – 415 yield a thin ($< 500 \text{ m}$) intermediate layer ($\sim 4.1 \text{ km s}^{-1}$) beneath. Only sparse

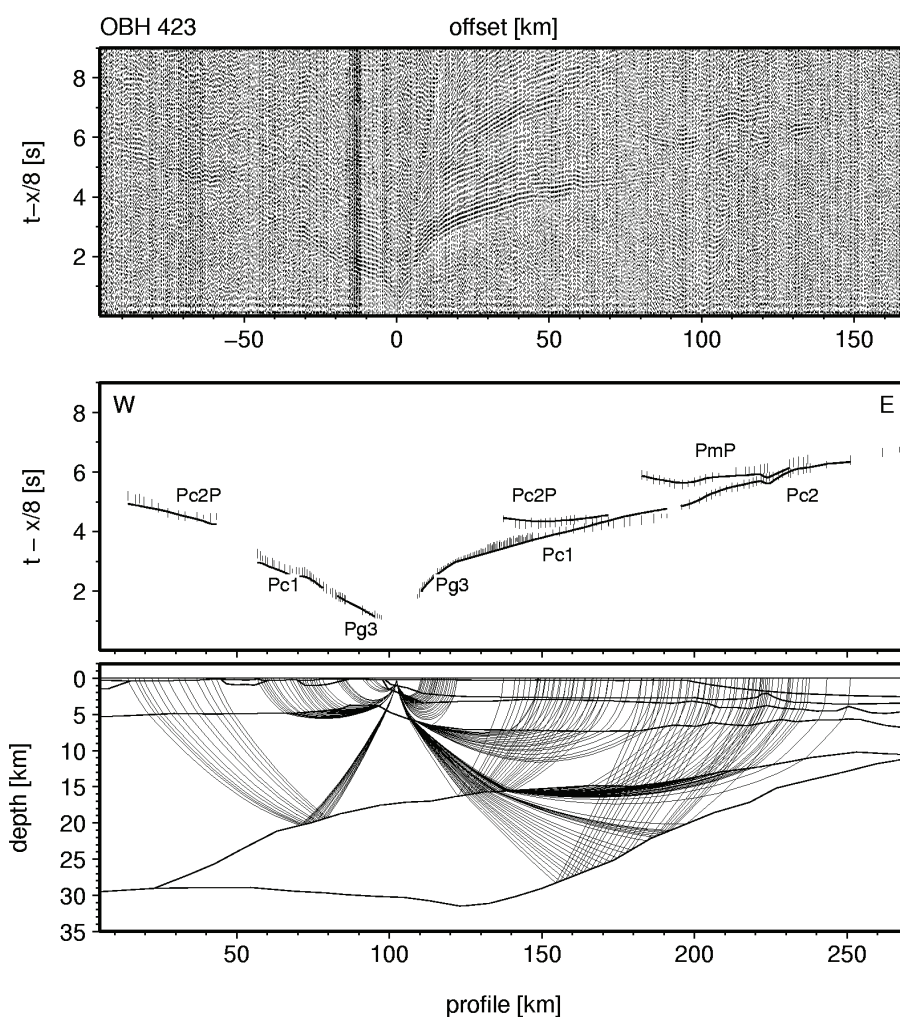


Figure 5.7: c) (Continued.)

reflections sample the top of this thin layer, which terminates seaward in the shallow feature interpreted as of volcanic origin (Pg2 arrivals of OBH 411 – 410) at km 224 (Figures 5.4 and 5.6b). Three crustal layers of the transition zone can be distinguished on the basis of their different velocity gradients. The upper part has a velocity gradient of $0.35 - 0.47 \text{ km s}^{-1} \text{ km}^{-1}$ with velocities between $4.6 - 5.5 \text{ km s}^{-1}$ at 3 km depth and $5.8 - 6.5 \text{ km s}^{-1}$ at 7 km depth. Two Pc1P' (Table 2) reflections constrained the boundary between km 205 and 220. In the middle part, an increasing velocity gradient of $0.04 \text{ km s}^{-1} \text{ km}^{-1}$ to 0.1

$\text{km s}^{-1} \text{ km}^{-1}$ is modelled from west to east. Seismic velocities range between $6.4 - 6.8 \text{ km s}^{-1}$ at 7 km depth and $6.8 - 7.1 \text{ km s}^{-1}$ at 13 – 17 km depth. Diving waves penetrate almost 2/3 of the crustal layer, and have their deepest turning points at 9 - 12 km depth (Figure 5.6b). Several Pc2P and Pc2P' (Table 2) reflections (Figures 5.4 and 5.6a) were modelled, constraining the intra-crustal and seaward rising reflector. The significant velocity contrast along this reflector, as modelled in the continental part of the profile, becomes less prominent to the east. A high velocity lower crustal layer ($7.15 - 7.4 \text{ km s}^{-1}$) yields a very low velocity gradient of $0.01 \text{ km s}^{-1} \text{ km}^{-1}$. PmP and PmP' resolved the Moho along the entire transition zone. The maximum thickness of the high velocity layer is 16 km at a depression in the Moho near km 124. Upper mantle velocities of 8.0 km s^{-1} were derived from Pn arrivals (Figures 5.4 and 5.6a) between km 140 and 250.

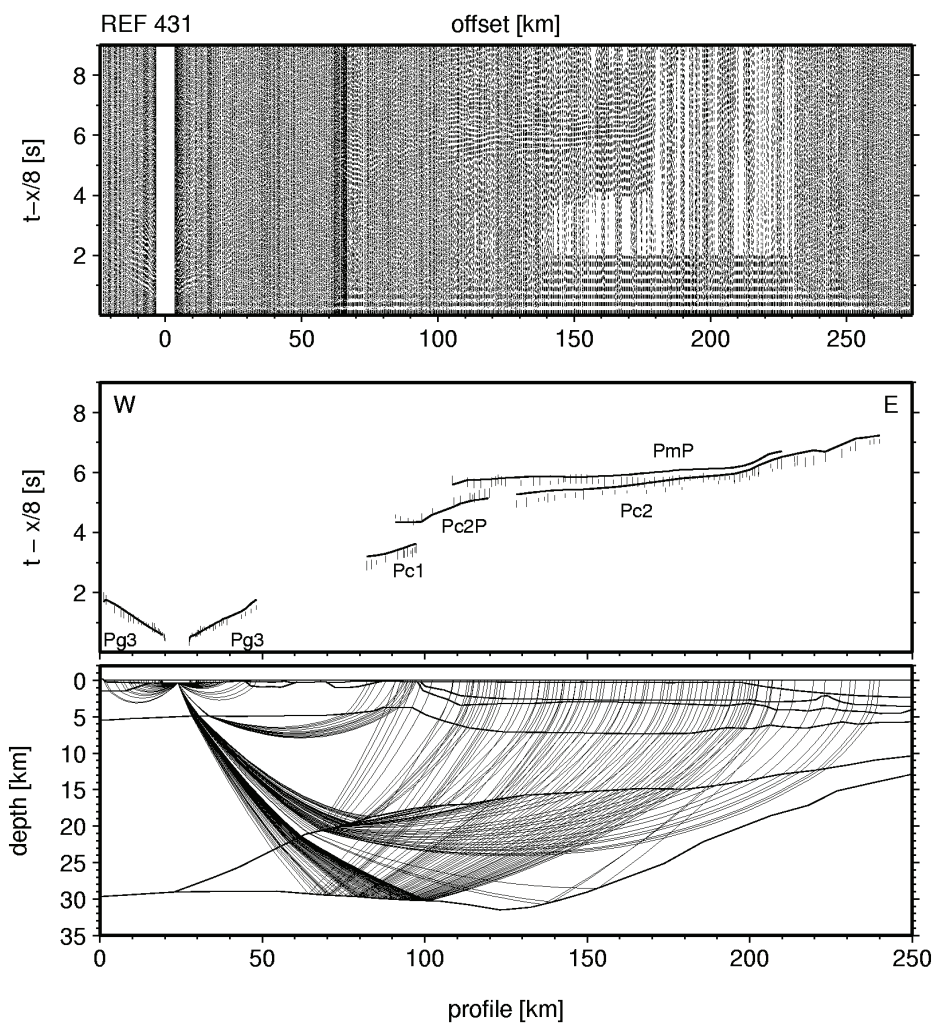


Figure 5.7: d) (Continued.)

5.5.1.3 Oceanic crust (224 – 320 km)

The eastern crustal unit of the profile has the characteristics of typical oceanic crust (White et al. 1992), consistent with the presence of the first clearly identified magnetic spreading anomaly, C22, near km 250/OBH 407. An upper sedimentary layer was modelled with velocities in the range $1.6 - 1.9 \text{ km s}^{-1}$ and thickness decreasing seawards from 1.25 to 0.75 km. A basal reflector is inferred for this unit from four P2P arrivals (Figures 5.6a and 5.9). Upper oceanic crust was modelled to consist of two layers with

different velocity gradients. The upper layer has velocities of $3.2 - 5.0 \text{ km s}^{-1}$, the lower one velocities $4.6 - 6.0 \text{ km s}^{-1}$, which is well defined by Pg3 arrivals (Fig 6b). At the eastern end of the profile, between km 280 and 320, MCS data show rough topography (AWI unpublished data; see *Jokat et al.* (2004) as reference). A lower 4 – 5 km thick oceanic layer was modelled, with P-wave velocities of $6.6 - 6.7 \text{ km s}^{-1}$ at the top and $6.9 - 7.0 \text{ km s}^{-1}$ at the base. The velocity gradient of the lower layer falls in the range for standard lower oceanic layers (White et al. 1992). Pc1P arrivals at OBHs 402 – 409 resolved a distinct reflector in the oceanic crustal part of the profile. Beneath this, thickened oceanic crust was modelled from Pc2 arrivals with velocities of $7.2 - 7.4 \text{ km s}^{-1}$. PmP and PmP' arrivals (Figure 5.6a) resolved the Moho in 10.1 – 15.8 km depth, and show a decrease in total thickness of the oceanic crust from 13.7 to 6.8 km between km 224 and 300. An upper mantle velocity of 8.0 km s^{-1} was modelled from several observed Pn arrivals.

5.5.2 The Kejser Franz Joseph Fjord profile (KFJF) AWI-20030500

Profile AWI-20030500 has a total length of 460 km. Seven land stations recorded seismic signals at distances of up to 250 km. OBHs and OBSs recorded arrivals of refraction and reflection waves out to an average distance of 80 km with a maximum of 170 km. This profile overlaps with profile 94320 (Schlindwein and Jokat 1999) for a distance of almost 120 km (Figure 5.2). The overlapping part of the crustal transect was used as a starting model for the continental part of profile AWI-20030500. Only minor adjustments were necessary due to the different orientations of both transects. In the eastern, oceanic, part, between km 280 and 460, horizons of the two top sedimentary layers were digitized from time migrated multi-channel seismic data (AWI unpublished data; see *Jokat et al.* (2004) as reference). Fig 10 shows the corresponding P-wave velocity model. The following description of the results is organised as for profile AWI-20030400.

5.5.2.1 Continental crust (0 – 130 km)

The top continental sediment layer ($5.2 - 6.0 \text{ km s}^{-1}$) reveals average velocity gradients of $0.13 \text{ km s}^{-1} \text{ km}^{-1}$. A 1.5 km – deep basin is imaged by short offset arrivals ($3.6 - 5.0 \text{ km s}^{-1}$) (Figure 5.5, OBH 531) west of Bontekoe Ø (km 85 – 125). The top velocities decrease to 3.2 km s^{-1} beneath the outcrop of plateau basalts (Escher and Pulvertaft 1995). Between km 0 and 70, upper crustal velocities ($6.1 - 6.5 \text{ km s}^{-1}$) fall within the global average range of velocities for continental crust (Christensen and Mooney 1995). Further east, the values increase constantly (Figure 5.10) and the velocity gradient increases from $0.02 - 0.05 \text{ km s}^{-1} \text{ km}^{-1}$. Pc2P and PmP reflections revealed a west dipping mid-crustal reflector at 17 – 20 km depth and a similar – dipping Moho at 27 – 31 km depth between km 50 and 100 (Figures 5.6 and 5.10). A Moho plateau is modelled at 26 km depth from further PmP reflections (Figure 5.5 REF 533, 532 and OBH 524). The strong horizontal velocity increase in the lower crustal layer near km 50 (Figure 5.10) was adopted from profile 94320 (Schlindwein and Jokat 1999). Similar velocities of $6.8 - 7.2 \text{ km s}^{-1}$ were calculated from Pc2 arrivals but the modelling of this phase revealed major misfits (Figure 5.5 REF 537). Besides the Moho plateau, all crustal velocities and layer boundaries are in good agreement with the overlapping part of profile 94320.

5.5.2.2 Continent – ocean transition zone (130 – 260 km)

This 130 km long part of the model represents an area of increased crustal velocities compared to the continental crustal unit. Pg3 phases at OBH 529 - 527 witness the dip of the continental sedimentary layer landward of km 130 with velocities of $4.5 - 6.1 \text{ km s}^{-1}$ and the onset of another layer seaward of this point with velocities of $2.0 - 3.3 \text{ km s}^{-1}$ (Figures 5.5 and 5.10). The uppermost sedimentary layer ($2.0 - 2.4 \text{ km s}^{-1}$) pinches out to the west (km 210), and merges with a sedimentary basin in the oceanic crustal unit. A second dipping sedimentary layer is modelled with a strong velocity increase ($2.0 - 3.3 \text{ km s}^{-1}$) between km 130 and 230 and a lower velocity range ($2.5 - 4.2 \text{ km s}^{-1}$) further seaward between km 230 and 260. This layer also forms a deep basin in the oceanic crustal unit (Figure 5.10). The intra-

sedimentary layer boundaries were inferred from unpublished MCS data, but could not be confirmed by reflected P2P arrivals. Beneath, a layer extends and thins out from km 130 to 255, but with velocities ranging between $3.8 - 6.5 \text{ km s}^{-1}$ from top to bottom. Pg3 travel time arrivals (Figure 5.6d) yield an increase in the velocity gradient for this layer from an average of $0.13 \text{ km s}^{-1} \text{ km}^{-1}$ in the continental crust (see above) to an average of $0.55 \text{ km s}^{-1} \text{ km}^{-1}$ in the transitional unit. The top of the crystalline crust is not resolved by any Pc1P phases but most travel time curves show a variation of the velocity gradient at a mean depth of $6.3 \pm 0.5 \text{ km}$. Thus, within the upper crustal layer, velocities vary in the range $6.5 - 6.7 \text{ km s}^{-1}$ at the top and $6.9 - 7.0 \text{ km s}^{-1}$ at the bottom. Between km 180 and 255, Pc2P reflections trace a pronounced bowl shaped reflector. This reflector marks a velocity contrast from 6.9 km s^{-1} to 7.2 km s^{-1} . Thus, the velocity gradient within the upper crust increases marginally by up to $0.08 \text{ km s}^{-1} \text{ km}^{-1}$ from west to east, as is seen on profile AWI-20030400. Pc2P and PmP reflections constrain the topography of the intermittent reflector and the Moho (Figures 5.6 and 5.10).

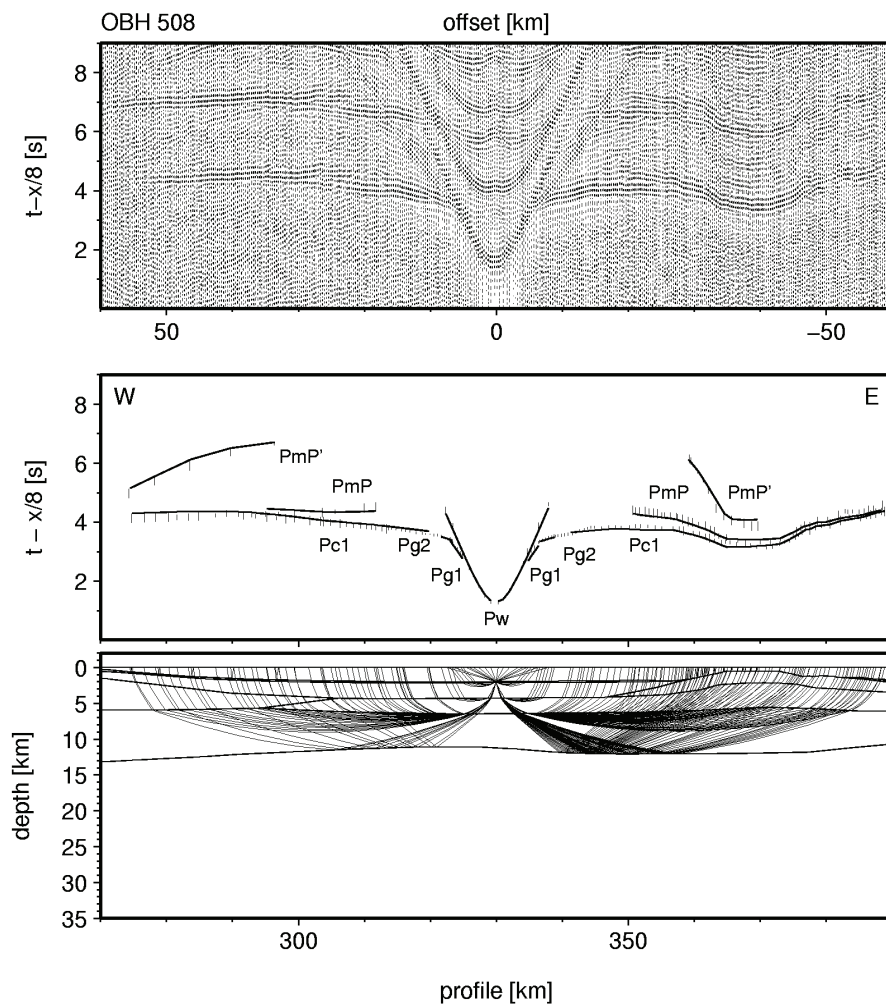


Figure 5.8: Examples of recorded seismic data from profile AWI-20030500. For data descriptions see Fig. 7. a) OBH 508 represents recordings of the oceanic basin west of the ridge and the eastern COT. Note the multiple reflected phase PmP' near $\pm 50 \text{ km}$. b) OBH 518 shows delayed arrivals due to thick Cenozoic sediments within the COT. c) OBH 529 is located at the landward termination of the COT. d) Continental crust, LCB and the western part of the COT are covered by station REF 536.

Between km 130 and km 218 a Moho depression is modelled with a maximum depth of 28.8 km. The resulting maximum thickness of the high velocity layer is 15 km, near km 165. Land stations REF 537, 536, 533 and OBH 531, recorded Pc2 phases at offsets of 100 - 240 km (Figure 5.5). Rough calculations of the travel time arrivals yield velocities between $7.2 - 7.4 \text{ km s}^{-1}$, but the upper crustal topography could not be resolved by Pc2 travel time fits without giving rise to large misfits of up to 300 ms (Fig5, REF 537, 536, 533 and OBH 531). The Moho slope between km 218 and 260 is not traced by any rays.

5.5.2.3 Oceanic crust (260 – 460 km)

The south eastern area of the profile, between km 290 and 460, shows typical oceanic crustal layering and velocities (White et al. 1992), correlating with the first clearly identified magnetic spreading anomalies C21 (Escher and Pulvertaft 1995). The dipping sedimentary layer from the transitional unit forms a 30 km wide basin ($3.2 - 4.2 \text{ km s}^{-1}$) between km 260 and 290. Between km 360 and 380 a ridge

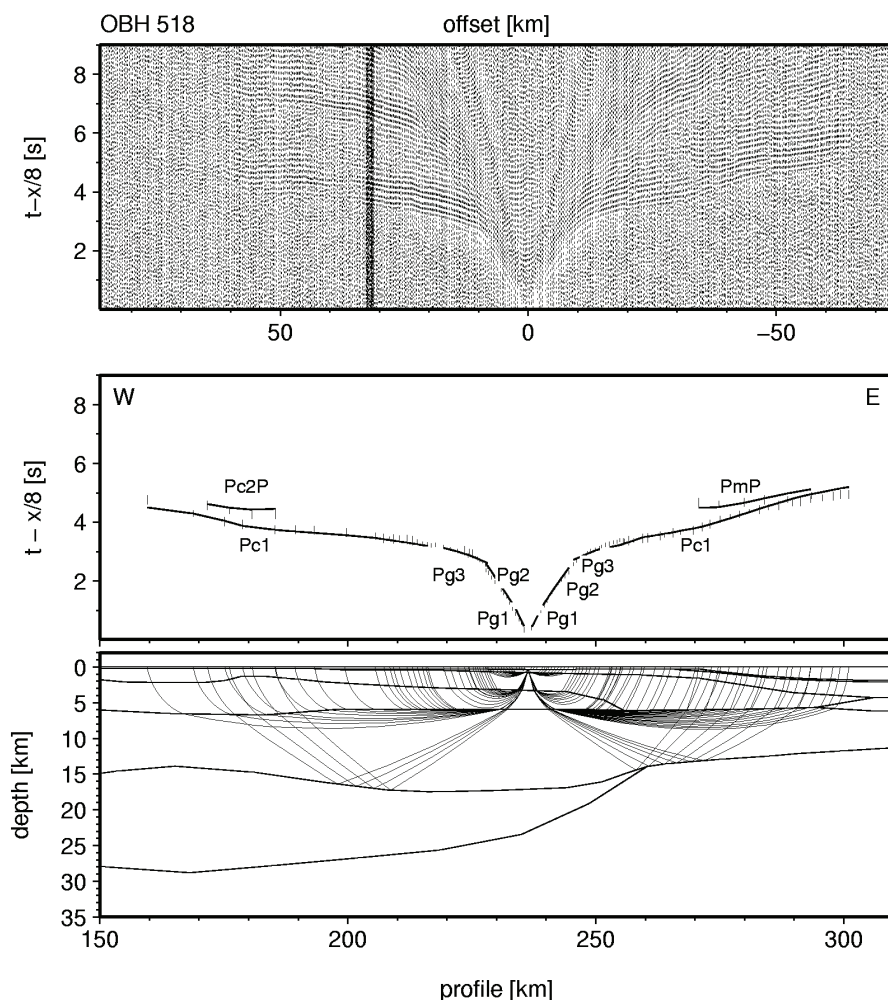


Figure 5.8: b) (Continued.)

domes up to separate two different sedimentary basins (Figure 5.10). Reflecting horizons for the two top sedimentary layers were picked from MCS data. In the west, between the shelf edge and the ridge (km 290 – 350), the basin fill consists of a thin (100 m) upper layer ($1.9 - 2.0 \text{ km s}^{-1}$) and the layer extending from the transitional unit ($2.1 - 3.0 \text{ km s}^{-1}$) (Figure 5.10). The maximum thickness is 1.8 km. A thin

(750 m) upper layer ($1.6 - 1.9 \text{ km s}^{-1}$) and a second thin (1 km, $2.5 - 3.2 \text{ km s}^{-1}$) sedimentary layer were inserted into the model east of the ridge. Observed P1P and P2P arrivals from OBS 501 and 502 (Figure 5.6c) confirm the horizons. The upper part of the ridge is modelled between km 350 and 430, with velocities of 3.0 to 4.0 km s^{-1} increasing from west to east. These values are derived from Pg2 arrivals at OBHs 502 – 505. Beneath this, P-wave velocities strongly increase between km 290 and 460, from 4.5 to 6.3 km s^{-1} down to $\sim 6.5 \text{ km}$ depth. In the lower oceanic crust, velocities range between 6.6 km s^{-1} and 7.0 km s^{-1} within a $2.5 - 4 \text{ km}$ thick layer (Figure 5.10). The Moho depth was constrained to $11 - 14 \text{ km}$ between km 260 and 330 by Pn arrivals from stations 514 – 516 (Figures 5.5 and 5.6d) and PmP arrivals from stations 511, 512 and 517 – 519 (Figures 5.7 and 5.8c). Further east, the Moho decreases to 8.6 km depth with a small root (12 km depth) beneath the ridge. The location of the Moho is based on numerous PmP, PmP', Pn and Pn' arrivals (Figures 5.8c and d). Traveltime arrivals of OBS 501 – 505 and 507 associated as mantle phases were assumed to be critically refracted and travelling as head waves along the Moho and with the upper mantle acoustic velocity of 8.0 km s^{-1} (Figures 5.6c and 5.10). The oceanic crustal thickness decreases from west to east, from 7.0 km to 4.8 km . However, the maximum thickness of the ridge in the oceanic crust reaches 11.5 km .

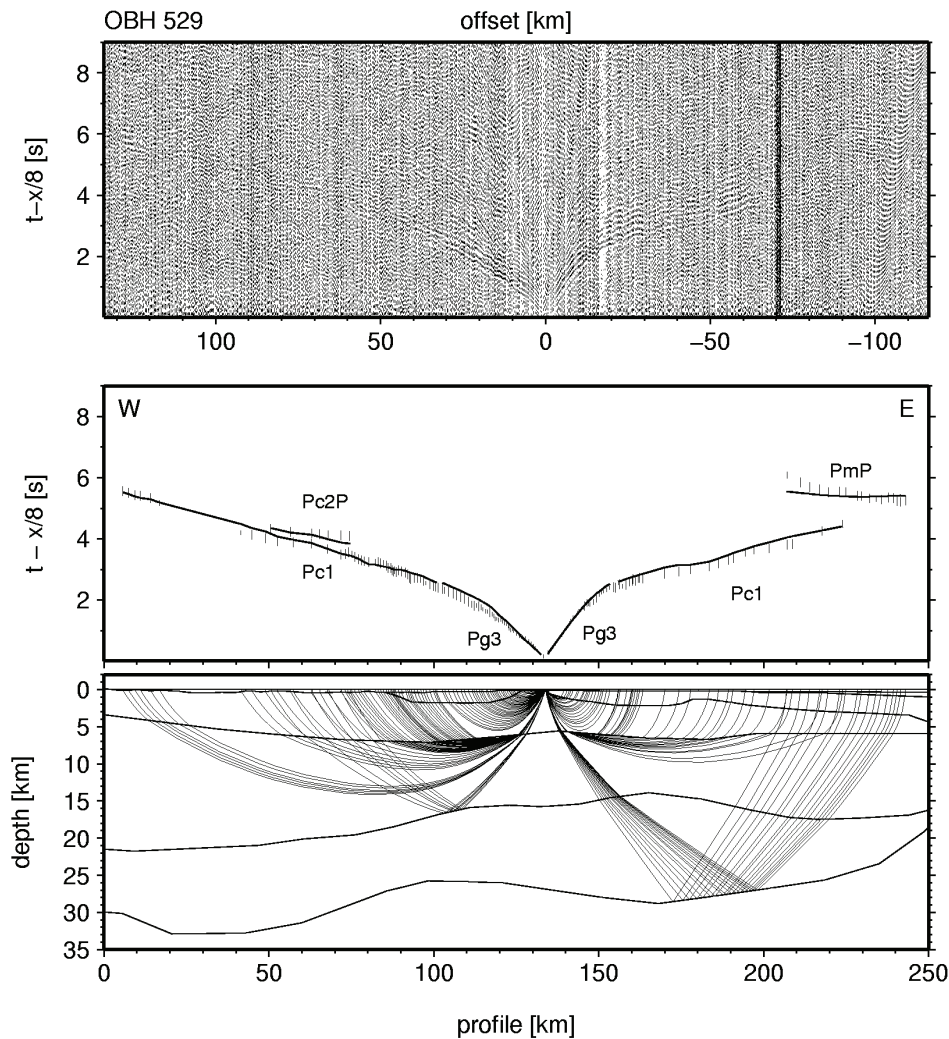


Figure 5.8: c) (Continued.)

5.5.3 Gravity models

2-D gravity modelling was performed for both transects to verify the consistency of the P-wave velocity models with the observed Bouguer anomalies. An initial density model was derived from conversion of all P-wave velocity nodes to density using a Nafe and Drake curve (Nafe and Drake 1957) approximation after Ludwig *et al.* (1970). Velocity layers were partly split into separate polygons with different densities where appropriate, but each polygon was assigned with a constant density value. Adjustments to the mantle density were necessary in order to fit the gentle rise of the observed gravity data towards the oceanic part of the models. Thus, the sub-continental mantle was set to 3.31 g cm^{-3} and beneath the oceanic crust to $3.24 - 3.26 \text{ g cm}^{-3}$. The first approximation with a constant density of 3.05 g cm^{-3} for the lower crustal layer caused also a major misfit. A constant density of 3.15 g cm^{-3} provided a better fit. Minor adjustments were applied to the upper and middle crustal layers to obtain an even closer fit of the calculated and measured gravity anomalies. The final gravity models yield maximum deviations (residuals) to the observed gravity anomalies of 15.4 mGal for AWI-20030400 and 19.3

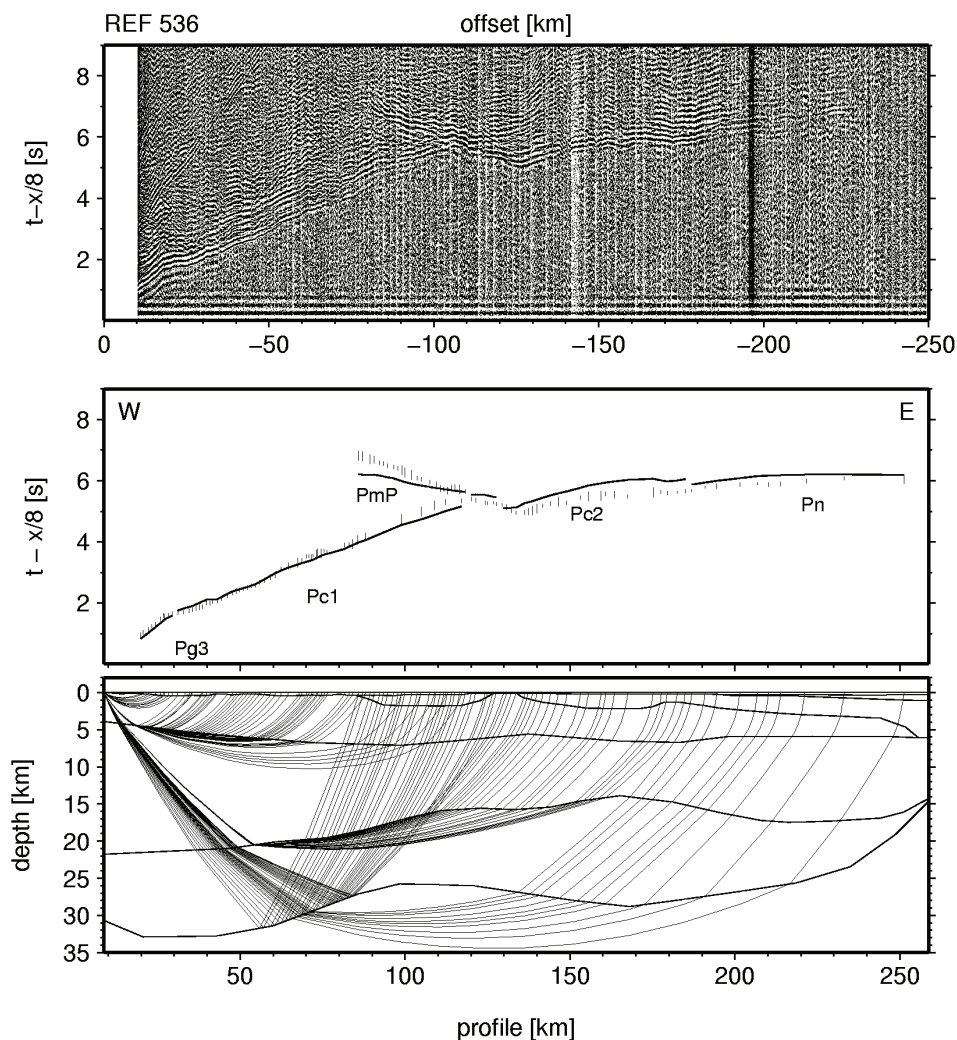


Figure 5.8: d (Continued.)

mGal for AWI-20030500. Density variations larger than $\pm 0.02 \text{ g cm}^{-3}$ for sedimentary and upper crustal layers and $\pm 0.01 \text{ g cm}^{-3}$ for lower crustal layers and the mantle would yield significant misfits to the observed Bouguer anomalies. The results of the gravity modelling are shown in Figures 5.9 and 5.10. Corresponding densities for the polygons are given in g cm^{-3} . The derived P-wave velocity models

can be verified very well with the gravity models. Oceanic mantle adjustments result from a simple approximation with respect to a warmer temperature compared to the sub-continental mantle and is applied commonly for volcanic rifted margins (Breivik et al. 1999; Schmidt-Aursch and Jokat 2005b). Three minor misfits occur at profile AWI-20030500 while the approximation for profile AWI-20030400 is excellent. In the continental part between km 0 and 140, misfits can be related to 3-D effects of intrusions and/ or sediment basins, which can not be constrained in details by the 2-D model. Misfits within the continent-ocean transition zone between km 200 and 290 might result also from the unresolved crust-mantle boundary between km 220 and 240 (Figures 5.6 and 5.10). The top of the ridge between km 360 and 390 was modelled with a low density of 2.1 g cm^{-3} in order to match the measured gravity values.

5.6 Interpretation and discussion

First-order structural interpretations derived from the P-wave velocity models and the magnetic data are presented in Figures 5.11 and 5.12. Since both velocity models are quite similar, we provide a joint interpretation of both profiles. Prominent features of each transect are outlined and discussed in detail. Figure 5.13 shows an overview of the tectonic and magmatic results of the interpretations. A comparison with the conjugate Vøring margin will be discussed according to the profiles shown in Figure 5.14.

5.6.1 Continental crust

The onshore geology shown in Figure 5.1 (Escher and Pulvertaft 1995) allows us to interpret Devonian to Carboniferous/Mesozoic sediments in the upper western layers of the seismic profiles (Figures 5.11 and 5.12). We have extrapolated this interpretation along the profiles, considering the P-wave velocities and the gradients, up to km 100 (Figure 5.11) and km 130 (Figure 5.12). However, a significant change in the velocity parameters occurs at these locations. Further eastward of them, the sedimentary layers tilt down and the velocity gradients increase. Additionally, a layer with much slower velocity ($2.0 - 3.0 \text{ km s}^{-1}$) appears on top, which consists presumably of Cenozoic sediments (Figures 5.9 – 5.12). Around Bontekoe Ø (Figures 5.1, 5.2 and 5.12), slower velocities ($3.2 - 5.0 \text{ km s}^{-1}$) in the 40 km wide and 1.5 km deep basin allow us to conclude the presence of volcanically intruded sediments consistent with the exposed plateau basalts on the island (Figure 5.1). An equivalent interpretation for the two 0.7 km deep basins imaged on profile AWI-20030400 (Figure 5.11) near km 50 and 80 is most likely. The transition to the crystalline continental crust at 5 – 6 km depths is interpreted from the change to a lower velocity gradient (Figures 5.9 and 5.10). A Pc2P - reflector and the Moho at ~30 km depth is well resolved on both profiles (Figures 5.6a/c, 5.9 and 5.10). The westward dipping character of the reflectors was also observed on profile 94320 (Schlindwein and Jokat 1999; 2000) and attributed to Mesozoic – Tertiary extensional thinning of the continental crust from 45 km to ~22 km. Those authors concluded that large scale intrusions (Escher and Pulvertaft 1995) in the Mesozoic sedimentary basins and the formation of a magmatic underplate at the base of the continental crust are both consequences of a Tertiary magmatic event. Short wavelength magnetic variations (Figures 5.3, 5.11 and 5.12) that correlate with the area of increasing seismic velocities in the continental crust support this interpretation. A high velocity lower crust is also observed, and its further extent to the east is a notable result of this study. A detailed discussion of this pronounced layer is undertaken in one of the next sections. The coincidence of the eastward lateral increase of seismic velocities, the short wavelength magnetic anomaly pattern, and the onset of magmatic underplating is also remarkable. It indicates an eastward increasing amount of magmatic intrusions in the continental crust and its sedimentary basins during an episode of excess magmatism. We suggest the beginning of the COT occurs at this location (km 100 at AWI-20030400 and km 130 at AWI-20030500) due to major rift-related changes in the crustal structure.

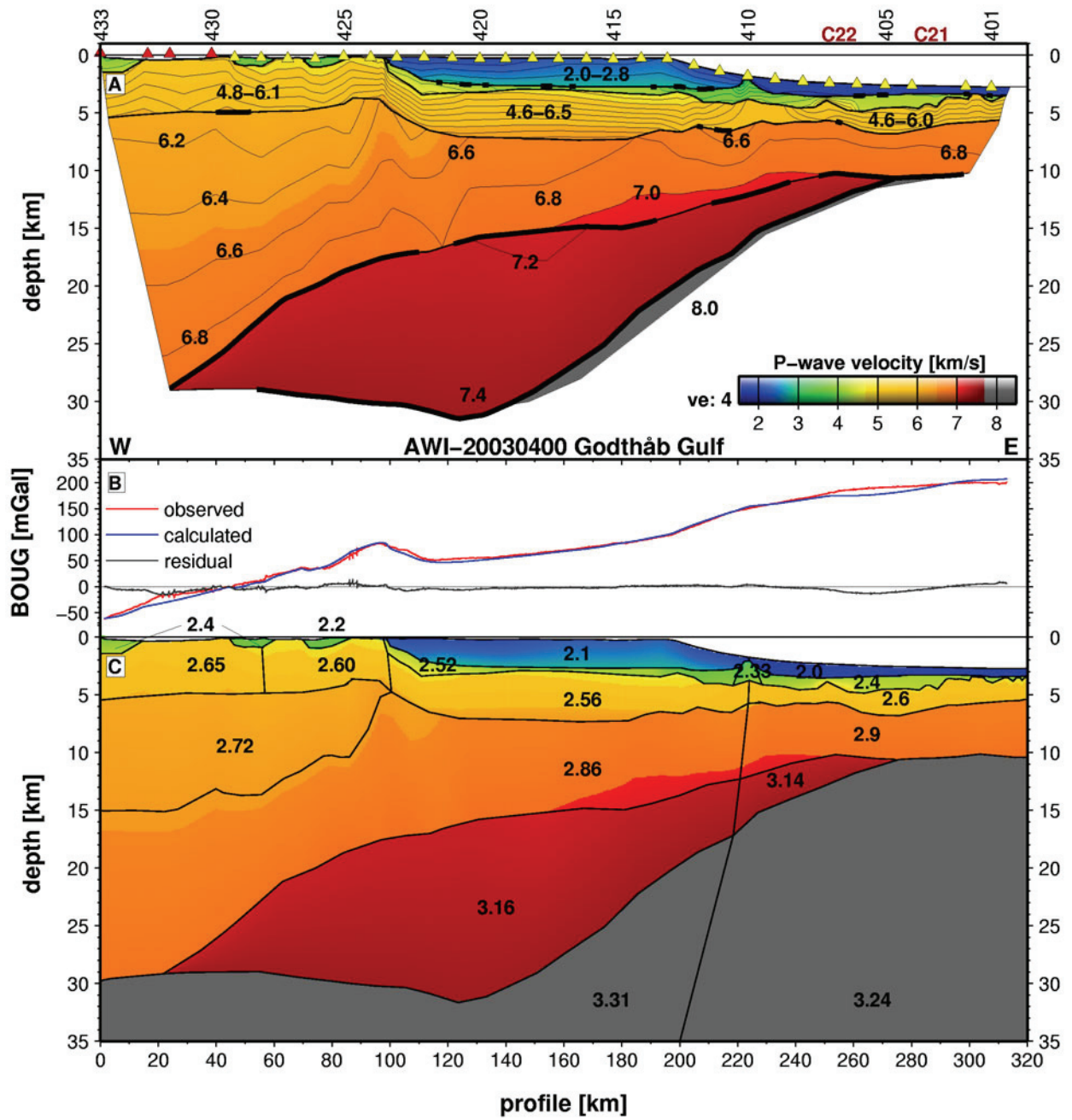


Figure 5.9: A) Interpolated P-wave velocity model for profile AWI-20030400. Contour lines are from 1.6 to 7.4 km s⁻¹ every 0.2 km s⁻¹. Selected contours are individually labelled. Reflectors are marked by thick black lines. The minimum and maximum velocities are shown in the upper layers. See text for other areas with no velocities labelled. Triangles show receiver locations. C21 and C22 mark the position of magnetic ocean spreading anomalies (Figure 5.3). Vertical exaggeration is 4 and comparable to Figures 5.10 – 5.12. The model is only shown where it is constrained by rays. B) Observed and calculated Bouguer gravity anomalies given in mGal. Black line shows residuals. C) 2D gravity modelling for profile AWI-20030400. Background shows velocity grid as above. Black lines mark density polygons. Velocity layers were split into individual polygons where appropriate. P-wave velocities were converted to density using a formal approximation after Ludwig et al. (1970). Water was assigned with 2.67 g cm⁻³ and no terrain correction was applied within the fjord. Densities are given in g cm⁻³.

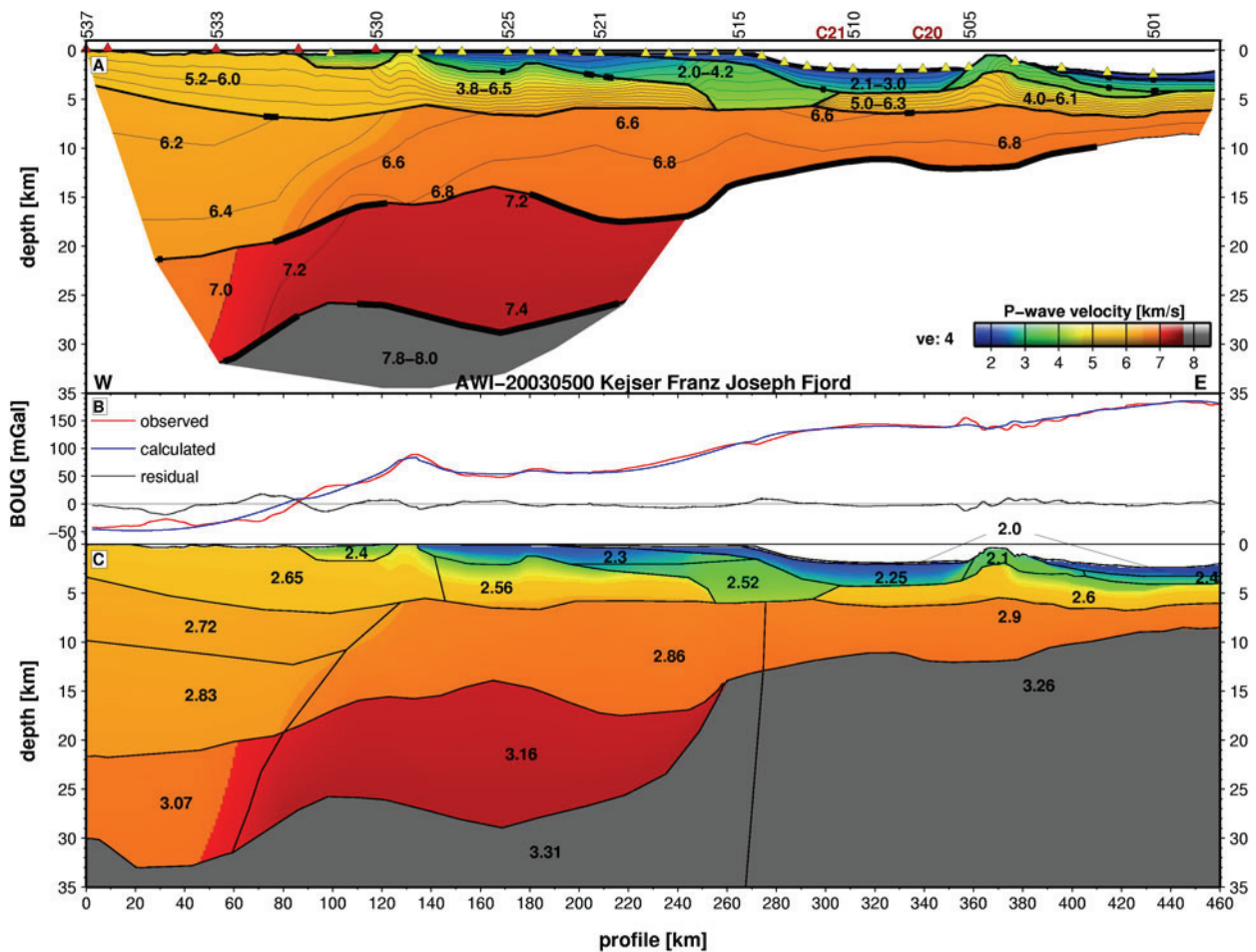


Figure 5.10: A) Interpolated P-wave velocity model for profile AWI-20030500. Model descriptions are as in Figure 5.9. C20 and C21 mark position of magnetic ocean spreading anomalies. B) Observed and calculated Bouguer gravity anomalies given in mGal. Black line shows residuals. C) 2-D gravity modelling for profile AWI-20030500. Model descriptions are as in Figure 5.9C.

5.6.2 The continent – ocean transition (COT)

Earlier, we adopted the definition of the COT by *Whitmarsh & Miles (1995)* for a rough division into the three crustal units, continental, transitional and oceanic crust. Along the two profiles, significant crustal structure variations provide additional constraints for the westward and eastward termination of the COT. The landward terminations are dominated by an increase in seismic velocities in the upper continental crust, and thickening of the lower crustal layer (Figures 5.9 – 5.12). A comparison of the eastern ends of both COTs with wide-aperture CDP profiles published by *Hinz et al. (1987)* (Figure 5.2) provide a pronounced correlation with their identified seaward dipping reflector sequences (SDRs). The following interpretations describe the crustal structure of both COTs in detail:

1. The top sedimentary layer is interpreted as Cenozoic sediments and can clearly be distinguished from the underlying layer by its much slower seismic velocities ($2.0 - 3.0 \text{ km s}^{-1}$). We assume that the seismic velocities of $3.2 - 4.1 \text{ km s}^{-1}$ between km 200 and 250 of profile AWI-20030400 (Figure 5.9) represent an area of basalts extruded in a deep water regime. We associate the basement high at km 225 as a volcano with increased lava flows to the west. This region correlates with the area where *Hinz et al. (1987)* identified SDRs on profile 46 (Figure 5.2) westward of a basement high, which is similar to the one we found at km 225. East of that point,

the crust was described as normal oceanic crust. A projection of SDRs identified on profile 46 would fall into the crustal layer beneath, between km 200 and 225 and in 3 – 7 km depth (Fig 11). *Hinz* (1981) suggested that SDRs were erupted over highly extended continental crust prior to seafloor spreading. Thus, we suggest the seaward termination of the COT at km 230. A similar interpretation is applicable to the sedimentary basin between km 255 and 295 for profile AWI-20030500. The seismic velocities in the lower part of the basin (3 – 6 km depth) show the same range of values (Figure 5.10) as described above. *Hinz et al.* (1987) identified two sequences of SDRs on profile 61 north of profile AWI-20030500 (Figure 5.2), a landward sequence projecting onto km 245 – 255, and an outer sequence onto km 295 – 300. These locations correlate with our modelled termination of the sub-Cenozoic layer for the inner ones in and with the first clearly identified spreading anomaly C21 for the outer ones (Figure 5.12) in 3 – 6 km depth. However, we assume that the low velocities of the deep sedimentary basin between km 255 - 295 (Figures 5.12 and 5.14) are likely to be the result of volcanic intrusions or sills that may have formed at the same time as the emplacement of the SDRs. We discuss this relationship further in the next section. We suggest that the COT terminates east of the inner SDRs at km 255 because the outer location of SDRs correlates with C21 (Figure 5.12).

2. The weakening of the short wavelength magnetic anomalies correlates with increasing depths to the high velocity gradient layers (Figures 5.3, 5.11 and 5.12) and the area of the COT zone is dominated by discontinuous magnetic anomalies with wavelengths of tens of kilometres. In our model the COT zone was formed during a long lasting rift event, which might have had a duration of several million years. During this time Late Cretaceous sediments as well as volcanic material was deposited. While the seismic velocities show an abrupt change at the boundary of this layer, we suggest that it consists mainly out of basalts. This is confirmed through the existence of a volcanic structure at km 180 of profile AWI-20030500 and the basaltic extrusive layer of profile AWI-20030400 as described above. However, the amount of syn-rift sediments compared to the basalts is unknown. The strong velocity gradient in the up to 4.5 km thick layers ($\sim 0.5 \text{ km s}^{-1} \text{ km}^{-1}$ average of both profiles) might suggest that volcanic material dominates. Thus, the long wavelength magnetic anomalies in the transitional zone might originate most likely from this basaltic layer and probably also from middle crustal intrusions. It might have formed before its subsidence together with the onshore basaltic rocks a large volcanic province.
3. Higher crustal velocities, of 6.4 to 6.9 – 7.0 km s^{-1} , compared to 6.45 km s^{-1} for the global average in continental crust (Christensen and Mooney 1995) seem to support an interpretation of magmatically intruded crust in the COT. The significant increase of the velocities in the crystalline crust correlates with the location of the short wavelengths magnetic anomalies and the pronounced negative anomaly (Figures 5.3, 5.9 and 5.10). Thus, we suggest to locate the landward termination of the COT at km 100 for profile AWI-20030400 and at km 130 for profile AWI-20030500. The high velocity (7.15 – 7.4 km s^{-1}) in the lower crustal layer has previously been interpreted as the result of Tertiary magmatic underplating (Schlindwein and Jokat 1999). A detailed discussion is provided in the next section.
4. The pronounced Moho topography on profile AWI-20030500 and the steep increase in Moho depth along profile AWI-20030400 indicates further stretching, and crustal thinning from ~ 30 km to less than 15 km.
5. The intermittent lower crustal reflector, already identified in the continental crustal unit of profile AWI-20030400, merges with the Moho at the seaward end of the transitional unit. Similar reflectors were identified, with gaps, along profile AWI-20030500, and by *Schlindwein & Jokat* (1999).
6. The first clearly identified seafloor spreading anomalies are C22 and C21 (Figures 5.3, 5.11 and 5.12), marking the beginning of normal oceanic crustal accretion.

Scott (2000) placed the continent – ocean boundary (COB) near our landward termination of the COT (Figure 5.13). His arguments were based on magnetic lineations that he interpreted as evidence for oceanic crust. *Scott* (2000) attributed the incoherency of the lineations to thick Cenozoic sediments overlying the area, and to be overprinted by intrusions associated with the separation of the Jan Mayen block from the East Greenland margin. Our data confirm the presence of up to 3 – 5 km thick Cenozoic sediments across the shelf region, and do not preclude a magmatic influence of the Jan Mayen break-up in that area. However, the seismic data reveal a concealed basaltic and syn-rift sedimentary layer extending close to the proposed location of SDRs (*Hinz et al.* 1987), which rest on highly extended continental crust.

The COB of *Tsikalas et al.* (2002), based mainly on plate reconstructions, is located 50 - 70 km west of C22, near OBH 417 on profile AWI-20030400 and OBH 521 on profile AWI-20030500 (Figure 5.13). The profiles show no distinct structural changes in the seismic velocity models in this area and thus, do not support a COB at that location.

The above summaries of the structure of the transitional area and of the COB controversy lead us to conclude that it is only possible to define a COT at the East Greenland margin. According to *Schlindwein & Jokat* (1999), tectonic activity shifted from west to east in Mesozoic times and led to crustal extension. These authors proposed crustal thinning, magmatic intrusion and underplating continued into Tertiary times. The transitional zones of both profiles contain evidence for all these processes. The near surface magmatic intrusions interpreted from magnetic data, and the increase of upper crustal velocities from west to east, provide constraints on the landward limit of the COT. For the seaward termination of the COT, we applied the definition of *Hinz* (1981), that the eruption of SDRs occurs over highly extended continental crust during the final phases of rifting. The projection of *Hinz et al.*'s (1987) SDRs onto our profiles, and the presence of magnetic spreading anomalies C22 and C21, constrain the seaward edges of the COTs along the seismic profiles. Thus, we propose a COT width of 125 km on profile AWI-20030400 (km 100 – 225) and also 125 km on profile AWI-20030500 (km 130 – 255). The total crustal thicknesses of the COTs decrease from west to east from 29 to 13 km (AWI-20030400) and 27 to 10 km (AWI-20030500), respectively. There is no evidence on either profile for either rotated fault blocks to shift the landward boundaries of the COTs further east, or SDRs/oceanic crust to shift the seaward termination further west.

COT zones for volcanic rifted margins have a wide range in width. Seismic profiles from south-east Greenland reveal a range of 50 – 70 km (*Holbrook et al.* 2001). and only up to 50 km is reported from the Norwegian margins (*Kodaira et al.* 1995; *Mjelde et al.* 2001; *Mjelde et al.* 2005). Wider transition zones of 80 - 100 km are reported from the U.S. Atlantic margin (*Holbrook et al.* 1994a; *Holbrook et al.* 1994b) and 150 – 200 km wide from the Namibia margin (*Bauer et al.* 2000). In contrast, the COT of the East Greenland volcanic margin is also exceptionally wide and the landward and seaward boundaries cannot be unequivocally identified. However, the architecture of the East Greenland transition zone mirrors exceptional and long-lived rifting prior to break-up.

5.6.3 The oceanic crust

Clearly identifiable magnetic spreading anomalies mark the onset of oceanic crust along both profiles (Figures 5.3). Paleocene - Eocene sediments (Figures 5.11 and 5.12) conceal the basement layers, which can be related to typical oceanic layers 2 and 3 due to their seismic velocities and velocity gradients.

On profile AWI-20030400, the magmatic underplating merges into a lower oceanic layer, with velocities consistent with layer 3B (*Fowler* 2005), between km 230 and 270 (Figure 5.11). The oceanic crust is ~11 km thick east of the volcanic basement high (km 230) and thins further eastward to 7 km near anomaly C21. But in this part of the layer it is impossible to establish a boundary between the magmatic underplating and oceanic layer 3B.

The oceanic crustal thickness along profile AWI-20030500 varies within the mean range of 4.8 – 7 km but increase to a maximum of 11.5 km beneath the ridge. The ridge is linked to the Jan Mayen Fracture

Zone (Figure 5.1). The velocity model is consistent with a volcanic character. A thick pile of low velocity sediments is located between the termination of the Mesozoic sediments and the onset of normal oceanic crust (km 255 – 295). Velocities increase slowly, to 4.2 km s^{-1} in 6 km depth, with a strong contrast to 6.6 km s^{-1} below. Similar velocities were obtained from Profile 61 (Hinz et al. 1987; Mutter and Zehnder 1988) in the vicinity of this region (Figure 5.2) and SDRs east and west of it. Mutter & Zehnder (1988) classified also this region also as oceanic crust. A projection of spreading anomaly C22, as shown by Tsikalas et al. (2002), falls into the same region. The new seismic data give reasonable witness of the presence of 6 – 7 km thick oceanic crust based on the Moho depth in 12 – 14 km but an oceanic layer 2 could not be identified due to strong reverberations. We do not preclude the presence of such a layer but if it is present, it must be very thin with a strong velocity gradient. However, a precise identification of an anomaly C22 from the magnetic data (Figure 5.3) between km

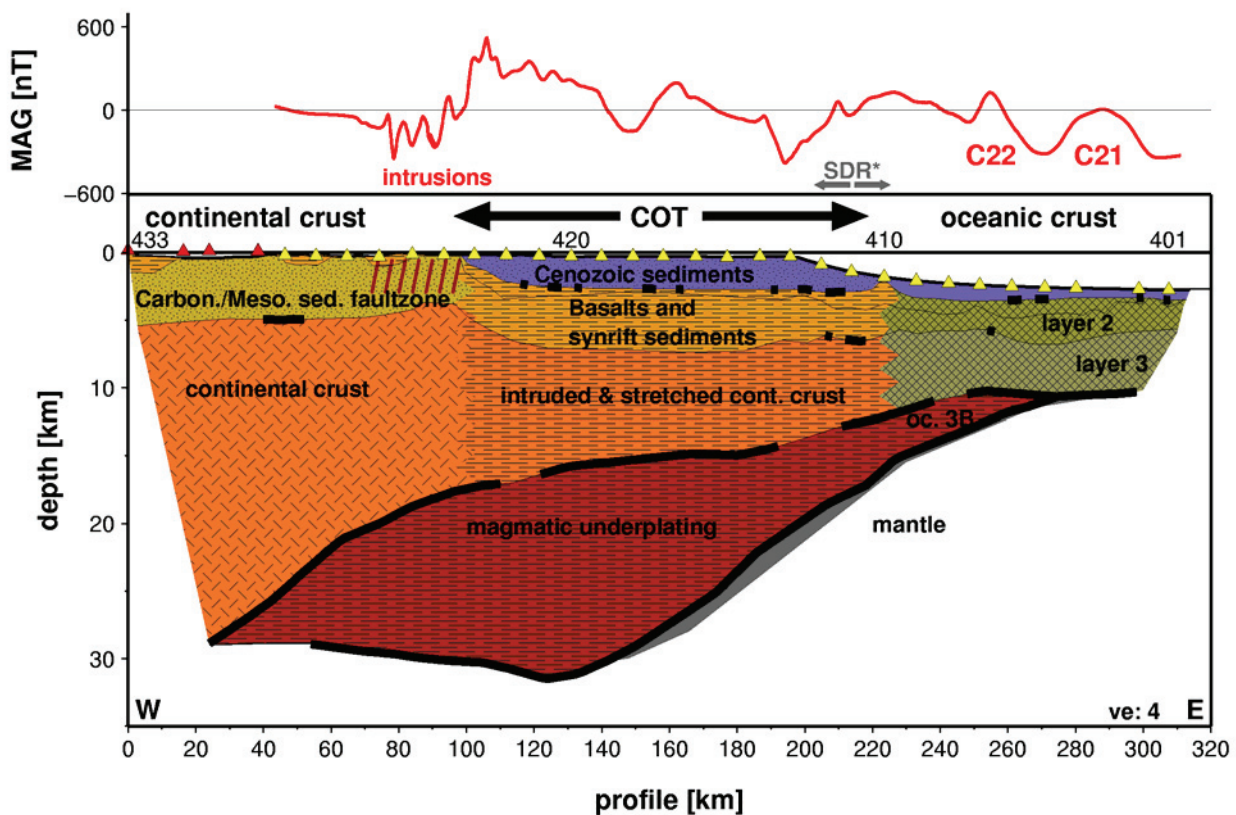


Figure 5.11: Bottom: Interpretation of the P-wave velocity model of profile AWI-20030400. Thick black lines mark wide-angle reflections. Geological units are indicated. COT: continent – ocean transition zone. oc. 3B: oceanic layer 3B. SDR*: Projection of the area of seaward dipping reflectors from profile 46 after Hinz et al. (1987) (see text). Parallel red lines symbolize the location of shallow intrusions as seen in the magnetic data. Different geological units are marked by different patterns. Note the wide COT and the thick magmatic underplating. Top: Red curve shows projected magnetic anomalies (MAG) along the seismic line. Data derived from 5 km magnetic grid (not shown) of the newly acquired airborne data. Note the high amplitude and short wavelength variations within the area of the pronounced negative magnetic anomaly (see Figure 5.2). C22 and C21 mark magnetic ocean spreading anomalies.

255 and 295 on profile AWI-20030500 is not possible owing to the weakening signal strength of the anomaly towards southwest. We suggest a relation of the magnetic anomaly to intrusions into the sedimentary basin during the emplacement of SDRs, and that this part of the profile (km 255 – 295) marks the earliest stage of oceanic crustal accretion, located seawards of the proposed inner SDRs (Hinz et al. 1987).

5.6.4 The lower crustal body (LCB)

A striking result of the P-wave modelling is the thick high velocity ($7.15 - 7.4 \text{ km s}^{-1}$) lower crustal body (LCB), underlying continental crust and the entire COT, which terminates in thickened oceanic crust. The top of the LCB and the Moho are very well constrained by numerous travel time arrivals (Figures 5.6a and 5.6c). Along profile AWI-20030400, the LCB thins gradually towards the east and west while it seems to end abruptly for profile AWI-20030500. The maximum dimensions of the LCB are shown in Table 5.3. Gravity modelling supports the dimensions of the LCBs with densities of $3.14 - 3.16 \text{ g cm}^{-3}$, which differs significantly from normal lower crustal as well as upper mantle densities. Other high velocity layers in the lower crust were interpreted as the result of serpentinized mantle (Holbrook and Kelemen 1993; Kelemen and Holbrook 1995), oceanic layer 3B (Mjelde et al. 2005) or accreted igneous material (Bauer et al. 2000). *Schlindwein & Jokat* (1999) interpreted the LCB off East Greenland as due to Tertiary magmatic underplating and suggest it coincides with a pronounced negative magnetic anomaly extending SE-NW along the margin in the fjord region (Figure 5.2). *Schlindwein & Meyer* (1999) show that the magnetic anomaly is most probably related to Tertiary magmatism, as the basins are intruded by Tertiary dikes and sills and partly overlain by Tertiary tholeiitic basalts (Escher and Pulvertaft 1995). However, the eastward extent of the LCB remained unknown due to the lack of seismic data coverage seawards of the margin. The new data show a completely different picture of a remarkably wide and thick LCB off the East Greenland fjord region whose full extent is estimated in Figure 5.13. We suggest the LCB is due to magmatic underplating that terminates eastward in a thin and immediately decreasing oceanic layer 3B. The southern termination is given by evidence for further magmatic underplating identified on profile 94340 (Schlindwein and Jokat 1999) (Figure 5.2). The negative magnetic anomaly terminates in a magnetic quiet zone further north, where coincidentally, no LCB was identified on seismic refraction profiles south of Shannon Island (*Schlindwein* 1998). The landward limits in Figure 13 are restricted by the models after *Schlindwein & Jokat* (1999) and interpolated along the margin with respect to the west dipping character of the LCB on

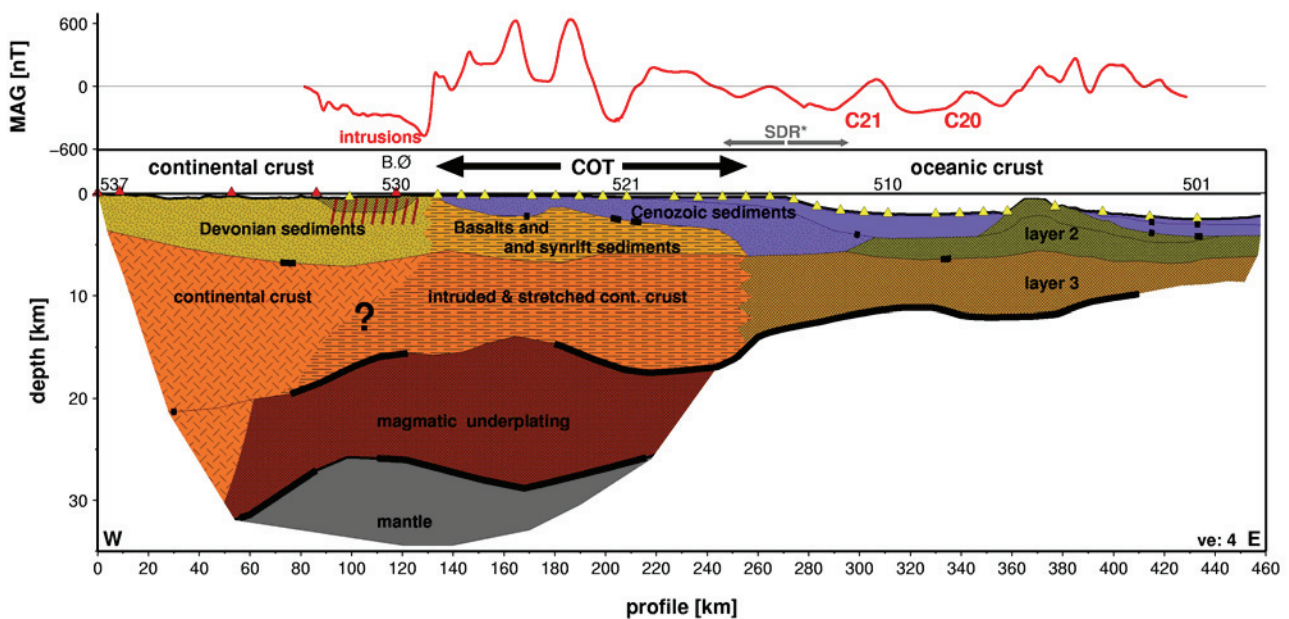


Figure 5.12: Interpretation of the P-wave velocity model of profile AWI-20030500. See Figure 5.11 for descriptions. B.Ø: Bontekoe Ø. SDR*: Projection of the area of seaward dipping reflectors (see text) from profile 61 after *Hinz et al.* (1987). Large question-mark marks the questionable landward boundary of the COT within the crust due the lateral increase of seismic velocities (see Figure 5.10).

profile AWI-20030400 (Figure 5.11). Thus, it is possible to interpret almost the entire shelf as being underlain by a magmatic underplate, from Kong Oscar Fjord to probably south of Shannon Island.

Profile	Width LCB	Thickness LCB	Reference
East Greenland AWI-20030400	~225 km	16 km	this paper
East Greenland AWI-20030500	~190 km	15 km	this paper
Southeast Greenland (P III)	150 km	9 km	1
Vøring Margin P99 (Figure 5.12)	~150 km	12.5 km	2
US – East Coast	100 – 190 km	10 – 15 km	3, 4
Namibia	150 – 200 km	~18 km	5, 6
Hatton Bank	90 km	15 km	7

Table 5.3: Maximum widths and thicknesses of lower crustal bodies (LCB). References for LCBs: 1. (Hopper et al. 2003); 2. (Mjelde et al. 2005); 3. (Holbrook and Kelemen 1993); 4. (Kelemen and Holbrook 1995); 5. (Gladchenko et al. 1998); 6. (Bauer et al. 2000); 7. (Morgan et al. 1989).

5.6.5 Rift propagation

It is interesting to speculate whether underplating developed during a single event in Tertiary times, or if other pre-rift or post-break-up processes fed magma into the lower crust. On the other hand, the wide COT implicates a pinch-out of the spreading anomalies along the margin (Figure 5.13) from north to south which gives rise to debate about rift propagations. Three scenarios could be possible, as follows: Shifting of the rift-axis led to long – term rifting across the margin in the vicinity of the Kejsler Franz Joseph Fjord and gave rise to the unusually wide COT in Mesozoic to Tertiary times. Direct evidence for shifts of the rift-axis can be seen in the pronounced Moho topography (Schlindwein and Jokat 1999). Several Moho slopes and plateaus exist off Kejsler Franz Joseph Fjord, but the Godthåb Gulf profile shows only a steep but steady decrease of the Moho to the onset of oceanic crust. Investigations on the conjugate Lofoten and Vøring margin, off Norway, have also revealed vertical and lateral variations in crustal structure and composition resulting from a complex rifting history during the late Cretaceous and early Tertiary times (Mjelde et al. 1997; Mjelde et al. 1998; Raum et al. 2002; Mjelde et al. 2005; Tsikalas et al. 2005). The long – term rifting supported excessive upwelling of magmatic material, and intruded the stretched crust and, probably, sedimentary basins.

A second scenario involves the separation of the Jan Mayen block from East Greenland in Oligocene/Miocene times (Gudlaugsson et al. 1988). *Scott* (2000) assumed the presence of intrusions related to this event. In the first stage, Tertiary rifting was accompanied by magmatic underplating in this region (Schlindwein and Jokat 1999). Subsequently, more magmatic material was emplaced prior to the break-up of the Jan Mayen microcontinent (25 Ma). But the velocity models reveal no any evidence for two stages of emplacement, however. In such a case one might expect a reflection from inside the high velocity body, which would support this interpretation.

Another possible interpretation from the newly derived results is an episode of rift propagation from north to south, with retarded break-up and initiation of seafloor spreading in this region. The study area shows many characteristics consistent with having been part of a ‘locked zone’ on the spreading axis (*Courtillot* 1982; *Vink* 1982). Break-up started with chron C24B in the north and the oblique angle of the anomalies C24A, C23 and C22 along the margin between Shannon Island and the Jan Mayen Fracture Zone (Figure 5.13) is consistent with a N – S rift propagation. The magnetic data provide good evidence that magnetic anomalies C24A-C21 terminate against the East Greenland COT rather than continuing beneath the shelf like in other interpretations.

Magmatic material generated during break-up remained pooled beneath the locked zone until lithospheric separation was completed in this area. Average propagation velocities of $47 \pm 5 \text{ km Ma}^{-1}$ (Figure 5.13c) can be calculated from the anomaly identifications along the margin with the errors related to picking uncertainties. A preliminary calculation of the half spreading rates along a transect is shown in Figures 5.13a and 5.13b. The calculation relates to the zero crossings between the reversed

older and normal younger anomaly. Oceanic half spreading velocities decreased from 27 km Ma⁻¹ to 11.7 km Ma⁻¹, which is much slower than the rift propagation. Further south of C21, younger spreading anomalies terminate towards the Mayen Fracture Zone (Figure 5.2).

The existence of a wide COT and voluminous magmatic underplating is direct evidence of a long-term rifting process and rift-related magmatism. The reasons for the long – term rifting or the existence of a locked zone within a propagating rift might be related to pre-rift processes, which are not fully understood yet. *Schlindwein & Jokat* (1999) concluded, from the large differences of volcanic extrusion and crustal intrusions north and south of Kong Oscar Fjord, that pre-existing lithospheric structures guided the magmatic activity. However, the complexity of these tectonic and magmatic events is mirrored in the asymmetry of adjacent and conjugate margin architectures.

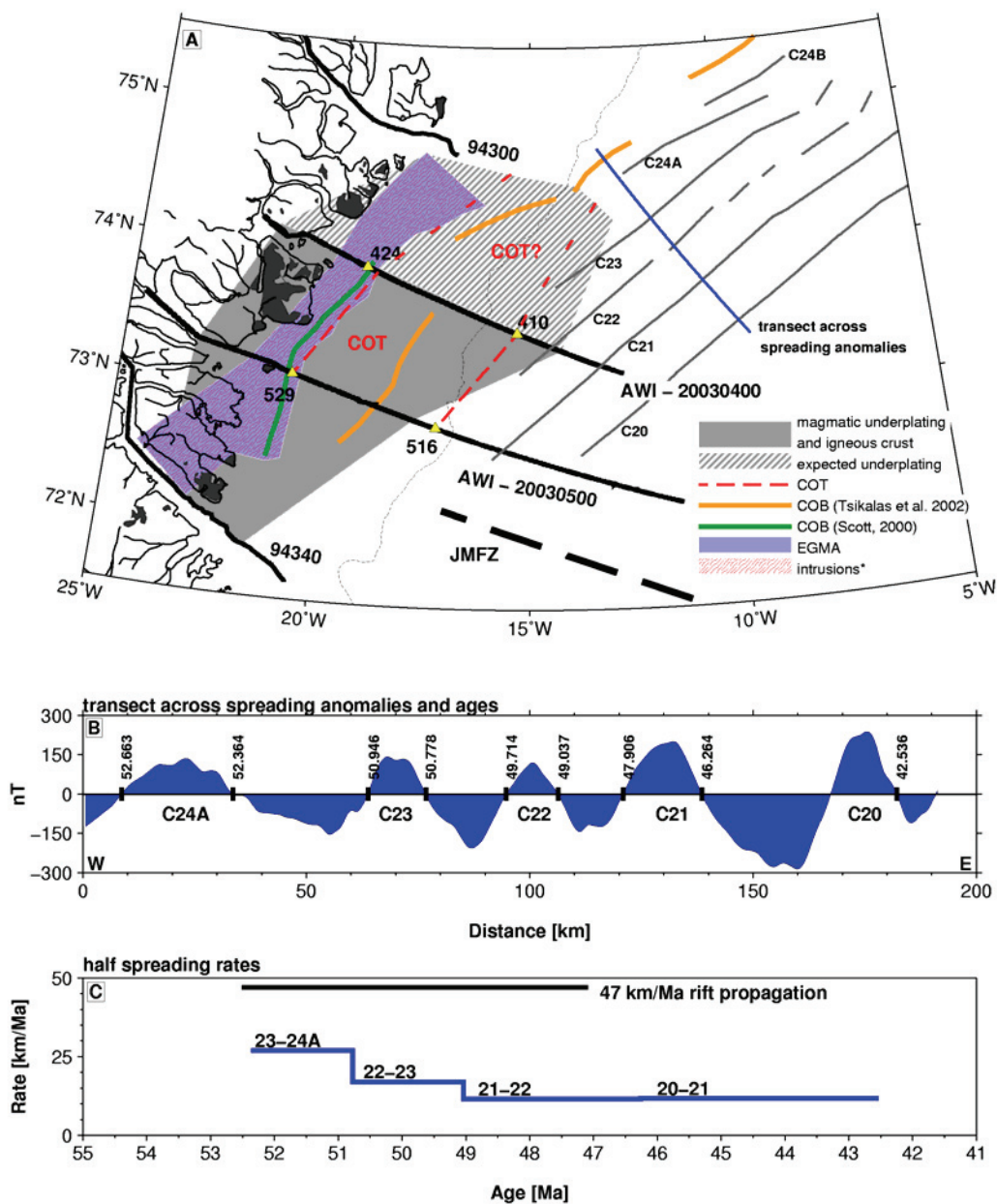
5.6.6 Competitive interpretation of the conjugate margins

A comparison of the conjugate margin structures off East Greenland and Norway provides constraints of the processes involved in the volcanic margin formation and evolution. On the conjugate margin numerous OBS profiles were acquired to investigate the crustal structure of the Vøring Plateau (Mjelde et al. 1997; Mjelde et al. 2001; Raum et al. 2002; Mjelde et al. 2005). Profile 99, across the outer Vøring Margin (Mjelde et al. 2005), turns out to be an adequate counterpart to profile AWI-20030400 (Figure 5.14c). A reconstruction model after *Rowley and Lottes* (1988) with an interpolated angle of 9.68° for a C22 rotation shows a good approximation of the anomalies and a ~65 km offset of the two conjugate profiles. Thus, a comparison of the two seismic profiles of the conjugate margins should be seen as a general consideration within the limits of the reconstruction models.

Both profiles extend from continental to oceanic crust, crossing an area of complex magnetic anomalies (Figures 5.14a and 5.14b). Both profiles show similar crustal layering at spreading anomaly C22 (Figure 5.14c), where thickened oceanic crust (~9 km) is modelled. An increase to 18.5 km towards C23 at profile 99 is in contrast to the area east of the volcanic basement high at km 225 in our model. The absence of pre-C22 magnetic anomalies in our data is a major difference between the models. On the East Greenland margin, we related the magnetic anomalies landward of C22 to strong intrusions in the stretched continental crust. If the margins were symmetrical, then profile AWI-20030400 should show anomaly C24B near km 170 (Figure 5.14c). In contrast, we have presented good evidence for stretched and intruded transitional crust beneath thick Cenozoic and Mesozoic sediments at this location, rather than oceanic crust. On the other hand, the interpretation of C24B off the Vøring Margin is questionable due to the ambiguous magnetic anomaly pattern around the Vøring Plateau (5. 14a). The landward increase of Moho depth to ~30 km along profile AWI-20030400 is a further major difference to the Moho depth of

20 km on the conjugate margin. The eastern and western boundary structures seem similar of the COT on the conjugate profiles. The landward boundaries of the COTs are characterised by a lateral increase of seismic velocities and thickening of the transitional crust. The seaward boundaries are located near the proposed inner SDRs. But the widths of the COTs are different. *Mjelde et al.* (2005) suggested a width of 25 km on profile 99. The East Greenland margin, however, has undergone long term stretching and, thus, the transitional zone is 125 km.

The controversy surrounding the interpretation of the magnetic anomalies significantly influences the structural models. Although local similarities in the crustal structures of the continental margin can be identified, the major and tectonically most relevant features, the COT and LCB differ greatly in their extents and thicknesses. The asymmetric crustal architecture of conjugate margins requires also a complex history of rifting and/or post-rifting events were involved but not considered so far. Further examinations of tectonic and magmatic features along the conjugate margin profiles and direct line-up comparisons could bring some more light into the processes involved in the margin formations.



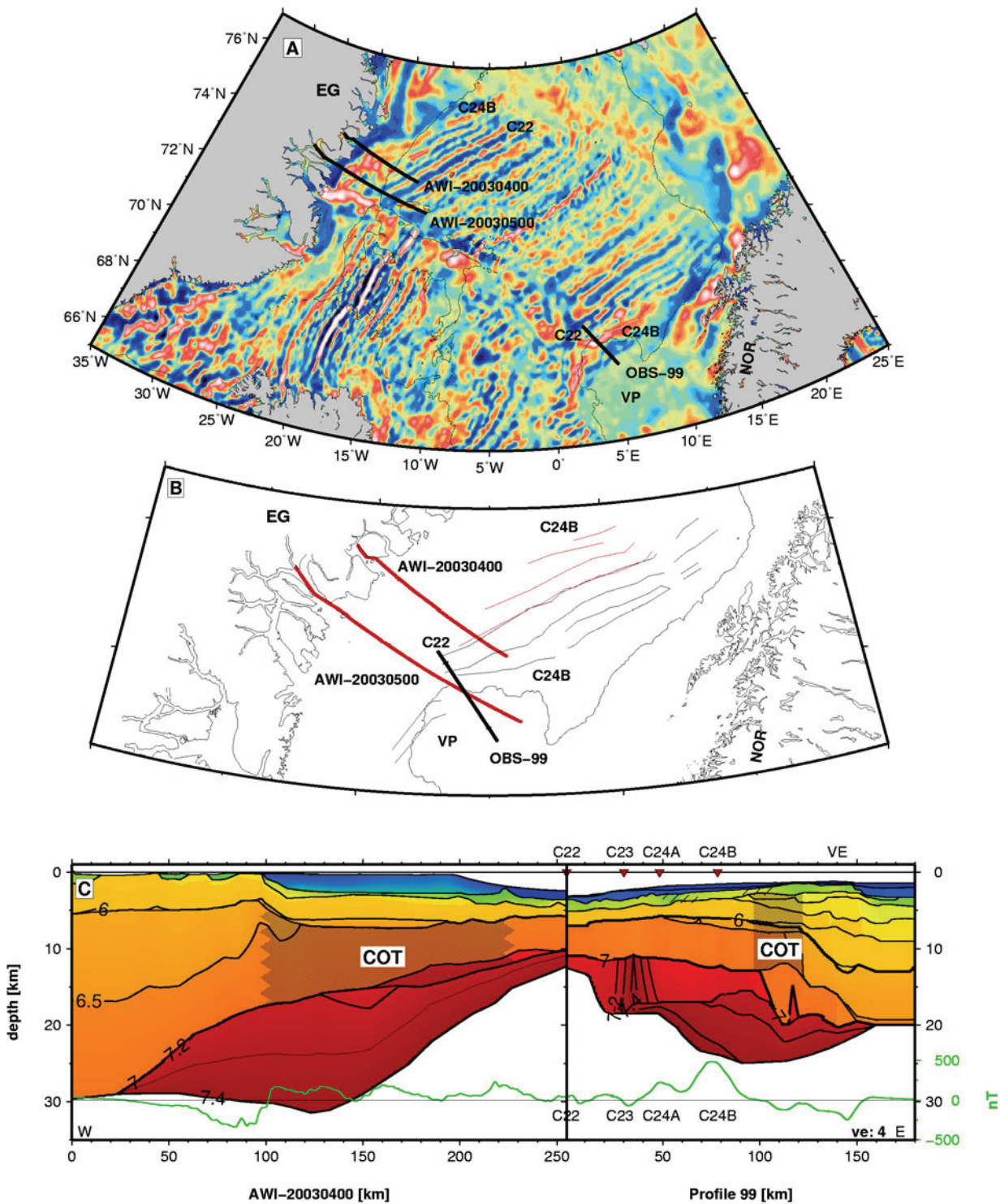


Figure 5.14: Comparison of the East Greenland profile AWI-20030400 and the Vøring Margin seismic profile OBS-99 after Mjelde et al. (2005). A) Present day location of seismic profiles shown as black lines. Background shows regional magnetic grid (Verhoef et al. 1996). White lines mark spreading anomalies. C22 and C24B are labelled. Thin black lines represent the 1500m bathymetric contour. B) 49.7 Ma (C22) reconstruction after Rowley and Lottes (1988). Thick lines show seismic profiles. Thin red lines mark locations of western magnetic anomalies C24b – C22. Thin black lines mark eastern spreading anomalies. The present day 1500 m contour is shown as reference. C) Line-up of both P-wave velocity models in same scale (vertical exaggeration: 4). Colours equivalent to 5. 9. Selected contour lines are shown and labelled (6.0, 6.5, 7.0, 7.2 and 7.4 km s⁻¹). Shading marks the COTs. Green line shows regional magnetic data along the transects. Spreading anomalies are shown after Mjelde et al. (2005). Note the different occurrence of the anomalies on both sides. VE: Vøring Escarpment.

5.7 Conclusion

Regional models were established along two profiles across the East Greenland continental margin between 72°N and 74.5°N. This dataset provides an insight into the lower crustal architecture in the prolongation of Godthåb Gulf and Kejser Franz Joseph Fjord. The consistency of the P-wave velocity models were verified by 2-D gravity modelling and were interpreted in combination with regional magnetic data and an additional improved high resolution airborne magnetic data set. In this study we focused on the examination of the COT and the extent of a lower crustal body associated with magmatic underplating.

One main result is the existence of a 120 – 130 km wide COT, that is characterized by high seismic velocities in the stretched and thinned continental crust ($6.6 - 7.0 \text{ km s}^{-1}$) and by a thick high velocity lower crustal body ($7.15 - 7.4 \text{ km s}^{-1}$). The maximum thicknesses of the lower crustal bodies are 15 – 16 km with lateral extents of 190 – 225 km. A well defined intra-crustal reflector is assumed to merge with the Moho in both directions. The Moho shows a distinct topography within the COT and rises from ~30 km to 11 – 14 km near the onset of oceanic crust. The P-wave velocity models reveal a concealed basaltic layer mixed with synrift sediments whose presence supports the interpretation of long term rifting and a highly extended transitional crust across almost the entire shelf. Given this interpretation, the presence of ocean spreading anomaly C23 – C24B is unlikely between the Godthåb Gulf and Jan Mayen Fracture Zone. The magnetic anomalies are rather related to magmatic intrusions into the transitional crust and the basaltic/synrift sedimentary basin.

A N – S rift propagation between Shannon Island and the Jan Mayen Fracture Zone can be deduced from the SW - NE orientation of the spreading anomalies C21 – C24B, and is consistent with the interpretation of tectonic and magmatic features on the seismic profiles.

Contrasting interpretations of the conjugate margin crustal structures of East Greenland and the Vøring Margin reveal significant asymmetries of the crustal architecture. The major differences are a 10 km deeper Moho in the continental unit of the East Greenland margin, a wider COT, and a larger high velocity body, interpreted as magmatic underplating rather than as oceanic layer 3B.

5.8 Acknowledgements

Data acquisition along these profiles and their analyses was supported by the European Science Foundation (ESF) and the Deutsche Forschungsgemeinschaft within the EUROMARGINS project. The manuscript improved greatly by comments from V. Schlindwein, M.C. Schmidt-Aursch, G. Eagles and the anonymous reviewers. All figures were created with GMT (Wessel and Smith 1998). Magnetic data processing and 2-D gravity modelling was performed with the commercial software *LCT* provided by *Fugro*.

5.9 References

- Bauer, K., S. Neben, B. Schreckenberger, R. Emmermann, K. Hinz, N. Fechner, K. Gohl, A. Schulze, R. B. Trumbull and K. Weber (2000). "Deep structure of the Namibia continental margin as derived from integrated geophysical studies." Journal of Geophysical Research **105**(B11): 25829-25853.
- Breivik, A. J., J. Verhoef and J. I. Faleide (1999). "Effect of thermal contrasts on gravity modeling at passive margins: Results from the western Barents Sea." Journal of Geophysical Research **104**(B7): 15293-15311.
- Cande, S. C. and D. V. Kent (1995). "Revised calibration of the geomagnetic polarity timescale for the Late Cretaceous and Cenozoic." Journal of Geophysical Research **100**(B4): 6093-6095.

Christensen, N. I. and W. D. Mooney (1995). "Seismic velocity structure and composition of the continental crust: a global view." Journal of Geophysical Research **100**(B7): 9761-9788.

Courtillot, V. (1982). "Propagating rifts and continental breakup." Tectonics **1**(3): 239-250.

Escher, J. and T. Pulvertaft (1995). "Geological Map of Greenland, 1:2 500 000." Geological Survey of Greenland.

Fechner, N. and W. Jokat (1996). "Seismic refraction investigations on the crustal structure of the western Jameson Land basin, east Greenland." Journal of Geophysical Research **101**(B7): 15867-15881.

Fowler, C. M. R. (2005). "The solid earth: an introduction to global geophysics." **2nd ed.**

Gladchenko, T. P., J. Skogseid and O. Eldholm (1998). "Namibia volcanic margin." Marine Geophysical Researches **20**: 313-341.

Gudlaugsson, S. T., K. Gunnarson, M. Sand and J. Skogseid (1988). Tectonic and volcanic events at the Jan Mayen Ridge microcontinent, in A. C. Morton and L. M. Parson (ed.), Early Tertiary Volcanism and the Opening of the NE Atlantic, Geological Society Special Publication. **39**: 85-93.

Henriksen, N., A. Higgins, F. Kalsbeek and T. Pulvertaft (2000). "Greenland from Archaean to Quarternary; descriptive text to the geological map of Greenland, 1: 2 500 000." Geol. Greenland Surv. Bull. **185**: 1-93.

Hinz, K. (1981). "A hypothesis on terrestrial catastrophes wedges of very thick oceanward dipping layers beneath passive continental margins; their origin and palaeoenvironmental significance." Geologisches Jahrbuch **E2**: 3-28.

Hinz, K., J. C. Mutter, C. M. Zehnder and N. S. Group (1987). "Symmetric conjugation of continent-ocean boundary structures along the Norwegian and East Greenland margins." Mar. Petrol. Geol. **3**: 166-187.

Holbrook, W. S. and P. B. Kelemen (1993). "Large igneous province on the US Atlantic margin and implications of magmatism during continental breakup." Letters of Nature **364**: 433-436.

Holbrook, W. S., H. C. Larsen, J. Korenaga, T. Dahl-Jensen, I. D. Reid, P. B. Kelemen, J. R. Hopper, G. M. Kent, D. Lizarralde, S. Bernstein and R. S. Detrick (2001). "Mantle thermal structure and active upwelling during continental breakup in the North Atlantic." Earth and Planetary Science Letters **190**: 251-266.

Holbrook, W. S., G. M. Purdy, R. E. Sheridan, L. Glover III, M. Talwani, J. Ewing and D. Hutchinson (1994b). "Seismic structure of the U.S. Mid-Atlantic continental margin." Journal of Geophysical Research **99**(B9): 17871-17891.

Holbrook, W. S., E. C. Reiter, G. M. Purdy, D. Sawyer, P. L. Stoffa and J. Makris (1994a). "Deep Structure of the U.S. Atlantic continental margin, offshore South Carolina, from coincident ocean bottom and multichannel seismic data." Journal of Geophysical Research **99**(B5): 9155 - 9178.

- Hopper, J. R., T. Dahl-Jensen, W. S. Holbrook, H. C. Larsen, D. Lizarralde, J. Korenaga, G. M. Kent and P. B. Kelemen (2003). "Structure of the SE Greenland margin from seismic reflection and refraction data: Implications for nascent spreading center subsidence and asymmetric crustal accretion during North Atlantic opening." Journal of Geophysical Research **108**(B5): 2269.
- Jakobsson, M., N. Z. Cherkis, J. Woodward, R. Macnab and B. Coakley (2000). "New grid of Arctic bathymetry aids scientists and mapmakers." EOS Transactions of the American Geophysical Union **81**: 89, 93, 96.
- Jokat, W., D. Berger, H. Bohlmann, V. Helm, M. Hensch, D. Joussetin, C. Klein, N. Lensch, P. Liersch, H. Martens, A. Medow, U. Micksch, L. Rabenstein, C. Salat, M. Schmidt-Aursch and A. Schwenk (2004). "Marine Geophysics." Reports on Polar and Marine Research **475**: 11-34.
- Kelemen, P. B. and W. S. Holbrook (1995). "Origin of thick, high-velocity igneous crust along the U.S. East Coast Margin." Journal of Geophysical Research **100**(B7): 10077-10094.
- Kodaira, S., A. Goldschmidt-Rokita, J. M. Hartmann, H. B. Hirschleber, T. Iwasaki, T. Kananzawa, H. Krahn, N. Tomita and H. Shimamura (1995). "Crustal structure of the Lofoten continental margin, off N. Norway, by OBS refraction studies." Geophys. J. Int. **121**: 907-924.
- Larsen, H. C. and C. Marcussen (1992). Sill-intrusion, flood basalt emplacement and deep crustal structure of the Scoresby Sund region, east Greenland, in B. C. Storey, T. Alabaster and R. J. Pankhurst (ed.), Magmatism and the Causes of Continental Break-up, Geological Society Special Publication. **68**: 365-386.
- Ludwig, W. J., J. E. Nafe and C. L. Drake (1970). Seismic refraction, in M. A.E. (ed.), The Sea, Wiley-Interscience. **vol. 4**: 53-84.
- Mandler, H. and W. Jokat (1998). "The crustal structure of central east Greenland: results from combined land-sea seismic refraction experiments." Geophys. J. Int. **135**: 63-76.
- Mjelde, R., P. Digranes, H. Shimamura, H. Shiobara, S. Koaira, H. Brekke, T. Egebjerg, N. Sørenes and S. Thorbjørnsen (1998). "Crustal structure of the northern part of the Vøring Basin, mid-Norway margin, from wide-angle seismic and gravity data." Tectonophysics **293**: 175-205.
- Mjelde, R., P. Digranes, M. Van Schaak, H. Shimamura, H. Shiobara, S. Kodaira, O. Naess, N. Sørenes and E. Vagnes (2001). "Crustal structure of the outer Vøring Plateau, offshore Norway, from ocean bottom seismic and gravity data." Journal of Geophysical Research **106**(B4): 6769-6791.
- Mjelde, R., S. Kodaira, H. Shimamura, T. Kananzawa, H. Shiobara, E. W. Berg and O. Riise (1997). "Crustal structure of the central part of the Vøring Basin, mid-Norway margin, from ocean bottom seismographs." Tectonophysics **277**: 235-257.
- Mjelde, R., T. Raum, B. Myhren, H. Shimamura, Y. Murai, T. Takanami, R. Karpuz and U. Naess (2005). "Continent-ocean transition on the Voring Plateau, NE Atlantic, derived from densely spaced ocean bottom seismometer data." Journal of Geophysical Research **110**.
- Morgan, J. V., P. J. Barton and R. S. White (1989). "The Hatton Bank continental margin-III. Structure from wide-angle OBS and multichannel seismic refraction profiles." Geophys. J. Int. **98**: 367-384.

Mutter, J. C. and C. M. Zehnder (1988). "Deep crustal and magmatic processes: The inception of seafloor spreading in the Norwegian-Greenland Sea." Geol. Soc. Spec. Publ. London **39**: 35-48.

Nafe, J. E. and C. L. Drake (1957). "Variations with depth in shallow and deep water marine sediments of porosity, density and the velocity of compressional and shear waves." Geophysics **22**: 523-552.

Raum, T., R. Mjelde, P. Digranes, H. Shimamura, H. Shiobara, S. Kodaira, G. Haatvedt, N. Sørenes and S. Thorbjørnsen (2002). "Crustal structure of the southern part of the Vøring Basin, mid-Norway margin, from wide-angle seismic and gravity data." Tectonophysics **355**: 99-126.

Rowley, D. B. and A. L. Lottes (1988). "Plate-kinematic reconstructions of the North Atlantic and Arctic: Late Jurassic to Present." Tectonophysics **155**: 73-120.

Saunders, A. D., J. G. Fitton, A. C. Kerr, M. J. Norry and R. W. Kent (1997). The North Atlantic Igneous Province, in J. J. Mahoney and M. F. Coffin (ed.), Large Igneous Provinces, American Geophysical Union Monograph. **100**: 45-94.

Schindwein, V. (1998). Architecture and evolution of the continental crust of east Greenland from integrated geophysical studies. Reports on Polar and Marine Research. Bremerhaven. **270**: 1-148.

Schindwein, V. and W. Jokat (1999). "Structure and evolution of the continental crust of northern east Greenland from integrated geophysical studies." Journal of Geophysical Research **104**(B7): 15227-15245.

Schindwein, V. and W. Jokat (2000). "Post-collisional extension of the East Greenland Caledonides: a geophysical perspective." Geophys. J. Int. **140**: 559-567.

Schindwein, V. and W. Meyer (1999). "Aeromagnetic study of the continental crust of northeast Greenland." Journal of Geophysical Research **104**(B4): 7527-7537.

Schmidt-Aursch, M. and W. Jokat (2005a). "The crustal structure of central East Greenland-I: From the Caledonian orogen to the Tertiary igneous province." Geophys. J. Int. **160**: 736-752.

Schmidt-Aursch, M. and W. Jokat (2005b). "The crustal structure of central East Greenland-II: From the Precambrian shield to the recent mid-oceanic ridges." Geophys. J. Int. **160**: 753-760.

Scott, R. A. (2000). "Mesozoic-Cenozoic Evolution of East Greenland: Implications of a Reinterpreted Continent-Ocean Boundary location." Polarforschung **68**: 83-91.

Tsikalas, F., O. Eldholm and J. I. Faleide (2002). "Early Eocene sea floor spreading and continent-ocean boundary between Jan Mayen and Senja fracture zones in the Norwegian-Greenland Sea." Marine Geophysical Researches **23**: 247-270.

Tsikalas, F., O. Eldholm and J. I. Faleide (2005). "Crustal structure of the Lofoten-Vesterålen continental margin, off Norway." Tectonophysics **404**: 151-174.

Upton, B. G. J. (1988). "History of Tertiary igneous activity in the N Atlantic borderlands." Geol. Soc. Spec. Publ. London **39**: 429-453.

- Upton, B. G. J., C. H. Emeleus and N. Hald (1980). "Tertiary volcanism in the northern E Greenland: Gauss Halvø and Hold with Hope." J. geol. Soc. London **137**: 491-508.
- Verhoef, J., W. R. Macnab, R. Arkani-Hamed and J. M. o. t. P. Team (1996). "Magnetic anomalies of the Arctic and North Atlantic Oceans and adjacent land areas; Open File 3125." Geological Survey of Canada.
- Vink, G. E. (1982). "Continental rifting and the implications for plate tectonic reconstructions." Journal of Geophysical Research **87**(B13): 10677-10688.
- Weigel, W., E. R. Flüh, H. Miller, A. Butzke, G. A. Dehghani, V. Gebhardt, I. Harder, J. Hepper, W. Jokat, D. Kläschen, S. Kreymann, S. Schüßler and Z. Zhao (1995). "Investigations of the east Greenland continental margin between 70° and 72°N by deep seismic sounding and gravity studies." Marine Geophysical Researches **17**: 167-199.
- Wessel, P. and W. Smith, H. F. (1998). "New, improved version of Generic Mapping Tools released." EOS Transactions of the American Geophysical Union **79**(47): pp. 579.
- White, R. S. and D. McKenzie (1989). "Magmatism at rift zones: The generation of volcanic continental margins and flood basalts." Journal of Geophysical Research **94**(B6): 7685-7729.
- White, R. S., D. McKenzie and R. K. O'Nions (1992). "Oceanic Crustal Thickness From Seismic Measurements and Rare Earth Element Inversions." Journal of Geophysical Research **97**(B13): 19683-19715.
- Whitmarsh, R. B. and P. R. Miles (1995). "Models of the development of the West Iberia rifted continental margin at 40°30'N deduced from surface and deep-tow magnetic anomalies." Journal of Geophysical Research **100**(B3): 3789-3806.
- Zelt, C. A. and R. B. Smith (1992). "Seismic Traveltime inversion for 2-D crustal velocity structure." Geophysical Journal International **108**: 16-34.

6 Variations in magmatic processes along the East Greenland volcanic margin

Max Voss, Mechita C. Schmidt-Aursch and Wilfried Jokat

Alfred Wegener Institute for Polar and Marine Research, Columbusstrasse, 27568 Bremerhaven, Germany

E-mails: Max.Voss@awi.de (MV); Mechita.Schmidt-Aursch@awi.de (MSA); Wilfried.Jokat@awi.de (WJ)

6.1 Summary

Seismic velocities and the associated thicknesses of rifted and igneous crust are important for understanding the formation of rifted margins. The measurement of these parameters provides key constraints on the rifting history of, and the differentiation between, non-volcanic and volcanic rifted margins. The driving force of magmatism at volcanic margins, i.e. active or passive upwelling and the temperature anomaly in the lithosphere is often inferred from these geophysical observables. Seismic transects of the East Greenland margin are important for the evaluation of the influence of the mantle plume as the driving force of continental break-up and the formation of the North Atlantic Igneous Province. Here, a compilation of 30 wide-angle seismic velocity models from several publications along the entire East Greenland margin is used to create maps of the depth to basement, depth to Moho, crustal thickness and thickness of high velocity lower crust (HVLC; with velocities above 7.0 km s^{-1}). Firstly, we present two new wide-angle seismic transects, which contribute to the compilation at the northeast Greenland margin and over the oceanic crust between Shannon Island and the Greenland Fracture Zone. Raytracing modelling reveals total traveltime rms-misfits of 100 to 120 milliseconds and χ^2 values of 3.7 and 2.3 for the northern and southern profiles with respect to the data quality and structural complexity. 2D gravity modelling is used to verify the structural and lithologic constraints. The northernmost profile, AWI-20030200, reveals a magma starved break-up and a rapidly thinning oceanic crust until magnetic anomaly C21 (47.1 Ma). The southern seismic transect, AWI-20030300, exhibits a positive velocity anomaly associated with the Shannon High, and a basin of up to 15 km depth beneath flood basalts between Shannon Island and the continent – ocean boundary. Break-up is associated with minor crustal thickening and a rapidly decreasing thickness of oceanic crust out to anomaly C21. The continental region is proposed to be only sparsely penetrated by volcanism and unusually is not underplated by magmatic material at all compared to the vast amount of magmatism further south. Break-up is proposed to have occurred at the seaward boundaries of the continent – ocean transition zones at between ~ 50 and ~ 54 Ma, propagating from north to south based on a joint analysis incorporating transects from the Kejsers Franz Joseph Fjord and Godthåb Gulf. Secondly, we discuss the variation of the HVLC along the East Greenland margin from 60° to 77° N. A distribution chart from East Greenland and transects of its conjugate margin invokes inverted emplacement of prominent landward and seaward HVLC thickness portions from north to south. The northward extent of plume-related magma flow is questioned for the northern parts of the margin. Based on the similar distance to the hotspot track but the great differences in the distribution and thickness of the HVLC, three hypothetical models are presented for the northeast Greenland margin, to explain the observed structural styles. One infers a major feeder dyke and assumes a transfer zone/detachment acting as a barrier to northward magma flow. The second suggests the role of underplating to be taken on by thicker and highly intruded lower crust with several small scale feeder dykes that locally increase the lower crustal velocities. A third model picks up the possibility of a second magmatic event associated with the separation of the Jan Mayen microcontinent. Lithospheric-scale inhomogeneities might be responsible for the heterogeneous melt generation, the inversion of the HVLC distribution in continental and oceanic domains and

differences in its velocities.

Keywords: crustal structure, East Greenland, ray tracing, rifted margin

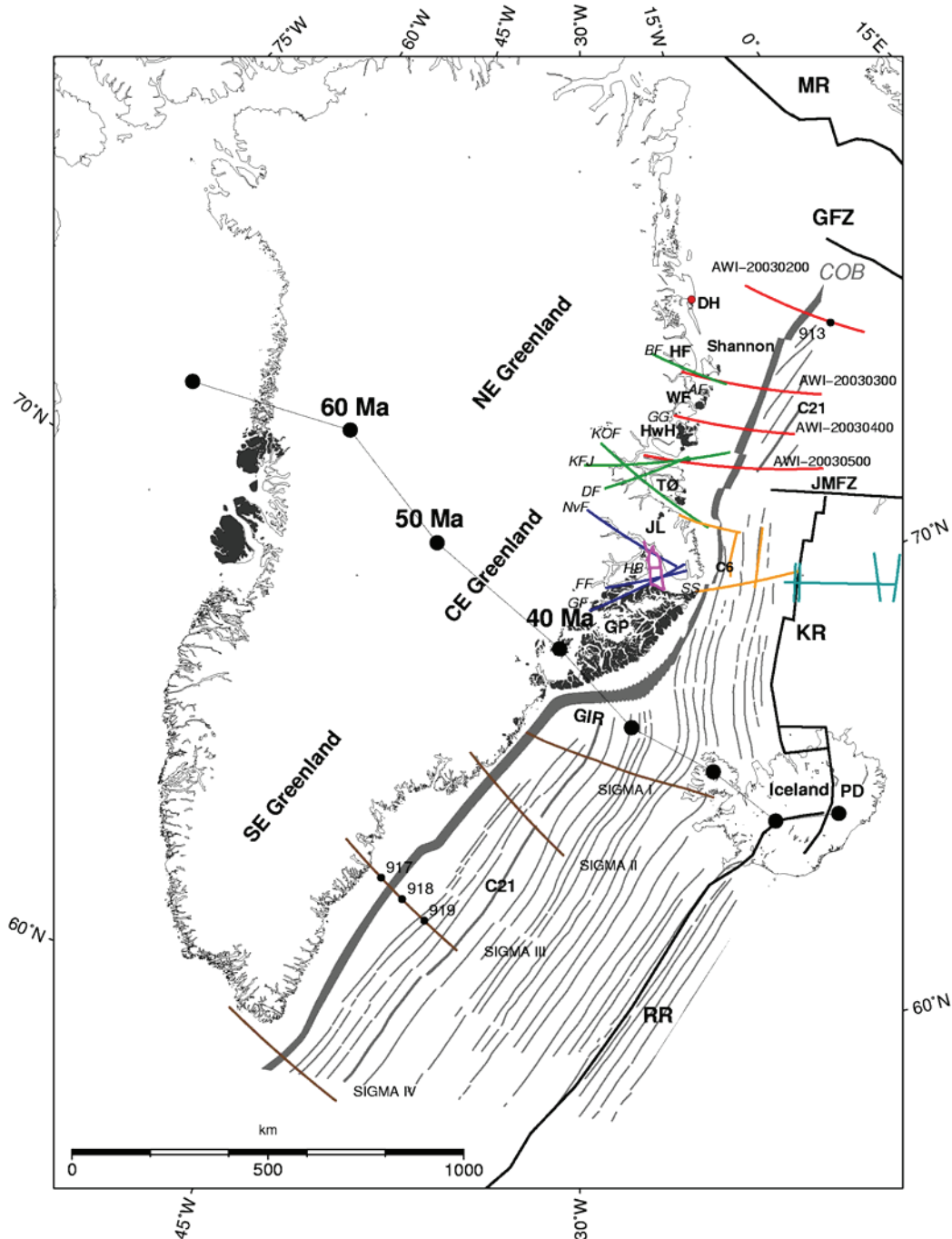


Figure 6.1: The map of East Greenland shows the margin segmentation into northeast (NE), central-east (CE) and southeast (SE) Greenland. Grey shaded continent-ocean boundary (COB), magnetic anomaly lineaments and onshore flood basalts from Escher and Pulvertaft (1995). Magnetic anomalies C21 (marked as thicker gray line) and C6 are labelled. Ridges and fracture zone from Hopper et al. (2003). Hotspot track and location proposed by Lawver and Müller (1994). AWI-2003xxxx lines and SIGMA xx lines (see Table 6.4) are labelled. Colours of seismic lines refer to different sources as described further in the text (Table 6.4). Small black dots mark ODP sites 9xx. Red dot marks Danmarkshavn (DH). Abbreviations are AF, Ardencaple Fjord; BF, Brede Fjord; DF, Dickson Fjord; FF, Føn Fjord; GF, Gåse Fjord; GFZ, Greenland Fracture Zone; GG, Godthåb Gulf; GIR, Greenland Iceland Ridge; GP, Geikie Plateau; HB, Hall Bredning; HF, Hochstetter Foreland; HwH, Hold with Hope; JL, Jameson Land; JMFZ, Jan Mayen Fracture Zone; KFJ, Kejsers Franz Joseph Fjord; KOF, Kong Oscar Fjord; KR, Kolbeinsey Ridge; MR, Mohns Ridge; NvF, Nordvest Fjord; PD, present day location of the Iceland hotspot; RR, Reykjanes Ridge; SS, Scoresby Sund; WF, Wollaston Foreland. Scale is valid for 70° N.

6.2 Introduction

The majority of the North Atlantic margins are of the volcanic rifted type (White et al. 1987; White and McKenzie 1989; Eldholm and Grue 1994). The main characteristics of such margins are (1) seaward dipping reflector sequences (SDRS) (Hinz 1981; Hinz et al. 1987), (2) a high velocity lower crust (HVLC) with seismic velocities exceeding 7.0 km s^{-1} (White and McKenzie 1989; Kelemen and Holbrook 1995) and (3) up to three times thicker than normal initial oceanic crust (e.g. Mutter et al. 1988; White and McKenzie 1989; Eldholm and Grue 1994). Alternative interpretations of HVLC at non-volcanic margins invoke shallow serpentinized mantle rather than magmatic material (e.g. Whitmarsh et al. 1996; Funck et al. 2003). Conductive cooling of decompressed melt can explain the exhumation of mantle material and sparsity of magmatism during long-term and pure-shear rifting (Bown and White 1995) at such margins. They have shown that melt thickness increases with lithospheric thicknesses, extension ratios and mantle temperatures, but reduces significantly with the duration of an extensional episode.

SDRS at volcanic margins are generally observed with reflection seismic methods and have been closely analysed in drillholes (Eldholm et al. 1989; Saunders et al. 1998), while the lower crustal structure is inferred from wide-angle seismic (seismic refraction) modelling. Bulk velocities and thicknesses of the crustal layers obtained from seismic P-wave velocity models, and the corresponding density models are essential for understanding the formation of volcanic rifted margins (White et al. 1987; Mutter et al. 1988; White and McKenzie 1989; Bown and White 1995; Kelemen and Holbrook 1995; Korenaga et al. 2002). These parameters are effective indicators of the temperatures attained during melt production, and of the melting processes, rift duration and the mantle composition.

New seismic refraction data were acquired in the summer of 2003 (Jokat et al. 2004) along four cross-margin profiles between the Jan Mayen and Greenland fracture zones (Figure 1) in order to assess the temporal and spatial evolution of the northeast Greenland margin. Older seismic lines imaged the structure of the continental crust and sedimentary basins beneath the fjords, and these were extended where appropriate. The aims of the transects are to provide a more detailed image of the continent – ocean transition zone (COT) and the rift-related architecture of the continental crust. The COT, generally well observed at non-volcanic margins, is characterized by continental fault blocks, and with the clear onset of oceanic crust marked by magnetic ocean spreading anomalies (Whitmarsh and Miles 1995). Consequently, the continent – ocean boundary (COB) marks the seaward termination of the extended transitional zone. The COB can also be inferred from lateral velocity variations between the continental domain and the newly accreted igneous crust. The COT is commonly less clear at volcanic rifted margins due to the thick wedges of basalts that give rise to seaward dipping reflector sequences, and the large amounts of magmatic intrusions that smear out lateral velocity contrasts. The results of the two southern profiles AWI-20030400 and AWI-20030500 (Figure 6.1) reveal a large scale high velocity lower crust and a high degree of magmatic intrusion into the upper crust over a $\sim 130 \text{ km}$ wide continent – ocean transition zone (Voss and Jokat 2007).

The aim of this study is to provide key constraints on the rifting system and timing of continental break-up drawn from the detailed study of the COT, the rift-related crustal architecture, the distribution of magmatic intrusions and flood basalts, and the extent of the HVLC at the northeast Greenland margin. Along-strike variations of the northeast Greenland margin and its crustal architecture will be discussed, and compared with the southern profiles AWI-20030400 and AWI-20030500. A direct line-up of two conjugate transects, AWI-20030300 and a conceptual model of the Lofoten margin, emphasizes their asymmetric structures. The distribution of the HVLC of the East Greenland and the conjugate margins is shown in relation to the mantle plume distance according to an analysis after Barton and White (1995). Three hypothetical models for the formation of the northeast Greenland margin

are developed from these observations.

6.3 Brief review of geodynamic models for volcanic rifted margin

McKenzie and Bickle (1988) and White and McKenzie (1989) inferred the thick basaltic crust at volcanic rifted margins is the result of enhanced melting due to the passive upwelling of mantle material with anomalously high lithospheric temperatures. A hotspot model developed for the North Atlantic (e.g. Morgan 1971; White et al. 1987; White and McKenzie 1989; Skogseid et al. 2000) assumes a plume head up to 2000 km wide with a 100 – 200° C thermal anomaly, which enhanced decompression melting and increased volcanism during lithospheric extension. Kelemen and Holbrook (1995) deduced mantle compositions, i.e. the depth of melt generation and migration, from the bulk velocity and thickness of igneous crust. Pure passive upwelling is related to an increased depth range of melt production and higher temperatures, which in turn are associated with higher magnesium and lower silicon contents that are responsible for high average seismic velocities. The formation of the North Atlantic Igneous Province (NAIP) has been associated with the generally accepted model of elevated temperatures from a mantle plume (Iceland hotspot), which has also been supposed to have triggered North Atlantic continental break-up (e.g. White and McKenzie 1989; White 1992; Saunders et al. 1997). Lawver and Müller (1994) suggested the mantle plume was located beneath central Greenland in Late Cretaceous/Early Tertiary times (Figure 6.1). Thus, the Tertiary volcanism of the North Atlantic margins prior to and during break-up is associated with mantle plume activity within a circle of radius ~1200 km.

Systematic seismic investigations along the East Greenland margin over the last 20 years yield an improved image of its crustal structure (Figure 6.1) and have prompted different models of melt generation with or without a mantle plume. The southeast Greenland margin is investigated along four wide angle seismic profiles which show thick igneous crust in the continent – ocean transition zone (COT) and on the first oceanic lithosphere produced after break-up (Korenaga et al. 2000; Holbrook et al. 2001; Hopper et al. 2003). The varying structural styles along the southeast Greenland margin and the presence of the high velocity igneous crust have been linked to their distance from the Iceland plume. Holbrook et al. (2001) suggests, from the bulk velocities and thicknesses of the igneous high velocity lower crust, that a modest margin-wide mantle thermal anomaly was present during break-up (~56 Ma), which was exhausted by 43 Ma. Active upwelling is proposed for the proximal zone of the plume head, whereas the lateral emplacement of warm plume head material over 500 km (e.g. Sleep 1996) into the distal zone is explained by pure passive upwelling. Active upwelling is understood as the rapid vertical flux of material compared to lithospheric spreading, and may also generate increased seismic velocities of thick igneous crust, but without a thermal anomaly (Kelemen and Holbrook 1995; Holbrook et al. 2001; Korenaga et al. 2002). Convective partial melting is proposed to result from lateral thermal gradients in the lithosphere, which passively induce small-scale convection (Mutter et al. 1988). Edge-driven small scale convection cells were proposed to explain the flood basalt provinces at volcanic rifted margins (King and Anderson 1995; 1998). These authors suggest that a step in the lithosphere, e.g. at the edge of a thick craton, would control the flow of mantle material into a melting zone, while extension and faulting would allow melt transportation to the surface. Callot et al. (2002) propose a model of localized melting domains, similar to small scale mantle diapirs which arise from the channelled and focused ascent of hot plume material due to such possible edge effects. Such ‘soft spots’ are invoked to explain the segmentation and along-strike variation of magmatism at the southeast to central-east Greenland margin. Anderson (2000) proposed normal potential temperatures for the upper mantle of $1400 \pm 200^\circ$ C, and rapid convection giving rise to 3D-heterogeneities in the lithosphere that are responsible for the excess magmatism. Nielsen and Hopper (2004) found that the effect of lithospheric thickness differences was insufficient to produce all the observed igneous crust at the

southeast Greenland margin as a result of edge-effect convection. They propose, instead, that a hot sub-lithospheric layer is responsible for the temporal evolution of the southeast Greenland igneous crustal thickness. Increased mantle temperatures due to the proximal Iceland plume are also assumed for central-east Greenland (Weigel et al. 1995; Fechner and Jokat 1996; Schlindwein and Jokat 1999). Alternatives to the mantle plume hypothesis were proposed to explain large scale melt production and mantle temperatures above 1200° C (McKenzie and Bickle 1988; Anderson 2000). Foulger and Anderson (2005) considered mantle heterogeneities, resulting from the introduction of subducted slab of oceanic crust beneath the Laurasian continent during the Paleozoic closure of the Iapetus ocean. Other modelling experiments considered mantle upwelling rates that are higher than plate extension rates (van Wijk et al. 2001), resulting in the melting of a large amount of normal-temperature mantle material around break-up. Other processes and scenarios were proposed and reviewed for the formation of the North Atlantic Igneous Province by Meyer et al. (2007).

The northeast Greenland margin (72° N – 78° N) is bounded to the south by the western Jan Mayen Fracture Zone (JMFZ) and by the Greenland Fracture Zone (GFZ) to the north (Henriksen et al. 2000). Significant variations in the onshore geology (e.g. the Caledonian orogen, post-Caledonian sediment basins and the distribution of flood basalts (Escher and Pulvertaft 1995; Henriksen et al. 2000)), and in offshore features like the width of the shelf region, and magnetic pattern, led to increased interest in the crustal structure of this part of the Greenland margin. Wide aperture CDP profiles and extended spread profiles (ESP) (Hinz et al. 1987; Mutter and Zehnder 1988) focused locally on the COT, and the onset of oceanic crust. Multichannel seismic (MCS) profiles cover the shelf region and parts of the transition from continental to oceanic crust up to ~73° N (Larsen 1990). Schlindwein and Jokat (1999; 2000) proposed an eastward shift of Mesozoic rifting which preserved the Devonian structures in the region north of Kong Oscar Fjord (Figure 6.1) while further thinning and weakening of Devonian crust to the south allowed Tertiary melts to ascend to the surface. Their models did not provide constraints on the COT or on the onset of oceanic crust. Several seismic and potential field investigations along the opposing Scandinavian margin provide important constraints on the evolutionary history of the Norwegian-Greenland Sea (Mjelde et al. 1997; Mjelde et al. 1998; Raum et al. 2002; Mjelde et al. 2003; Mjelde et al. 2005; Tsikalas et al. 2005). Complementary data from the northeast Greenland margin, with comparable coverage and a similar cross-margin extent to those in southeast Greenland, were missing until now. It is debatable therefore, which of the models mentioned above is applicable to the northeast Greenland margin.

6.4 New transects of the northeast Greenland margin

The northernmost transect, AWI-20030200, located ~140 km offshore from Danmarkshavn (Figure 6.1), extends across the deep sedimentary basins and shelf slope into the Greenland basin, approximately 200 km south of the Greenland Fracture Zone. Line AWI-20030300 is a prolongation of a previously acquired seismic line 94300 (Schlindwein 1998), and crosses the shelf south of Shannon Island. Profile AWI-20030400 follows the Godthåb Gulf across the shelf, and AWI-20030500 is an extension of the earlier transect 94320 (Schlindwein and Jokat 1999) off the Kejser Franz Joseph Fjord. This contribution presents results for the northern profiles, AWI-20030200 and AWI-20030300.

6.4.1 Processing and modelling

Data were acquired using the R/V *Polarstern*, with a seismic source array of 77 litres (5x9 L +32 L) (Jokat et al. 2004). Ocean bottom hydrophones (OBH) and seismometers (OBS) were deployed offshore and REFTEK stations with geophones were distributed onshore along the Ardencaple Fjord for profile AWI-20030300 (Figure 6.2). In-line instrument relocation of 30

to 260 m was performed for those OBH/S of both profiles that showed asymmetric parabola of the direct wave arrivals in the shot gathers in reduced travel time display. Bandpass filtering (4 – 20 Hz) enhanced the data quality for picking arrivals. A projection of the receiver locations from the great circle onto a straight line is obligatory for the ray-tracing. A straight line fit through stations 201 and 225 was used for profile AWI-20030200 and revealed a maximum shift of 3.6 km for station 210. The maximum shift, for ocean bottom station 314 on profile AWI-20030300, is 4.3 km for a line through stations 301 and 325 and 14.1 km for the westernmost land station 331 (Figure 6.2). The true offsets of the shots and therefore of the observed P-wave arrivals, remained unchanged. The contraction of profile AWI-20030300 by a couple of tens of metres within the line, and of approximately 1.2 km within the fjord, due to the projection results in averaging of laterally inhomogeneous crustal structures due to the different ray paths between the real profile and the approximation. However, these errors are expected to have only a minor influence in the overall structural style along the profiles. Individual seismic sections and their ray coverage are shown in Figures 6.3a-f. In the following we describe the applied modelling methodology for the two transects:

- 1) P-wave travel time arrivals were picked with the *ZP* software from *B.C. Zelt* (available at <http://www.soest.hawaii.edu/~bzelt/zp/zp.html>). Associated error values for the picks range between 0.04 and 0.15 s and depend on the signal to noise ratio, as calculated by the software in a 0.25 s time window before and after each pick time. A constant error of 0.05 s was used for profile AWI-20030200. First crustal arrivals were weak at stations 202 (Figure 6.3c), 210 and 212 of profile AWI-20030200, but could be distinguished better in the first multiples between the station and sea surface.
- 2) Velocity models (V_p) were obtained by forward modelling with 2D ray-tracing software *RAYINV* (Zelt and Smith 1992) equivalent to the procedure applied by Voss and Jokat (2007). 2D inversion was used in questionable areas of the model but was not the major modelling tool. The error analysis of the individual phases used for the final P-wave velocity models are summarized in Tables 6.1 and 6.2. The phase numbers refer to the layer of the velocity model, e.g. P2 means refracted rays in layer 2, and P2P means reflections at the base of layer 2. Reflections at the crust-mantle boundary (Moho) are labelled with PmP, upper mantle refractions with Pn. Occasionally, these refracted waves could not be modelled properly due to the very low vertical gradient of the upper mantle velocities. In these cases the identified arrivals were approximated by a head wave propagating along the Moho and assigned as Pn'. The ray-tracing software is able to model multiples at the shot location and the associated phase numbers are labelled with an asterisk. Multiples at the station locations are labelled equally but require manual adjustments prior to ray-tracing. A static time shift was applied to the individual picks of the multiples of the above mentioned deep sea stations. The final values are 4.75 s and 4.6 s for the left and right sides of station 202 (3587 m), 4.13 s (left) and 4.16 s (right) for station 210 (3174 m) and 3.1 s for both sides of station 212 (2325 m) depth, which are ± 0.1 s of the travel time path through the water column above the stations. This approximation of the multiples revealed acceptable results, which were used to test the sparse first arrivals of these stations and the layer parameters. Modelling of weak identified arrivals led to large normalized chi-squared (χ^2) values and large RMS misfits between identified and calculated travel times. Thus, we spent more effort on fitting the slope of the first arrivals than on minimizing residuals. The remaining deviations between observed and calculated travel times should be seen as a best compromise. General resolution tests require equidistant layer and velocity node distributions, which were not appropriate in our models. Thus, the resolution and quality of the final models are obtained from

the ray coverage (Figures 6.4A and 6.6A) and the fitting parameters. Rays were traced for 97 per cent of 2040 picks (arrivals from the seafloor excluded) for profile AWI-20030200, and 98 per cent of 3550 picks for AWI-20030300 (Figures 6.4 and 6.6). A velocity error of $\pm 0.1 \text{ km s}^{-1}$ is estimated for the well-covered portions of the oceanic, and the top layer of the continental parts of the profiles. Velocities for the middle and lower continental parts of profile AWI-20030300 (Figures 6.6 and 6.7) could not be modelled with errors smaller than $\pm 0.2 \text{ km s}^{-1}$. Layer boundaries were introduced where wide-angle reflections were identified. In all other instances, the layer boundaries were shifted to fit the velocity gradients within the layers. The uncertainties of layer locations were tested by varying the depths until unacceptable misfits occurred for ray-tracing. Thus, we estimate the accuracy of layer depths to $\pm 0.1 \text{ km}$ for the top reflections (P2P) and the oceanic layers, and $\pm 0.5 \text{ km}$ for mid-crustal and Moho reflections.

- 3) The final P-wave velocity models were verified by 2D gravity modelling using commercial software, *LCT*. A predicted gravity model was calculated by converting all velocity nodes of the V_p -models to density nodes using a polynomial formula after Funck et al. (2004) approximating the Nafe-Drake curve (Nafe and Drake 1957; Ludwig et al. 1970). Polygons of homogeneous densities were defined within the layer boundaries already determined from wide-angle reflections in order to simplify the initial starting model. A homogenous mantle density (3.31 or $3.26 \times 10^3 \text{ kg m}^{-3}$) yields a large error of the modelled gravity. Modifications to crustal layer densities would have only short wavelength effects. A thickness variation of the lower lithosphere, i.e. a higher asthenosphere in the oceanic domain, is assumed to reveal an effect with too large wavelengths. An additional influence on density contrasts might be associated with lateral and vertical thermal gradients between the continental and oceanic lithosphere (Breivik et al. 1999). Thus, the density for sub-continental upper mantle was set to $3.31 \times 10^3 \text{ kg m}^{-3}$, and that for oceanic mantle lithosphere to $3.25 - 3.26 \times 10^3 \text{ kg m}^{-3}$ (Figures 6.5 and 6.7). Both values should be seen as first order approximations. Equivalent values were used for gravity modelling of the two southern profiles (Voss and Jokat 2007). Densities of the individual polygons were successively modified to fit the short wavelength variations in the measured Bouguer anomalies (Figures 6.5 and 6.7). Adjustments within a range of $0.05 \times 10^3 \text{ kg m}^{-3}$ were necessary until residuals increased significantly. The depths of layer boundaries within the velocity models were left unchanged.
- 4) The geological interpretation of seismic velocities in the continental part of profile AWI-20030300 follows that of velocities in the southern profiles (Voss and Jokat 2007). Detailed lithologic interpretations were not possible due to the lack of boreholes and rock samples. Thus, the velocity models are classified stratigraphically and structurally. Velocities of up to 4.0 km s^{-1} are attributed to post-rift Cenozoic sediments. The velocity variations within this range reflect burial depth and grade of compaction of these sediments. Continental sediments, most likely Mesozoic/Cretaceous syn-rift sediments, and basaltic extrusive rocks are suggested the source of P-wave velocities between 4.5 km s^{-1} and 6.0 km s^{-1} . P-wave velocities typical for granitic/granodioritic crystalline crust range between 6.0 km s^{-1} at the top and $6.6 - 6.9 \text{ km s}^{-1}$ at the base of the crust (Christensen and Mooney 1995). Higher velocities in the lower crust of between 7.0 km s^{-1} and 7.4 km s^{-1} appropriate for the average velocity of intrusions into the lower crust and/or to magmatic underplate trapped between the upper mantle and lower crust (e.g. White and McKenzie 1989). Typical oceanic velocity layering corresponds to sediments ($1.6 - 3.0 \text{ km s}^{-1}$), oceanic layer 2 ($4.0 - 6.5 \text{ km s}^{-1}$) and oceanic layer 3 ($6.5 - 6.9 \text{ km s}^{-1}$) (Fowler 2005). An oceanic layer 3B with velocities of $>7.0 \text{ km s}^{-1}$ is commonly associated with increased melt

production and thickened oceanic crust (White and McKenzie 1989; Eldholm and Grue 1994; Mjelde et al. 2001; Tsikalas et al. 2005).

- 5) Half spreading rates were calculated from regional magnetic data (Verhoef et al. 1996) along profiles AWI-20030200 and AWI-20030300 as well from high resolution aeromagnetic data acquired along the two southern profiles. The results are discussed in a comparison with other calculations of oceanic spreading rates of the East Greenland (Mosar et al. 2002b), and Norwegian Møre margins (Breivik et al. 2006).

Layer	Phase	AWI – 20030200			
		n	t_{RMS}	χ^2	
1	Water	not modelled			
2	top sediments	P2	69	0.055	1.227
		P2P	163	0.186	13.893
3	Oceanic layer 2A	no assigned picks			
4	Oceanic layer 2B	P4	318	0.092	3.413
5	Oceanic layer 3	P5	618	0.081	2.611
		PmP	653	0.091	3.291
	multiples of oceanic layer 3	PmP*	105	0.073	2.168
6	mantle (head wave)	Pn'	77	0.078	2.439
	multiples mantle (head waves)	Pn'*	37	0.057	1.337
	TOTAL		2040	0.097	3.735

Table 6.1: Phase nomenclature for individual phases of profile AWI-20030200 with associated number of used observations (n), RMS misfit between calculated and picked travel times (t_{RMS}) in seconds and normalized χ^2 . Phases with asterisks are multiples at the receiver locations. Pn' means head waves (details in the text).

6.4.2 Profile AWI-20030200

The 330 km long profile AWI-20030200 runs NW-SE from the continental shelf across a large basement high into the abyssal plain of the Greenland Basin. In total, 25 ocean-bottom hydrophones and seismometers (OBH/S) were deployed (Figure 6.2). The eight ocean-bottom stations on the shelf (station 218-225) show a complex pattern of sedimentary phases, as shown in Figure 6.3a for OBS 224. Most stations recorded no phases from the crystalline crust, which is most probably a consequence of a deep basin, and a complex sedimentary structure with low-velocity layers and scattering. The base of the sediments could not be derived from the wide-angle data, or from MCS data (Berger, personal communication). For this reason, only the eastern 210 km of the model, containing parts of the continent-ocean transition and the oceanic layers, will be shown and discussed in this contribution. Figure 6.3b shows the recording and modelling for OBH 209, which is located near the COB. OBH 202 covers a region of decreasing oceanic crustal thickness and includes modelled multiples, as described above (Figure 6.3c). In total, six layers were used for modelling between km 120 and 330. The first layer represents the water, layers 2 to 5 represent sediments and crustal layering and the sixth layer was used for the upper mantle (Figure 6.5).

6.4.2.1 Continent – ocean transition

Only the eastern part of the COT, including the Greenland Escarpment and an outer high, could be modelled, and the western extent of the transition zone is currently unknown. Near the shelf edge, the sedimentary layer shows seismic velocities between 2.2 km s^{-1} at the top and 3.9 km s^{-1} at 4 km depth (Figure 6.5).

The top of the basement high between km 160 and 200 and the basement depth east and west of it has been constrained by MCS data (Berger, personal communication) and by reflections in the wide-angle seismic sections (Figure 6.4A/B). The crustal structure below the sedimentary layer west of the high (km 120 – 150) is highly speculative. The Greenland Escarpment, at km 160, and the outer high were modelled with seismic velocities of between

4.5 km s^{-1} and 6.5 km s^{-1} . In the lower part of the COT seismic velocities of $6.6 - 7.1 \text{ km s}^{-1}$ were found. Although this area is not well covered by rays (Figures 6.3b and 6.4), the modelling results indicate that a large high-velocity body is unlikely.

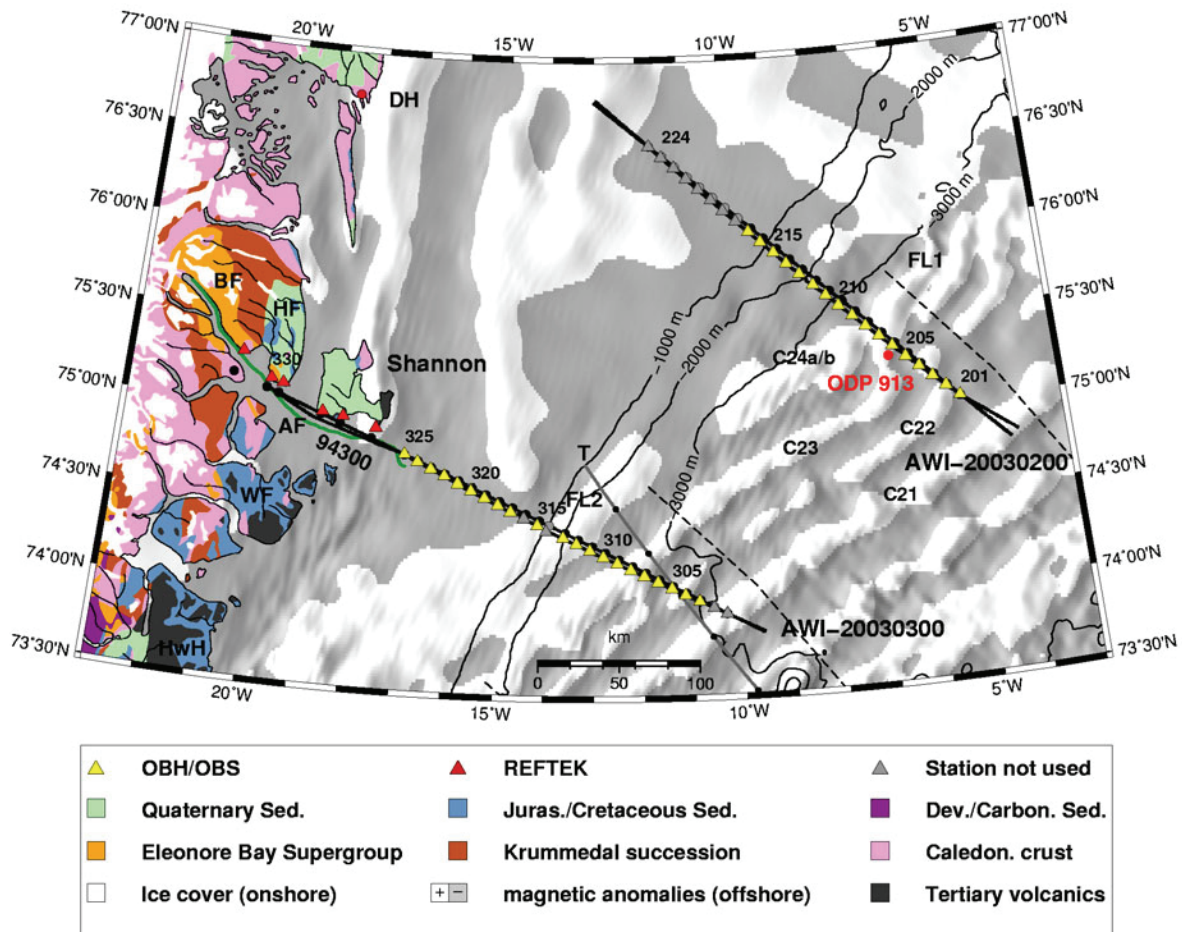


Figure 6.2: Locations and instruments setup of the seismic refraction profiles AWI-20030200 and AWI-20030300. Background shows regional magnetic grid (Verhoef et al. 1996) with white regions for positive and grey regions for negative polarisations. Spreading anomalies are labelled with Cxx. Thin black lines represent bathymetric contours after Jakobsson et al. (2000). Onshore geology after Escher and Pulvertaft (1995). Yellow triangles show locations of the OBS/OBS, red triangles represent REFTEK land stations. Black dots show the locations of the receivers projected onto a straight line, as described in the text. Gray triangles and dots mark unused receiver stations. Every fifth station location is labelled. Green line represents seismic refraction profile 94300 of Schlindwein (1998). Dashed thin lines represent synthetic flowlines using the rotation poles of Rowley and Lottes (1988). Thick grey line marks reference transect from Voss and Jokat (2007) with black dots marking picks of spreading anomalies. Abbreviations are as in Figure 6.1 and FL1 and FL2, flowlines; T, reference transect. Scale is valid for 75° N .

6.4.2.2 Oceanic section

The crustal layers have typical velocity ranges for oceanic crust (White et al. 1992; Fowler 2005). The deep-sea sediments, with a maximum thickness of 1 km, were modelled as one layer ($1.6 - 2.4 \text{ km s}^{-1}$). The depth of the basement was derived from MCS data and constrained by reflected phases picked in the wide-angle data (Figure 6.4B). The basement topography is quite rough, leading to strong undulations in the crustal phases. Oceanic layer 2A is too small to be resolved by the wide-angle data, but a thin layer ($4.3 - 4.4 \text{ km s}^{-1}$, max. 0.4 km thick) had to be included in order to model the delayed onset of refracted waves from layer 2B. Layer 2B shows seismic velocities between 4.8 km s^{-1} at the top and 6.6 km s^{-1} at the bottom at $\sim 6 \text{ km}$ depth. Velocities of up to 6.7 km s^{-1} were found west of magnetic anomaly C24. In this area, the lower oceanic crustal layer also shows slightly higher velocities

(6.8 - 7.1 km s⁻¹) than towards the end of the profile in the east at anomaly C21 (6.6 - 7.0 km s⁻¹). The Moho depth decreases from 13 km east of the outer basement high (km 200) to 9.5 km in the deep Greenland Basin (Figures 6.3b/c and 6.5). The crustal thickness, without sediments, ranges between 9 km near the transition zone (km 200) and 5 km near C21 (km 300).

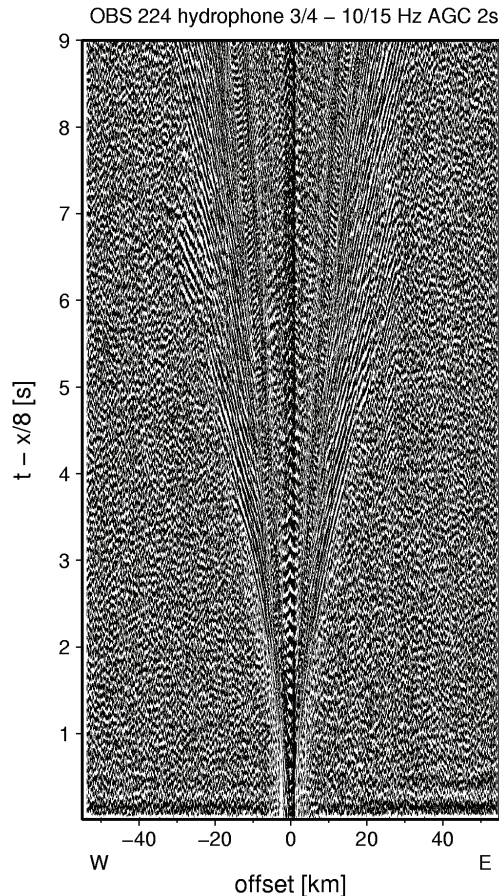


Figure 6.3: Examples of recorded seismic data. The traveltimes are reduced for 8 km s⁻¹. Observed phases are labelled (see Tables 6.1 and 6.2). The ray coverage of each station is marked in the lower model. a) OBS 224 on profile AWI-20030200, hydrophone channel. A 3 to 15 Hz band pass filter and automatic gain control window of 2 s is applied. Note the location in Figure 6.2 and the scattering of the sediment basin (as deep as 9 s). b) Station OBH 209 on profile AWI-20030200 shows the loss of signals at the outer high (3 – 25 Hz and AGC window of 1 s). c) Station OBH 202 on profile AWI-20030200. Note that phases marked with an asterisk are multiple reflections at the receiver point and shifted statically. Pn' marks arrivals from head waves along the Moho. d) Land station REF 330 on profile AWI-20030300 shows clearly the Shannon High velocity anomaly. e) Station OBS 319 on profile AWI-20030300 shows the loss of signals due to the western basin. Note that P6* is a multiple reflection at the shot point. f) OBS 309 of profile AWI-20030300 is located on oceanic crust. Note the late arrivals of the multiples P6* and P6P* and the head waves Pn'.

6.4.2.3 Gravity modelling

A simple 2D density model (Figure 6.5) verifies typical oceanic crustal densities with values comparable to other models (e.g. Voss and Jokat 2007). Minimum and maximum deviations of the calculated versus measured Bouguer gravity are in the range of ± 11 mGal near the Greenland Escarpment and the outer high (Figure 6.5). Further uncertainty results from the unresolved model landward of the outer high. Constraints on the density of the sedimentary layer of the ocean basin were obtained from drilling results ODP drillhole 913 (Myhre and Thiede 1995), located near km 242 (Figure 6.5), yields an average grain-density of $2.5 - 2.7 \times 10^3 \text{ kg m}^{-3}$ and porosities of 30 – 60 per cent, which would result in densities of $2.2 - 2.6 \times 10^3 \text{ kg m}^{-3}$ for compaction between 0.3 and 0.6 (Sawyer 1985). P-wave velocities between 1.6

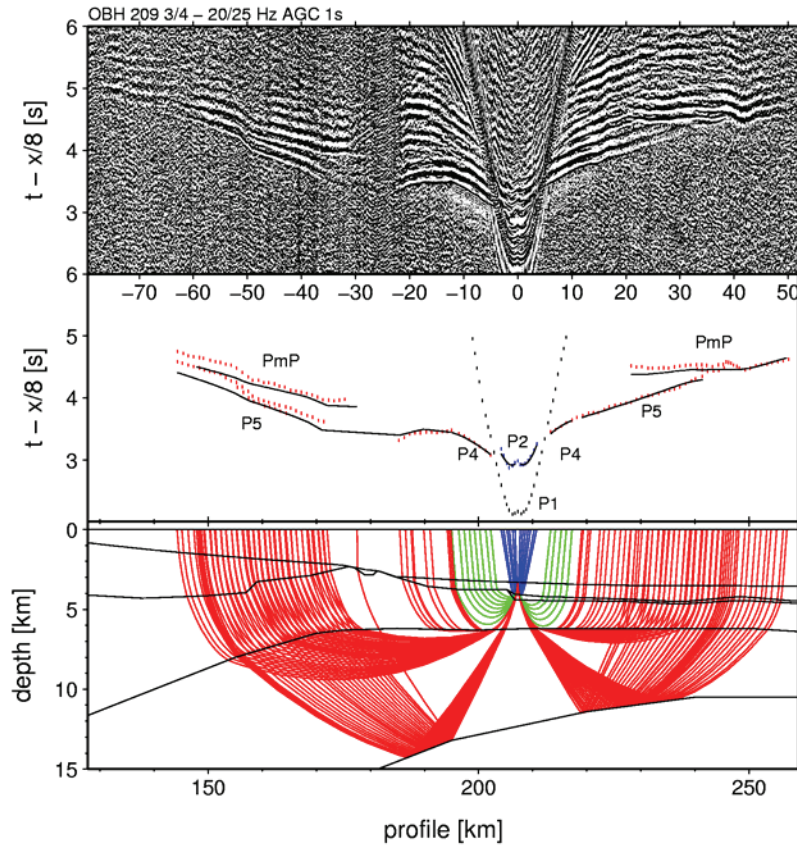


Figure 6.3: b) (Continued.)

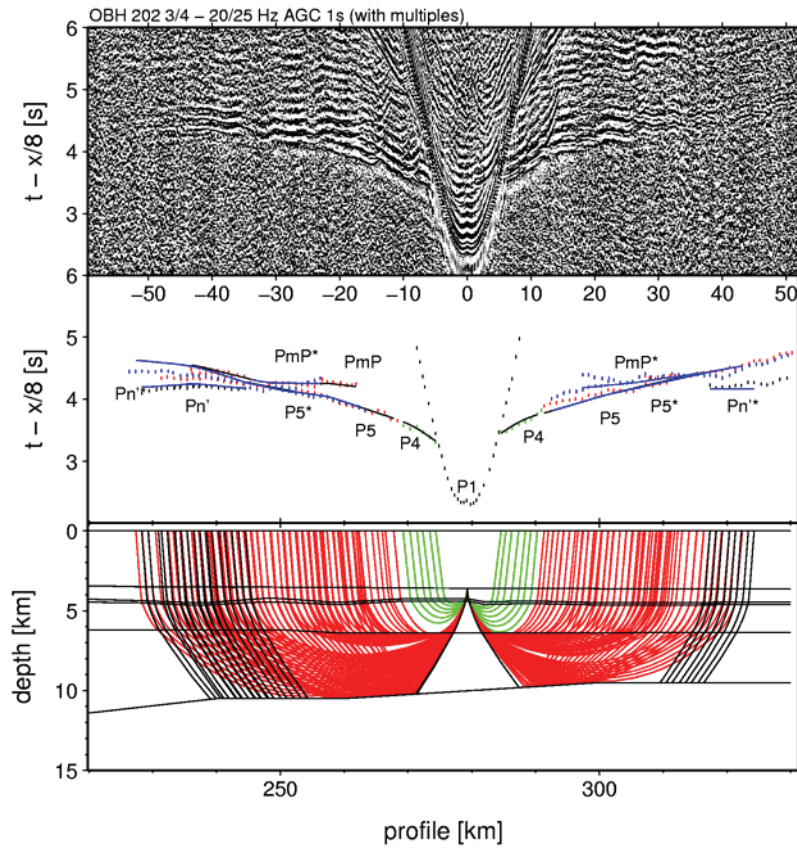


Figure 6.3: c) (Continued.)

and 2.4 km s^{-1} are related to densities of 1.65 ± 0.3 and $2.05 \pm 0.2 \times 10^3 \text{ kg m}^{-3}$ (Nafe and Drake 1957). Thus, $2.15 \times 10^3 \text{ kg m}^{-3}$ is an acceptable average for the top sedimentary layer. The higher velocities ($> 7.0 \text{ km s}^{-1}$) in the lower oceanic layer were assigned a slightly higher density of $3.03 \times 10^3 \text{ kg m}^{-3}$, which yield a closer fit of the calculated to the observed gravity. The outer high has densities that are lower than those typical of volcanic structures, which might be attributed to the unresolved model landwards, and/or an unknown internal structure of the outer high. Hinz et al. (1987) also found low velocities within the rise seaward of the Greenland Escarpment. A change from $3.31 \times 10^3 \text{ kg m}^{-3}$ to $3.26 \times 10^3 \text{ kg m}^{-3}$ marks the transition from sub-continental to sub-oceanic upper mantle as described above.

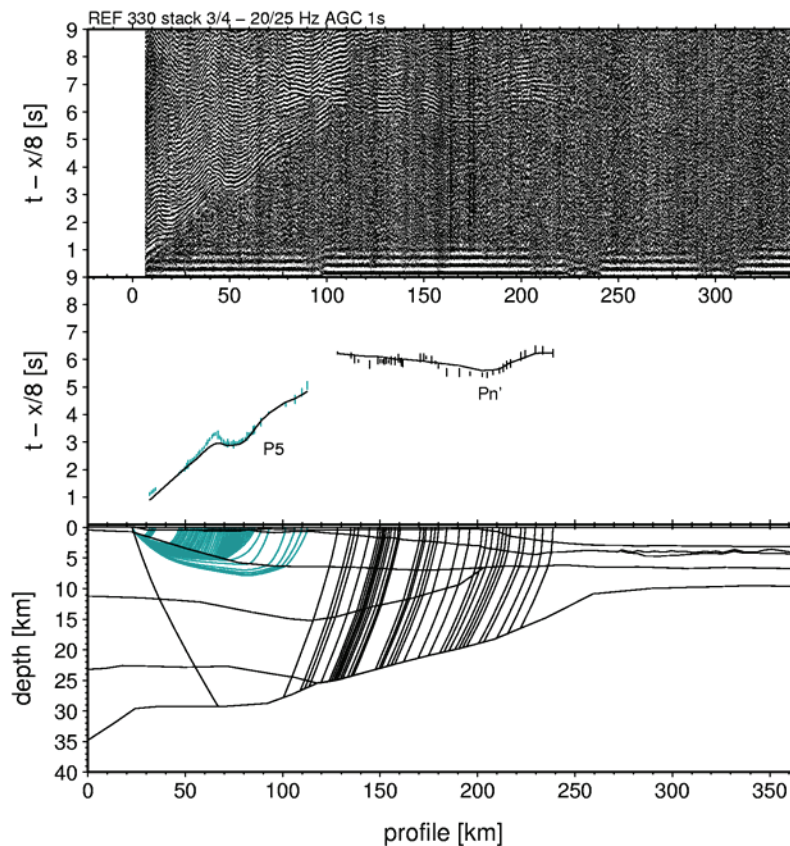


Figure 6.3: d) (Continued.)

6.4.2.4 Stratigraphic and structural interpretation of AWI-20030200

The oceanic magnetic spreading anomalies provide good constraints on the location of the COB along this transect. Anomalies C24A and C24B form a wide normal polarity anomaly, and can not clearly be distinguished from one another (Figure 6.5A). Berger and Jokat (personal communication) confirmed the Greenland Escarpment along MCS lines across the Greenland Fracture Zone, and suggest that the basalts were emplaced on continental crust prior to break-up to form the outer high (Figure 6.5D). Therefore, we propose the COB to lie at km 200, 20 km east of the outer high within the reversed part of anomaly C24A/B. Seismic velocities of the sediments to the west of this location are significantly higher than the post-break-up sediments east of it. Sediments accumulated landward of the basement high are probably more highly compacted, and were buried by Paleogene to Neogene sediments during thermal subsidence and lying now 2 – 4 km deep (Figure 6.5D).

The top oceanic crustal layers, 2A and 2B, are integrated into oceanic layer 2 (Figure 6.5D) and can clearly be distinguished from layer 3A on the base on their velocities, gradients and density. An oceanic layer 3B with an initial thickness of up to 2 km terminates near C23. The

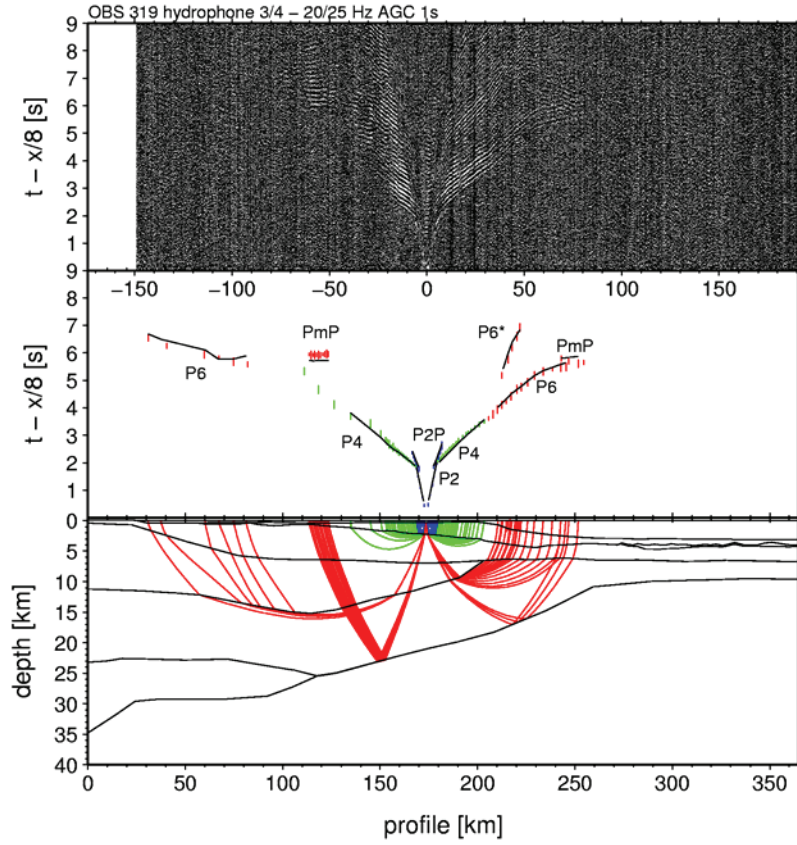


Figure 6.3: e) (Continued.)

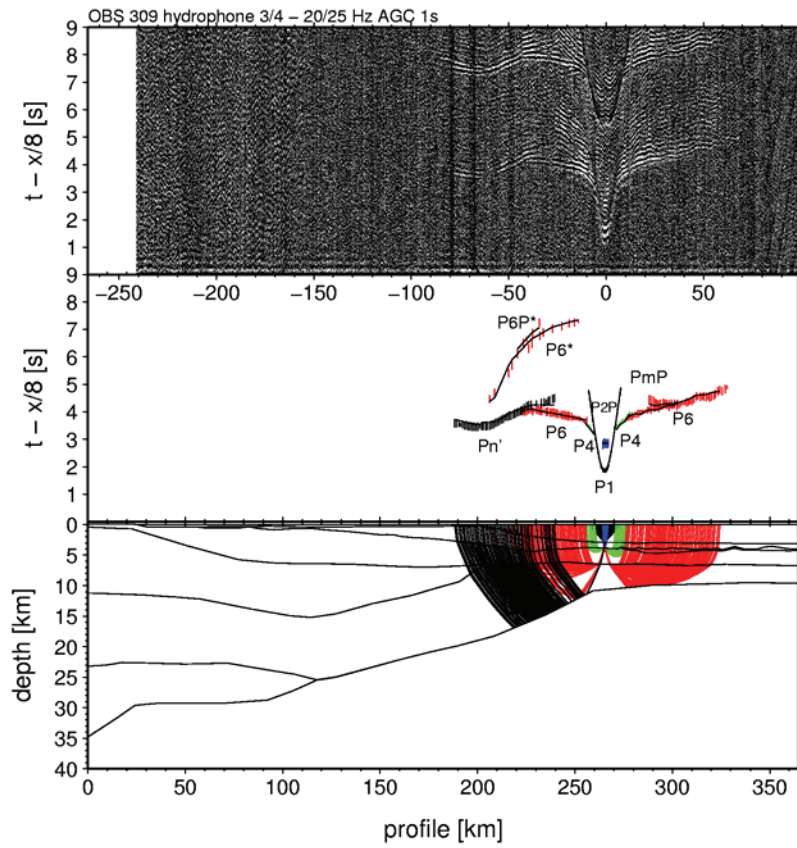


Figure 6.3: f) (Continued.)

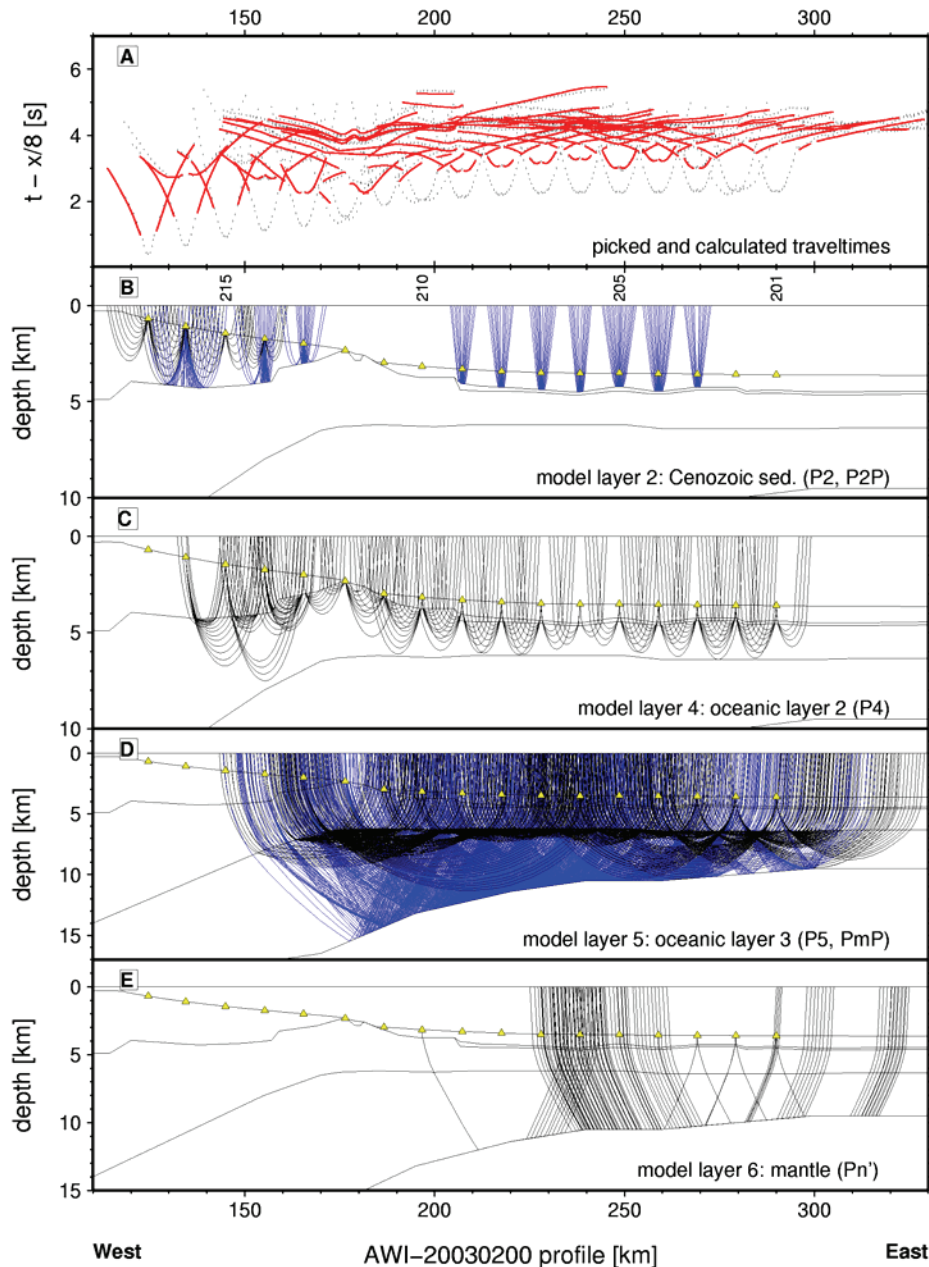


Figure 6.4: Ray coverage for stations 201 – 217 along transect AWI-20030200. The first 120 km of the profile were not modelled (see text). A) Observed and calculated P-wave arrivals. The traveltimes reduction is 8 km s^{-1} . Picks of arrivals are marked with 50 ms vertical error bar. Red lines show the calculated arrivals (not for picks within the water column). Note that for station 202, 210 and 212 multiples were also modelled. B) Refractions and reflections within the top sedimentary layer. Yellow triangles mark receiver locations were every fifth is labelled. C) Refractions and reflections of the upper part of the continental basin and oceanic layer 2. D) As in (C) but for oceanic layer 3. E) Arrivals interpreted as mantle phases either as refractions or as head waves travelling along the Moho (see text for further explanations).

total thickness of the oceanic crust decreases rapidly seawards, over a distance of 20 km, from 9 to 7 km, near the peak of C24A/B. It decreases to 6 km near the normal polarity part of C23 and further to 5 km near C21. The crustal structure landward of the COB on profile AWI-20030200 contrasts strongly with that derived for the southern profiles AWI-20030400 and AWI-20030500 (Voss and Jokat 2007). This will be discussed further below.

6.4.3 Profile AWI-20030300

The 365 km long seismic transect AWI-20030300 south of Shannon Island includes 14 OBS, 11 OBH and 6 REFTEK land stations. Stations 301, 302, 314 and 316 (Figures 6.2 and 6.6) were not used for modelling due to bad recordings. Phase identification at all other stations was difficult, and could not be eased by deconvolution filters. The entire velocity model consists of eight layers; the water column, six layers for sediments and the crust, and one layer for the upper mantle (Figures 6.6 and 6.7). Five layers were used to model the continental part of the profile (km 0 – 210), and four layers for the oceanic part (km 210 – 365). The westerly 100 km of profile AWI-20030300 overlap with an older seismic profile, 94300, that extends from Shannon Island landwards into the Bredefjord (Schlindwein 1998) and provides additional constraints on the poorly covered (Figure 6.6E) and weakly resolved continental crust. The most likely range of the continent – ocean transition zone and its seaward termination (COB in Figure 6.7D) will be discussed further below.

Layer	Phase	AWI – 20030300			
		n	t_{RMS}	χ^2	
1	Water	P1	306	0.149	7.082
2	top sediments	P2	139	0.075	2.034
		P2P	146	0.119	2.065
3	Oceanic layer 2A	no assigned picks			
4	basalts, continental sediments and	P4	699	0.092	1.778
	Oceanic layer 2B	P4P	33	0.109	1.343
	multiples of oceanic layer 2B	P4P*	12	0.108	0.914
5	intermediate continental layer	P5	281	0.130	2.983
		P5P	81	0.123	1.719
6	lower crust, oceanic layer 3	P6	960	0.093	1.019
		P6P/PmP	431	0.124	1.471
		P6*	89	0.100	0.639
		PmP*	21	0.118	0.657
7	continental sub-lower crustal layer	PmP	92	0.286	9.577
8	upper mantle	Pn	61	0.059	0.354
	upper mantle (head wave)	Pn'	149	0.168	2.340
TOTAL			3500	0.120	2.265

Table 6.2: Phase nomenclature for individual phases of profile AWI-20030300 with associated number of used observations (n), RMS misfit between calculated and picked travel times (t_{RMS}) in seconds and normalized χ^2 . Phases with asterisk are multiples at the shot point location.

6.4.3.1 Continental section

The top sedimentary layer, east of Shannon Island, has P-wave velocities of 2.0 – 2.3 km s⁻¹ at the top and up to 3.5 km s⁻¹ (km ~200) in 3 km depth. Its thickness increases continuously to 2.7 km (Figure 6.7) near km 210. The top of a seaward-necking horizon is constrained by reflections in 0 – 3 km from numerous stations almost continuously between km 145 and 210 (Figure 6.6B). This second continental layer was modelled with velocities, from top to bottom, of between 4.0 and 5.7 km s⁻¹. Wide-angle reflections were inferred from OBS 325, 324 and 320 and constrain the depth of the layer to 6 – 7 km between km 110 and 160 (Figures 6.6C and 6.7). A significant velocity anomaly was found beneath Shannon Island (km 65 and 80). The velocities increase from 4.0 km s⁻¹ east and west of the island to 6.0 km s⁻¹ beneath it. This positive velocity anomaly is also modelled in layer 5 with a maximum velocity of 6.55 km s⁻¹ in 5 km depth and 6.6 km s⁻¹ in 13 km depth. Only land stations 331 – 326 gave constraints on this velocity anomaly (Figures 6.3d and 6.6). West of the anomaly, seismic velocities were modelled at between 5.6 and 6.4 km s⁻¹ in layer 5 and show a lower velocity gradient than that in the model of the overlapping profile 94300 (Schlindwein 1998). Poor deeper ray coverage by refractions in layer 5 between kms 50 and 200 (Figure 6.6) leave

the velocities for the lower part poorly constrained. Wide angle reflections provide constraints on a likely boundary, and help adjust the velocity gradients within the layer (Figure 6.6D). It remains questionable if the reflections sampled along the same lithological boundary (Figure 6.7). However, layer 5 velocities range between 5.6 - 5.8 km s⁻¹ at the top and 6.0 - 6.2 km s⁻¹ at the bottom excluding the Shannon Island anomaly (Figure 6.7). The base of this layer seems to rise from 15 km to 6.5 km depth between profile kms 115 and 190 (Figures 6.3e and 6.6D).

The lower part of the crustal model (km 0 – 120) consists of two layers inferred from profile 94300 in the western overlap (Schlindwein 1998; Figs. 2, 6 and 7). Only two very weak reflections (P6P; Figure 6.6E) support such a differentiation of the lower crustal layer but no diving waves were obtained from the deepest crustal layer between km 0 and 120. The crust-mantle boundary is well imaged by wide-angle reflections and arrivals modelled as head waves (Figures 6.3d and 6.6F). The latter constrain the range of P-wave velocities in these layers to 6.4 – 7.0 km s⁻¹ (top to bottom, kms 20 – 170) and to 8.0 km s⁻¹ in the upper mantle (Figure 6.7). Slightly increased velocities beneath Shannon Island were also necessary to minimize the misfits of PmP reflections (Figures 6.6 and 6.7). Large velocity gradient variations towards km 210 necessitated velocities of up to 7.3 km s⁻¹ between km 170 and km 210 (Figures 6.3c, d, 6.6 and 6.7). A further westward extent of the high velocity lower crustal layer could be precluded from the move out of the PmP reflections (Figure 6.6). Thus, an almost continuous decrease in Moho depth was modelled, from 30 km beneath Shannon Island to 18 km at the onset of oceanic crust.

6.4.3.2 Oceanic section

The oceanic section between km 210 and 365 (Figure 6.7) shows typical seismic velocities, similar to those on profile AWI-20030200 (Figures 6.5 and 6.7). The top sedimentary layer (1.6 – 2.4 km s⁻¹) shows only slightly increased velocities of up to 3.5 km s⁻¹ near the COB (km 220). Its thickness varies from 2.7 km to less than 1 km with increasing seafloor depth to 3.1 km. The top oceanic crustal layer is too small to be resolved in wide-angle data, but its existence was derived from MCS data (Berger, personal communication). A thin layer (4.3 - 4.4 km s⁻¹, max. 0.7 km thick) added to the model between km 270 – 365 (Figure 6.7) explains, therefore, the delay of refractions for the layers beneath. Velocities of 4.3 – 6.6 km s⁻¹ are well resolved in layer 4 from numerous P4 arrivals (Figure 6.6). A significant lower vertical velocity gradient (4.3 – 5.5 km s⁻¹) was necessary between kms 230 and 280 (Figures 6.3f and 6.7). The boundary between the two major oceanic layers 2 and 3 (model layers 4 and 6) is inferred from the significant change in velocity gradient due to the lack of any P4P reflections (Figure 6.6). The lower oceanic layer reveals velocities of 6.7 – 7.1 km s⁻¹. Several PmP reflections and Pn arrivals mark the Moho, whose depth increases from 9.5 to 18 km from east to west.

6.4.3.3 Gravity modelling

The final density model was obtained from the predicted P-wave model, as described above, with only minor changes ($\pm 0.1 \times 10^3 \text{ kg m}^{-3}$) for the density polygons within the continental part (Figure 6.7). Minimum and maximum deviations of the calculated to measured Bouguer gravity are in the range of $\pm 8.5 \text{ mGal}$ near km 210 and the large Shannon anomaly, respectively. A more significant change for upper mantle densities, similar to that described above, led to the use of densities of $3.31 \times 10^3 \text{ kg m}^{-3}$ for the sub-continental and $3.25 \times 10^3 \text{ kg m}^{-3}$ for the oceanic upper mantle. The deep velocity anomaly beneath Shannon Island required an introduction of a density anomaly of $0.02 - 0.2 \times 10^3 \text{ kg m}^{-3}$ higher than the adjacent values. Additionally, a higher lower crustal density ($2.98 \times 10^3 \text{ kg m}^{-3}$) beneath the Shannon high was necessary for a satisfactory match to the observed anomalies. Slightly

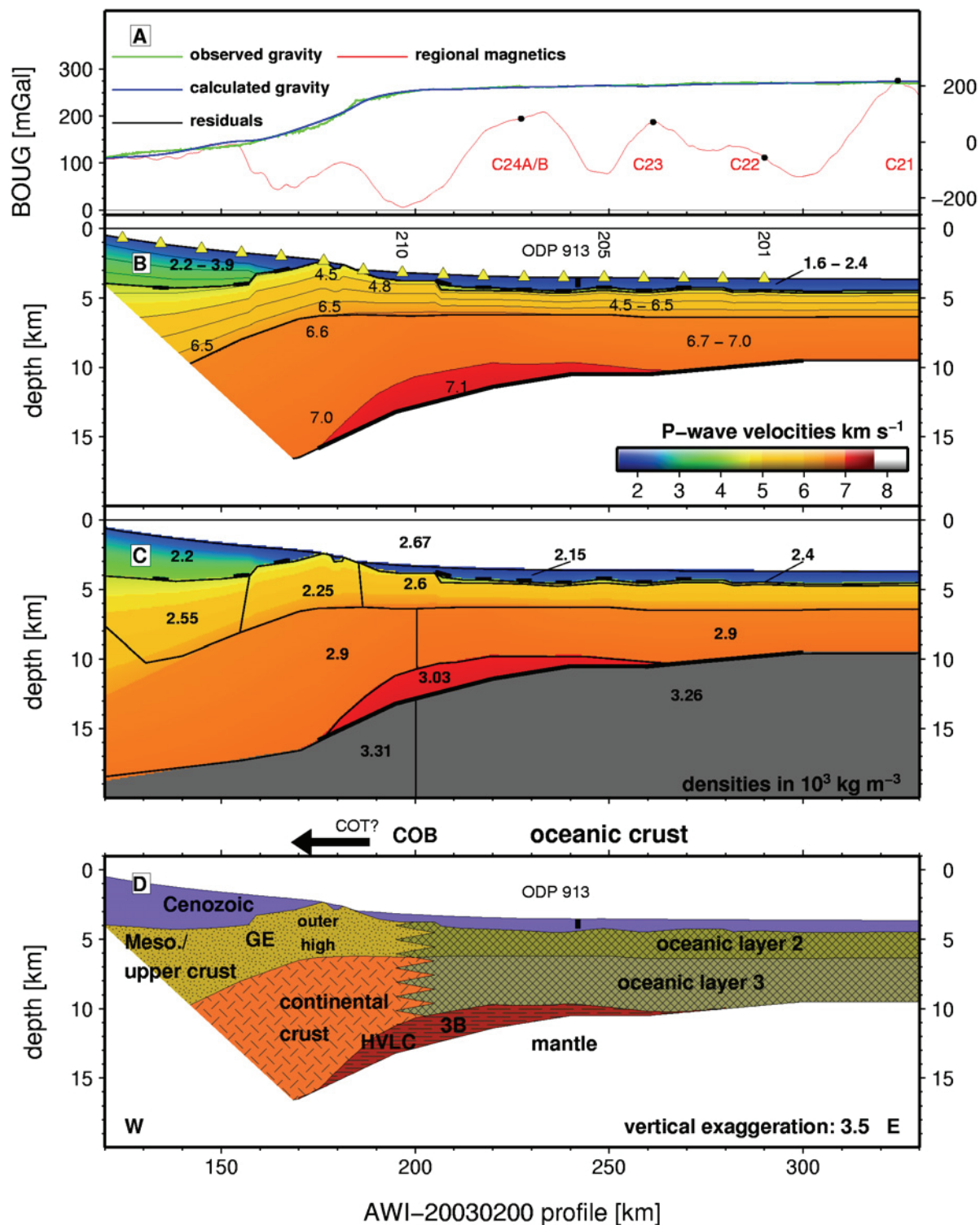


Figure 6.5: Modelling of profile AWI-20030200. A) Potential field data along the transect. Magnetic spreading anomalies are labelled. Black dots mark centres of normal polarisation locations for calculations of half spreading rates (see text). Observed and calculated Bouguer gravity and residuals refer to (C). B) P-wave velocity model. Numbers mark velocities of the layers. Contour lines between 2.5 and 7.0 km s^{-1} every 0.5 km s^{-1} . Yellow triangles mark ocean bottom recording locations. Thick black lines outline wide-angle reflections. C) 2D density model. Thin black lines mark polygons of constant densities. Colours represent velocity model from (B). The good approximation to the observed gravity is shown by residuals in (A). Note that the splitting of the upper mantle density is a simplification of the thermal effect of sub-oceanic mantle (see text). D) Lithologic interpretation based on the models above. The continent – ocean boundary (COB) marks the seaward end of the transition zone (COT). Abbreviations are GE, Greenland Escarpment; HVLC, high velocity lower crust; Meso., Mesozoic sediments; W/E, west and east.

increased velocities ($\sim 6.2 \text{ km s}^{-1}$) in 10 – 13 km depth at km 120 correlate with a gravity anomaly. This anomaly might suggest that the velocities are probably underestimated within the range of uncertainties in this poorly covered region (Figure 6.6). The density model verifies the inferred continental crustal velocity model and constrains the crustal structure and depth to Moho additionally to the seismic results.

6.4.3.4 Stratigraphic and structural interpretation of AWI-20030300

The top layer, from the shelf into the ocean basin, is related to post-rift Cenozoic sedimentation. The velocities and density model west of Shannon Island (km 0 – 50) suggest that a thick pile of Neoproterozoic Eleonore Bay Supergroup (EBS) sediments are concealed beneath Cretaceous sediments, which were deposited between the fjord and Shannon Island (Figure 6.7D). The onshore geology shows EBS sediments along the Brede and Ardencaple Fjord (Figure 6.2) and outcrops on Hochstetter Foreland and Shannon Island indicate the presence of Cretaceous sediments beneath Quaternary sediments (Escher and Pulvertaft 1995; Figure 6.2). Constraints on the thickness of the EBS sediments can be drawn from the interpretation of profile 94300 (Schlindwein 1998), where velocities of between 5.6 and 6.0 km s^{-1} indicate a pile of 4 km thickness. Applying an equivalent interpretation of the velocities, EBS sediments west of Shannon Island would be up to twice as thick (8 km) considering the 6.0 km s^{-1} contour line as the deepest limit (Figure 6.7).

The two units beneath the Cenozoic sediments east of Shannon Island (km 90 – 200) are interpreted to represent a deep (up to 15 km) rift-basin with a low vertical velocity gradient, and an unresolved thickness of basalts erupted close to break-up. We also assume that the basin east of Shannon Island has a more complex structure with horsts, graben and probably minor volcanic intrusions at greater depths than can be resolved by the velocity model, which is rather uniform. Scattering, and the absorption of seismic energy, prevents sufficient ray coverage in this part of the profile, and does not allow identifying such structures in detail. Large t_{rms} and χ^2 values (Table 6.2) for arrivals of model layer 4 leave the exact depth of this likely Paleozoic/Mesozoic syn-rift basin debatable (Figure 7). We interpret the velocity variations and densities between km 90 and 210 as an average taken over this faulted rift zone. The slightly higher velocity and density at 11 – 15 km depth (km 120) suggest another structural high that is buried deeper in the basin. The sedimentary cover yields a weaker Bouguer anomaly and there is no magnetic anomaly associated with this. Such a deep basin can also be inferred from the regionally low magnetic field anomalies (Figure 7A) between kms 100 and 200. The short wavelength anomalies suggest shallow sources, which can most likely be attributed to flood basalts. This interpretation is consistent with other findings: Larsen (1990) suggested coast-parallel basins and highs across the shelf from aeromagnetic data; Hamann et al. (2005) inferred (from MCS reflection data) that deep basins ($< 13 \text{ km}$) offshore Shannon Island contain rock successions of Devonian to recent age. The deep sedimentary basins of East Greenland developed during a Devonian phase of extensional collapse (Surlyk 1990). Presumably Mesozoic deposits buried the Devonian strata during uniform extension and subsidence of the basin, equivalent to the situation in the Jameson Land basin. We assume that the Shannon basement high (Figure 7, km 50 – 90) also served as a magma conduit inferred from magnetic data and widespread extrusive rocks like those seen in outcrops on Shannon Island. Plateau basalts of Tertiary age with inter-basaltic sediments crop out on Shannon Island and have been related to the Lower Plateau Lava Series, i.e. $\sim 56 \text{ Ma}$ (Watt 1994), although no correlation with other flows on Wollaston Foreland was possible (Figure 6.2). The positive magnetic anomaly is, however, consistent with volcanism during the normal polarity part of chron C25 (55.9 – 56.4 Ma; Cande and Kent 1995). The strong reflections between the Cenozoic and older sediments (Figure 6.6B) are attributed to a cover with a layer of flood basalts but with an unresolved thickness.

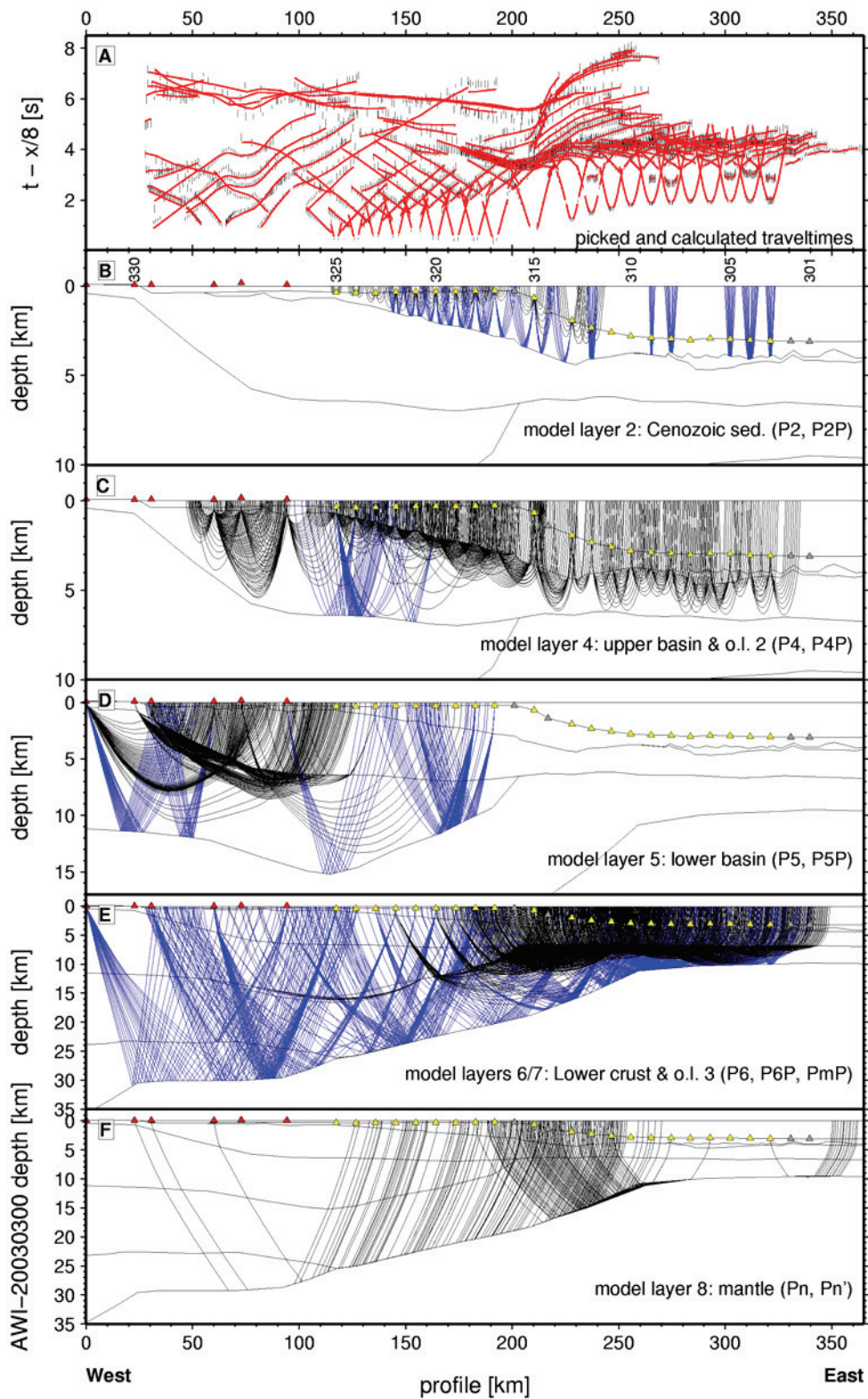


Figure 6.6: Ray coverage along transect AWI-20030300. A) Observed and calculated P-wave arrivals of all rays. See Figure 6.3 for further descriptions. B) Refractions and reflections within the top sedimentary layer. C) Refractions and reflections of the upper part of the continental basin and oceanic layer 2. D) As in (C) but for the lower part of the continental basin. E) Lower continental crustal rays, oceanic layer 3 and Moho reflections. F) Arrivals interpreted as mantle phases either as refractions or as head waves travelling along the Moho (see text for further explanations). Abbreviations are o.l., oceanic layer.

Crystalline basement of continental crust is inferred from velocities greater than 6.0 km s^{-1} . Its thickness decreases significantly from west to east, from nearly 25 km (km 60) just west of the Shannon high to less than 11 km at km 210. Reflection arrivals were modelled at only one station (REF 326) in 23 km depth near profile km 60. This lower crustal reflector represents no significant velocity contrast but is consistent with the model of profile 94300 (Schlindwein 1998). A lithological difference can only be assumed from the gravity modelling. The increased density, and the occurrence of basalts on Shannon Island, supports the existence of a higher degree of magmatic intrusion in the lower crust. As inferred for the profiles off Godthåb Gulf and Kejser Franz Joseph Fjord (Voss and Jokat 2007), there is no evidence of magmatic underplating, as velocities do not exceed 7.0 km s^{-1} , and densities are lower than $3.0 \times 10^3 \text{ kg m}^{-3}$. However, we suggest magmatic intrusions do occur in the lower crust between kms 170 and 210, where the increased seismic velocities and the density of a distinct continent – ocean transition zone cannot be defined due to the weakly resolved structure of the basin between Shannon Island and the oceanic crust. The first magnetic anomaly seems to correspond to C24A/B and therefore constrains the eastward limit of the COT. We propose the onset of oceanic crust and, with it, the location of the seaward COB at km 210, which is well constrained by the oldest magnetic spreading anomaly, the density model for the upper mantle and the evidence for magmatic intrusion of the lower crust. The top oceanic crustal layers 2A and 2B are integrated into oceanic layer 2 (Figure 6.7D), and can clearly be distinguished from oceanic layer 3 on the basis of their velocities, gradients and density (Figure 6.7D). An interface between the continental sediment-basalt mixture and oceanic layer 2 (km 210 and 280) might contain an outer section of SDRS deduced from the slightly reduced velocities and densities (Figure 6.7B/C). However, in such a position these basaltic wedges would obviously overlay oceanic crust. The total oceanic crustal thickness decreases from 13 km at the COB (km 210) to only 7 km near C23 (km 260) within only 40 km and to only 5.5 km at the end of the profile near C21; a value that is thinner than normal oceanic crust (White et al. 1992).

6.4.4 Comparison of structural style with the conjugate Lofoten-Verstålen margin

The region between Shannon Island and the Greenland Fracture Zone is conjugate to the Lofoten-Verstålen Margin off Norway. Comparable margin transects are selected by constructing synthetic flowlines from the Mohns Ridge to the margins (Figure 6.8A), using the rotation poles of Rowley and Lottes (1988). Based on these, two transects, T1 and T4, are suitable for structural style comparisons. Structural interpretations of the Norwegian transects are based on seismic refraction and magnetic/gravity modelling (Kodaira et al. 1995; Tsikalas et al. 2002; Tsikalas et al. 2005). Voss and Jokat (2007) compared profile AWI-20030400 and the Vøring Plateau profile OBS-99 (Mjelde et al. 2005), based on a similar reconstruction.

AWI-20030200 opposes transect T4 off the Verstålen margin segment (Figure 6.8A), where no HVLC is observed (Tsikalas et al. 2005). Normal oceanic crust (~8 km) is up to 3 km thicker than on line AWI-20030200 (Figure 6.8B). The COBs mark the landward increase in Moho depths, which seems gentle on both margins. The structural styles differ further landward. A marginal outer high bounded by the landward escarpment, as seen on line AWI-20030200 (Figures 6.5 and 6.8B), is absent on the conjugate margin. Although no crustal structure is modelled along the East Greenland line west of it, the general basin style is not symmetric to the conjugate Verstålen margin (e.g. Tsikalas et al. 2001; e.g. Hamann et al. 2005).

A simplified model of transect T1 after Tsikalas et al. (2005) is aligned with a simplified structural model of the conjugate profiles 94300 and AWI-20030300 (Figure 6.9) at anomaly C23 (Figure 6.8C). The major difference is the clear core complex structure at the Lofoten margin segment. There are also clear differences in the widths and depths of sedimentary

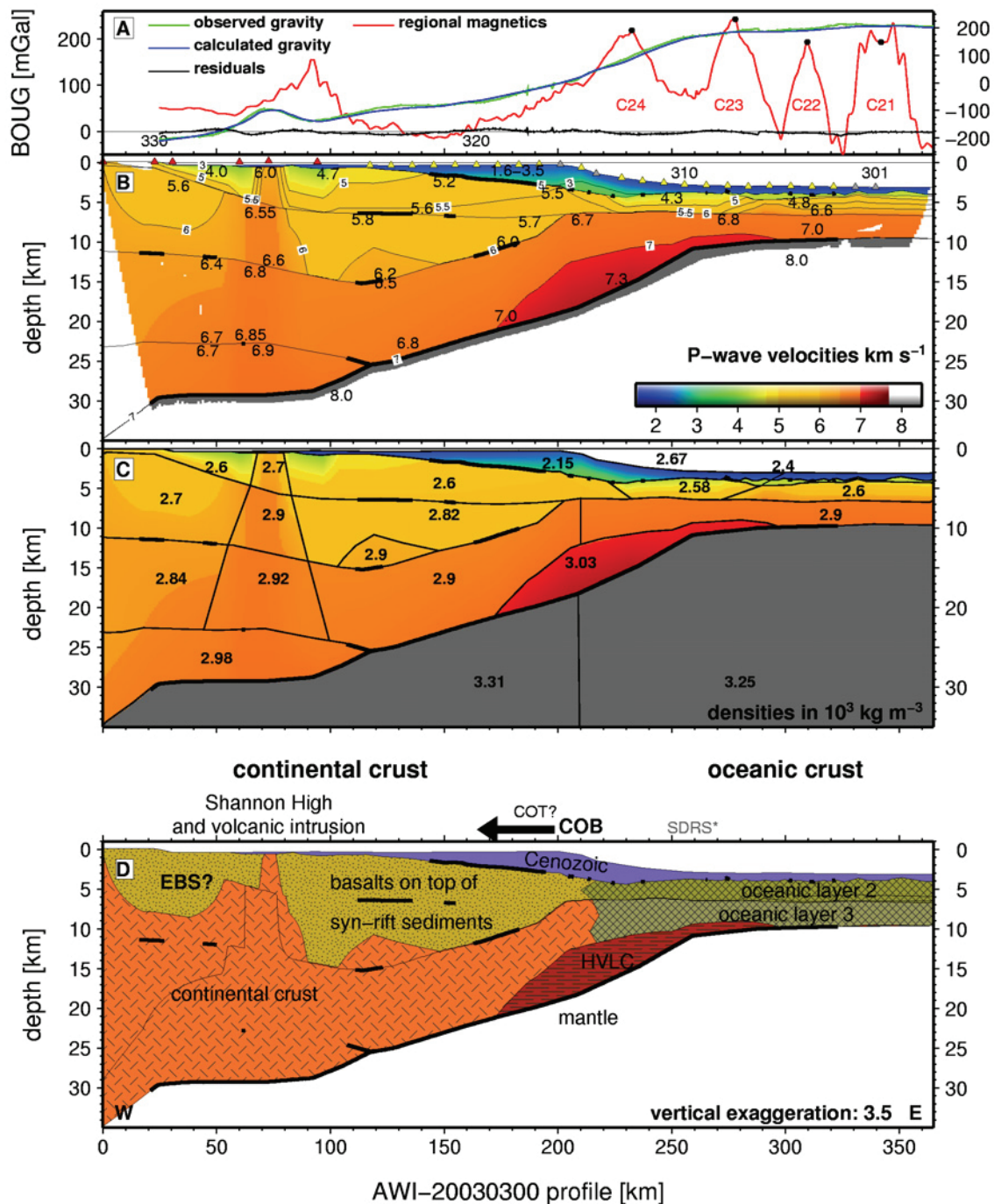


Figure 6.7: Modelling for profile AWI-20030300. Explanations as in Figure 6.5. A) Potential field data and Bouguer gravity model along the line. B) P-wave velocity model. C) 2D density model with marked polygons of constant density. D) Interpretation of the lithology. Note the likely area for seaward dipping reflectors in the oceanic section between km 220 and 280. Abbreviations are as in Figure 6.5 and EBS, Eleonore Bay Supergroup sediments; SDRS*, likely location of seaward dipping reflector sequences.

basins, and Moho depth. The oceanic crust is also approximately 2 km thicker near C23 on the eastern margin. The definition of the COT of the Lofoten margin differs in that it includes the area between C23 and the COB (Figure 6.8C), although both COBs are located near the reverse polarity part of the earliest magnetic spreading anomaly (Tsikalas et al. 2002; this paper), i.e. 70 – 80 km landward of C23 and seaward of extremely thinned continental crust. The lens-shaped HVLC extends on both transects from C23 into the continental domain and is thickest near the COB. The depth range differs beyond the COB, which correlates with the steady increase of Moho depth on the Greenland side. Tsikalas et al. (2005) proposed the

HVLC, absent further north (Tsikalas et al. 2005), as we have suggested for the Greenland side, despite the slightly higher velocities beneath the COB on line AWI-20030200. An adjacent basaltic basin cover is also suggested off Shannon Island but its thickness is not unresolved. Seaward dipping reflectors are proposed for both margin segments between the COB and C23, although they are weakly constrained. Continental crust is thinnest between the COB and the Røst High, which is located approximately 75 km eastwards. An equivalent (albeit more deeply buried) high is suggested on line AWI-20030300, ~90 km landward of the COB (Figure 6.8B), where continental crust is also thinnest. Both highs are marked by gravity anomalies, although the east Greenland anomaly is weaker and lacks a corresponding magnetic anomaly (Figure 6.7A). Further landwards, the Shannon High shows strong similarities to the Lofoten Ridge. Both are distinct highs with proposed increased lower crustal density anomalies. The thinnest crust beneath the Lofoten Ridge is attributed to core-complex development during large scale Mesozoic extension (Tsikalas et al. 2005). High grade, lower crustal rocks, and accreted decompressional melt brought to shallower levels are the likely sources of the higher density. The East Greenland margin shows no core-complex structure but magmatic intrusions are proposed consistent with the emplacement of flood basalts on Shannon Island. Thus, accretion of decompressional melt can not be excluded, and the age of this and its possible relationship to Late Cretaceous/Early Paleocene rifting remains a subject for debate.

The variable oceanic Moho depths, crustal thicknesses, definitions of the COT and the absence of a core-complex emphasize the general asymmetry of these conjugate margins. The outlined small-scale similarities in structural styles and interpretations permit the assumption, however, of a more symmetrical conjugate margin pair than the Vøring and East Greenland margins (Voss and Jokat 2007).

6.5 Half spreading rates and time of break-up

Voss and Jokat (2007) proposed a north to south rift propagation during oceanization of the Greenland Basin north of the Jan Mayen Fracture Zone. This proposal is based on the obliquity of the continent – ocean transition zone deduced from crustal structure models of profiles AWI-20030400 and AWI-20030500 with respect to the oldest magnetic spreading anomalies. The new constraints on the seaward terminations of the continent – ocean transition zone developed here (Figure 6.9) allow us to determine the time of break-up (Table 6.3) along the northeast Greenland margin. Minimum and maximum estimates of the timing were derived from calculations of half spreading rates along the profiles, and also by using the average of the half rates over all four profiles, as shown in Figure 6.9.

A major difficulty in this is to distinguish between ocean spreading anomalies C24A and C24B along the transects AWI-20030200 and AWI-20030300. On both profiles, only one distinct maximum can be seen that relates to these spreading anomalies (Figures 6.5A, 6.7A and 6.9). Therefore, we average over the time period after Cande and Kent (1995) and estimate a C24 normal polarisation maximum at 52.9 Ma. A similar approach for anomalies C20 – C23 results in normal polarisation maxima at 43.16 Ma, 47.09 Ma, 49.36 Ma and 51.4 Ma. The differences between these age maxima were used for the durations of the spreading intervals. Half spreading rates were determined for C20 – C24 along the profiles and corrected for spreading direction (Table 6.3), based on synthetic flowlines from the Mohs Ridge generated using the rotation poles of Rowley and Lottes (1988). A change in spreading direction occurred after C22. The main uncertainty is in the identification of the peaks of normal polarity anomalies (Figures 6.5A and 6.7A), with 2 km shifts yielding an error of 1.5 km Ma^{-1} in the modelled half spreading rate. An offset in magnetic anomaly C22 near stations OBS 201 and 202 on profile AWI-20030200 (Figure 6.2) appears on the regional magnetic grid. Here, we have used a projection of the linear part of the anomaly from further southwest. Similar calculations on the southern profiles AWI-2003400 and AWI-20030500 constrain the

half spreading rates for the intervals between C21 – C23 and C20 – 22, respectively (Table 6.3).

For the northern lines, early seafloor half spreading rates range between 22 and 29 km Ma⁻¹ (Figure 6.10). Later on, rates dropped to 13 - 15 km Ma⁻¹ (average 14 km Ma⁻¹) between C23 (51.4 Ma) and C22 (49.4 Ma) and to 13 – 17 km Ma⁻¹ (average 14.7 km Ma⁻¹) for the interval C22 to C21 (47.1 Ma). A further drop at C21 – C20 (43.2 Ma) to below 10 km Ma⁻¹, was determined along line AWI-20030500. These values closely fit published half rates for the intervals between C21 and C23 (Figure 6.10). It has to be noted that Voss and Jokat (2007) determined half spreading rates along a transect perpendicular to the magnetic anomalies (Figure 6.2), however, judging from the old edges of normal polarity anomalies giving rise to an apparent shift in the determined age of rate changes (Figure 6.10).

Mosar et al. (2002b) calculated half spreading rates along tectonic flowlines and found much slower rates than we have for the interval between C23 – C24, but identical rates for later intervals. Results from the Møre margin (Breivik et al. 2006) also resemble our results quite well. Hopper et al. (2003) determined initial half spreading rates of 33 km Ma⁻¹ for the southeast Greenland margin between 56 Ma and ~53 Ma, with a drop to 19 km Ma⁻¹ between ~53 Ma and 50.8 Ma and a further decrease to 17 km Ma⁻¹ until 47.8 Ma. These rates are comparable to the observations of northeast Greenland, despite the fact that break-up is proposed to be earlier (~56 Ma).

Based on our half rate calculations, we propose a time of break-up (Table 6.3) of 54 ± 0.2 Ma at profile AWI-20030200 and 53.8 ± 0.2 at AWI-20030300. The seaward boundaries of the COT, i.e. the COBs, on profiles AWI-20030400 and AWI-20030500 (Voss and Jokat 2007) can be dated to 51.5 ± 0.2 Ma and 50.1 ± 0.3 Ma, respectively (Figure 6.9).

h.s.r. in kmMa ⁻¹ on profile location	C20 – C21 (3.93 Ma)	C21 – C22 (2.27 Ma)	C22 – C23 (2.04 Ma)	C23 – C24 (1.5 Ma)	break-up at seaward boundary of COT [Ma]
AWI-20030200	-	14.8 (11°)	14.0 (5°)	22.6 (5°)	54.0 ± 0.2
AWI-20030300	-	13.1 (23°)	14.9 (16.5°)	29.0 (16.5°)	53.8 ± 0.2
AWI-20030400	-	13.4 (24.5°)	13.2 (18°)	-	51.5 ± 0.2
AWI-20030500	8.1 (27.5°)	17.1 (27.5°)	- (22°)*	-	50.0 ± 0.3

Table 6.3: Half spreading rates and timing of break-up calculated four north-eastern seismic lines. Angles behind half spreading rates were used to correct for spreading directions. Angle with asterisk was used for break-up calculation.

6.6 Offshore crustal architecture of the East Greenland margin

In this section, we summarize offshore crustal models derived from seismic refraction modelling, which extend over the southeast and northeast Greenland margins. MCS data were not included, since we focus on velocity models from basement to the depth to the Moho. Therefore, the resolution of the maps is simply based on the resolution of the P-wave velocity models. Two major uncertainties might thus affect the reliability of the maps. Navigation data were not accessible for some seismic lines, for which the locations of the transects were instead digitized from publications. Where endpoints were available, an equidistant interpolation linked the navigation and the model layers along the profiles. This may result in a modest offset of less than 5 km. Uncertainties also result from digitizing crustal models and identifications of layer boundaries, i.e. crystalline basement, Moho and high velocity lower crust (HVLC). Here, we assume maximum errors of less than 500 m for layer depths identifications and, therefore, an error of less than 1 km for layer thicknesses. Note, that we performed no crossover corrections for the variations in thicknesses and layer depths observed at profiles crossing points, which result from different shot directions and modelling constraints. The gridding algorithm (adjustable tension continuous curvature surface gridding;

Smith and Wessel 1990) smoothed these areas of large gradients of layer depths and thicknesses, resulting in deviations between the maps and source model profiles.

Profile ID	Geographic location	Line colour	Reference	Basement [km]	Moho [km]
	Northeast Greenland				
20030200	south GFZ – COT	red	this paper	120 – 330	170 – 330
94300	Bredefjord	green	2	0 – 210	50 – 180
20030300	Ardencaple Fjord – COT	red	this paper	0 – 365	20 – 355
20030400	Godthåb Gulf - COT	red	3	0 – 313	20 – 300
94320	Keiser Franz Joseph Fjord	green	4	0 – 375	75 – 250*
20030500	Keiser Franz Joseph Fjord - COT	red	3	0 – 465	50 – 450
94340	Kong Oscar Fjord	green	4	0 – 350	87 – 300
94360	Dickson Fjord	green	4	0 – 230	40 – 200
	Central East Greenland				
94410	Nordvest Fjord - Hall Bredning	dark blue	5	0 – 270	50 – 255
90320	Føn Fjord - Hall Bredning	dark blue	5	0 – 210	40 – 195
94400	Gåse Fjord - Hall Bredning	dark blue	4,5	0 – 270	70 – 250
90537	N–S Hall Bredning	pink	6	0 – 116	0 – 116
90538	W–E Hall Bredning (south)	pink	6	0 – 36	0 – 36
90539	N–S Hall Bredning (southern)	pink	6	0 – 85	0 – 85
90540	N–S Hall Bredning (northern)	pink	6	0 – 34	0 – 34
90549	W–E Hall Bredning (north)	pink	6	0 – 42	0 – 42
90554	W–E Hall Bredning (central)	pink	6	0 – 36	0 – 36
88300	W–E Scoresby Sund - Kolbeinsey Ridge	orange	7	155 – 417	155 – 417
88400	N–S Scoresby Sund (C5)	orange	7	0 – 165	0 – 165
88500	N–S Scoresby Sund (C6?)	orange	7	0 – 120	0 – 120
88600	NE Jameson Land	orange	7	0 – 164	0 – 164
	Kolbeinsey Ridge - Jan Mayen Basin				
L1	N–S eastern flank of Kolbeinsey Ridge	light blue	8	0 – 98	0 – 98
L2	N–S 12 km east of Kolbeinsey Ridge	light blue	8	0 – 99	0 – 99
L3	W–E Kolbeinsey Ridge - Jan Mayen Basin	light blue	8,9,10	0 – 284	0 – 284
L5	eastern Jan Mayen Basin	light blue	9	0 – 125	0 – 125
L6	western Jan Mayen Basin	light blue	9	0 – 125	0 – 125
	Southeast Greenland				
SIGMA I	Greenland - Iceland Ridge	brown	12	0 – 500	0 – 500
SIGMA II	SE Greenland - ocean basin	brown	11,12	0 – 350	0 – 350
SIGMA III	SE Greenland - ocean basin	brown	12,13	0 – 391	0 – 391
SIGMA IV	southern tip of Greenland	brown	12	0 – 348	0 – 348

Table 6.4: Wide-angle seismic line numbers of the corresponding P-wave velocity models used for this compilation. Geographic locations and line colours correspond to lines in Figure 6.1. The resolution of the basement and Moho is given in km along the profiles. See references for details of the profiles: 1) Fechner and Jokat (1996); 2) Holbrook et al.(2001); 3) Hopper et al.(2003); 4) Kodaira et al. (1997); 5) Kodaira et al. (1998a); 6) Kodaira et al. (1998b); 7) Korenaga et al. (2000); 8) Schlindwein (1998); 9) Schlindwein and Jokat (1999); 10) Schmidt-Aursch and Jokat (2005a); 11) Voss and Jokat (2007); 12) Weigel (1995). Abbreviations of locations are C5,C6?, magnetic chrons off Scoresby Sund; COT, continent ocean transition zone; GFZ, Greenland Fracture Zone; N – S, north to south; W – E, west to east; NE, northeast; SE, southeast.

6.6.1 Seismic profiles

The entire length of the East Greenland margin (~3000 km) is covered with ~50 wide-angle seismic profiles, which constrain the crustal structure from the top sedimentary cover to the Moho (Figure 6.1). We used a set of crustal models based on 30 wide-angle seismic lines (Table 6.4). Four lines, SIGMA I – IV (Korenaga et al. 2000; Holbrook et al. 2001; Hopper et al. 2003), cover the area between the Greenland-Iceland Ridge (SIGMA I) and the southern tip of Greenland (SIGMA IV). For these, in situ sample control from ODP drillholes exists (Larsen et al. 1994). The quality of the P-wave velocity models of SIGMA II – IV is excellent. SIGMA II is based on seismic tomography (Korenaga et al. 2000) and layer

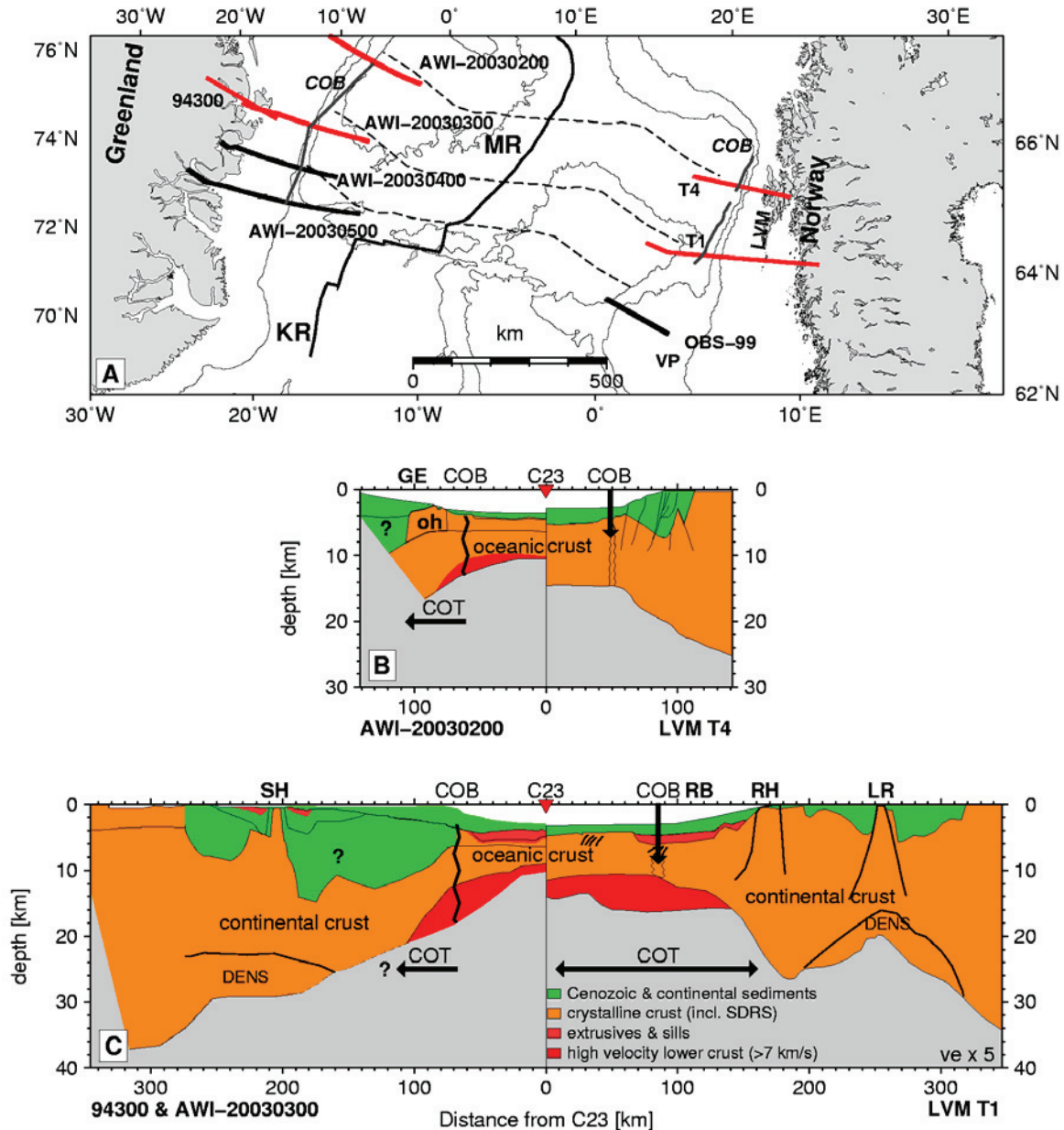


Figure 6.8: Comparison of profiles from northeast Greenland and Lofoten-Vesterålen Margin (LVM). A) Line location map. Thick lines mark seismic profiles. Red lines are compared below. Dashed thin lines represent flowlines (Figure 6.2) from the Mohns Ridge (MR). Gray lines mark proposed COBs. Thin black lines are bathymetric contours of 1000, 2000 and 3000m. See text for line references. Abbreviations are KR: Kolbeinsey Ridge, VP: Vøring Plateau. Scale valid for 75° N. B) + C) Line-up of simplified conceptual models at chron C23. LVM T1 and T4 after Tsikalas et al. (2005). Note that profile lengths are inverted to distance from C23. Hatched lines mark SDRS. Black lines outline structural features. Abbreviations are COB/COT: continent-ocean boundary and transition zone, GE: Greenland Escarpment, DENS: marked lower crustal region with proposed increased density, oh: outer high, LR: Lofoten Ridge, RB: Røst Basin, RH: Røst High, SDRS: Seaward dipping reflector sequences, SH: Shannon High.

boundaries were derived from velocity contour lines. Constraints from SIGMA I (Holbrook et al. 2001) might contain larger uncertainties due to the moderate quality of the published model.

Between the Greenland – Iceland Ridge (GIR) and Scoresby Sund, i.e. offshore the Geikie Plateau (Figure 6.1), wide angle seismic data are insufficient for this region to be included in the presented maps.

The region of Hall Bredning and Scoresby Sund is constrained on profiles by several authors

(Fechner and Jokat 1996; Mandler and Jokat 1998; Schmidt-Aursch and Jokat 2005a). A selection of six north-south and east-west trending lines (90537-90540, 90548 and 90554) along and across Hall Bredning are included after Fechner and Jokat (1996), which surround further of their lines, and provide a good approximation to the crustal structure in this region. Using all of their lines would not change the overview of the East Greenland margin. Velocity models from profiles 94410 (Nordvestfjord), 90320 (Føn fjord) and 94400 (Gåsefjord) were used in this compilation from Schmidt-Aursch and Jokat (2005a), who remodelled previous transects (Mandler and Jokat 1998) with additional recording units.

Weigel et al. (1995) presents crustal structure models off Scoresby Sund and south of Kong Oscar Fjord. The offshore network of lines 88300 – 88600 provide good to moderate constraints on the younger oceanic crust from the west flank of the Kolbeinsey Ridge. Moho depths are occasionally weakly resolved. Therefore, a simplified model structure is used for mapping. From the eastern flank of the younger ridge system to the Jan Mayen basin, the crustal structure is imaged by a network of wide-angle lines L1, L2, L3, L5 and L6 from Kodaira et al. (1997; 1998a; 1998b).

The crustal structure and the continental sedimentary basins of the Fjord region north of the Jan Mayen Fracture Zone are resolved by profiles in the Dickson Fjord (94360), Kong Oscar Fjord (94340), Keiser Franz Joseph Fjord (94320) and Brede Fjord (94300) (Schlindwein 1998; Schlindwein and Jokat 1999; 2000; Schmidt-Aursch and Jokat 2005a). Line 94320 is extended in the prolongation of the Keiser Franz Joseph Fjord with profile AWI-20030500. The COT and onset of oceanic crust are imaged by this transect, together with lines AWI-20030400 and AWI-20030300. Profile AWI-20030200 marks the northernmost limit of the East Greenland mapping region. Crustal models of CDP profiles 41, 46 and 61 are excluded (Hinz et al. 1987; Mutter and Zehnder 1988) due to their proximity to the higher-resolution profiles AWI-20030200-500.

6.6.2 Depth to crystalline basement

The top of crystalline basement in the offshore continental parts of the margin is defined at the 6.0 km s^{-1} velocity contour, which is consistent with global studies (Christensen and Mooney 1995). Basaltic layers within the sedimentary units of the COT are not considered as basement units. This yields a maximum discrepancy of 1.2 km between the depth of the 6.0 km s^{-1} contour line and the interpreted basement within the COT on profiles AWI-20030400 and AWI-20030500. In order to be consistent in this compilation, the 6.0 km s^{-1} isopach is used for both the continental and COT domains.

Within the oceanic crust, the top of oceanic layer 2A (White et al. 1992) is chosen as the top basement layer. Within the oceanic part of profile SIGMA II, a 4.0 km s^{-1} isopach approximates the top of oceanic basement reasonably well, and is consistent with our seismic profiles of northeast Greenland.

The depth to the basement is mapped over the full extent of the profiles (Table 6.4), which sum up to almost 6648 km. Figure 6.11 illustrates the results. The largest deviations, of up to 6.4 km, occur between the grid and line data near the Shannon High (AWI-20030300). Here, the steep gradient on the eastern margin of the high is smoothed out in the mapped representation of basement depth.

The map clearly shows the relatively uniform and shallow depth to basement in the south compared to the more structural central to northeast Greenland margin. The deep sedimentary basins observed in Scoresby Sund (Weigel et al. 1995) and on Jameson Land (Fechner and Jokat 1996; Schlindwein and Jokat 1999; Schmidt-Aursch and Jokat 2005a) (Figures 6.1 and 6.11) die out towards the Jan Mayen Fracture Zone. Larsen (1990) proposed, and Henriksen et al. (2000) outlined, the central- and northeastern offshore sedimentary basins, which are deeper than 3 km, and are fairly well matched in Figure 6.11. Voss and Jokat (2007)

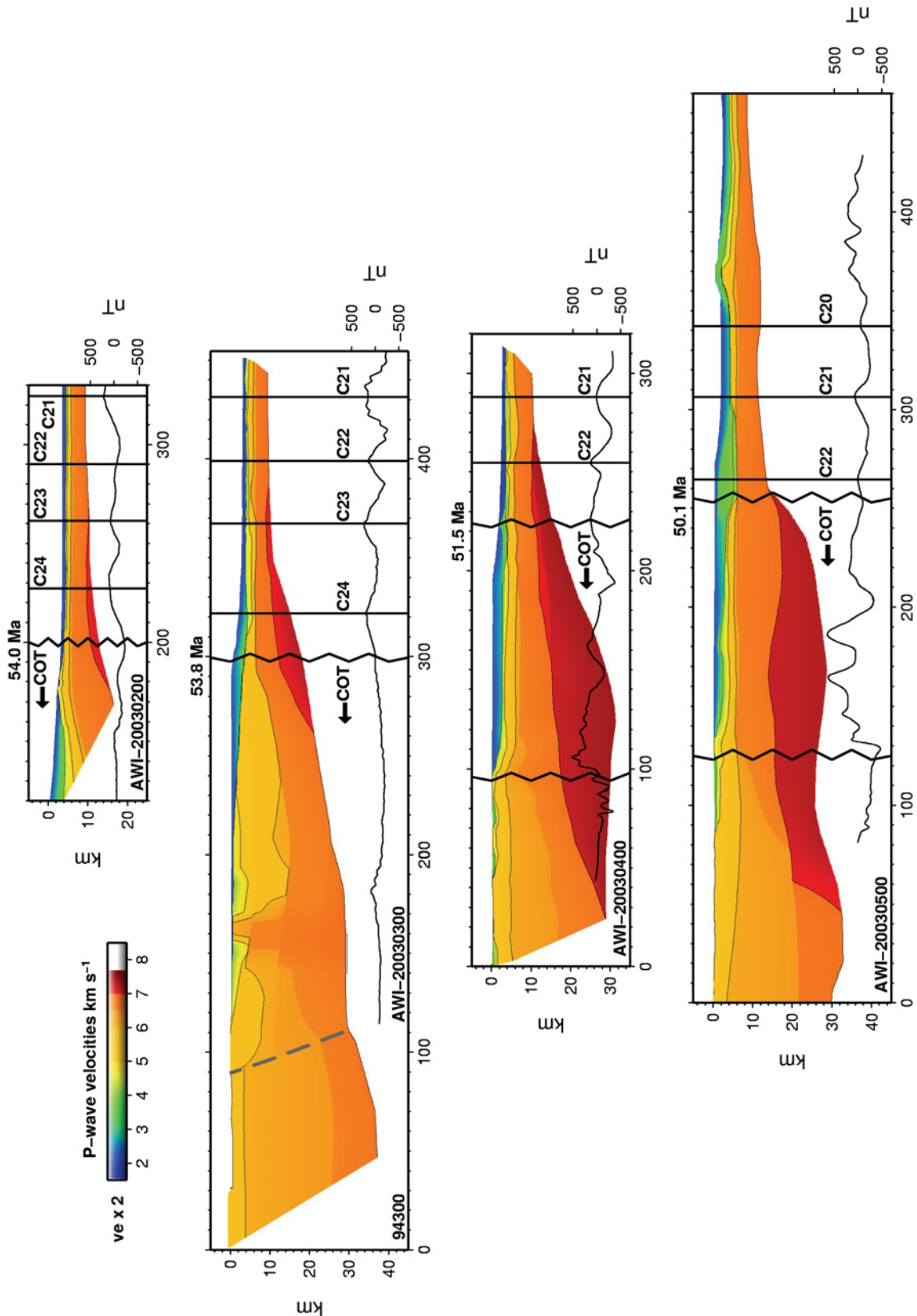


Figure 6.9: Compilation of northeast Greenland P-wave velocity models between the Jan Mayen and Greenland fracture zones. Locations are in Figure 6.1. All models are shown with vertical exaggeration of 2 and velocity contours of 4, 5, 6 and 7 km s⁻¹. Model for 94300 refers to Schlindwein (1998), models of AWI-20030400 and AWI-20030500 to Voss and Jokat (2007). Boundary of merged profiles 94300 and AWI-20030300 is outlined with grey dashed line. Lower right scale relates to along-line magnetic data as shown at the bottom of the models. Spreading anomalies and seaward COB of the transition zones are marked with vertical lines and labelled. The age given above the COB refers to calculated time of break-up (see text).

suggested that the basin north of the Jan Mayen Fracture Zone consists of 4 km of syn-rift sediments mixed with basalts, overlain by post-break-up sediments forming the present day shelf region. Additional constraints on the extent of the >8 km deep sedimentary basins off Shannon Island and further north, outline a change in rifting style between lines AWI-20030400 and AWI-20030300.

6.6.3 Depth to Moho

The Moho is not resolved at the beginning and end of several seismic lines, due to the lack of ray coverage. In order to minimize extrapolation of unresolved regions, we trimmed the lines to the resolved Moho (Table 6.4). In all, 5973 km of Moho depth values were used for mapping (Figure 6.12). The largest averaging effect occurs at the end of line 94360, at its intersection with profile AWI-20030500. Here, the Moho decreases by ~3.6 km, which matches reasonably well with the better-constrained Moho of profile AWI-20030500. A slight step in the Moho at kms 170 – 200 of profile 94410 (Schmidt-Aursch and Jokat 2005a) is smoothed and raised by up to 3.6 km in the grid. A shallower Moho depth of up to 5 km compared to a 3D gravity model (Schmidt-Aursch and Jokat 2005b) is based mainly on the additional contribution of seismic lines in the Jan Mayen basin after Kodaira et al. (1998a) and the new constraints of the COT and oceanic crust from the profiles AWI-20030200 – 500.

6.6.4 Crustal thickness

Crustal thicknesses are derived from the line data before interpolation, i.e. the difference between the top crystalline basement and the depth to the Moho. Syn- and postrift sediments and basalts are not included and the thickness of the crust was only calculated where Moho depths could be picked. The largest deviations occur as a result of smoothing the basement near the Shannon High of profile AWI-20030300. Moderate variations occur on several other line intersections in the central-east Greenland region most likely due to the different resolutions and interpretations of the profiles and/or steep gradients in the derived thicknesses.

The major differences in the oceanic crustal thickness of the northeastern and southeastern margin are obvious (Figure 6.13). Between the Jan Mayen and Greenland fracture zones, oceanic crustal thickness decreases rapidly from 10 – 13 km just east of the COB to normal and even thinner values (7 – 5 km). Along all profiles of the northeast Greenland margin, a rapid decrease to thinner than normal oceanic crust occurs prior to C21. Igneous crust decreases from 18 – 30 km to ~8 km thickness along the southern profiles SIGMA-II, -III and IV. C24 – C21 aged oceanic crust south of the Greenland-Iceland Ridge (GIR) is up to 5 km thicker than that north of the Jan Mayen Fracture Zone. The extreme crustal thickness of 25 – 35 km, derived from line SIGMA-I, is clearly associated with the GIR (Holbrook et al. 2001), and contrasts with the younger and thinner crust (~5 – 10 km) off Scoresby Sund.

6.6.5 Thickness of high velocity lower crust

Several seismic models in this compilation show a high velocity lower crust (HVLC; velocities exceeding 7.0 km s^{-1}) each of which is associated with increased magmatism during break-up by the corresponding authors. The thickness of the HVLC along the East Greenland margin is illustrated in Figure 6.14, ignoring the varying interpretations of it as representing sub-continental pure magmatic underplating (Schlindwein and Jokat 1999; Voss and Jokat 2007), igneous transitional crust and/or thickened oceanic crust (Weigel et al. 1995; Kodaira et al. 1997; Kodaira et al. 1998a; Kodaira et al. 1998b; Korenaga et al. 2000; Holbrook et al. 2001; Hopper et al. 2003). None of these authors suggested the possibility of serpentinized mantle or eclogitic material, which display similar high seismic velocities and density

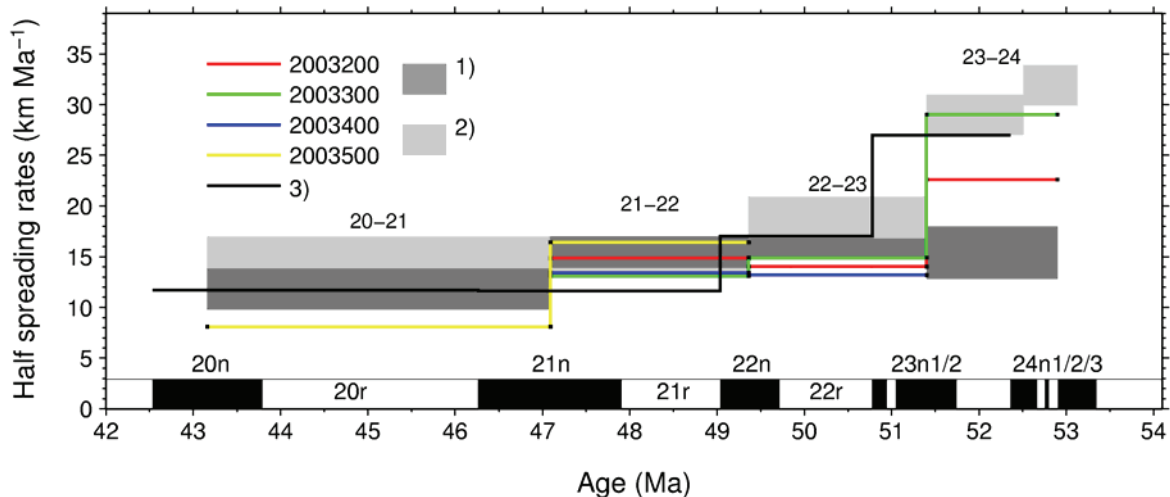


Figure 6.10: Half spreading rates calculated along seismic lines. Calculations by other authors are included as reference. Dark grey (1) refers to Mosar et al. (2002b), light grey (2) to Breivik et al. (2006). The half spreading rates of Voss and Jokat (2007) (3) are based on the beginning of each positive polarity anomaly while all others used the maxima of normal polarities. Polarities of the magnetic chrons are shown at the base of the diagram after Cande and Kent (1995).

anomalies and have been considered as alternatives to magmatic layers beneath the Norwegian margin (Mjelde et al. 2002; Gernigon et al. 2003; Gernigon et al. 2004; Ebbing et al. 2006). Major misfits and averaging occurred at the Keiser Franz Joseph Fjord between lines 94320, 94360 and AWI-20030500 at the landward end of the HVLC. Schlindwein and Jokat (1999) resolved high velocities only at the end of the lines while Voss and Jokat (2007) imaged the full extent of this body. However, gridding causes a reduction of the thickness by 3.1 - 6.4 km between km 60 and 75 on profile AWI-20030500 (Figure 6.9). Misfits of less than 3.5 km occur locally near the Kolbeinsey Ridge (88300 and L1), the extension of the Kong Oscar Fjord (94360 and 88600) and on lines SIGMA-I, -III and -IV (Figure 6.1).

The map shows strong variations in the dimensions of the HVLC, with two different styles. The southern margin shows a widespread high velocity lower crust. The moderate to great thicknesses of 5 - 10 km (SIGMA II - IV) underlie the oceanic crust as well as landward of the COB. A maximum thickness is reached along the GIR (SIGMA-I), at more than 15 km. No HVLC was identified within the continental crust of Hall Bredning and Scoresby Sund (Fechner 1994; Schlindwein and Jokat 1999; Schmidt-Aursch and Jokat 2005a) (Fig1), and there is insufficient seismic coverage to image the lower crust beneath the basalt-covered Geikie Plateau. The young oceanic crust west of the Kolbeinsey Ridge, however, contains a 5 - 10 km thick HVLC (Weigel et al. 1995), greater than on the eastern side of the ridge, where it decreases to less than 5 km (L1 - L6) (Kodaira et al. 1997; Kodaira et al. 1998a; Kodaira et al. 1998b).

Near the Jan Mayen Fracture Zone, and further north, the pattern of the high velocity lower crustal thickness shows more variations with great local maxima which probably is due to the more closely spaced data. The HVLC identified on the Kong Oscar Fjord profile 94360 (Schlindwein and Jokat 1999) (Figure1) increases from 5 km thickness to a maximum of 15 km on the nearby profile 88600 (Weigel et al. 1995), where almost the entire oceanic crust contains velocities of greater than 7.0 km s^{-1} . North of the fracture zone, the maximum thickness of the HVLC exceeds 10 - 15 km (AWI-20030400 and AWI-20030500) (Voss and Jokat 2007), and is found landward of and along the COT, with a strong decrease in thickness towards the onset of oceanic crust and towards the north. From C23 and C22 eastwards, no high velocity oceanic layer ($>7.0 \text{ km s}^{-1}$) appears in the seismic models. This is in strong contrast to the southern margin, where the oceanic crust apparently has a high velocity lower layer of more than 5 km thickness at similar crustal ages.

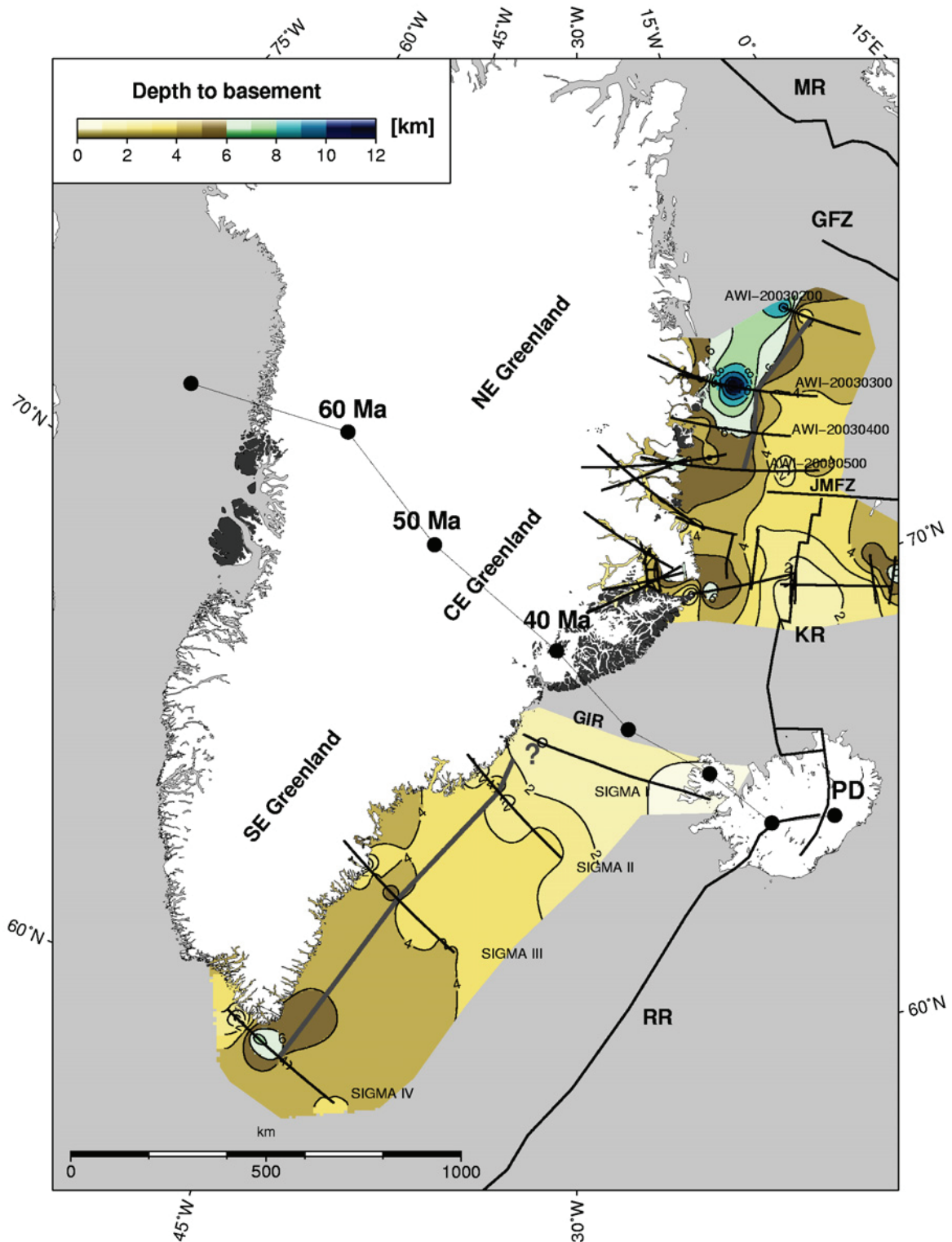


Figure 6.11: Map of generalized depth to crystalline basement based on published seismic lines shown in Figure 6.1 and listed in Table 6.4. Basement is defined at the 6.0 km s⁻¹ contour line in the continental domain, and at the top of oceanic layer 2A in the oceanic domain. Onshore dark grey regions mark flood basalts. Outline of mapped region excludes large scale extrapolations. Contours every 1 km are included as reference. Thick grey line marks the break-up location along the SIGMA profiles in Southeast Greenland after Holbrook et al. (2001). Question mark denotes unknown location of the line of break-up. The same line marks the seaward COB of the transition zones as in Figure 6.8 along profiles AWI-2003200–500 in northeast Greenland. Black lines mark profile locations. Abbreviations are as in Figure 6.1. Scale is valid for 70° N.

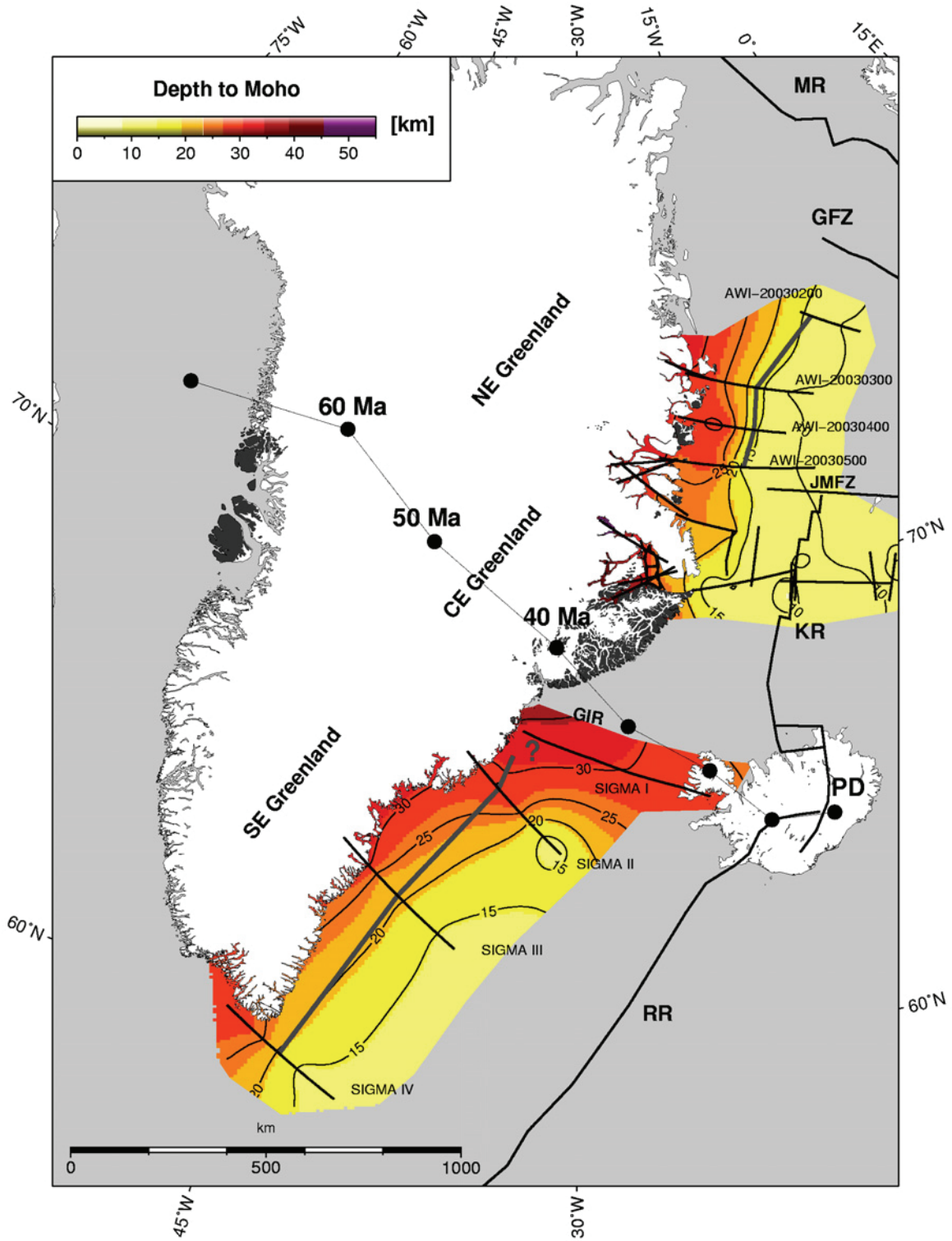


Figure 6.12: Map of depth to Moho. Moho depths are only used where constrained by ray coverage or outlined in other published models. In general it coincides with the 8.0 km s⁻¹ velocity contour line. Depth contours are outlined every 5 km. Format of map is equivalent to Figure 6.11.

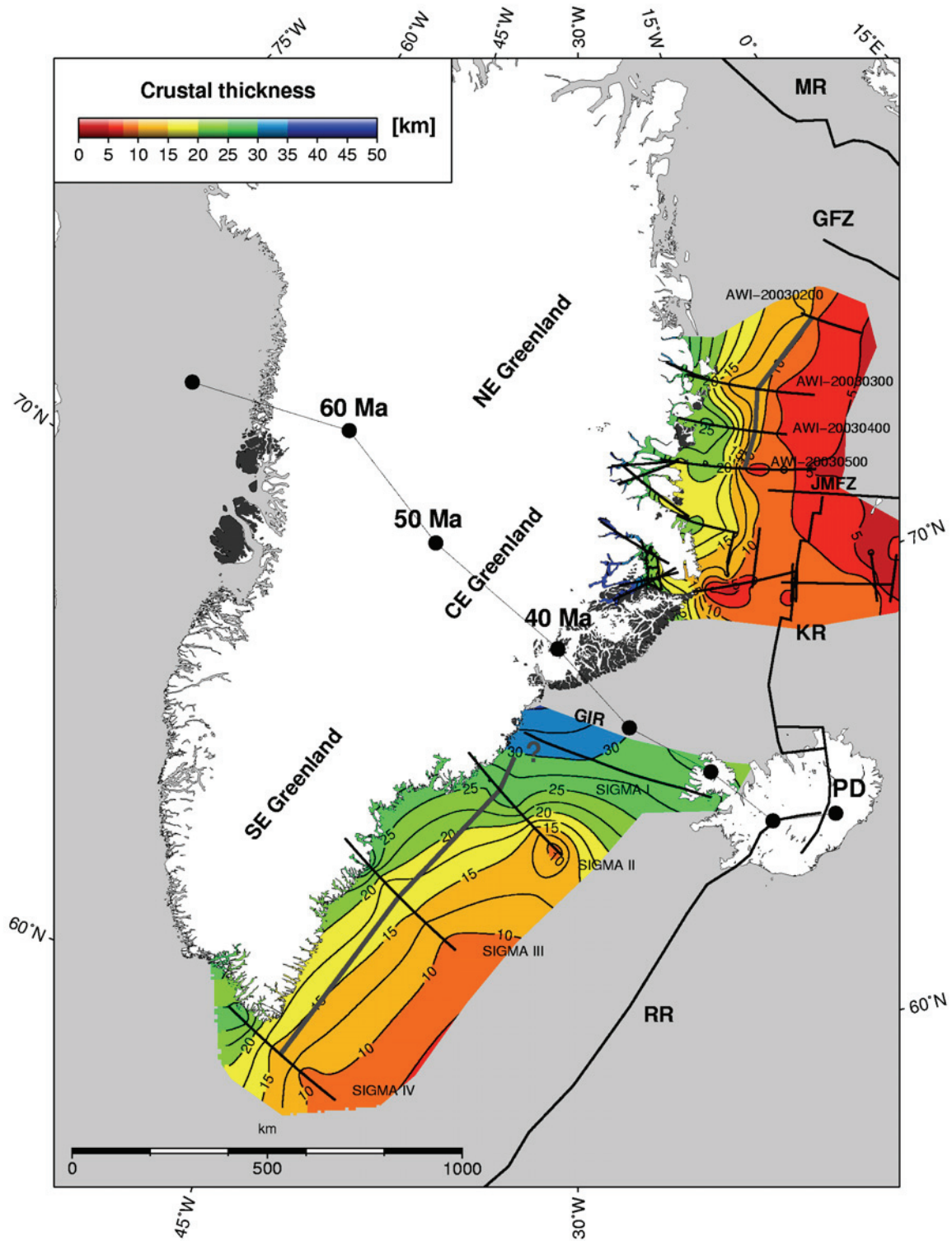


Figure 6.13: Crustal thickness map, with thicknesses calculated from line data (Moho – basement) prior to mapping. Contour lines every 2.5 km. Note the different thicknesses seaward of the grey line in the northeast and southeast Greenland margins. Format of map is equivalent to Figure 6.11.

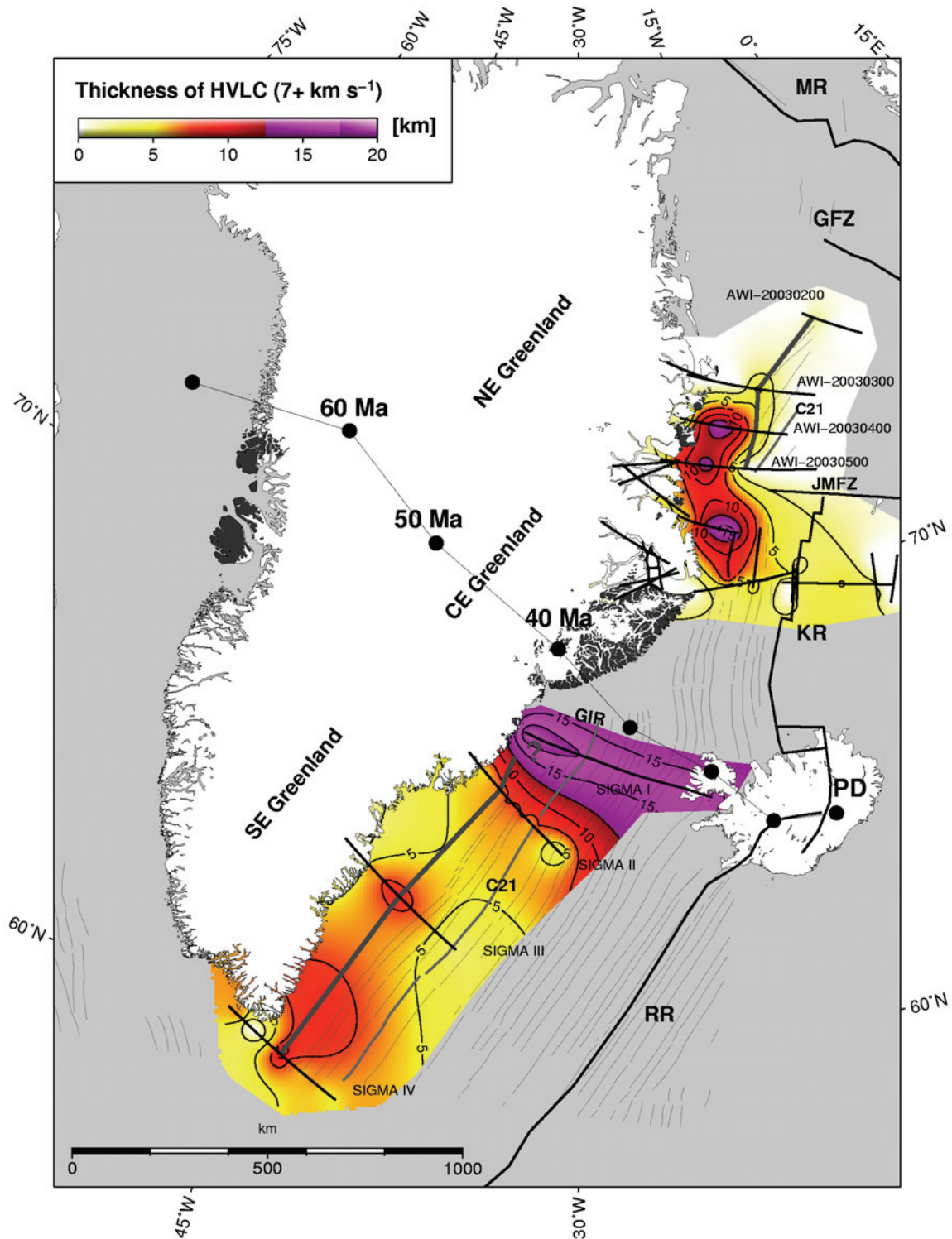


Figure 6.14: Thickness map of high velocity lower crust (HVLC), including seismic velocities of $>7.0 \text{ km s}^{-1}$ along the East Greenland margin. It includes igneous crust and sub-continental magmatic underplating. Contour interval 2.5 km. Magnetic spreading anomalies are included and C21 is highlighted for reference. Note the different distributions of the thicknesses between southeast and northeast Greenland. Format of map is equivalent to Figure 6.11.

6.7 Discussion

The heterogeneous style of the northeast Greenland margin domain differs significantly from the more regular style in the south-eastern domain in almost all maps. This might be influenced by the much smaller distance between northern seismic lines and the spatial extent of about 800 km from the Scoresby Sund to the northern end compared to almost 1200 km along the south-eastern margin. The maps emphasize, however, the strong variations of the northern and southern regions in terms of the dimension, distribution and extent of the HVLC, and the thickness of the oceanic crust.

The presented profiles are all located within a radius of ~1300 km from the proposed location of the Iceland plume track (Lawver and Müller 1994). Despite the similar distances of the seismic lines AWI-20030200-500 and SIGMA I – IV to the Icelandic thermal anomaly, the heterogeneous distribution of the HVLC along the Greenland margins suggests strong variations in margin formation processes. The first major difference is that the majority and maxima of the HVLC are interpreted as pure magmatic underplating beneath extended continental crust (Voss and Jokat 2007) near the Jan Mayen Fracture Zone, but HVLC is absent only 100 km further to the north, where only minor intrusions appear near the COB. Emplacement of high velocity igneous crust landward of the COB is less for the southern Greenland region, but continues much further out into the transitional and oceanic domains.

The second difference is in the maximum thickness of the HVLC. SIGMA II – IV lines show an almost continuous distribution of the HVLC and its thickness while in the north it appears more concentrated on the vicinity of the Jan Mayen Fracture Zone (Figure 6.14), where it is less widespread but almost twice as thick as off southeast Greenland.

The third major difference is the thickness age and content of the oceanic HVLC. Between break-up and C21 (47.1 Ma) (C21 marked in Figure 6.14), the oceanic crust in the northern region loses its HVLC and thins rapidly to about 5 km. Off southeast Greenland, the oceanic crust near C21 still has a HVLC and its thickness is in the range 8 – 10 km.

6.7.1 HVLC distribution at North Atlantic conjugate margins

Regional melt distribution prior to and shortly after break-up along the East Greenland and conjugate margins can be estimated from HVLC thicknesses. Average thicknesses are estimated for the East Greenland margin landward of the line of break-up (Holbrook et al. 2001), and the proposed northeastern COB (Figures 6.9 and 6.14), and out to magnetic chron C21 for the oceanic domain. The distances of the East Greenland margin profiles from the plume head are related to SIGMA I (Figure 6.14) which is located along the Greenland – Iceland Ridge (GIR). The contributions of profiles 94340 and 88600 (Weigel et al. 1995; Schlindwein and Jokat 1999) are included, even if this region is influenced by Late Oligocene to Miocene rifting. Profile Cam77 (Barton and White 1995) of the Edoras Bank margin (EB) and line NI8 from Hatton Bank (HB) (Fowler et al. 1989; Morgan et al. 1989) are appropriate conjugate transects for the southeast Greenland margin (Holbrook et al. 2001; Hopper et al. 2003). Profiles OBS-99 from the Vøring margin (Mjelde et al. 2005) and T1 from the Lofoten margin (Tsikalas et al. 2005), as previously shown (Voss and Jokat 2007; this paper), oppose the northeast Greenland lines (Figure 6.8). Spatial distances on the conjugate margin are related to the Faeroe-Iceland Ridge (FIR) (Bott and Gunnarson 1980), the eastward prolongation of the GIR according to Barton and White (1995). These authors suggest a symmetric distribution of excess melt thickness north and south of the FIR. The decreased melt thicknesses at the peripheries of the region indicate decreased asthenospheric temperatures with increasing distance to the plume location. An increased temperature of approximately 100° C associated with the Iceland plume is assumed to result in passive upwelling and the emplacement of large amounts of melt compared to the succeeding oceanic

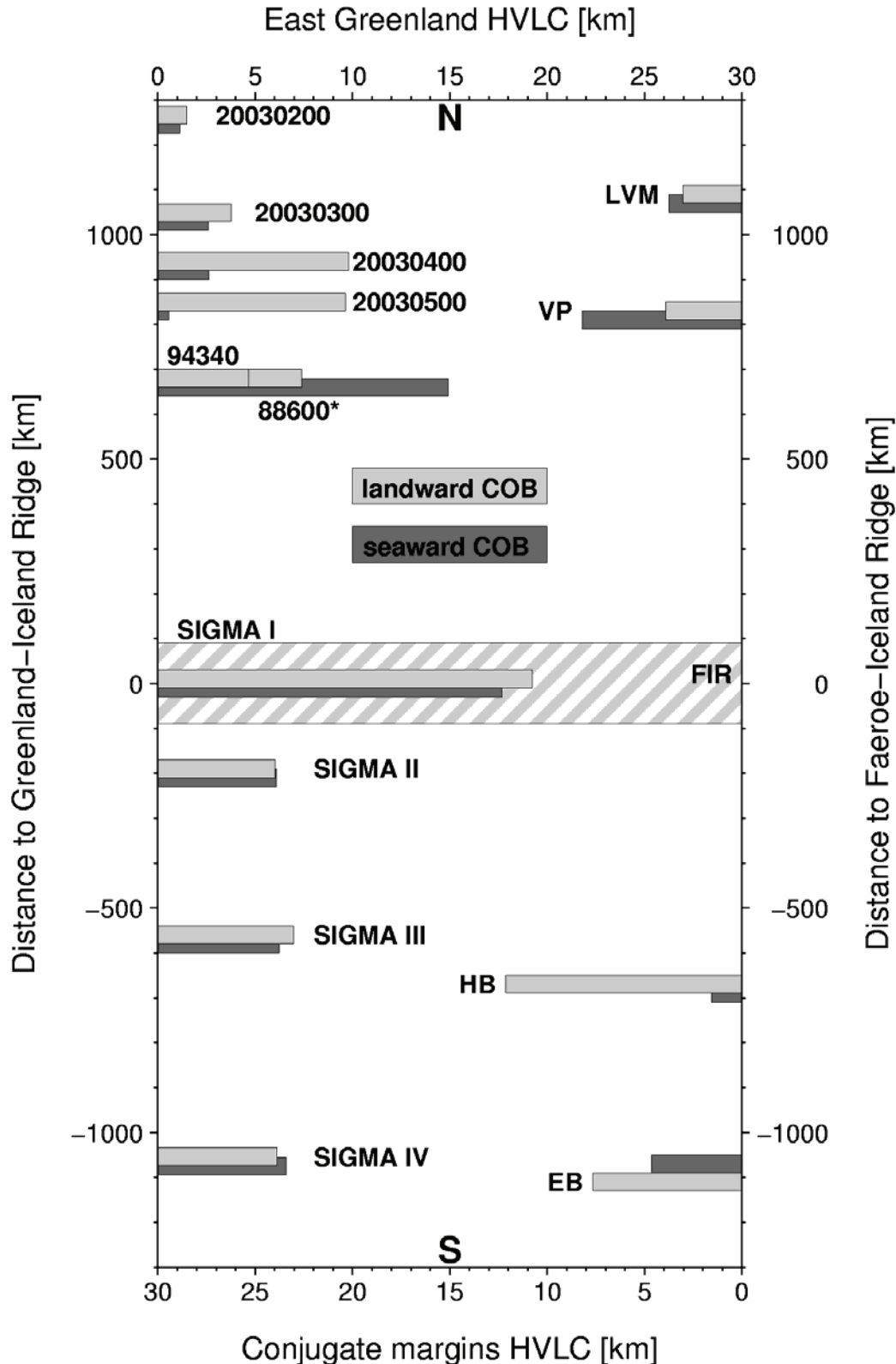


Figure 6.15: N-S distribution of HVLC thicknesses of East Greenland and conjugate margin transects. Separation of landward and seaward portions according to associated COBs. Distances are related to SIGMA I location near the Greenland Iceland Ridge for the East Greenland side and to the Faeroe-Iceland Ridge for conjugate profiles. Abbreviations are COB: Continent-ocean boundary, EB: Edoras Bank, FIR: Faeroe-Iceland Ridge, HB: Hatton Bank, LVM: Lofoten-Vesterålen Margin, VP: Vøring Plateau. Asterisk mark profile across oceanic crust of different age than others. See text for details.

crust. Considering sub-continental and oceanic HVLC thicknesses separately, a surprising inversion of the melt distribution appears (Figure 6.15). The general trend of decreasing melt volume away from the plume (GIR and FIR) is marked by asymmetry. Thicker HVLC landward of the COBs opposes thinner oceanic HVLC increasingly to the north. The strong northward decrease is displayed on both margins, as previously commented. The southern regions reveal, even for the distal regions, moderate average thicknesses landwards of the COBs. However, peak values of sub-continental HVLC content appear only locally distributed and seems to have a much smaller spatial extent north of the Jan Mayen Fracture Zone (Figures 6.14 and 6.15). The outstanding HVLC thickness in the oceanic domain at 670 km (profile 88600) (Figures 6.14 and 6.15) correlates with the margin segment that was involved in the separation of the Jan Mayen microcontinent and the early spreading of the Kolbeinsey Ridge (Weigel et al. 1995). The heterogeneous distribution of the HVLC suggests, however, different sources of melt generation and emplacement. The width of transition zones and the spatial extent of decreasing thickness of the HVLC has also been shown as strongly asymmetric off conjugate margins (e.g. Hopper et al. 2003; Voss and Jokat 2007), which has important implications for volumetric magma quantifications associated with the opening of the North Atlantic (Eldholm and Grue 1994).

6.7.2 Northeast Greenland melt distribution and margin formation models

In general, the observed structural styles of the North Atlantic volcanic margins are associated with the influence of a mantle plume and two end-member melt generation models exist (e.g. White and McKenzie 1989; Kelemen and Holbrook 1995; e.g. Holbrook et al. 2001; Korenaga et al. 2002). Passive upwelling is understood to produce thicker high velocity crust at higher temperatures due to the enriched magnesium content from deep-seated melt generation in the mantle. Melt generation from shallower mantle regions and a moderate thermal anomaly cause active upwelling without substantial crustal velocity variations. The development of the southeast Greenland margin was proposed to be influenced by a hotspot (Holbrook et al. 2001) or thin spot (Hopper et al. 2003) with proximal active upwelling (SIGMA I and II). Passive upwelling and a decrease of the thermal anomaly from break-up to C21/C20 is inferred for the regions of SIGMA III and IV from the crustal thicknesses and bulk velocities. Lateral flow of warm material to distal areas (Sleep 1996) was supposed to reach the southern tip of Greenland (Holbrook et al. 2001), a distance of ~1200 km, and to be responsible for the thick oceanic crust there. Exhaustion of the thermal anomaly at 45 Ma and the reduction of the plume head radius from ~300 km to less than 200 km reduced the production of high velocity lower oceanic crust and igneous crustal thickness (Holbrook et al. 2001; Hopper et al. 2003). To the north, similar distances from the possible plume location at 56 Ma, or indeed from the present-day Iceland thermal anomaly, would extend beyond profile AWI-20030200. But, it has been shown that the HVLC distribution differs substantially in such a way that large scale magmatism is almost absent at the northern periphery. Mjelde et al. (2003) postulated intervening active and passive rifting components from the regional structural styles of the Vøring margin. The decrease of magmatism with increasing plume distance is consistent with an active portion. The proposal that crustal lineaments acted as barriers to melt emplacement, documents the passive component. Local indications of HVLC thickness and velocity variations have also been related to a heterogeneous asthenospheric source. Three hypothetical models are considered to explain our observations from the northeast Greenland margin.

Model 1 - Pre-Paleogene long-term rifting and melt accumulation from one major feeder dyke

The northeast Greenland margin seems to have an outstanding structural style, including highly extended continental crust together, locally, with large scale magmatism. Similar

highly extended continental crust exists further north, but within 100 km excess magmatism seems restricted to the point of break-up and is almost absent near the Greenland Fracture Zone. Long-term rifting is generally associated with minor melt production due to conductive cooling during rifting (Bown and White 1995), consistent with the observations off Shannon Island (AWI-20030300). Thus, long-term rifting and crustal thinning is assumed to have started long before the Tertiary magmatic event. We deduce from the above analysis that the direct influence of a mantle plume head, active upwelling, widespread lower crustal magma flows, and/or other proposed models seem plausible explanations for the southern region of the East Greenland margin. We therefore assume for this model that a feeder dyke, originating from the distal plume head, sufficiently supported magmatism into the region of the increased HVLC north of the Jan Mayen Fracture Zone (AWI-20030400/500). The decrease in magmatism and variations in the HVLC along the northeast Greenland margin provide, in this case, supporting arguments to the melt barrier model. The different structural styles between the margins covered by AWI-200400/500 and AWI-20030300 allow us to assume the existence of a transfer zone or detachment that acted as a barrier to the Tertiary magmatism. This region marks a transition from the highly volcanic margin in the south (AWI-20030400/500) to magma-poor rifting and break-up further north. Assuming the HVLC of the two southern profiles is the result of pure magmatic underplating, i.e. subtracting it from the total crustal thickness, a pre-magmatic Moho is much shallower than on the northern profile (Figure 6.9). By contrast, a greater basin depth appears in the north lying along the prolongation of major Caledonian extensional detachments known from onshore observations (Hartz et al. 2002). The thick portion of magmatic underplating can then be interpreted as an accumulation-point of Tertiary magmatism, where Moho depths were lowest. Melt migration or lower crustal flow, as proposed for southeast Greenland, might probably have been channelled away from the thick continental crust and the Caledonian root structure to the west (Schmidt-Aursch and Jokat 2005b) and the transfer zone/detachment to the north. Such a model resembles the edge driven small scale convection model of King and Anderson (1995; 1998) or the soft spot model of Callot et al. (2002). Conductive cooling decreased upper mantle temperatures and the amount of igneous crustal accretion following the initiation of seafloor spreading, which explains the rapid decrease in oceanic crustal thickness. Tsikalas et al. (2002) proposed a conjugate transfer zone system along the East Greenland margin, based on regional magnetic data and the projections of major structures on the Norwegian margin. The across-margin extents of profiles AWI-20030200-400 are most likely located to cross these proposed features but no evidence for them is found on the seismic lines. Recent publications of potential field data from the Norwegian-Greenland Sea rejected also many of the previously proposed lineaments and fracture zones on both sides of the North Atlantic (Ebbing et al. 2006; Olesen et al. 2007). Therefore, according to these observations, we agree that small scale lineaments do not exist at this part of the margin. However, a major detachment fault between Godthåb Gulf and Ardencaple Fjord (Shannon Island) could explain the sudden decrease of magmatic underplating to the north and find support from the presented different structural styles.

Model 2 – Highly intruded thick continental crust and several small feeder dykes

Magmatic production from several small scale local volcanic feeders at the northeast Greenland margin might explain the larger thickness but smaller spatial extent of the HVLC, compared to the southeast Greenland margin. The thickness of the HVLC shows large gradients in all directions, while along the southeast Greenland margin it is distributed more homogeneously (except for the increase towards the Greenland Iceland Ridge). Voss and Jokat (2007) classified the HVLC as Tertiary magmatic underplating, which is a reasonable explanation according to previous interpretations of the region and the conjugate margin (Schlindwein and Jokat 1999; Mjelde et al. 2002; Mjelde et al. 2005). Supporting arguments

come from the increased velocities and densities, the distinct top reflector and Moho reflections, the shallower basin depth compared to the adjacent margin segments and the complex magnetic anomaly pattern offshore and prior to the ocean spreading anomalies. However, it is unclear how the remaining highly extended continental crust could have resisted oceanization in the face of such an excess in melt supply, and how excess melt production can be linked with long-term rifting (Bown and White 1995). Interpreting the HVLC instead as highly intruded lower crust including components of continental crust, addresses the same arguments but qualifies the delay between magmatism and break-up. The difference here is that the HVLC is not attributed to a pure magmatic body ponded beneath highly thinned continental crust. Instead, several small scale feeder dykes penetrate the rifted continental crust, and the top lower-crustal reflections are off major sills. Small volcano-like features occur at km 220 and 190 on profiles AWI-20030400 and AWI-20030500 respectively (Figure 6.9) (Voss and Jokat 2007). The magnetic anomaly pattern can be attributed to the magmatic lower crustal intrusions. The increased Cenozoic sediment thicknesses on these profiles are a result of isostatic subsidence due to the weight of the intruded crust compared to AWI-20030300. Minor volcanism occurred further north, at Shannon Island. The strong decrease in oceanic crustal thickness might be seen as a result of decreasing mantle temperature after break-up (Barton and White 1995), but also supports the possibility of more localized volcanism rather than large scale plume-related magma flow. The difference of the HVLC content in the oceanic domain also supports a significantly smaller northern melt generation.

Although this model seems plausible, it has difficulties to explain why the top reflector of the HVLC clearly dips towards the west and whether sills can cause such clear reflections in the lower crust. Additional constraints could be obtained from a comprehensive subsidence analysis, which investigates the thermal-tectonic subsidence of the COT due to intrusions or if it was uplifted due to underplating. Evidence of sediment erosion during latest Cretaceous to earliest Paleocene exhumation has been found in the onshore fjord region (Hartz et al. 2002).

Model 3 – Secondary magmatic event according to the Jan Mayen separation

Price et al. (1997) dated tholeiitic basalts on Traill Ø and related these to the Iceland plume magmatic event (~54 Ma). A second alkaline magmatic event dated to ~36 Ma is proposed to have been regionally significant in East Greenland. Slightly younger plateau basalts (~33 Ma; Upton et al. 1995) were found on Hold with Hope. Despite the difference in measurement techniques, it seems obvious that increased magmatism occurred between the onset of spreading along the Kolbeinsey Ridge and the final separation of Jan Mayen (Gudlaugsson et al. 1988). This process could explain the localized distribution of the HVLC north and south of the Jan Mayen Fracture Zone, which appears almost symmetrical (Weigel et al. 1995; Kodaira et al. 1997; Kodaira et al. 1998a; Voss and Jokat 2007). This model implies that the initial crustal structural style might have been similar to the model off Shannon Island. The primary magmatic event revealed intrusions during extension and the formation of onshore plateau basalts. Break-up occurred along the northeast Greenland margin between 54 and 50 Ma (Figure 6.9), emplacing SDRS (Hinz et al. 1987; Mutter and Zehnder 1988) and a limited amount, if any, magmatic underplating. It is possible that primary Early Tertiary magmatism acted to reduce crustal permeability and prevent the ascent of younger upwelling magma in this region. The second event started with initiation of the Kolbeinsey Ridge system and the separation of the Jan Mayen microcontinent (Gudlaugsson et al. 1988). Thick oceanic crust accreted to the central-east Greenland margin south of the Jan Mayen Fracture Zone. Ascending melt ponded beneath the primary sealed and thinned continental crust (COT of AWI-20030400 and 500) and formed the local thick magmatic underplate there. The complex magmatic pattern is therefore attributed to primary intrusions. If the secondary magmatic underplating contributes the magnetic anomalies depends on its depth relatively to the depth-

level of the Curie temperature. The resulting uplift might have caused erosion of the early basalts on- and offshore, which suggests that the shelf region might have had a widespread cover of flood basalts, if not similar to the flood basalts exposed on the Geikie Plateau (Figure 6.1). According to this model, the observed underplating from Kong Oscar Fjord, Kejser Franz Joseph Fjord and Godthåb Gulf is most likely related to Late Eocene rather than Late Paleocene/Early Eocene magmatism. The melt production affects margin formation in a small radius of less than 200 km, leaving the region off Shannon Island and south of Scoresby Sund unaffected. A difficulty of this model is the explanation of the thinner oceanic crust off Kejser Franz Joseph Fjord, which opposes also the Kolbeinsey Ridge across the Jan Mayen Fracture Zone.

The models presented form three end-members. Some combination of these might best describe the evolution of the northeast Greenland margin. These models contrast with those for the formation of the southeast Greenland margin, emphasizing the strong variations along East Greenland. Plate reconstruction models need to invoke such variations and the asymmetries of conjugate margins, since they have a significant impact in the evaluation of the timing of magmatism, melt quantities, rift durations (e.g. Hopper et al. 2003), uplift history (e.g. Clift et al. 1995) and the hydrocarbon potential of offshore continental margin basins (Hinz et al. 1993). Lithospheric-scale inhomogeneities must be responsible for the heterogeneous melt generation according to the variations and inversion of the HVLC distribution in continental and oceanic domains, and differences in its velocities (Figures 6.14 and 6.15). However, whether or not a mantle plume or other processes are responsible for the melt production, it seems difficult to deduce a solution from geometrical and velocity constraints alone.

6.8 Conclusion

New crustal structure models based on wide-angle seismic data are presented, and 30 seismic models from the southern tip of Greenland to the Greenland Fracture Zone in the north were used to compile maps for regional seismic interfaces within the crust.

Interpretation of P-wave velocity models of the profiles AWI-20030200 and AWI-20030300 revealed important constraints on the extent of magmatism along the northeast Greenland margin between the Jan Mayen and Greenland fracture zones. Significant variations were found in the presented models, and the previous published structural models of the two southern profiles AWI-20030400 and AWI-20030500 (Voss and Jokat 2007). The main results are as follows:

1. Between the present-day coastline and shelf edge, there is a significant variation in crustal architecture beneath the basaltic layers that form the volcanic province of the East Greenland margin. A sedimentary basin up to 15 km deep and with a low velocity gradient, a crustal layer with moderate lower crustal velocities, and the confinement of increased velocities to the COB, define a completely different weak-magmatic evolution of the northeastern margin compared to the highly magmatic evolution of the southern profiles. The continental lithosphere is proposed to have been only sparsely penetrated by melts and not to have been magmatically underplated, whereas excess volcanism further south was voluminous. This difference correlates with the magnetic record along the profiles within these regions. However, Moho depths along the three transects across the northeast margin seem similar, decreasing from 30 km to almost 10 km at the onset of oceanic crust, albeit strongly depending on the width and thickness of the HVLC.
2. The thicknesses of the Cenozoic sediments differ between profiles AWI-20030300, AWI-20030400 and AWI-20030500 across the present day shelf region. Along AWI-20030300 they gradually thicken up to 2.7 km towards the shelf slope, while on the two southern profiles, the sediments have an almost constant thickness of 2.5 – 3 km. This variation

might be linked to variations in subsidence and uplift caused by different magmatic processes, as shown by the observed variability in crustal structure.

3. A significant velocity anomaly is observed underneath the Shannon High, but not on the two southern profiles. The absence of a significant HVLC beneath the Shannon High and the COT, and a positive magnetic anomaly rather than a chaotic magnetic signature as in the south leads us to conclude that the emplacement of plateau basalts on Shannon Island was probably related to a local volcanic event, independent of rather than linked to the upper and lower plateau lava sequences on Wollaston Foreland and Hold with Hope (Watt 1994).
4. Oceanic crustal thicknesses in the Greenland Basin decrease slightly towards the north and away from the COB, from approx. 9 – 13 km at break-up to almost 5 km near chron C21.
5. Half spreading rates were calculated along the four seismic lines between the Greenland and Jan Mayen fracture zones and provide age constraints on the time of break-up. The rates suggest that break-up propagated from north to south in the period from ~54 to ~50 Ma, based on identifications of the seaward COBs.

A line-to-line comparison with a crustal transect across the conjugate Lofoten margin reveals surprising similarities in the structural style despite the presence of a unique major tectonic feature, the Lofoten core-complex.

A systematic compilation of 30 crustal models from wide-angle seismic lines along the entire East Greenland margin yields a regional crustal image and its variations. The major differences are the interpretation of the HVLC as pure magmatic underplating and/or accretion seaward of the COB, the distribution of the maximum high velocity lower crust and the thickness of the oceanic crust north and south of Iceland. We could demonstrate that the average thicknesses of the HVLC landward and seaward of proposed COBs differs inversely from north to south from the East Greenland margin profiles and their conjugate counterparts when plotted according to their distance from the Greenland-Iceland-Faeroe Ridge.

From this heterogeneous distribution we deduced three possible models for the formation of, and melt generation at the northeast Greenland margin. The first model infers a major feeder dyke linked to the plume head and a transfer zone/detachment between Godthåb Gulf and Shannon Island. A second model suggests thicker continental crust, rather than pure magmatic underplating, and volcanism sourced from several small feeder dykes. The third model involves a second magmatic event which is associated with the separation of the Jan Mayen microcontinent and the formation of the Kolbeinsey Ridge system.

6.9 Acknowledgements

Data acquisition along these profiles was supported by the Deutsche Forschungsgemeinschaft. Funding was provided for data processing of the wide-angle seismic lines by Statoil and by the European Science Foundation within the EUROMARINS project. We thank John Hopper who provided the digital velocity models of the SIGMA II – IV profiles. The manuscript was improved greatly by comments from Daniela Berger, Erik Lundin, Asbjørn Breivik and Graeme Eagles. We thank Bob Trumbull, Robert White and two anonymous reviewers for their inspiring comments. All figures were created with GMT (Wessel and Smith 1998). Seismic velocity models were created with *RAYINV*R provided by Collin Zelt (Zelt and Smith 1992). 2D gravity modelling was performed with the commercial software *LCT* provided by *Fugro*.

6.10 References

- Anderson, D. L. (2000). "The thermal state of the upper mantle; no role for mantle plumes." Geophysical Research Letters **27**(22): 3623-3626.
- Barton, A. J. and R. S. White (1995). "The Edoras Bank continental margin: Continental break-up in the presence of a mantle plume." J. geol. Soc. London **152**: 971-974.
- Bott, M. H. P. and K. Gunnarson (1980). "Crustal structure of the Iceland-Faeroe Ridge." J. Geophys. **47**: 221-227.
- Bown, J. W. and R. S. White (1995). "Effect of finite extension rate on melt generation at rifted continental margins." Journal of Geophysical Research **100**(B9): 18,011-18,029.
- Breivik, A. J., R. Mjelde, J. I. Faleide and Y. Murai (2006). "Rates of continental breakup magmatism and seafloor spreading in the Norway Basin-Iceland plume interaction." Journal of Geophysical Research **111**(B07102).
- Breivik, A. J., J. Verhoef and J. I. Faleide (1999). "Effect of thermal contrasts on gravity modeling at passive margins: Results from the western Barents Sea." Journal of Geophysical Research **104**(B7): 15293-15311.
- Callot, J. P., L. Geoffroy and J. P. Brun (2002). "Development of volcanic passive margins: Three-dimensional laboratory models." Tectonics **21**(6): 1052-1064.
- Cande, S. C. and G. M. Kent (1995). "Revised calibration of the geomagnetic polarity timescale for the Late Cretaceous and Cenozoic." Journal of Geophysical Research **100**(B7): 9761-9788.
- Christensen, N. I. and W. D. Mooney (1995). "Seismic velocity structure and composition of the continental crust: a global view." Journal of Geophysical Research **100**(B7): 9761-9788.
- Clift, P. D., J. Turner and O. D. P. L. S. Party (1995). "Dynamic support by the Iceland plume and vertical tectonics of the northeast Atlantic continental margins." Journal of Geophysical Research **100**(B12): 24473-24486.
- Ebbing, J., E. Lundin, O. Olesen and E. K. Hansen (2006). "The mid-Norwegian margin: a discussion of crustal lineaments, mafic intrusions, and remnants of the Caledonian root by 3D density modelling and structural interpretation." Journal of Geological Society, London **163**: 47-49.
- Eldholm, O. and K. Grue (1994). "North Atlantic volcanic margins: Dimensions and production rates." Journal of Geophysical Research **99**(B2): 2955-2968.
- Eldholm, O., J. Thiede and E. Taylor (1989). "Evolution of the Vøring volcanic margin." Proc. Ocean Drill. Program Sci. Results **104**: 1033-1065.
- Escher, J. and T. Pulvertaft (1995). "Geological Map of Greenland, 1:2 500 000." Geological Survey of Greenland.

- Fechner, N. (1994). Detailed refraction seismic investigations in the inner Scoresby Sund / East Greenland. Reports on Polar Research. Bremerhaven, Alfred Wegener Institute of Polar and Marine Research. **143**: 1-196.
- Fechner, N. and W. Jokat (1996). "Seismic refraction investigations on the crustal structure of the western Jameson Land basin, east Greenland." Journal of Geophysical Research **101**(B7): 15867-15881.
- Foulger, G. R. and D. L. Anderson (2005). "A cool model for the Iceland hotspot." Journal of Volcanology and Geothermal Research **141**: 1-22.
- Fowler, C. M. R. (2005). "The solid earth: an introduction to global geophysics." **2nd ed.**
- Fowler, S. R., R. S. White, G. D. Spence and G. K. Westbrook (1989). "The Hatton Bank continental margin - II. Deep structure from two-ship expanding spread seismic profiles." Geophys. J. Int. **96**: 295-309.
- Funck, T., J. R. Hopper, H. C. Larsen, K. E. Loudon, B. E. Tucholke and W. S. Holbrook (2003). "Crustal structure of the ocean-continent transition at Flemish Cap: Seismic refraction results." Journal of Geophysical Research **108**: 2531-2551.
- Funck, T., H. R. Jackson, K. E. Loudon, S. A. Dehler and Y. Wu (2004). "Crustal structure of the northern Nova Scotia rifted continental margin (eastern Canada)." Journal of Geophysical Research **109**(B09102).
- Gernigon, L., J. C. Ringenbach, S. Planke and B. Le Gall (2004). "Deep structures and breakup along volcanic rifted margins: insights from integrated studies along the outer Vøring Basin (Norway)." Marine and Petroleum Geology **21**: 363-372.
- Gernigon, L., J. C. Ringenbach, S. Planke, B. Le Gall and H. Jonquet-Kolstø (2003). "Extension, crustal structure and magmatism at the outer Vøring Basin, Norwegian margin." Journal of Geological Society, London **160**: 197-208.
- Gudlaugsson, S. T., K. Gunnarson, M. Sand and J. Skogseid (1988). Tectonic and volcanic events at the Jan Mayen Ridge microcontinent, in A. C. Morton and L. M. Parson (ed.), Early Tertiary Volcanism and the Opening of the NE Atlantic. **39**: 85-93.
- Hamann, N. E., R. C. Whittaker and L. Stemmerik (2005). Geological development of the Northeast Greenland Shelf, in A. G. Doré and B. A. Vining (ed.), Petroleum Geology: North-West Europe and Global Perspectives-Proceedings of the 6th Petroleum Geology Conference, Geological Society, London: 887-902.
- Hartz, E., E. A. Eide, A. Andresen, P. Midbøe, K. V. Hodges and S. N. Kristiansen (2002). "⁴⁰Ar/³⁹Ar geochronology and structural analysis: Basin evolution and detrital feedback mechanisms, Hold with Hope region, East Greenland." Norwegian Journal of Geology **82**: 341-358.
- Henriksen, N., A. Higgins, F. Kalsbeek and T. Pulvertaft (2000). "Greenland from Archaean to Quaternary; descriptive text to the geological map of Greenland, 1: 2 500 000." Geol. Greenland Surv. Bull. **185**: 1-93.

Hinz, K. (1981). "A hypothesis on terrestrial catastrophes wedges of very thick oceanward dipping layers beneath passive continental margins; their origin and palaeoenvironmental significance." Geologisches Jahrbuch **E2**: 3-28.

Hinz, K., O. Eldholm, M. Block and J. Skogseid (1993). "Evolution of North Atlantic volcanic continental margins." from Perol. Geol. of Northwest Europe: Proceedings of the 4th Conference: 901-913.

Hinz, K., J. C. Mutter, C. M. Zehnder and N. S. Group (1987). "Symmetric conjugation of continent-ocean boundary structures along the Norwegian and East Greenland margins." Mar. Petrol. Geol. **3**: 166-187.

Holbrook, W. S., H. C. Larsen, J. Korenaga, T. Dahl-Jensen, I. D. Reid, P. B. Kelemen, J. R. Hopper, G. M. Kent, D. Lizarralde, S. Bernstein and R. S. Detrick (2001). "Mantle thermal structure and active upwelling during continental breakup in the North Atlantic." Earth and Planetary Science Letters **190**: 251-266.

Hopper, J. R., T. Dahl-Jensen, W. S. Holbrook, H. C. Larsen, D. Lizarralde, J. Korenaga, G. M. Kent and P. B. Kelemen (2003). "Structure of the SE Greenland margin from seismic reflection and refraction data: Implications for nascent spreading center subsidence and asymmetric crustal accretion during North Atlantic opening." Journal of Geophysical Research **108**(B5): 2269.

Jakobsson, M., N. Z. Cherkis, J. Woodward, R. Macnab and B. Coakley (2000). "New grid of Arctic bathymetry aids scientists and mapmakers." EOS Transactions of the American Geophysical Union **81**: 89, 93, 96.

Jokat, W., D. Berger, H. Bohlmann, V. Helm, M. Hensch, D. Jouselin, C. Klein, N. Lensch, P. Liersch, H. Martens, A. Medow, U. Micksch, L. Rabenstein, C. Salat, M. Schmidt-Aursch and A. Schwenk (2004). "Marine Geophysics." Reports on Polar and Marine Research **475**: 11-34.

Kelemen, P. B. and W. S. Holbrook (1995). "Origin of thick, high-velocity igneous crust along the U.S. East Coast Margin." Journal of Geophysical Research **100**(B7): 10077-10094.

King, S. D. and D. L. Anderson (1995). "An alternative mechanism for flood basalt formation." Earth and Planetary Science Letters **136**: 269-279.

King, S. D. and D. L. Anderson (1998). "Edge-driven convection." Earth and Planetary Science Letters **160**: 289-296.

Kodaira, S., A. Goldschmidt-Rokita, J. M. Hartmann, H. B. Hirschleber, T. Iwasaki, T. Kananzawa, H. Krahn, N. Tomita and H. Shimamura (1995). "Crustal structure of the Lofoten continental margin, off N. Norway, by OBS refraction studies." Geophys. J. Int. **121**: 907-924.

Kodaira, S., R. Mjelde, K. Gunnarson, H. Shiobara and H. Shimamura (1997). "Crustal structure of the Kolbeinsey Ridge, North Atlantic, obtained by use of ocean bottom seismographs." Journal of Geophysical Research **102**(B2): 3131-3151.

Kodaira, S., R. Mjelde, K. Gunnarson, H. Shiobara and H. Shimamura (1998a). "Structure of

- the Jan Mayen microcontinent and implications for its evolution." Geophys. J. Int. **132**: 383-400.
- Kodaira, S., R. Mjelde, K. Gunnarson, H. Shiobara and H. Shimamura (1998b). "Evolution of the oceanic crust on the Kolbeinsey Ridge, north of Iceland, over the past 22 Myr." Terra Nova **10**: 27-31.
- Korenaga, J., W. S. Holbrook, G. M. Kent, P. B. Kelemen, R. S. Detrick, H. C. Larsen, J. R. Hopper and T. Dahl-Jensen (2000). "Crustal structure of the southeast Greenland margin from joint refraction and reflection seismic tomography." Journal of Geophysical Research **105**(B9): 21591-21614.
- Korenaga, J., P. B. Kelemen and W. S. Holbrook (2002). "Methods of resolving the origin of large igneous provinces from crustal seismology." Journal of Geophysical Research **107**(B9): 2178.
- Larsen, H. C. (1990). The East Greenland Shelf, (ed.), The Geology of North America, Geological Society of America, Boulder, Colo. **L**: 185-210.
- Larsen, H. C., A. D. Saunders and P. D. Clift (1994). "Proc. ODP, Init. Rep., 152 (Pt. 1)." Ocean Drilling Program, College Station, TX.
- Lawver, L. A. and D. R. Müller (1994). "Iceland "hotspot" track." Geology **22**: 311-314.
- Ludwig, W. J., J. E. Nafe and C. L. Drake (1970). Seismic refraction, in A. E. Maxwell (ed.), in: The Sea, Wiley-Interscience. **4**: 53-84.
- Mandler, H. and W. Jokat (1998). "The crustal structure of central east Greenland: results from combined land-sea seismic refraction experiments." Geophys. J. Int. **135**: 63-76.
- McKenzie, D. and M. J. Bickle (1988). "The volume and composition of melt generated by extension of the lithosphere." Journal of Petrology **29**: 625-679.
- Meyer, R., J. van Wijk and L. Gernigon (2007). The North Atlantic Igneous Province: A Review of the Models for its Formation, in G. R. Foulger and D. M. Jurdy (ed.), Plates, Plumes, and Planetary Processes, Geological Society of America Special Paper: 430 p.
- Mjelde, R., P. Digranes, H. Shimamura, H. Shiobara, S. Koaira, H. Brekke, T. Egebjerg, N. Sørenes and S. Thorbjørnsen (1998). "Crustal structure of the northern part of the Vøring Basin, mid-Norway margin, from wide-angle seismic and gravity data." Tectonophysics **293**: 175-205.
- Mjelde, R., P. Digranes, M. Van Schaak, H. Shimamura, H. Shiobara, S. Kodaira, O. Naess, N. Sørenes and E. Vagnes (2001). "Crustal structure of the outer Vøring Plateau, offshore Norway, from ocean bottom seismic and gravity data." Journal of Geophysical Research **106**(B4): 6769-6791.
- Mjelde, R., J. Kasahara, H. Shimamura, A. Kamimura, T. Kananzawa, S. Kodaira, T. Raum and H. Shiobara (2002). "Lower crustal velocity-anomalies; magmatic underplating or serpentinized peridotite? Evidence from the Vøring Margin, NE Atlantic." Marine Geophysical Researches **23**: 169-183.

- Mjelde, R., S. Kodaira, H. Shimamura, T. Kananzawa, H. Shiobara, E. W. Berg and O. Riise (1997). "Crustal structure of the central part of the Vøring Basin, mid-Norway margin, from ocean bottom seismographs." Tectonophysics **277**: 235-257.
- Mjelde, R., T. Raum, B. Myhren, H. Shimamura, Y. Murai, T. Takanami, R. Karpuz and U. Naess (2005). "Continent-ocean transition on the Vøring Plateau, NE Atlantic, derived from densely spaced ocean bottom seismometer data." Journal of Geophysical Research **110**.
- Mjelde, R., H. Shimamura, T. Kananzawa, S. Kodaira, T. Raum and H. Shiobara (2003). "Crustal lineaments, distribution of lower crustal intrusives and structural evolution of the Vøring Margin, NE Atlantic; new insights from wide-angle seismic models." Tectonophysics **369**: 199-218.
- Morgan, J. V., P. J. Barton and R. S. White (1989). "The Hatton Bank continental margin - III. Structure from wide-angle OBS and multichannel seismic refraction profiles." Geophys. J. Int. **98**: 367-384.
- Morgan, W. J. (1971). "Convection plumes in the lower mantle." Nature **230**: 42-43.
- Mosar, J., G. Lewis and T. H. Torsvik (2002b). "North Atlantic sea-floor spreading rates: implications for the Tertiary development of inversion structures of the Norwegian-Greenland Sea." Journal of Geological Society, London **159**: 503-515.
- Mutter, J. C., W. R. Buck and C. M. Zehnder (1988). "Convective partial melting 1. A model for the firmation of thick basaltic sequences duirng the initiation of spreading." Journal of Geophysical Research **93**(B2): 1031-1048.
- Mutter, J. C. and C. M. Zehnder (1988). "Deep crustal and magmatic processes: The inception of seafloor spreading in the Norwegian-Greenland Sea." Geol. Soc. Spec. Publ. London **39**: 35-48.
- Myhre, A. M. and J. Thiede (1995). "North Atlantic-Arctic Gateways." Proc. Ocean Drill. Program Initial Rep. **151**.
- Nafe, J. E. and C. L. Drake (1957). "Variations with depth in shallow and deep water marine sediments of porosity, density and the velocity of compresional and shear waves." Geophysics **22**: 523-552.
- Nielsen, T. K. and J. R. Hopper (2004). "From rift to drift: Mantle melting during continental breakup." Geochem. Geophys. Geosyst. **5**(7): 1-24.
- Olesen, O., J. Ebbing, E. Lundin, E. Maurant, J. J. Skilbrei, T. H. Torsvik, E. K. Hansen, T. Henningsen, P. Midbøe and M. Sand (2007). "An improved tectonic model for the Eocene opening of the Norwegian-Greenland Sea: Use of modern magnetic data." Marine and Petroleum Geology **24**: 53-66.
- Price, S., J. Brodie, A. Whitham and R. Kent (1997). "Mid-Tertiary rifting and magmatism in the Traill Ø region, East Greenland." J. geol. Soc. London **154**: 419-434.
- Raum, T., R. Mjelde, P. Digranes, H. Shimamura, H. Shiobara, S. Kodaira, G. Haatvedt, N.

Sørensen and S. Thorbjørnsen (2002). "Crustal structure of the southern part of the Vøring Basin, mid-Norway margin, from wide-angle seismic and gravity data." Tectonophysics **355**: 99-126.

Rowley, D. B. and A. L. Lottes (1988). "Plate-kinematic reconstructions of the North Atlantic and Arctic: Late Jurassic to Present." Tectonophysics **155**: 73-120.

Saunders, A. D., J. G. Fitton, A. C. Kerr, M. J. Norry and R. W. Kent (1997). The North Atlantic Igneous Province, in J. J. Mahoney and M. F. Coffin (ed.), Large Igneous Provinces, American Geophysical Union Monograph. **100**: 45-94.

Saunders, A. D., H. C. Larsen and S. W. J. Wise (1998). Proceedings of the Ocean drilling Program, Scientific Results, (ed.), Ocean Drilling Program, College Station, TX. **152**.

Sawyer, D. S. (1985). "Total tectonic subsidence: A parameter for distinguishing crust type at the U.S. Atlantic continental margin." Journal of Geophysical Research **90**(B9): 7751-7769.

Schlindwein, V. (1998). Architecture and evolution of the continental crust of east Greenland from integrated geophysical studies. Reports on Polar and Marine Research. Bremerhaven. **270**: 1-148.

Schlindwein, V. and W. Jokat (1999). "Structure and evolution of the continental crust of northern east Greenland from integrated geophysical studies." Journal of Geophysical Research **104**(B7): 15227-15245.

Schlindwein, V. and W. Jokat (2000). "Post-collisional extension of the East Greenland Caledonides: a geophysical perspective." Geophys. J. Int. **140**: 559-567.

Schmidt-Aursch, M. C. and W. Jokat (2005a). "The crustal structure of central East Greenland-I: From the Caledonian orogen to the Tertiary igneous province." Geophys. J. Int. **160**: 736-752.

Schmidt-Aursch, M. C. and W. Jokat (2005b). "The crustal structure of central East Greenland-II: From the Precambrian shield to the recent mid-oceanic ridges." Geophys. J. Int. **160**: 753-760.

Skogseid, J., S. Planke, J. I. Faleide, T. Pedersen, O. Eldholm and F. Neverdal (2000). NE Atlantic continental rifting and volcanic margin formation, in A. Nøttvedt (ed.), Dynamics of the Norwegian Margin, Geological Society Special Publication, London. **167**: 295-326.

Sleep, N. H. (1996). "Lateral flow of hot plume material ponded at sublithospheric depths." Journal of Geophysical Research **101**: 28065-28083.

Smith, W. H. F. and P. Wessel (1990). "Gridding with continuous curvature splines in tension." Geophysics **55**: 293-305.

Surlyk, F. (1990). Timing, style and sedimentary evolution of Late Palaeozoic-Mesozoic extensional basins of East Greenland, in R. F. P. Hardman and J. Brooks (ed.), Tectonic Events Responsible for Britain's Oil and Gas Reserves, Geol. Soc. Spec. Publ. **55**: 107-125.

Tsikalas, F., O. Eldholm and J. I. Faleide (2002). "Early Eocene sea floor spreading and

continent-ocean boundary between Jan Mayen and Senja fracture zones in the Norwegian-Greenland Sea." Marine Geophysical Researches **23**: 247-270.

Tsikalas, F., O. Eldholm and J. I. Faleide (2005). "Crustal structure of the Lofoten-Vesterålen continental margin, off Norway." Tectonophysics **404**: 151-174.

Tsikalas, F., J. I. Faleide and O. Eldholm (2001). "Lateral variations in tectono-magmatic style along the Lofoten-Verstålen volcanic margin off Norway." Marine and Petroleum Geology **18**: 801-832.

Upton, B. G. J., C. H. Emeleus, D. C. Rex and M. F. Thirlwall (1995). "Early Tertiary magmatism in northeast Greenland." J. geol. Soc. London **152**: 959-964.

van Wijk, J. W., R. S. Huismans, M. Ter Vorrde and S. A. P. L. Cloetingh (2001). "Melt generation at volcanic continental margins: No need for a mantle plume?" Geophysical Research Letters **28**: 3995-3998.

Verhoef, J., W. R. Macnab, R. Arkani-Hamed and J. M. o. t. P. Team (1996). "Magnetic anomalies of the Arctic and North Atlantic Oceans and adjacent land areas; Open File 3125." Geological Survey of Canada.

Voss, M. and W. Jokat (2007). "Continent – ocean transition and voluminous magmatic underplating derived from P-wave velocity modelling of the East Greenland continental margin." Geophys. J. Int. **170**: 580-604.

Watt, S. W. (1994). "Stratigraphy and correlation of the Tertiary plateau basalts in North-East Greenland." Rapp. Grønlands geol. Unders. **162**: 195-200.

Weigel, W., E. R. Flüh, H. Miller, A. Butzke, G. A. Dehghani, V. Gebhardt, I. Harder, J. Hepper, W. Jokat, D. Kläschen, S. Kreymann, S. Schübler and Z. Zhao (1995). "Investigations of the east Greenland continental margin between 70° and 72°N by deep seismic sounding and gravity studies." Marine Geophysical Researches **17**: 167-199.

Wessel, P. and W. Smith, H. F. (1998). "New, improved version of Generic Mapping Tools released." EOS Transactions of the American Geophysical Union **79(47)**: pp. 579.

White, R. and D. McKenzie (1989). "Magmatism at rift zones: The generation of volcanic continental margins and flood basalts." Journal of Geophysical Research **94(B6)**: 7685-7729.

White, R. S. (1992). Magmatism during and after continental break-up, in B. C. Storey, T. Alabaster and R. J. Pankhurst (ed.), Magmatism and the Causes of Continental Break-up, Geological Society Special Publication. **68**: 1-16.

White, R. S., D. McKenzie and R. K. O'Nions (1992). "Oceanic Crustal Thickness From Seismic Measurements and Rare Earth Element Inversions." Journal of Geophysical Research **97(B13)**: 19683-19715.

White, R. S., G. D. Spence, S. R. Fowler, D. McKenzie, G. K. Westbrook and A. N. Bowen (1987). "Magmatism at rifted continental margins." Nature **330**: 439 - 444.

Whitmarsh, R. B. and P. R. Miles (1995). "Models of the development of the West Iberia

rifted continental margin at 40°30'N deduced from surface and deep-tow magnetic anomalies." Journal of Geophysical Research **100**(B3): 3789-3806.

Whitmarsh, R. B., R. S. White, S. J. Horsefield, J. C. Sibuet, M. Recq and V. Louvel (1996). "The ocean-continent boundary off the western continental margin of Iberia; crustal structure of Galicia Bank." Journal of Geophysical Research **101**(28291-28314).

Zelt, C. A. and R. B. Smith (1992). "Seismic Traveltime inversion for 2-D crustal velocity structure." Geophysical Journal International **108**: 16-34.

7 From Devonian extensional collapse to Early Eocene continental break-up: an extended transect of the Kejser Franz Joseph Fjord of the East Greenland margin

Max Voss and Wilfried Jokat

Alfred Wegener Institute for Polar and Marine Research, Columbusstrasse, 27568 Bremerhaven, Germany
E-mails: Max.Voss@awi.de (MV); Wilfried.Jokat@awi.de (WJ)

7.1 Summary

Seismic investigations along East Greenland's Fjord Region completed during the last decade provide fundamental insights into the region's crustal structure and tectonic history. A summary of models along a transect through the Kejser Franz Joseph Fjord provides a view from the Precambrian Shield to the Eocene oceanic crust. We conclude that a change of rifting geometry from an upper to a lower plate-style margin occurred in early Mesozoic times and formed the >350 km wide rift zone. Despite the demonstrated asymmetry of the northeast Greenland and conjugate Vøring margins, the change of rift geometries and the direction of rift jumps remain debatable. A combined model for productivity and duration of magmatism is proposed for the northeast Greenland fjord region. We suggest that magmatism started slowly at 58.8 ± 3.6 Ma with a production rate of $1.5 \times 10^{-4} \text{ km}^3 \text{ km}^{-1} \text{ a}^{-1}$, which is similar to the productivity of onshore upper and lower lava sequences on the Geikie Plateau. A peak of $9.4 \times 10^{-4} \text{ km}^3 \text{ km}^{-1} \text{ a}^{-1}$ for 0.5 m.y., and a subsequent productivity of $4.4 \pm 0.3 \times 10^{-4} \text{ km}^3 \text{ km}^{-1} \text{ a}^{-1}$ for 2.5 m.y. between 53.3 and 50.8 Ma, produced the majority of melt, but break-up did not occur immediately afterwards. Continuous production of melt, similar to the rate of ocean spreading until C22 (~50 Ma), contributed to massive magmatic underplating until break-up at 50 Ma. The volumes and production rates show similarities to those obtained from a profile off the southeast Greenland margin but with a major difference in the regional spatial extent.

Key words: crustal structure, East Greenland, rifted margin

7.2 Introduction

The northeast Greenland margin opposes the well-explored Norwegian margin across the northern North Atlantic. Margin evolution concepts and rift geometries on the Greenland margin are often assumed to be the same as on its Scandinavian conjugate (e.g. Mosar et al. 2002a). A lack of detailed crustal structure models, especially for the post-Devonian to Tertiary parts of the margin, make this assumption hard to evaluate. Deep seismic experiments in the last decade (Mandler and Jokat 1998; Schlindwein and Jokat 1999; Voss and Jokat 2007; Voss et al. submitted), and potential field modelling (Schmidt-Aursch and Jokat 2005b) have provided fundamental data for rift system analysis at the northeast Greenland margin. Schlindwein and Jokat (1999; 2000) proposed a model for the late Caledonian extension, but did not discuss post-Devonian events. In this paper, we summarize and review the extensional structures on a traverse from the Precambrian shield west of the Greenland Caledonides, across the continental sedimentary basins and shelf region, and into the oceanic basin off the Kejser Franz Joseph Fjord (Figure 7.1). The objective of this study is to provide an overview of the crustal structures formed during tectonic extension that started with Devonian extensional collapse and culminated in Early Eocene opening of the North Atlantic. The Early Tertiary magmatic episodes, i.e. the duration of magmatism based on predicted production rates, will be discussed on this northeast Greenland margin cross-section.

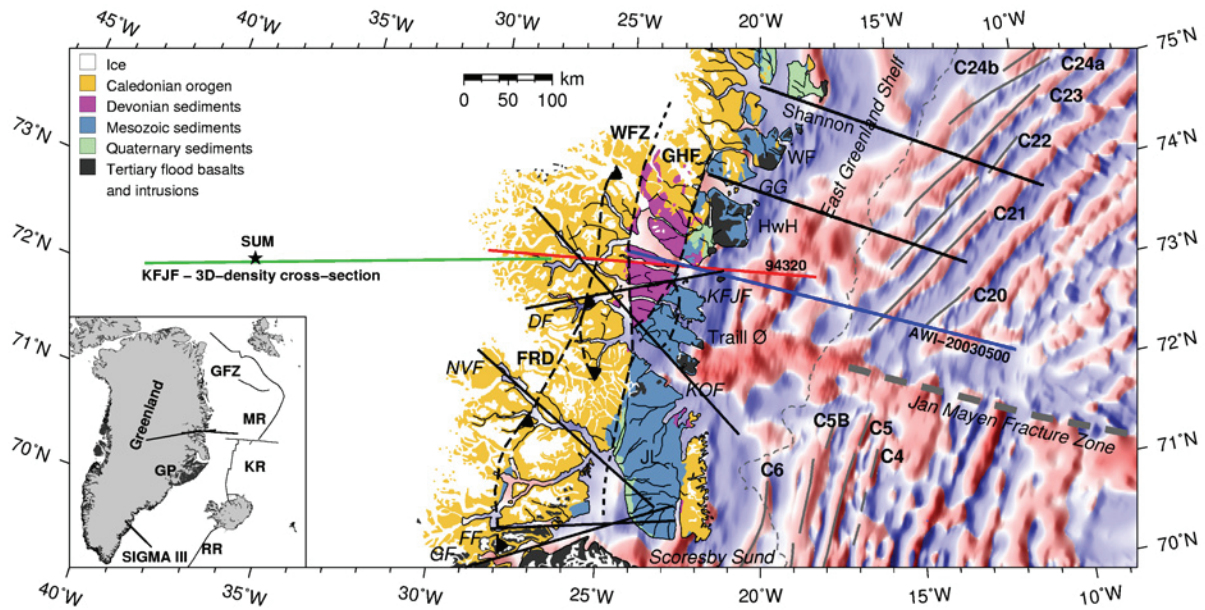


Figure 7.1: Location of the merged transect from the Precambrian shield west of the Greenland Caledonides into the oceanic basin off the Kejsler Franz Joseph Fjord. Green line marks KFJF – 3D density cross-section after Schmidt-Aursch and Jokat (2005b), profile 94320 (red) after Schlindwein and Jokat (1999), and AWI-20030500 (blue) after Voss and Jokat (2007). Black solid lines mark other seismic profiles. Background shows regional magnetic grid (Verhoef et al. 1996) with red regions positive and blue regions negative polarisations. Spreading anomalies are marked with grey lines and labelled with Cxx. Thin black lines represent bathymetric contours after Jakobsson et al. (2000). Thick dashed grey line marks the Jan Mayen Fracture Zone. Thin dashed grey line marks smoothed shelf edge (330m). Onshore geology after Escher and Pulvertaft (1995) (copyright Geological Survey of Denmark and Greenland) and Henriksen et al. (2000). Continental extensional detachments and fault zones are marked by black dashed lines. The overview map contains additionally ridges, onshore plateau basalts (dark grey) and locations of the southeast Greenland profile SIGMA III. Abbreviations are DF, Dickson Fjord; FF, Fonsfjord; FRD, Fjord Region Detachment; GF, Gåsefjord; GFZ, Greenland Fracture Zone; GG, Godthåb Gulf; GHF, Gauss Halvø Fault; GP, Geikie Plateau; HwH, Hold with Hope; KFJF, Kejsler Franz Joseph Fjord; KOJ, Kong Oscar Fjord; KR, Kolbeinsey Ridge; MR, Mohns Ridge; NVF, Nordvestfjord; SUM, Summit station; WF, Wolaston Foreland; WFZ, Western Fault Zone. Scale is valid for 72°N.

7.3 Geological background

The Iapetus Ocean closed during continent-continent collision of Baltica and Laurentia in mid-Silurian times (~425 Ma). The westward subduction of Baltic crust caused extreme crustal thickening in the Caledonian Belt (Torsvik et al. 1996). The early stage of post-collision extension and formation of the fault belt (Figure 7.1) occurred in middle to late Silurian times, perhaps due to gravitational collapse and pure shear stretching of the lower crust (Andersen and Jamveit 1990; Milnes et al. 1997). An alternative model is that the subduction reverted to exhumation (Fossen and Rykkeliid 1992; Rey et al. 1997) along a pre-existing, west-dipping shear zone (Schlindwein and Jokat 2000). Discrete extensional phases followed the lithospheric collapse (McClay et al. 1986; Dewey 1988) for almost 350 million years. Extensional detachments (Hartz and Andresen 1995), fault-controlled Devonian basins (Larsen and Bengaard 1991), and syn-extension granitic intrusions along the detachment faults (Hartz and Andresen 1995) testify to the post-Caledonian extension, which ceased in late-Devonian to early Carboniferous time. Price et al. (1997) suggested minor crustal stretching occurred associated with a Carboniferous rifting event on Traill Ø (Figure 7.1), but larger amounts of stretching are suggested for Jameson Land (Larsen 1990; Larsen and Marcussen 1992). Existing seismic refraction data in this area (Fechner 1994; Mandler and Jokat 1998) also show evidence for thinning of the Devonian crust. The most prominent rifting event took place in late Jurassic to early Cretaceous times (Surlyk 1990), when marine sediments were deposited

over the Devonian sediments on Jameson Land. North of Kong Oscar Fjord these two sequences are juxtaposed (Figure 7.1) and separated by the Gauss Halvø Fault (Schlindwein and Jokat 1999; Peacock et al. 2000). Cenozoic magmatism accompanied the final stage of rifting and the opening of the North Atlantic in the early Eocene. Price et al. (1997) provide a detailed analysis of the onshore exposures of the Cenozoic rift-related and magmatic rocks. The contrasting rifting histories north and south of the Kong Oscar Fjord led to the assumption that pre-existing crustal structures had an influence on magmatism (Schlindwein and Jokat 1999). The total amount of volcanic extrusives in the fjord region between Kong Oscar Fjord and Shannon Island (Figure 7.1) is still under debate. The relatively minor tholeiitic and alkaline basalts exposed onshore may either be evidence for weak activity, or they may alternatively represent relics of larger amounts of intrusions which were since eroded (Upton 1988; Larsen et al. 1989). Schlindwein and Jokat (1999) and Voss and Jokat (2007) proposed major melt production from deep seismic crustal velocity models in the region between Kong Oscar Fjord, Kejser Franz Joseph Fjord and the Godthåb Gulf. Observations of high seismic velocities ($> 7.0 \text{ km s}^{-1}$) in the lower crust are consistently interpreted in this region as magmatic underplating of the northeast Greenland continental crust. The seismic evidence of underplating diminishes rapidly northward (Voss et al. submitted). Voss and Jokat (2007) proposed the presence of concealed basaltic extrusives mixed with syn-rift sediments in $\sim 2 - 6$ km depth within the shelf region, based on seismic velocities and gravity modelling (Figure 7.1). The opening of the North Atlantic between Greenland and Scandinavia is associated with a south to north propagation of the Early Eocene continental break-up, starting at around 56 Ma (Larsen 1988). The earliest seafloor spreading is marked by the oldest ocean spreading anomaly, C24B (~ 54 Ma), along the North Atlantic margins (Figure 7.1). Voss and Jokat (2007) proposed a delay in break-up in a zone north of the Jan Mayen Fracture Zone (JMFZ), which was locked as a result of long term extension of the continental crust. Based on the location of the continent ocean boundary (COB) and its obliquity with respect to seafloor spreading anomalies, Voss et al. (submitted) estimated break-up not earlier than 51.5 ± 0.2 Ma (C23) and 50.1 ± 0.3 Ma (C22) off Godthåb Gulf and Kejser Franz Joseph Fjord, respectively, which is about 3.5 m.y. later than that further north. Initially, enhanced oceanic crustal accretion started with half spreading rates of about 30 cm a^{-1} (Voss et al. submitted), and decreased rapidly to $14 - 17 \text{ cm a}^{-1}$ and gave rise to the production of thinner than normal ($5 - 7$ km) oceanic crust (White et al. 1992). In contrast, the oceanic crust forming off southeast Greenland at the same time is $8 - 12$ km thick (Korenaga et al. 2000; Holbrook et al. 2001; Hopper et al. 2003).

7.4 Crustal scale characteristics of rift episodes

A 3D density model (Schmidt-Aursch and Jokat 2005b) covered parts of the Caledonian hinterland, the fjord region and the Greenland Sea basin up to the Mohns Ridge. Inferences on the structure of the continental crust and sedimentary basins based on six deep seismic profiles (Schlindwein and Jokat 1999; Schmidt-Aursch and Jokat 2005a) over Kong Oscar Fjord (KOF), Keiser Franz Joseph Fjord (KFJF), Dickson Fjord (DF), Nordvestfjord (NVF), Føn fjord (FF), and Gåsefjord (GF) (Figure 7.1). A distinct continent – ocean transition zone (COT) was not interpreted due to its unknown complexity, and the COB after Escher and Pulvertaft (1995) was used instead. Constraints for the ocean basin came from Klingelhöfer et al. (2000a). The error in extrapolated Moho depths was estimated to ± 5 km for the continental domain, and ± 3 km in the ocean basin (Schmidt-Aursch and Jokat 2005b). A major uncertainty remains because of poorly-known surface geology and westward extent of the Caledonides, hidden beneath the Greenland ice sheet. The newly observed and modelled COT along profile AWI-20030500 (Voss and Jokat 2007) prompts a revised conceptual cross-section through the Kejser Franz Joseph Fjord (Figure 7.1). A composite 1020 km long

traverse is shown in Figure 7.2, based on three profiles of seismic refraction data and 3D density modelling. The traverse provides an excellent basis for re-examining the rifting history and the development of the crustal structural style during post-Caledonian extensional collapse through to the final stage of continental break-up. Multi-channel seismic data are not included due to the major focus on crustal structural styles, which is best addressed using wide-angle seismic data. We refer readers to the original studies for details of the velocities, densities, resolutions and uncertainties of the seismic models of the following transects, which provide sufficient overlap for full and continuous coverage:

- 1) The crustal model from the Precambrian shield to the Caledonian mountains (kms 0 – 460) is deduced from a 3D density cross-section after Schmidt-Aursch and Jokat (2005b). The inland-direction is a prolongation of the offshore seismic transects of the Kejsler Franz Joseph Fjord, and connects to the location of Summit Station (Dahl-Jensen et al. 2003) (Figure 7.1). The schematic surface topography (Figure 7.2) was not included in the density model (Schmidt-Aursch and Jokat 2005b). The profile merges with its eastern neighbour between km 400 at the top and km 460 at the bottom (Figure 7.2).
- 2) The post-Caledonian structure of the continental crust and sedimentary basins is based on seismic refraction profile 94320 (Figure 7.1) in the seaward prolongation of Kejsler Franz Joseph Fjord (Schlindwein and Jokat 1999), between kms 400 and 620 (Figure 7.2). Intra-crustal reflections were located with an accuracy of ± 2 km, and the Moho with ± 3 km. The transition to the eastern-most profile cuts through kms 560 and 620 from top to bottom.
- 3) Profile AWI-20030500 covers the COT and the onset of oceanic crust in the Greenland basin. It forms the youngest part of the cross section from km 560 at the top and km 620 at the bottom to the eastern end at km 1020. The greater number of recording stations and higher ray-coverage results in an estimated accuracy of ± 0.5 km for upper layers and ± 2 km for lower layer boundaries and the Moho (Voss and Jokat 2007). 2D Bouguer gravity modelling revealed similar densities for the crustal layers, sedimentary basin, and upper mantle in the two profiles just described, and it confirms the COT location and the high-velocity lower crust.

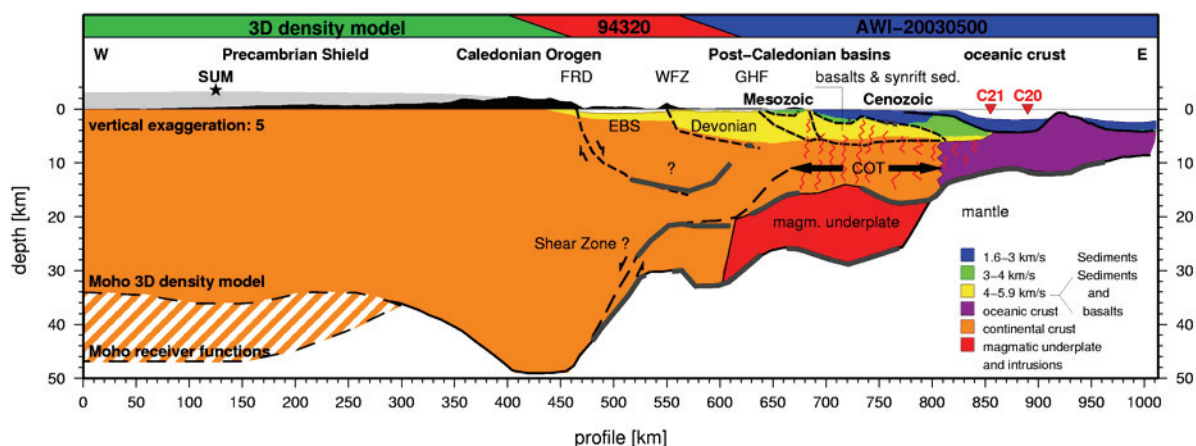


Figure 7.2: Conceptual crustal model of the merged transects. Coloured bars at top mark extents of single profiles and overlapping regions (see Figure 7.1). Colours mark crustal segments and velocity ranges of the sediments and basalts. Grey dashed line marks modelled Moho after 3D-gravity model. Striped region marks high density lower crustal layer (see text for details). Solid grey lines mark seismic reflectors. Black short dashed lines mark tectonic structures and/or structural boundaries of basins. Black long dashed line mark possible crustal shear zone. Magnetic spreading anomalies are marked and labelled Cxx. Abbreviations are as in Figure 7.1, plus COT, continent ocean transition; EBS, Eleonore Bay Supergroup sediments; magm., magmatic; sed., sediments.

A review of the typical crustal units (Figure 7.2) follows the interpretations of these studies, in combination with the geological maps of Escher and Pulvertaft (1995) and Henriksen et al. (2000). The surface geology, faults, and large scale crustal structures are correlated, and the main tectonic events are summarized, in a simplified time scale on Figure 7.3.

7.4.1 Precambrian Shield and Caledonian orogen

Gravity modelling yielded a thickness of the Proterozoic crust of 35 km (0 - 300 km) with moderate ($2.93 - 3.00 \times 10^3 \text{ kg m}^{-3}$) lower crustal densities (Schmidt-Aursch and Jokat 2005b). A 35 km thick crust is consistent with the average of other Precambrian shields world wide (Meissner 1986; Durrheim and Mooney 1994; Christensen and Mooney 1995; Zandt and Ammon 1995). However, Dahl-Jensen et al. (2003) inferred a Moho depth of 47 km from receiver function analysis at the Summit station (SUM), which is about 5 km off the gravity transect near km 125 (Figures 7.1 and 7.2). Schmidt-Aursch and Jokat (2005b) provided an alternative gravity model using this deeper Moho in the landward prolongation of the Kejser Franz Joseph Fjord. They showed that doing so required a density increase from $2.93 - 3.0 \times 10^3 \text{ kg m}^{-3}$ between 25 km and 35 km to densities of $3.1 \times 10^3 \text{ kg m}^{-3}$ and $3.2 \times 10^3 \text{ kg m}^{-3}$ in the 12 km thick additional lower crustal layer, in order to fit the Bouguer anomaly for the Moho (Fig 2). There is no independent evidence to favour either set of densities, although lower crustal layers with high densities and seismic velocities have been predicted (Durrheim and Mooney 1994) beneath Proterozoic shields. We prefer the simple model associated with the shallower Moho, consistent lower crustal densities and a reasonable Moho topography, but without rejecting the other model.

The distinct crustal root (350 – 500 km) beneath the Caledonian orogenic belt has a maximum Moho depth of 49 km, deeper than either of the alternative Moho depths modelled to the west (Figure 7.2). Clear evidence for this root came from a deep seismic profile in the Nordvestfjord (Mandler and Jokat 1998; Schmidt-Aursch and Jokat 2005a; Figure 7.1), and was confirmed by 3D gravity modelling (Schmidt-Aursch and Jokat 2005b). The significant Bouguer anomaly low correlates with the highest surface elevations and the crustal root, revealing an overall crustal thickness of 51 km. On the other hand, a crustal root is absent beneath the conjugate Scandinavian Caledonides (Meissner 1986; Kinck et al. 1991) where a significant Bouguer anomaly low is instead attributed to lower densities in the mantle (Theilen and Meissner 1979; Bannister et al. 1991). Schmidt-Aursch and Jokat (2005b) thoroughly discuss different orogenic roots and their associated gravity anomalies. A crustal root was also found beneath the Proterozoic Torngat Orogen, northeast Canada, between 35 – 38 km thick Archean crust in the west and the Nain Province in the east, which has been preserved for ~1.8 Gyr (Funck and Loudon 1999). A wide Bouguer anomaly low coincides with the ~50 km deep root, whose formation is suggested either to be the result of a flip in subduction direction (eastward to westward) or, alternatively, from westward underthrusting in a late stage of collision. However, Funck and Loudon (1999) attributed the preservation of the crustal root to the absence of postorogenic heating and ductile reworking, consistent with the lack of post-collisional magmatism. The East Greenland Caledonian crustal root formed in Silurian time (~425 Ma) during the palaeo-westward subduction of Baltic crust (Torsvik et al. 1996). Schlindwein and Jokat (2000) considered gravitational collapse or subduction reverted to exhumation along a west-dipping shear zone, which can be expected to have initiated the removal of the crustal root. The question of whether later heating (e.g. due to the Iceland plume thermal anomaly) also affected the crustal root has not yet been considered.

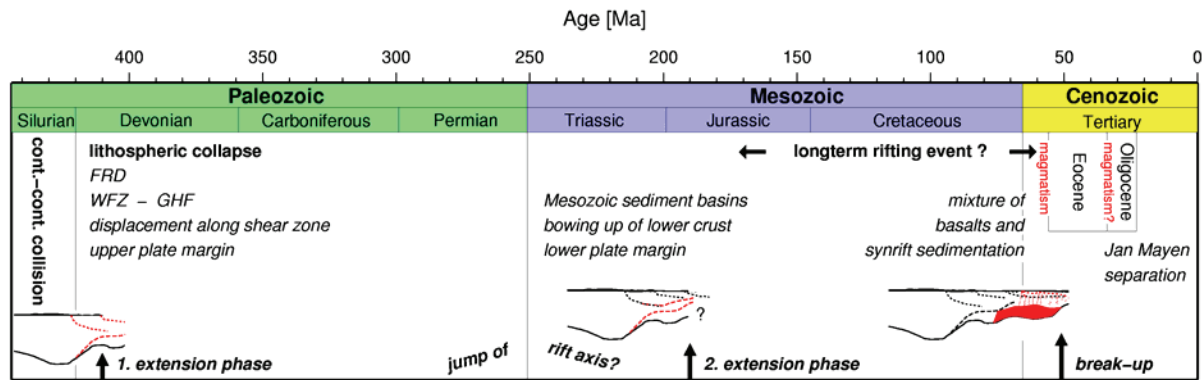


Figure 7.3: Simplified time scale with main tectonic and magmatic events. A sketch of the transect shows activated structures with red dashed lines. Note the possible jump of the rift axis between Paleozoic and Mesozoic times. Abbreviations are cont., continent, lith., lithospheric, and as in Figure 7.2.

7.4.2 Post-Caledonian Basins

Devonian Basin

The major east-dipping Fjord Region Detachment (Figure 7.2, FRD) (Hartz and Andresen 1995; Andresen et al. 1998) separates an area unaffected by significant upper crustal extension to the west (Andresen et al. 1998), from the Eleonore Bay Supergroup to the east (450 - 550 km). The FRD overlies a steeply westward dipping Moho at 40 to 30 km depth. Schlindwein and Jokat (2000) proposed the FRD terminates at a lower crustal reflector in ~13 km depth, and that it therefore does not represent a crustal-scale detachment. Those authors proposed that the overthickened post-orogenic Caledonian crust collapsed along a west-dipping shear zone between km 500 and 600, which is marked by a prominent lower crustal reflector. They suggest lower crustal displacement along this shear zone, following either a simple shear or a delamination model. The Western Fault Zone (Figure 7.2, WFZ) developed during the Devonian subsidence of the thinned crust, and the basin filled with Devonian continental sediments (Larsen and Bengaard 1991; Escher and Pulvertaft 1995). The location of the WFZ at the surface correlates with a Moho high in 30 ± 3 km depth. Schlindwein and Jokat (2000) concluded that this step in the Moho was preserved when the first major rifting phase gradually shifted to the east between late-Devonian and early-Carboniferous times.

Mesozoic Basins

The initiation of a second major rifting phase in middle Jurassic times (Surlyk 1990) led to the evolution of Mesozoic sedimentary basins, which lie to the east of the Devonian basin. Middle to upper Jurassic sediments were deposited in fluvial and shallow marine settings (Price et al. 1997). A second Moho slope developed during that rifting episode, underlying the Gauss Halvø Fault (Figure 7.2, GHF) between the two major sedimentary sequences. The increased seismic velocities of the lower crust in 16 - 30 km depth between km 600 and 680 were interpreted to be a result of (1) the displacement of lower crustal material along the west-dipping shear zone (Schlindwein and Jokat 2000) as described above, and (2) as a result of Tertiary magmatism (Schlindwein and Jokat 1999; Voss and Jokat 2007). The strong lateral velocity gradient at km 600 can be thought of either a structural boundary between rifted lower continental crust and a pure magmatic underplated body, or as the crust of a gradual increase in lower crustal intrusions. The correlation between a strong negative magnetic anomaly off the coast (Figure 7.1) and the expected magnetisation of a lower crustal body led Schlindwein and Jokat (1999) to conclude that the high velocities between km 600 and 680 represent a magmatic underplate.

Continent - ocean transition zone

Long term rifting persisted until Late Cretaceous/Early Tertiary times and formed deep-marine clastic wedges of up to 2600 m thickness exposed in Wolaston Foreland (Surlyk 1978; 1990). Voss and Jokat (2007) suggested that the latest stage of the Cretaceous to Tertiary rifting phase might have been accompanied by magmatism that significantly influenced the style of the COT. Extrusive basalts intercalated with syn-rift sediments form the up-to-5.4 km-thick layer between kms 690 and 810 (Figure 7.2). A further conclusion was that a large degree of magmatic intrusions had resulted in an increase in seismic crustal velocities between kms 670 and 800 in 6 – 18 km depth (Voss and Jokat 2007) to values ($6.6 - 6.8 \text{ km s}^{-1}$) that are significantly above the global average for extended crust at such depths (Christensen and Mooney 1995). Voss and Jokat (2007) related magnetic anomalies to such intrusions.

A major structure of the COT is a 210 km wide and up to 15 km thick lower crustal body, interpreted as a solidified magmatic underplate beneath the rifted continental crust (Voss and Jokat 2007). The current transition to mantle rocks occurs beneath the underplate at a depth of 26 – 28 km, shallowing rapidly eastwards towards oceanic crust. Schlindwein and Jokat (1999) concluded from the presence of minor exposures of onshore Tertiary plateau basalts on Bontekoe Ø (km 670), Hold with Hope and Traill Ø (Figure 7.1), that the underplate formed contemporaneously with the Tertiary plateau basalts on the Geikie Plateau south of Scoresby Sund (Figure 7.1). We cannot preclude the possibility that the thick high velocity lower crustal body contains fragments of inherited and exhumed Caledonian crust, as in the Norwegian Vøring basin (Gernigon et al. 2004). A major difference is, however, the complex magnetic pattern in the northeast Greenland margin associated with major intrusions in the crustal layers. To what extent the HVLC contributes to these magnetic anomalies is open to question, given its depth range of 15 – 30 km and the unknown level of the Curie temperature (540 – 570 °C). Schlindwein and Jokat (1999) attributed the large negative magnetic anomaly off the northeast Greenland fjord region (Figure 7.1) to the magmatic underplate and expected the demagnetisation level to lie below 20 km. We favour, for further consideration, a massive magmatic body and assume the majority of the melt accumulated at the crust-mantle boundary.

Cenozoic Basins

Thermal subsidence of the Norwegian-Greenland rift system initiated the deposition of Cenozoic sediments (Figure 7.2, km 690 – 820), which form the top layer of the present East Greenland shelf. The onset of oceanic crust is marked by a deep Cenozoic sedimentary basin (km 810 – 840) and a steep rise of the Moho to ~14 km (Voss and Jokat 2007). The accumulation of the magmatic underplate terminated at the time of break-up, and normal accretion of oceanic crust began.

Voss and Jokat (2007) proposed rift propagation from north to south along the Fjord region margin. Break-up was estimated to have occurred last off the Kejsler Franz Joseph Fjord, at close to C22 (~49.4 Ma) time. Anomaly C21 (~47.1 Ma) is the first clearly identified magnetic ocean spreading anomaly, at km 850 (Figs.1 and 2). The total thickness of the Early Eocene oceanic crust decreases from 7 km (km 820) to 4.8 km (km 980), but with a local maximum of 11.5 km beneath a fragment of the Jan Mayen Fracture Zone (Voss and Jokat 2007) (km 925; Figure 7.2).

7.5 Rift geometries

The composite cross-section (Figure 7.2) demonstrates the relative dimensions and extents of tectonic and magmatic structures of the COT, the extensional basins and rifted continental crust. Compared to the Precambrian crust and the Caledonian crustal root, a high degree of crustal thinning occurred over a 350 km wide region from Devonian to Cretaceous times. Post-collision extension revealed a significant initial vertical movement of crustal material as seen on the eastern steep flank of the crustal root (kms 460 to 530; Figure 7.2). An effective

mechanism for crustal thinning and vertical displacement of crustal material can be explained by asymmetric crustal scale detachment models. The simple shear model (Wernicke 1985) requires a low-angle fault cutting through the entire lithosphere. Extension is accommodated along the fault, and produces related normal faults from upper crustal brittle deformation in the hanging wall. Here, fault-bounded basins develop and fill with clastic sediments. A Moho slope forms where the shear zone offsets it. An alternative scenario is the delamination model (Lister et al. 1986), which considers a detachment penetrating delaminated lithosphere. Extension along a shear zone produce equivalent normal faulting at the surface but runs horizontally beneath the brittle/ductile layer boundary of the crust and also beneath the Moho. In either case, asymmetric margins evolve depending on their location relative to the shear zone, as conceptually illustrated in Figure 7.4 after Lister et al. (1986). The hanging wall is referred to as the upper plate margin with rocks originally above the shear zone, and with a simple structured basement (Lister et al. 1986). Uplift of the continental crust is a response to lateral translation of dense lithospheric material and upwelling of warmer and less denser asthenosphere. Underplating of igneous material at the crust-mantle boundary and normal fault sequences dipping at the surface towards the newly developing ocean are characteristics of an upper plate margin configuration. The lower plate margin refers to the footwall, which exposes deeper crustal rocks and hosts wider sedimentary basins. Movement along the major detachment fault and the removal of upper crustal material accompanies crustal thinning, subsidence and upward buckling of the lower crust. Characteristics of both upper and lower plate margins can be identified along the margin transect in Figure 7.2. We propose a rifting model involving a change from an upper plate margin to a lower plate margin, and which involves subsequent magmatic overprinting.

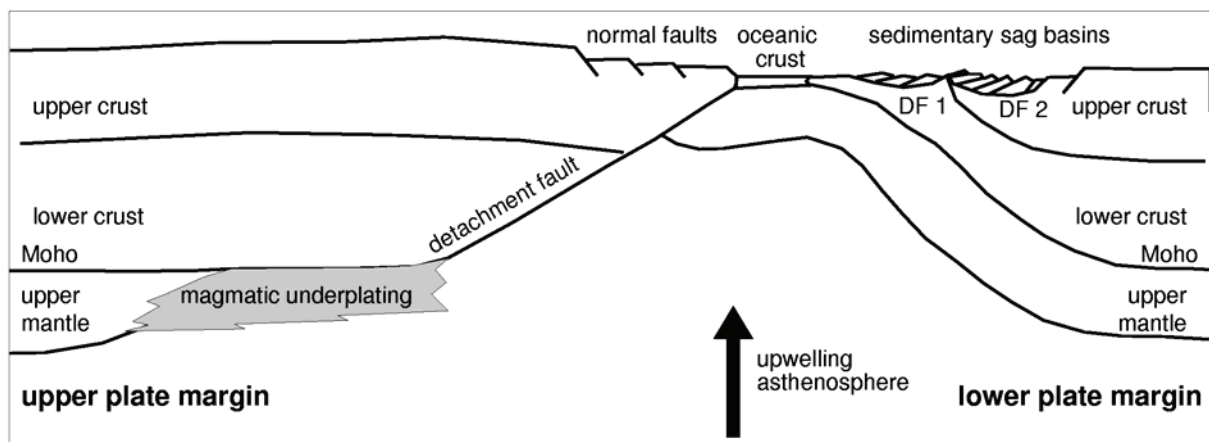


Figure 7.4: Detachment fault model with complementary asymmetric margin configurations after Lister et al. (1986). Upper plate unstructured, continental uplift due to magmatic underplating. Lower plate margin has complex structures. Illustration is not to scale. Abbreviations are DF, detachment faults.

7.5.1 Upper plate margin segment

The most significant feature similar to the upper plate margin geometry is the inferred westward dipping lower crustal shear zone (Figures 7.2 and 7.5a) with marked reflectivity in 22 – 40 km depth (Schlindwein and Jokat 2000). Fountain et al. (1984) related lower crustal reflectivity to the seismic anisotropy of mylonites along shear zones. The proposed shear zone can be associated with the landward dipping detachment fault (Lister et al. 1986), marked in Figure 7.4. Additional structures supporting this model are the major faults, FRD and WFZ, which initiated during the first stage of rifting (Figure 7.3). Initial vertical displacement of the lower Caledonian crust (Schlindwein and Jokat 2000) is consistent with the early stage of

evolution of an upper plate margin. An eastward prolongation of the proposed shear zone, which cuts through the upper crustal layer (Figure 7.5a), can be deduced from the strong lateral upper crustal velocity increase indicated by the dashed line in Figure 7.2, from $\sim 6.3 \text{ km s}^{-1}$ to $\sim 6.6 \text{ km s}^{-1}$ (Voss and Jokat 2007). Lavier and Manatschal (2006) describe differential crustal motion of up to 10 km vertically accommodated at a ductile shear zone in the thinning mode of the extensional rifting model for non-volcanic margins.

The eastward decrease in exposure of upper crustal material and the accompanying evolution of deep extensional basins underlain by large scale magmatic underplating, do not fit into a full upper plate margin model. Thus, we suggest a change from the upper plate margin configuration during the first Devonian/Carboniferous rifting stage to a lower plate margin configuration in the following rifting stages.

7.5.2 Lower plate margin segment

We propose a change to a lower plate margin with the initiation of the second major phase of rifting further east in the mid-Jurassic (Figure 7.3). Supporting evidence comes from Mosar et al. (2002a), who inferred as much from the extensional normal faults and the east-dipping FRD, WFZ and GHF. Extension was accommodated by wide fault blocks (Price et al. 1997) while, in lower Cretaceous times narrow fault blocks developed along detachment faults as a consequence of the movement of the eastern (upper) plate. Upper crustal material thinned to some degree during the extensional movement. It is not resolved and thus questionable, whether the post-Caledonian sedimentary basins show eroded half-graben structures at the bottom (Figure 7.5b). We assume that lower crustal material, vertically displaced along the crustal shear zone during the Devonian upper plate margin stage, bows further upwards during the lower plate margin stage. To some extent, the lateral velocity increase from ~ 6.6 to $\sim 6.8 \text{ km s}^{-1}$ between kms 600 and 650 (Voss and Jokat 2007) may mark the transition between brittle upper crust and ductile lower crustal material in 15 to 20 km depth, as well (as previously mentioned) the presence of later magmatic intrusions. A consequence of the great crustal thinning to less than 10 km was subsidence and the emplacement of syn-rift sediments. Lister et al. (1991) describe a similar sequence of crustal thinning and subsidence for Atlantic-type rifted margins based on observations from the US rifted margins. We suppose that intrusions into the rifted crust, during Tertiary magmatism at the end of the second rift phase (Figure 7.5c) additionally increased the seismic velocities within the COT, so that originally rifted upper and lower crust cannot be distinguished. We do not preclude stages of uplift during magmatic underplating, but neither can we quantify this or the accompanying erosion. However, post-magmatic thermal subsidence of $\sim 3 \text{ km}$ can be deduced from the thickness of the post-break-up sedimentary deposits (Figure 7.2).

It remains unresolved to what degree the rifted crust is intruded within the COT, and to what extent the high velocity lower crustal body consists of heavily intruded and stretched continental crust. It is assumed that sills in continental crust result in a more heterogeneous structural style with enhanced internal seismic reflectivity, but Schlindwein and Jokat (1999) and Voss and Jokat (2007) reported only clear top and bottom reflections of the high velocity lower crustal body, as shown in Figure 7.2.

7.5.3 Asymmetric rifting of conjugate margins

Torske and Prestvik (1991) proposed a rift-configuration model with an east-dipping main crustal detachment south of JMFZ, and a west-dipping one north of JMFZ, and suggested an upper plate style for the East Greenland margin and a lower plate type Vøring margin. Mosar et al. (2002a) demonstrated asymmetric rifting and the development of upper vs. lower plate margins for Norway and East Greenland based on cross-sections north and south of the Jan Mayen Fracture Zone. However, the latter authors proposed a lower plate margin development

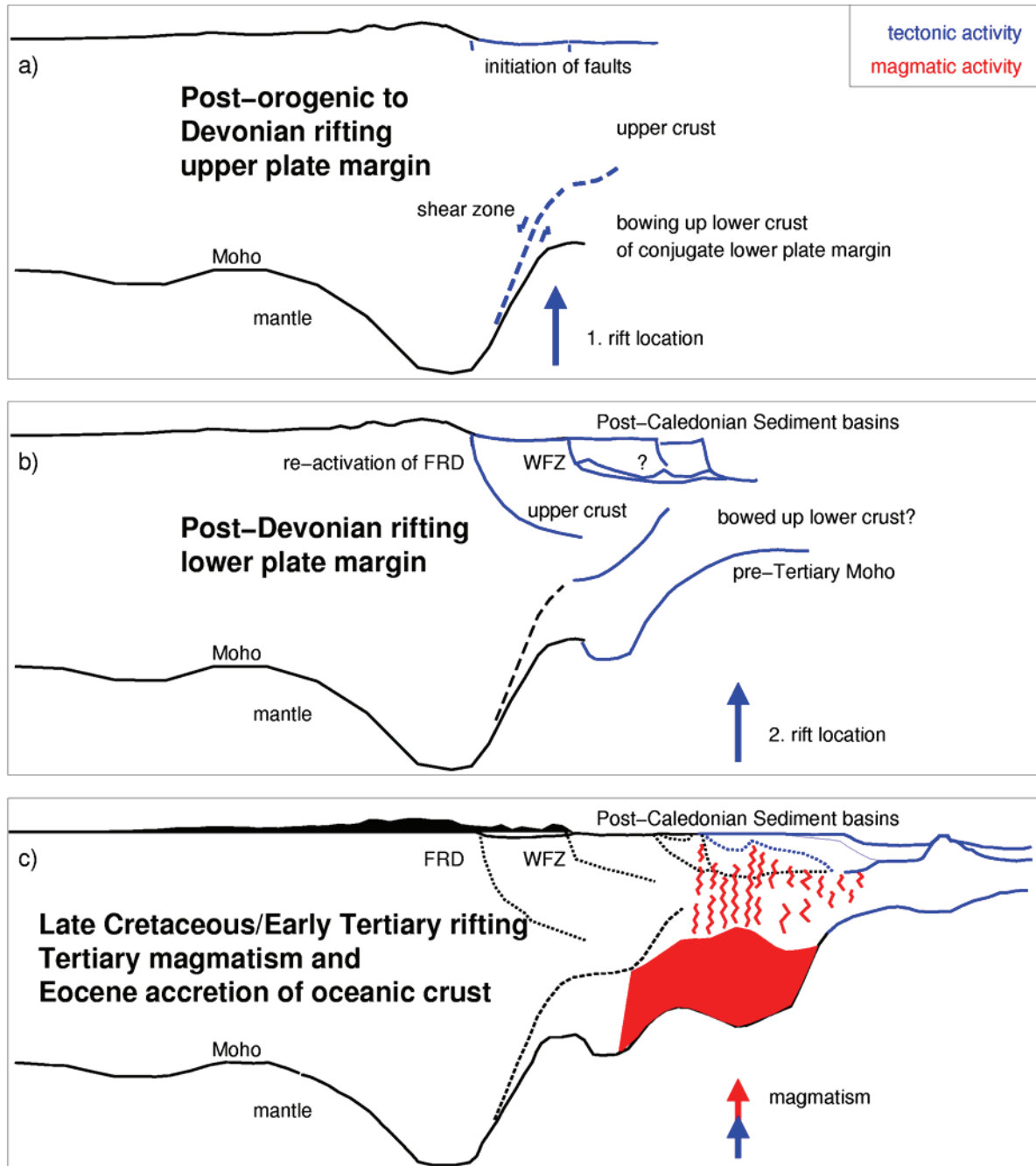


Figure 7.5: Sketch of the rift geometry and schematic margin evolution. Blue lines mark active faults and structures and red denotes magmatic activity. Arrows (blue and red) mark possible locations of rift and magmatic centres. a) Post-orogenic to Devonian rifting shows an upper plate margin configuration. A lower crustal shear zone marks the detachment of the upper and lower plate. Crust of the conjugate lower plate margin was bowed up. b) Configuration changed to a lower plate margin where former detachment faults were re-activated. A shallow pre-Tertiary Moho developed. Upper crust eroded by the eastward drift of the upper plate. c) Tertiary magmatism attached magmatic underplating and intruded the rifted continental crust. Break-up occurred and initiated accretion of oceanic crust.

for East Greenland north of the Jan Mayen Fracture Zone, and did not discuss the influence of magmatism for the latest stage of rifting at either margin. Mjelde et al. (2003) favoured a delamination model for the Vøring margin which started as a lower plate in late Cretaceous and early Tertiary times and switched to an upper plate geometry in response to the arrival of the Icelandic hotspot and a westward jump of the rifting axis. Our model shows a similar jump from an upper to lower plate margin, but suggests the timing of this jump was probably in mid-

Jurassic times. The detachment surface is proposed near the top of ductile and heavily intruded lower crust in both models. With respect to the uncertainties of the conjugate positions of Kejser Franz Joseph Profile and the Vøring Plateau profile (Voss and Jokat 2007), these two models agree on the evolution of asymmetric margins during the late stages of rifting. A major disagreement exists, however, in the timing of tectonic events and styles of rifting in the earlier stages.

7.6 Duration and production rates of northeast Greenland magmatism

The total magmatic volume within the COT of the Kejser Franz Joseph transect (Figure 7.2) is estimated per unit length (1 km) along-strike. Only rough calculations of the production rates and durations of magmatism are possible because of the large uncertainty in the amount of magma intruded into the lower crustal layer and the proportion of melt that was erupted as basalts. Furthermore, erosion might have locally removed extrusives to a large extent (Upton 1988; Larsen et al. 1989). It should be noted that these rates represent half production rates in units of km^3 per unit length per year ($\text{km}^3 \text{ km}^{-1} \text{ a}^{-1}$) based on calculations along only one side of the rift zone.

Table 7.1 summarizes the total volumes for each part of the rift zone influenced by magmatism and the assumed proportion of melt within the layers. We cannot precisely predict the proportion of basalt and the sedimentary sequence at kms 690 and 810 (Figure 7.2). Thus we assume it to vary between 0 and 100% with an average of 50% volcanic material, i.e. $210 \pm 210 \text{ km}^3$ of basalts. Increasing seismic velocities within the continental crust (km 615 – 690) and the COT between kms 690 and 815 (Figure 7.2) could be due to the uplifted lower crust, as described above, but also due to volcanic intrusions. Therefore, we assume a variability of 0 – 20%, averaging 10%, of volcanic intrusions in the rifted continental crust, i.e. $210 \pm 210 \text{ km}^3$ (Table 7.1), which is most likely an underestimate. The magmatic underplate (kms 600 – 810) consists of entirely magmatic material and has a volume of 1990 km^3 (Table 7.1). The total magmatic volume of basalts, crustal intrusions and magmatic underplating is thus estimated to $2410 \pm 420 \text{ km}^3$. An equivalent amount can be assumed from the adjacent profile off the Godthåb Gulf (Voss and Jokat 2007).

Eldholm and Grue (1994) calculated full production rates for the North Atlantic assuming magmatism lasted for 3 m.y. after break-up (54.4 – 51.4 Ma) along the North Atlantic margins. Voss et al. (submitted) estimated propagating break-up at the northeast Greenland margin, starting at the Greenland Fracture Zone at 54.2 Ma and ending at 50 Ma off the Kejser Franz Joseph Fjord, based on the location of the seaward COB and oblique spreading anomalies. We assume, in a first approach, magmatism to have been continuous throughout this period and to have had a constant production rate (Table 7.2). Published half production rates are used for a second calculation and an alternative duration of magmatism is estimated for the region off the Kejser Franz Joseph Fjord (Table 7.3).

	Width	mean thickness	total volume	magmatic volume
basalts and sediments	120 km	3.5 km	420 km^3	$210 \pm 210 \text{ km}^3$ (0 – 100 %)
transitional/intruded crust	125/200 km	9.6/10.5 km	$1200/2100 \text{ km}^3$	$210 \pm 210 \text{ km}^3$ (0 – 20 %)
Magmatic underplating	210 km	9.5 km	1990 km^3	1990 km^3 (100 %)

Table 7.1: Summary of the total magmatic volumes of each part of the rift zone after Voss and Jokat (2007). Note that the volumes are rough estimates.

7.6.1 Productivity

Voss et al. (submitted) proposed break-up off the Kejser Franz Joseph Fjord at 50 Ma near the maximum of the normal polarization of C22. A constant half production rate as high as $5.7 \pm$

$1.0 \times 10^{-4} \text{ km}^3 \text{ km}^{-1} \text{ a}^{-1}$ must have continued for 4.2 m.y. in order to emplace the estimated basalts, intrusions and underplated material off the Kejser Franz Joseph Fjord. Eldholm and Grue (1994) estimated $8.3 \times 10^{-4} \text{ km}^3$ per km rift per year full production rate within 3 m.y. of crustal accretion for the entire North Atlantic Volcanic Province (NAVP). This yields a half rate of $4.15 \times 10^{-4} \text{ km}^3 \text{ km}^{-1} \text{ a}^{-1}$ (Table 7.2), which is both lower and sustained for 1.2 m.y. less than our estimate. As an alternative to constant production, the latter authors suggested melt production increased during break-up, and then underwent a gradual decrease.

Crustal accretion	Half production rates [$\text{km}^3 \text{ km}^{-1} \text{ a}^{-1}$]	crustal thickness [km]	time interval [Ma]	Reference
NAVP	4.15×10^{-4}		for 3 m.y.	after Eldholm and Grue (1994)
Mohs Ridge				
0.8 cm a^{-1}	0.3×10^{-4}	~ 4.0	0 – 20	after Klingelhöfer et al. (2000b)
1.4 cm a^{-1}	0.7×10^{-4}	~ 5.0	~49.4	after Voss et al. (submitted)
2.9 cm a^{-1}	2.9×10^{-4}	~ 10.0	~54.2	after Voss et al. (submitted)
SE Greenland				
3.3 cm a^{-1}	~ 5.3×10^{-4}	18.3 – 13.5	56.0 – 53.0	after Hopper et al. (2003) (SIGMA III)
1.95 cm a^{-1}	~ 2.3×10^{-4}	13.5 – 11.6	53.0 – 50.8	
1.7 cm a^{-1}	~ 1.9×10^{-4}	11.6 – 11.2	50.8 – 50.0	
KFJF	~ $5.7 \pm 1.0 \times 10^{-4}$		for 4.2 m.y.	this paper

Table 7.2: Half production rates for crustal accretion along the East Greenland margin. Locations and oceanic half spreading rates are given in the first column. Volumes for production rates are calculated per 1 km along the rifted margin. Note that the rates are half production rates. Thicknesses of the oceanic crusts and age intervals are shown in the second and third columns. See text for the time durations for NAVP and KFJF. Abbreviations are hsr, half spreading rate; KFJF, Kejser Franz Joseph Fjord; m.y., million years; NAVP, North Atlantic Volcanic Province; SE, southeast.

7.6.2 Duration

The present day Mohs Ridge (Figure 7.1) is an ultra-slow spreading ridge (~0.8 cm a^{-1}) (Klingelhöfer et al. 2000b) with a mean crustal accretion rate of $4.0 \pm 0.5 \text{ cm a}^{-1}$. This corresponds to a productivity of just $0.3 \times 10^{-4} \text{ km}^3 \text{ km}^{-1} \text{ a}^{-1}$ (Table 7.2). More recent publications (Mosar et al. 2002b) proposed initial half spreading rates of 1.3 – 1.8 cm a^{-1} for the Mohs Ridge and ~1.5 – 2.1 cm a^{-1} for the Aegir Ridge. Voss et al. (submitted) have shown that half spreading rates decreased from an initial maximum of 2.2 – 2.9 cm a^{-1} between C23 and C24 to about $1.4 \pm 0.1 \text{ cm a}^{-1}$ until C22 with a corresponding decreasing crustal thickness from ~10 to 5 km. These values would yield a production rate of $0.7 – 2.9 \times 10^{-4} \text{ km}^3 \text{ km}^{-1} \text{ a}^{-1}$ (Table 7.2). Comparable values were found for central-eastern Greenland plateau basalts (Table 7.3). The production rates range between 1.15 and $1.5 \times 10^{-4} \text{ km}^3 \text{ km}^{-1} \text{ a}^{-1}$ for the northern Geikie Plateau to ~ $2.0 \times 10^{-4} \text{ km}^3 \text{ km}^{-1} \text{ a}^{-1}$ for the southern Geikie Plateau, and the area between 69° N and Kangerdlugssuaq (Larsen et al. 1989). Basalts on Iceland and onshore East Greenland were emplaced at similar rates (Nielsen and Brooks 1981; Table 7.3).

Basalt provinces	Half production rates [$\text{km}^3 \text{ km}^{-1} \text{ a}^{-1}$]	Reference
Geikie Plateau	$1.15 – 2.0 \times 10^{-4}$	Larsen et al. (1989)
69° N – Kangerdlugssuaq	~ 2.0×10^{-4}	Larsen et al. (1989)
Iceland	$0.6 – 2.5 \times 10^{-4}$	Nielsen and Brooks (1981)
East Greenland basalts	$0.8 – 1.0 \times 10^{-4}$	Nielsen and Brooks (1981)
southeast Greenland	1.12×10^{-4}	Saunders et al. (1998)
KFJF	$1.5 \times 10^{-4} \rightarrow 16.1 \pm 2.8 \text{ m.y. duration}$	this paper

Table 7.3: Half production rates for basaltic provinces. Units are the same as in Table 7.2. Note that an average of all half production rates is used as an estimate for the KFJF. Abbreviations are as in Table 7.2.

Assuming a constant production rate of $1.5 \times 10^{-4} \text{ km}^3 \text{ km}^{-1} \text{ a}^{-1}$, based on an average of the published values for extrusive basalts, would result a time interval of $16.1 \pm 2.8 \text{ m.y.}$ to

produce the observed $2410 \pm 420 \text{ km}^3$ of magmatic material off the Kejser Franz Joseph Fjord. Hence, the initiation of magmatism would have been at around $66.1 \pm 2.8 \text{ Ma}$, which is older than most estimates of the initiation of magmatism. Lower plateau basalts were related to a 60 – 62 Ma igneous phase around Kangerdlugssuaq (Saunders et al. 1997) and from drill site 917 off southeast Greenland (Saunders et al. 1998). Plateau lavas on Hold with Hope and Wolaston Foreland were also related to the lower series (Upton et al. 1995). Price et al. (1997) concluded a main period of volcanism in northeast Greenland at 60 – 54 Ma.

7.6.3 Poly-productivity model

The two estimates, one with a production rate of $5.7 \pm 1.0 \times 10^{-4} \text{ km}^3 \text{ km}^{-1} \text{ a}^{-1}$ for 4.2 m.y., and one with a period of magmatism of $16.1 \pm 2.8 \text{ m.y.}$ for an average productivity of $1.5 \times 10^{-4} \text{ km}^3 \text{ km}^{-1} \text{ a}^{-1}$, represent end-member models. A model with a heterogeneous, rather than constant, productivity rate appears to be most likely. Such a model would not contradict a peak of melt production (Eldholm et al. 1989). The eastward increase in thickness of the magmatic underplate may point to an eastward (i.e. later) increase of productivity. Larsen et al. (1989) also calculated an increased productivity for the latter episode of NAVP volcanism (Table 7.3). We propose a four stage productivity model including production rates derived from onshore plateau basalts and crustal accretion rates of northeastern Greenland. The derived initial magmatism correlates well with the dating of earliest emplaced onshore basalts. Backwards calculation from the time of break-up is necessary in order to achieve the initial duration. Production rates, duration of the stages and produced magmatic volumes are listed in Table 7.4 and schematically shown in Figure 7.6. Half spreading rates for northeast Greenland's oceanic crust and average crustal thicknesses are taken from Voss et al. (submitted), and the ages of spreading anomalies from Cande and Kent (1995).

	Productivity [$10^{-4} \text{ km}^3 \text{ km}^{-1} \text{ a}^{-1}$]	Duration of magmatism [million years]	magmatic volume [km^3]
Stage IV	1.1 ± 0.1	0.8 (50.0 – 50.8 Ma)	88 ± 8
Stage III	4.4 ± 0.3	2.5 (50.8 – 53.3 Ma)	1100 ± 75
Stage II	9.4	0.5 (53.3 – 53.8 Ma)	470 ± 32
Stage I	1.5	5.0 ± 3.6 (53.8 – 62.4 Ma)	752 ± 535

Table 7.4: Poly-productivity model for the emplacement of magmatic material off the Kejser Franz Joseph Fjord. See also Figure 7.5. Note that the calculation proceeds backwards from the proposed break-up at 50 Ma in order to reveal the initial duration of magmatism for the given production rate.

Stage IV: The latest stage comprises the magmatic material, which was generally accreted as oceanic crust from C23 (50.8 Ma) on, but remained beneath the continent – ocean transition zone until the local break-up at 50 Ma. The average half spreading rate for this time interval is proposed as $1.4 \pm 0.1 \text{ cm a}^{-1}$ and an average crustal accretion of 8 km yields a production rate of $1.1 \pm 0.1 \times 10^{-4} \text{ km}^3 \text{ km}^{-1} \text{ a}^{-1}$, corresponding to a volume of $88 \pm 8 \text{ km}^3$ added to the total produced volume (Table 7.4).

Stage III: An average productivity of $4.4 \pm 0.3 \text{ km}^3 \text{ km}^{-1} \text{ a}^{-1}$ is deduced from studies of the NAVP ($4.15 \times 10^{-4} \text{ km}^3 \text{ km}^{-1} \text{ a}^{-1}$) after Eldholm and Grue (1994) and the minimum of the proposed rate for the region off KFJF of $4.7 \times 10^{-4} \text{ km}^3 \text{ km}^{-1} \text{ a}^{-1}$ (Tab. 2). This stage has a duration of 2.5 m.y., starting from C23 (50.8 Ma) and lasting until 53.3 Ma (C24B), and produce a magma volume of $1100 \pm 75 \text{ km}^3$.

Stage II: A peak of 0.5 m.y. and a productivity of $9.4 \times 10^{-4} \text{ km}^3 \text{ km}^{-1} \text{ a}^{-1}$ (Eldholm et al. 1989; Eldholm and Grue 1994) is assumed between 53.3 and 53.8 Ma. Assuming an equivalent error (of 7 %) to that for stage III, this results in a contribution of $470 \pm 32 \text{ km}^3$.

Stage I: The remaining magmatic volume produced in the initial stage would be $752 \pm 535 \text{ km}^3$ (Table 7.4) deduced from the difference of the total volume along the transect (2410 ± 420

km³) and the calculated volumes of the later three stages (1658 ± 115 km³). At a production rate of 1.5×10^{-4} km³ km⁻¹ a⁻¹, similar to that for the emplacement of the plateau basalts (Tables 3 and 4), the duration of stage I would be 5.0 ± 3.6 million years.

The model yields a total duration of magmatic melt production of 8.8 ± 3.6 m.y. (Table 7.4) and suggests an initiation of magmatism at between 55.2 and 62.4 Ma (Figure 7.6). This timing correlates well with the dating of lower plateau basalts (60 – 62 Ma) around Kangerdlugssuaq (Saunders et al. 1997) and the plateau lavas on Hold with Hope and Wolaston Foreland (60 – 54 Ma; Upton et al. 1995; Price et al. 1997).

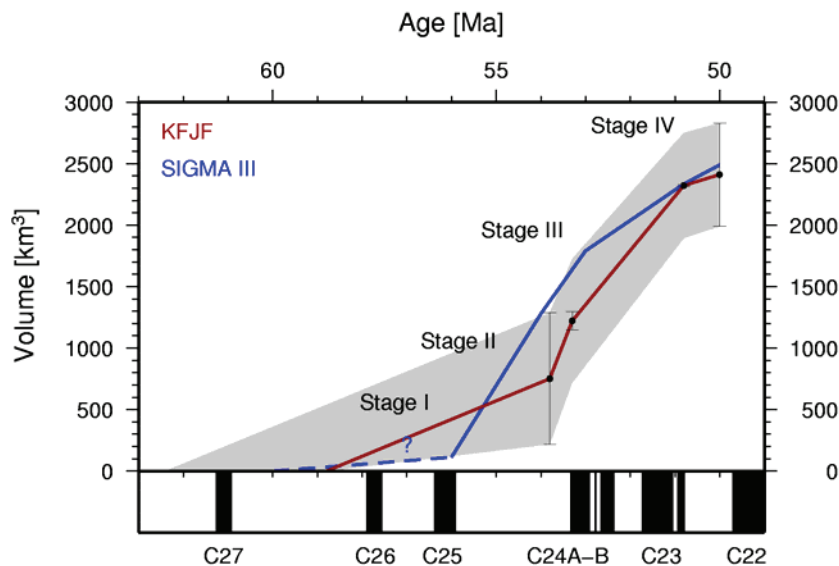


Figure 7.6: Poly-productivity model for the melt production off the Kejsjer Franz Joseph Fjord (KFJF) after Table 7.4. Stages I – IV mark the four different intervals of melt productivity. Duration of magmatism is 8.8 ± 3.6 Ma, initiation is estimated between 55.2 and 62.4 Ma. Red line marks mean values from KFJF, black marks corresponding error bars, grey fill outlines the error region. Production of oceanic crust of the southeast Greenland margin is shown in blue. Note that the question mark and the dashed blue line mark the production of the continental succession, which occurred over 1 m.y. within this period. Magnetic spreading anomalies with normal polarisation in black are shown as reference after Cande and Kent (1995).

7.7 Discussion

From the poly-productivity model we conclude that the maximum estimated magmatism at the northeast Greenland margin, i.e. off the Kejsjer Franz Joseph Fjord and probably also off the Godthåb Gulf, is consistent with the general estimated production rates of extrusives and intrusions for the NAVP. Initiation of magmatism is suggested to have started several million years before the maximum burst of magma in stage II and III (C24B; 53.8 Ma – C23; 50.8 Ma). However, whereas in other regions along the Greenland margin stage III coincides with break-up and emplacement of extensive SDRS basalts, this peak of magmatism off the fjord region preceded break-up there by a few million years. We infer from the change of upper plate to lower plate margin configuration and the associated seaward shift of the rifting centre that the rifted continental crust is only poorly weakened, which had an effect on the delayed break-up.

A similar sequence can be discerned at the southeast Greenland margin. Lower lava series on continental crust are dated at 60 – 60.5 Ma (Saunders et al. 1998) from ODP drillhole 917. Hopper et al. (2003) proposed a model of magmatism and accretion of oceanic crust along a seismic transect SIGMA III (Figure 7.1). These authors estimated an initial half spreading rate of 3.3 cm a⁻¹ and identified new igneous crust, which has accreted since 56 Ma. Igneous crustal thickness decreases from 18.3 km to 13.5 km within 3 m.y., giving an average productivity of 5.3×10^{-4} km³ km⁻¹ a⁻¹. The productivity decreased further to less than 2.3×10^{-4} km³ km⁻¹ a⁻¹.

until 50.8 Ma and to $1.9 \times 10^{-4} \text{ km}^3 \text{ km}^{-1} \text{ a}^{-1}$ until approximately 50 Ma (Table 7.2). Continental basalts were proposed to have been emplaced within 1 m.y. (at some time between 56 and 61 Ma) with a half production rate of $\sim 1.12 \times 10^{-4} \text{ km}^3 \text{ km}^{-1} \text{ a}^{-1}$ (Saunders et al. 1998; Table 7.3). The crustal thicknesses, half spreading rates, and the emplacement of the continental succession reveal a total volume of approximately 2490 km^3 (Figure 7.6). The volume produced off the northeast Greenland margin thus seems equivalent to that at the southeast Greenland margin. The major difference of these two regions is the regional extent of magmatism at the southeast Greenland margin compared to the more localised occurrence of large magmatic volumes off the fjord region (Voss et al. submitted). The poly-productivity model with its suggested production rates supports Voss et al.'s model of magmatism sourced from one major feeder dyke in the vicinity of the Icelandic mantle plume and provides a maximum estimate of melt production between 62.4 and 50 Ma for the region off the Kejsler Franz Joseph Fjord, and probably as far as off Godthåb Gulf, which comprises a similar amount of magmatic underplating (Voss and Jokat 2007). Voss et al. (submitted) proposed alternative models invoking highly intruded continental crust rather than pure magmatic underplating, or a second phase of magmatism linked to the Oligocene separation of the Jan Mayen microcontinent (Figure 7.3; Gudlaugsson et al. 1988; Upton et al. 1995; Price et al. 1997). Late Eocene, Oligocene and Miocene magmatism is not included into our model here, although onshore intrusions do indicate ongoing activity (Upton et al. 1995; Price et al. 1997) associated with the separation of the Jan Mayen and the 30 – 25 Ma initiation of ocean spreading at the Kolbeinsey Ridge (Larsen 1990; Kodaira et al. 1997). The proposed production rates well explain the observed amount of melt off the KFJF and correlates with dated onshore basalts. If the high velocity lower crustal body has a higher content of rifted continental crust, or if the volume of Oligocene magmatism was comparable to that of the initial Early Tertiary event, then the large production rates are over-estimated and need to be re-evaluated. But the degree of continental crustal content in the high velocity body and the amount of sill intrusion in upper crustal layers remains debatable and further investigations are necessary. However, slightly lower production rates and a portion of the volume associated with the earliest stage ($752 \pm 535 \text{ km}^3$) could be related to the Oligocene magmatism.

7.8 Conclusions

A merged crustal transect across the entire East Greenland passive margin is provided, based on deep seismic refraction data and 3D gravity data modelling. It extends from the Precambrian shield, and through the Caledonian Foreland, to the Early Eocene oceanic crust in the prolongation of Kejsler Franz Joseph Fjord. A polyphase rift history and magmatism based on crustal-scale structures can be summarized as follows:

- 1.) The lithospheric collapse of Caledonian crust initiated the configuration of an upper plate margin. Devonian rifting corresponds with the displacement of the lower crustal layer along a landward dipping detachment fault and the initiation of major seaward dipping faults at the surface. The reflectivity of the deep seated shear zone can be related to the velocity contrast and/or to mylonites along the shear zone.
- 2.) The geometry changed to a lower plate margin configuration with the initiation of the second long term rifting event in Jurassic times, as suggested by the pattern of velocity increase in the higher crustal levels. The ductile lower crust bowed up, and brittle upper crustal material was eroded away during the large scale extension accompanying the eastward movement of the eastern upper plate margin. Large low-angle oceanward-dipping faults developed, or were reactivated from the previous rifting event, forming sedimentary basins. An earlier crust-mantle boundary is assumed to be marked by the top reflector of the magmatic underplate at 15 – 17 km depth.

- 3.) Margin uplift is assumed with the initiation of Early Tertiary magmatism and the emplacement of the magmatic underplate. Basalts erupted either subaerially or in a shallow water setting on top of the uplifted lower crust. Intrusions additionally modified the rearranged and displaced upper and lower crust. The amount of material intruded into the rifted crust is difficult to tell, as is whether the lower crustal body is entirely magmatic or, to some degree, intruded lower continental crust.
- 4.) The history of asymmetric rifting for the northeast Greenland lower plate margin is consistent with the determination of an upper plate margin configuration on the Vøring Plateau in Early Tertiary. Our arguments concerning changes of the rift geometry and jumps of the rifting axis during earlier times are, however, at odds with previous studies.
- 5.) A four stage model is proposed to explain the production of the observed magmatic volume within the rift zone. Magmatism started at 58.8 ± 3.6 Ma, slowly, with the emplacement of onshore plateau basalts. A peak of magmatism led to break-up along most of the North Atlantic margins, but this failed in the region off the Kejsler Franz Joseph Fjord. Here, ongoing reduced magmatism weakened the highly extended crust and finally initiated break-up at C22 (50 Ma). The extruded basalts were concealed by the subsequent subsidence of approximately 3 – 6 km and Cenozoic sedimentation.
- 6.) A sequence of magmatism comprising four different production rates explains the suggested amount of melt and supports a model of magmatism from one major feeder dyke into the region off the Kejsler Franz Joseph Fjord and Godthåb Gulf. In the case that our melt volumes are overestimated due to a higher content of continental crust within the high velocity body or additional Oligocene magmatism associated with the separation of the Jan Mayen Ridge, other models would remain tenable.

7.9 Acknowledgements

We thank M.C. Schmidt-Aursch and V. Schlindwein, who provided the additional digital gravity and velocity models used for the full transect. The manuscript was also greatly improved by comments from V. Schlindwein and Graeme Eagles. The manuscript profited from the thorough reviews of Robert Trumbull and two other anonymous reviewers. All figures were created with GMT (Wessel and Smith 1998).

7.10 References

- Andersen, T. B. and B. Jamveit (1990). "Uplift of deep crust during orogenic extensional collapse: a model based on field studies in the Sogn-Sunnfjord region of western Norway." *Tectonics* **9**: 1097-1111.
- Andresen, A., E. Hartz and J. Vold (1998). "A late orogenic extensional origin for the infracrustal gneiss domes of the East Greenland Caledonides (72-74°N)." *Tectonophysics* **285**: 353-369.
- Bannister, S., B. Ruud and E. S. Husebye (1991). "Tomographic estimates of sub-Moho seismic velocities in Fennoscandia and structural implications." *Tectonophysics* **189**: 37-53.
- Cande, S. C. and G. M. Kent (1995). "Revised calibration of the geomagnetic polarity timescale for the Late Cretaceous and Cenozoic." *Journal of Geophysical Research* **100**(B7): 9761-9788.
- Christensen, N. I. and W. D. Mooney (1995). "Seismic velocity structure and composition of the continental crust: a global view." *Journal of Geophysical Research* **100**(B7): 9761-9788.

Dahl-Jensen, T., T. B. Larsen, I. Woelbern, T. Bach, W. Hanka, R. Kind, S. Gregersen, K. Mosegaard, P. Voss and O. Gudmundsson (2003). "Depth to Moho in Greenland: receiver-function analysis suggests two Proterozoic blocks in Greenland." Earth and Planetary Science Letters **205**: 379-393.

Dewey, J. F. (1988). "Extensional collapse of orogens." Tectonics **7**: 1123-1139.

Durrheim, R. and W. Mooney (1994). "Evolution of the Precambrian lithosphere: seismological and geochemical constraints." Journal of Geophysical Research **99**(B8): 15359-15374.

Eldholm, O. and K. Grue (1994). "North Atlantic volcanic margins: Dimensions and production rates." Journal of Geophysical Research **99**(B2): 2955-2968.

Eldholm, O., J. Thiede and E. Taylor (1989). "Evolution of the Vøring volcanic margin." Proc. Ocean Drill. Program Sci. Results **104**: 1033-1065.

Escher, J. and T. Pulvertaft (1995). "Geological Map of Greenland, 1:2 500 000." Geological Survey of Greenland.

Fechner, N. (1994). Detailed refraction seismic investigations in the inner Scoresby Sund / East Greenland. Reports on Polar Research. Bremerhaven, Alfred Wegener Institute of Polar and Marine Research. **143**: 1-196.

Fossen, H. and E. Rykkelid (1992). "Postcollisional extension of the Caledonian orogen in Scandinavia: structural expressions and tectonic significance." Geology **20**: 737-740.

Fountain, D. M., C. A. Hurich and S. B. Smithson (1984). "Seismic reflectivity of mylonite zones in the crust." Geology **12**: 195-198.

Funck, T. and K. E. Loudon (1999). "Wide-angle seismic transect across the Torngat Orogen, northern Labrador: Evidence for Proterozoic crustal root." Journal of Geophysical Research **104**(B4): 7463-7480.

Gernigon, L., J. C. Ringenbach, S. Planke and B. Le Gall (2004). "Deep structures and breakup along volcanic rifted margins: insights from integrated studies along the outer Vøring Basin (Norway)." Marine and Petroleum Geology **21**: 363-372.

Gudlaugsson, S. T., K. Gunnarson, M. Sand and J. Skogseid (1988). Tectonic and volcanic events at the Jan Mayen Ridge microcontinent, in A. C. Morton and L. M. Parson (ed.), Early Tertiary Volcanism and the Opening of the NE Atlantic. **39**: 85-93.

Hartz, E. and A. Andresen (1995). "Caledonian sole thrust of central East Greenland: a crustal-scale Devonian extensional detachment?" Geology **23**: 637-640.

Henriksen, N., A. Higgins, F. Kalsbeek and T. Pulvertaft (2000). "Greenland from Archaean to Quarternary; descriptive text to the geological map of Greenland, 1: 2 500 000." Geol. Greenland Surv. Bull. **185**: 1-93.

- Holbrook, W. S., H. C. Larsen, J. Korenaga, T. Dahl-Jensen, I. D. Reid, P. B. Kelemen, J. R. Hopper, G. M. Kent, D. Lizarralde, S. Bernstein and R. S. Detrick (2001). "Mantle thermal structure and active upwelling during continental breakup in the North Atlantic." Earth and Planetary Science Letters **190**: 251-266.
- Hopper, J. R., T. Dahl-Jensen, W. S. Holbrook, H. C. Larsen, D. Lizarralde, J. Korenaga, G. M. Kent and P. B. Kelemen (2003). "Structure of the SE Greenland margin from seismic reflection and refraction data: Implications for nascent spreading center subsidence and asymmetric crustal accretion during North Atlantic opening." Journal of Geophysical Research **108**(B5): 2269.
- Jakobsson, M., N. Z. Cherkis, J. Woodward, R. Macnab and B. Coakley (2000). "New grid of Arctic bathymetry aids scientists and mapmakers." EOS Transactions of the American Geophysical Union **81**: 89, 93, 96.
- Kinck, J. J., E. S. Husebye and C. E. Lund (1991). "The South Scandinavian crust: Structural complexities from seismic reflection and refraction profiling." Tectonophysics **189**: 117-133.
- Klingelhöfer, F., L. Géli, L. Matias, N. Steinsland and J. Mohr (2000a). "Crustal structure of a super-slow spreading centre: a seismic refraction study of Mohns Ridge, 72°N." Geophys. J. Int. **141**: 509-526.
- Klingelhöfer, F., L. Géli and R. S. White (2000b). "Geophysical and geochemical constraints on crustal accretion at the very-slow spreading Mohns Ridge." Geophysical Research Letters **27**(10): 1547-1550.
- Kodaira, S., R. Mjelde, K. Gunnarson, H. Shiobara and H. Shimamura (1997). "Crustal structure of the Kolbeinsey Ridge, North Atlantic, obtained by use of ocean bottom seismographs." Journal of Geophysical Research **102**(B2): 3131-3151.
- Korenaga, J., W. S. Holbrook, G. M. Kent, P. B. Kelemen, R. S. Detrick, H. C. Larsen, J. R. Hopper and T. Dahl-Jensen (2000). "Crustal structure of the southeast Greenland margin from joint refraction and reflection seismic tomography." Journal of Geophysical Research **105**(B9): 21591-21614.
- Larsen, H. C. (1988). A multiple and propagating rift model for the NE Atlantic, in A. C. Morton and L. M. Parson (ed.), Early Tertiary volcanism and the opening of the NE Atlantic, Geological Society Special Publication. **39**: 157-158.
- Larsen, H. C. (1990). The East Greenland Shelf, (ed.), The Geology of North America, Geological Society of America, Boulder, Colo. **L**: 185-210.
- Larsen, H. C. and C. Marcussen (1992). Sill-intrusion, flood basalt emplacement and deep crustal structure of the Scoresby Sund region, east Greenland, in B. C. Storey, T. Alabaster and R. J. Pankhurst (ed.), Magmatism and the Causes of Continental Break-up, Geological Society Special Publication. **68**: 365-386.
- Larsen, L. M., W. S. Watt and M. Watt (1989). "Geology and petrology of the Lower Tertiary plateau basalts of the Scoresby Sund region, East Greenland." Bull. Grønlands geol. Unders. **157**: 1-164.

Larsen, P. H. and H. J. Bengaard (1991). "Devonian basin initiation in East Greenland: a result of sinistral wrench faulting and Caledonian extensional collapse." J. geol. Soc. London **148**: 355-368.

Lavier, L. L. and G. Manatschal (2006). "A mechanism to thin the continental lithosphere at magma-poor margins." Nature **440**: 324-328.

Lister, G. S., M. A. Etheridge and P. A. Symonds (1986). "Detachment faulting and the evolution of passive continental margins." Geology **14**: 246-250.

Lister, G. S., M. A. Etheridge and P. A. Symonds (1991). "Detachment models for the formation of passive continental margins." Tectonics **10**: 1038-1064.

Mandler, H. and W. Jokat (1998). "The crustal structure of central east Greenland: results from combined land-sea seismic refraction experiments." Geophys. J. Int. **135**: 63-76.

McClay, K. R., M. G. Norton, P. Coney and G. H. Davis (1986). "Collapse of the Caledonian orogen and the Old Red Sandstone." Nature **323**: 147-149.

Meissner, R. (1986). "The continental crust - A geophysical approach." International Geophysics Series **34**.

Milnes, A. G., O. P. Wennberg, Ø. Skår and A. G. Koester (1997). Contraction, extension and timing in the South Norwegian Caledonides: the Sognefjord transect, in J.-P. Burg and M. Ford (ed.), Orogeny Through Time, Geol. Soc. Spec. Publ. **121**: 123-148.

Mjelde, R., H. Shimamura, T. Kananzawa, S. Kodaira, T. Raum and H. Shiobara (2003). "Crustal lineaments, distribution of lower crustal intrusives and structural evolution of the Voering Margin, NE Atlantic; new insights from wide-angle seismic models." Tectonophysics **369**: 199-218.

Mosar, J., E. A. Eide, P. T. Osmundsen, A. Sommaruga and T. H. Torsvik (2002a). "Greenland-Norway separation: A geodynamic model for the North Atlantic." Norwegian Journal of Geology **82**: 281-298.

Mosar, J., G. Lewis and T. H. Torsvik (2002b). "North Atlantic sea-floor spreading rates: implications for the Tertiary development of inversion structures of the Norwegian-Greenland Sea." Journal of Geological Society, London **159**: 503-515.

Nielsen, T. F. D. and C. K. Brooks (1981). "The East Greenland rifted continental margin: an examination of the costal flexure." J. geol. Soc. London **138**: 559-568.

Peacock, D. C. P., S. P. Price, A. G. Whitham and C. S. Pickles (2000). "The World's biggest relay ramp: Hold with Hope, NE Greenland." Journal of Structural Geology **22**: 843-850.

Price, S., J. Brodie, A. Whitham and R. Kent (1997). "Mid-Tertiary rifting and magmatism in the Traill Ø region, East Greenland." J. geol. Soc. London **154**: 419-434.

Rey, P., J.-P. Burg and M. Casey (1997). The Scandinavian Caledonides and their relationship to the Variscan belt, in J.-P. Burg and M. Ford (ed.), Orogeny Through Time, Geological Society Special Publication. **121**: 179-200.

Saunders, A. D., J. G. Fitton, A. C. Kerr, M. J. Norry and R. W. Kent (1997). The North Atlantic Igneous Province, in J. J. Mahoney and M. F. Coffin (ed.), Large Igneous Provinces, American Geophysical Union Monograph. **100**: 45-94.

Saunders, A. D., H. C. Larsen and S. W. J. Wise (1998). Proceedings of the Ocean drilling Program, Scientific Results, (ed.), Ocean Drilling Program, College Station, TX. **152**.

Schlindwein, V. and W. Jokat (1999). "Structure and evolution of the continental crust of northern east Greenland from integrated geophysical studies." Journal of Geophysical Research **104**(B7): 15227-15245.

Schlindwein, V. and W. Jokat (2000). "Post-collisional extension of the East Greenland Caledonides: a geophysical perspective." Geophys. J. Int. **140**: 559-567.

Schmidt-Aursch, M. C. and W. Jokat (2005a). "The crustal structure of central East Greenland-I: From the Caledonian orogen to the Tertiary igneous province." Geophys. J. Int. **160**: 736-752.

Schmidt-Aursch, M. C. and W. Jokat (2005b). "The crustal structure of central East Greenland-II: From the Precambrian shield to the recent mid-oceanic ridges." Geophys. J. Int. **160**: 753-760.

Surlyk, F. (1978). "Jurassic basin evolution of East Greenland." Nature **274**: 311-327.

Surlyk, F. (1990). Timing, style and sedimentary evolution of Late Palaeozoic-Mesozoic extensional basins of East Greenland, in R. F. P. Hardman and J. Brooks (ed.), Tectonic Events Responsible for Britain's Oil and Gas Reserves, Geol. Soc. Spec. Publ. **55**: 107-125.

Theilen, F. and R. Meissner (1979). "A comparison of crustal and upper mantle features in Fennoscandia and the Rhenish Shield, two areas of recent uplift." Tectonophysics **61**: 227-242.

Torske, T. and T. Prestvik (1991). "Mesozoic detachment faulting between Greenland and Norway: Inferences from Jan Mayen fracture zone system and associated alkalic volcanic rocks." Geology **19**: 481-484.

Torsvik, T. H., M. A. Smethurst, J. G. Meert, R. Van der Voo, W. S. McKerrow, M. D. Brasier, B. A. Sturt and H. J. Walderhaug (1996). "Continental break-up and collision in the Neoproterozoic and Palaeozoic - A tale of Baltica and Laurentia." Earth-Science Reviews **40**: 229-258.

Upton, B. G. J. (1988). "History of Tertiary igneous activity in the N Atlantic borderlands." Geol. Soc. Spec. Publ. London **39**: 429-453.

Upton, B. G. J., C. H. Emeleus, D. C. Rex and M. F. Thirlwall (1995). "Early Tertiary magmatism in northeast Greenland." J. geol. Soc. London **152**: 959-964.

Verhoef, J., W. R. Macnab, R. Arkani-Hamed and J. M. o. t. P. Team (1996). "Magnetic anomalies of the Arctic and North Atlantic Oceans and adjacent land areas; Open File 3125." Geological Survey of Canada.

Voss, M. and W. Jokat (2007). "Continent – ocean transition and voluminous magmatic underplating derived from P-wave velocity modelling of the East Greenland continental margin." Geophys. J. Int. **170**: 580-604.

Voss, M., M. Schmidt-Aursch and W. Jokat (submitted). "Variations in magmatic processes along the East Greenland volcanic margin." Geophys. J. Int.

Wernicke, B. P. (1985). "Uniform-sense normal simple shear of the continental lithosphere." Can. J. Earth Science **22**: 108-125.

Wessel, P. and W. Smith, H. F. (1998). "New, improved version of Generic Mapping Tools released." EOS Transactions of the American Geophysical Union **79**(47): pp. 579.

White, R. S., D. McKenzie and R. K. O'Nions (1992). "Oceanic Crustal Thickness From Seismic Measurements and Rare Earth Element Inversions." Journal of Geophysical Research **97**(B13): 19683-19715.

Zandt, G. and C. Ammon (1995). "Continental crust composition constrained by measurements of crustal Poisson's ratio." Nature **374**: 152-154.

8 Subsidence analysis

An analysis of the subsidence history of the presented seismic profiles AWI-20030200, -400 and -500 provides additional constraints on the subsidence of the ocean basin and the dimension and constitution of the high velocity lower crust (HVLC), and the existence of magmatic underplating off the East Greenland Fjord Region. Profile AWI-20030200 contributes solely to the subsidence analysis of the ocean basin.

8.1 Subsidence models

Rifted continental margins are characterised by subsidence and the formation of sedimentary basins during the rifting phase. Subsidence describes the mechanism of crustal lowering while stretching. The degree of thinning and subsidence is related to the thickness of unaffected crust, which is called “hinge zone”. In a simple shear type of rifting (Wernicke 1985), thinning increases with the distance from the hinge zone while it is constant in a pure shear type (McKenzie 1978). Intra-continental and marine sedimentation into the developed basins reveal additional support of subsidence due to the mass load. Further effects of vertical movements occur from magmatic intrusions into the rifted crust, depending on the change of density before and after intrusion. Magmatic underplating has an inverse effect of uplift of the system. The principles of these effects will be described below. An uniform stretching model of McKenzie (1978) is used to “predict” the depth of the top continental/transitional crustal layer. This model implies equal stretching factors for the crust and lithosphere. Predict means that the subsidence of the transitional zone is evaluated from given thicknesses and densities of the model layers, which are compared with the modelled depth to basement. Therefore, the interpretations of Cenozoic and syn-rift sediments, crustal layer, high velocity lower crust/magmatic underplating and upper mantle are extracted from the models, which are presented in section 4. A similar analysis is done for the depth of oceanic crust using the time dependent subsidence of ocean basins after Parson and Sclater (1977). Thermal subsidence, and subsidence due to the load of sediments, is calculated at the peak of spreading anomalies (for correct dating) and compared with the depth of oceanic crust derived from the seismic velocity modelling.

8.1.1 McKenzie model – Thermal tectonic subsidence

Le Pichon and Sibuet (1981) described the formation of rifted margins using the McKenzie (1978) model of uniform stretching. The total subsidence S_{MK} contains two components. The initial fault controlled subsidence S_i depends on the initial crustal thickness at the hinge zone, which is unaffected from extension, and the crustal stretching factor β (Figure 8.1). Assuming isostatic equilibrium of the crustal columns before and after stretching, the initial subsidence can be written as (Fowler 2005)

$$S_i = \frac{h_l (\rho_a - \rho_l) + h_c (\rho_l - \rho_c)}{\rho_a - \rho_w} \cdot \left(1 - \frac{1}{\beta}\right) \quad (\text{Eq. 8.1})$$

with h_l and ρ_l the thickness and density of the lithosphere, h_c and ρ_c the thickness and density of the crust, ρ_a the density of the asthenosphere, ρ_w the density of water and β the stretching factor. Is the temperature of the asthenosphere (T_a) is assumed to be constant and the temperature gradient in the lithosphere assumed to linear, ρ_c , ρ_l and ρ_a can be expressed as (Fowler 2005)

$$\begin{aligned}\rho_c &= \rho_{c0} \left(1 - \frac{\alpha T_a h_c}{2h_1} \right) \\ \rho_l &= \rho_{m0} \left(1 - \frac{\alpha T_a}{2} - \frac{\alpha T_a h_c}{2h_1} \right) \\ \rho_a &= \rho_{m0} (1 - \alpha T_a)\end{aligned} \quad (\text{Eq. 8.2})$$

using the crustal and mantle densities ρ_{c0} and ρ_{m0} at 0 °C, and the thicknesses h_c and h_1 . The coefficient of thermal expansion is α . The upwelling asthenosphere reveals a disbalance of the lithospheric thermal gradient (Figure 8.1).

The second component of the total subsidence is the thermal subsidence S_t , which occurs by relaxation of the lithospheric isotherms to the pre-stretching position and the thermal equilibrium. The gradually cooling of the lithosphere can be described with a one-dimensional heat-flow equation. A first approximation of the thermal subsidence is an exponential with a time constant, and assuming the temperature in the asthenosphere (T_a) to be constant, and temperature increasing linear with depth through the lithosphere (Fowler 2005) yields

$$S_t = E_0 r \cdot \left(1 - e^{-\frac{t}{\tau}} \right) \quad (\text{Eq. 8.3})$$

where

$$E_0 = \frac{4h_1 \rho_{m0} \alpha T_a}{\pi^2 (\rho_{m0} - \rho_w)}$$

is a constant of initial state values and

$$r = \frac{\beta}{\pi} \sin\left(\frac{\pi}{\beta}\right)$$

depends on the crustal stretching factor.

$$\text{The relaxation time is } \tau = \frac{h_l^2}{\pi^2 \kappa}.$$

The parameters are the time t and κ the thermal diffusivity. The total thermal-tectonic subsidence S_{MK} is the sum of both, and can be simply expressed for an infinite time by assuming Airy-type isostasy (Fowler 2005)

$$S_{MK} = h_c \frac{(\rho_{m0} - \rho_{c0}) \left(1 - \frac{\alpha T_a h_c}{2h_1} \right)}{\rho_a - \rho_w} \cdot \left(1 - \frac{1}{\beta} \right) \quad (\text{Eq. 8.4a})$$

The leading quotient can be expressed by a constant factor. In general, values are used from the Bay of Biscay (Le Pichon and Sibuet 1981) due to its characteristic magma-poor and non-volcanic rifted margin with

$$\begin{aligned}h_c &= 30 \text{ km} & h_l &= 125 \text{ km} \\ \rho_{m0} &= 3350 \text{ kg m}^{-3} & \rho_{c0} &= 2780 \text{ kg m}^{-3} & \rho_w &= 1030 \text{ kg m}^{-3} \\ \alpha &= 3.28 \times 10^{-5} \text{ }^\circ\text{C}^{-1} & T_a &= 1333 \text{ }^\circ\text{C}\end{aligned}$$

Equation 8.4a simplifies with equation 8.2 for ρ_a to

$$S_{MK} = 7.83 \cdot \left(1 - \frac{1}{\beta} \right) \quad (\text{Eq. 8.4b})$$

The total thermal-tectonic subsidence S_{MK} is estimated by determining the stretching factor β of the rifted margin in discrete steps along the profiles. The ratio of the thicknesses from the hinge zone and the crust at the discrete location is a simple approximation to the pure shear and uniform stretching model. A variation of the leading factor occurs, if values from the seismic models for the unaffected crustal thickness, and crustal and mantle densities are used for ρ_{m0} and ρ_{c0} . Varying one of the densities by $\pm 50 \text{ kg m}^{-3}$ yields a change for the leading factor of ± 0.75 . A variation in the temperature of $\pm 100^\circ \text{ C}$ yields only a change in subsidence of ± 0.03 .

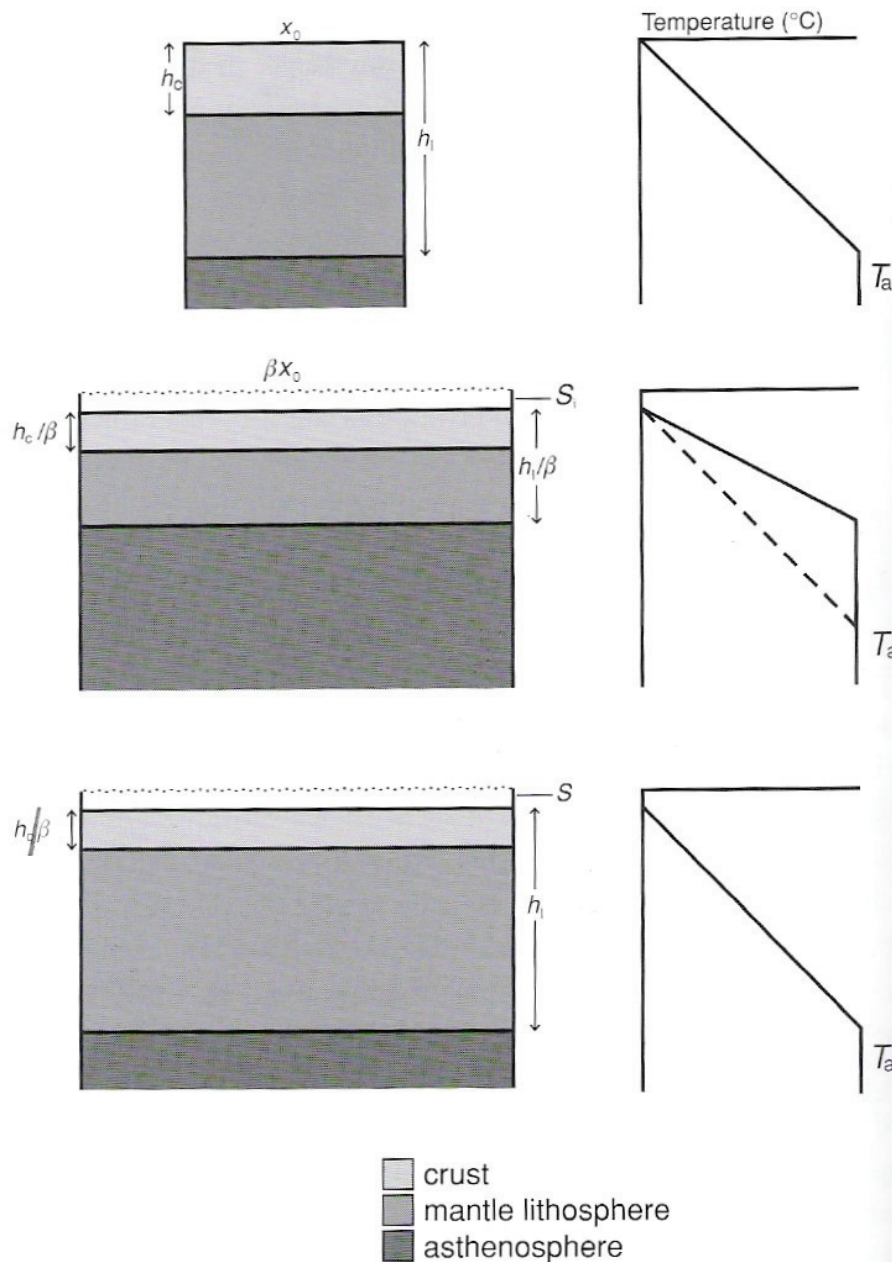


Figure 8.1: McKenzie model for the thermal-tectonic subsidence due to uniform stretching of the lithosphere (taken from Fowler 2005). TOP: The initial stage comprises lithospheric and crustal thicknesses h_l and h_c for continental lithospheric length x_0 . A linear temperature gradient for the lithosphere and constant temperature for the asthenosphere is assumed. MIDDLE: Instantaneous stretching by a factor β yields initial (tectonic) subsidence S_i , lithospheric layers h_c/β and h_l/β . Uprising hot asthenospheric material (with constant temperature) disturbs the thermal equilibrium (dashed line). BOTTOM: Cooling of the lithosphere reattains original thickness and temperature equilibrium. Initial subsidence S_i remains due to the replacement of light crustal material by dense mantle material. Further thermal subsidence S_t occurs due to lithospheric cooling. The final subsidence is $S = S_i + S_t$ (McKenzie 1978).

8.1.2 Subsidence by sediment load

Further subsidence occurs for a basin, which is originally filled with water. The replacement of a partial water column with sediments initiates subsidence due to the higher density. The final subsidence S_{Sed} by the loading effect of sediments is, for isostatic conditions, expressed by (Allen and Allen 1990)

$$S_{sed} = h_s - h_s \left(\frac{\rho_m - \rho_s}{\rho_m - \rho_w} \right) \quad (\text{Eq. 8.5})$$

with h_s : thickness of sediment layer
 ρ_s : density of sediments
 ρ_w : density of water
 ρ_m : density of mantle.

This equation describes the difference between a basin filled entirely with sediments of thickness h_s and its thickness (depth) it would have, if the sediments would be removed. Constant densities for crust, mantle and sediments are assumed to simplify calculations and due to lack of information for porosities and compaction coefficients of the sediments. The palaeo water depths and palaeo sea-level is neglected for the same reason. Sedimentation above sea-level was probably rather the case which also implies erosion. For this analysis, the present stage is considered, where the transitional zone is set beneath the shelf and below sea level. The present day water depth h_w has to be added to the subsidence S_{Sed} for determining the basement depth relative to the present day sea level.

8.1.3 Uplift by magmatic underplating

A crustal block is thickened by an underplated body of thickness h_{up} and density ρ_{up} . Uplift of the system occurs if $\rho_c < \rho_{up} < \rho_m$. Mantle material is replaced by lower density magmatic material, and a water column is replaced by the uplift. This is expressed by

$$U_{up} = h_{up} \left(\frac{\rho_m - \rho_{up}}{\rho_m - \rho_w} \right) \quad (\text{Eq. 8.6})$$

8.1.4 Subsidence by intrusion

Volcanic intrusions increase the density of a crustal layer and the system subsides, which can equivalently expressed by

$$S_{int} = h_{int} \left(\frac{\rho_{int} - \rho_c}{\rho_m - \rho_w} \right) \quad (\text{Eq. 8.7})$$

with h_{int} : thickness of intruded upper crust
 ρ_{int} : density of intruded upper crust
 ρ_c : density of unaffected (initial upper) crust

In order to constrain the dimension of magmatic underplating and/or lower crustal magmatic intrusions, the same subsidence can be calculated assuming the increase of lower crustal density to a value observed and interpreted as magmatic underplating. Thus, the subsidence S_{intl} caused by intrusions solely into the lower crust is

$$S_{intl} = h_{intl} \left(\frac{\rho_{intl} - \rho_{cl}}{\rho_m - \rho_w} \right) \quad (\text{Eq. 8.8})$$

with h_{intl} : thickness of intruded lower crustal layer
 ρ_{intl} : density of intruded lower crust and equivalent to ρ_{up}
 ρ_{cl} : density of unaffected (initial lower) crust

An end-member case is $h_{intl} = h_{up}$, where the proportion of magmatic underplating is totally assumed to be intruded lower crust. The total crustal thickness is then $h_{int} + h_{intl}$, which causes a smaller stretching factor β , and, therefore, a smaller thermal-tectonic subsidence.

8.1.5 Parson and Sclater model – Thermal subsidence of oceanic basins

An oceanic basin subsides with the age of the accreted crust due to the isostatic balance and lithospheric thermal cooling. At the ridge crest, the effect of the dense mantle column and the distal oceanic crust has to be in balance. Parson and Sclater (1977) describe the depth of an ocean basin D_{oc} by the square-root of time, which is expressed by

$$D_{oc} = d_r + \left(\frac{2\rho_a \alpha T_a}{\rho_a - \rho_w} \right) \times \left(\frac{\kappa t}{\pi} \right)^{\frac{1}{2}} \quad (\text{Eq. 8.9a})$$

with d_r : depth of ridge crest
 t : Age of oceanic crust in Ma.

Equation 8.9a simplifies to

$$D_{oc} = 2.5 + 0.36\sqrt{t} \quad (\text{Eq. 8.9b})$$

assuming a thermal diffusivity $\kappa = 10^{-6} \text{ m}^2 \text{ s}^{-1}$ (Fowler 2005) and a depth of the initial ridge crest of 2.5 km (other parameter values as described before), which is in agreement with observations of the North Atlantic and Pacific Ocean (Allen and Allen 1990). This approximation is valid for oceanic crust younger than 70 Ma, i.e. a depth of 5.5 km and is, thus, applicable for the estimation of the ocean basin off the East Greenland margin. Depth of oceanic basins increases more slowly with increasing age ($> 70 \text{ Ma}$) and is approximated by an equation with a negative exponential (Fowler 2005)

$$D_{oc(>70Ma)} = 5.65 - 2.47e^{-t/36} \quad (\text{Eq. 8.9c})$$

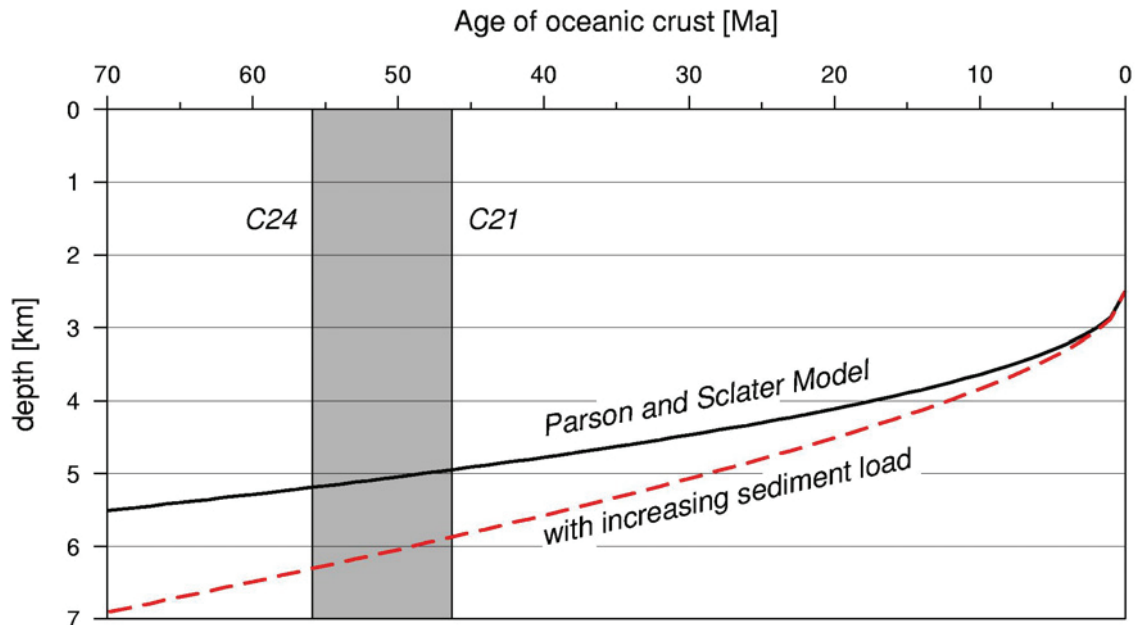


Figure 8.2 : Subsidence of oceanic crust after Parson and Sclater (1977). Thick black line shows depth of oceanic basement using equation 8.9b. Red dashed line includes an increasing sediment load, assuming subsidence by half of the increasing sediment thickness. Gray box marks region of East Greenland models between magnetic spreading anomaly C24 and C21 (55.9 – 46.3 Ma). Note that the red dashed line fits the thickness of approximately 2 km of sediments (~1 km subsidence) near 50 Ma similar to line AWI-20030500.

Assuming any sediment load onto the oceanic crust, the depth of the oceanic basement subsides (Eq. 8.5). Figure 8.2 shows an example for an increase of sediment load of 40 m per million years. Additional subsidence of approximately half the sediment thickness occurs by using densities of 1030, 2150 and 3260 kg m⁻³ for the water, marine sediments and the upper sub-oceanic mantle, respectively. The shaded region marks the time range between break-up near the end of chron C24r (55.9 Ma) and seafloor spreading until the beginning of chron C21n (46.3 Ma) of the East Greenland margin.

8.2 Oceanic basin and COT

The depth to basement of the Greenland basin is calculated along each seismic line (AWI-20030200 – 500) using equation 8.9b, and with respect to the effect of the observed sediment load. Stratigraphic age is determined by identification of magnetic spreading anomalies and the timescale after Cande and Kent (1995). Subsidence is calculated at the peaks of spreading anomalies along the oceanic parts of profile AWI-20030200 and AWI-20030300 for C21 – C24 (Figure 8.3). Possible locations of anomalies C22 – C24 were chosen from earlier publications (e.g. Tsikalas et al. 2002; Mosar et al. 2002b) off the East Greenland fjord region near profiles AWI-20030400 and AWI-20030500. This approach is used to constrain the interpretation of the proposed continent – ocean transition zone from the subsidence-point-of-view. However, for this case, the top of the layer of syn-rift sediment and basalts is seen as the top oceanic basement (Figure 8.3).

8.2.1 Predicted depths of ocean basin

The following simplifications were necessary, but are assumed to have a minor effect on the overall results:

- 1) The densities of the sediments are used from 2D gravity modelling (2150 kg m^{-3}) due to the lack of further physical parameters characterising the compaction, porosity and density. It has been shown in the section 6.3.2.3., that the modelled density of the sediments in the ocean basin fit in a certain range the results of drill-hole ODP 913 (Myhre and Thiede 1995).
- 2) Variations in palaeo water depth during the evolution of the ocean basin are neglected. Palaeo sea-level changes might have an effect on the presented results due to changes up to 200 m between Early Tertiary and the present day (Haq et al. 1987).
- 3) The spreading ridge crest in 2500 m depth is a well accepted value for mid-ocean ridges and is also valid with minor errors for the North Atlantic (Clift et al. 1995).
- 4) The most important assumption is that of local isostasy, and thus, a crust with a weak flexure. Clift et al. (1995) has shown that this is a reasonable approximation by comparing the East Greenland margin with other similar aged margins.

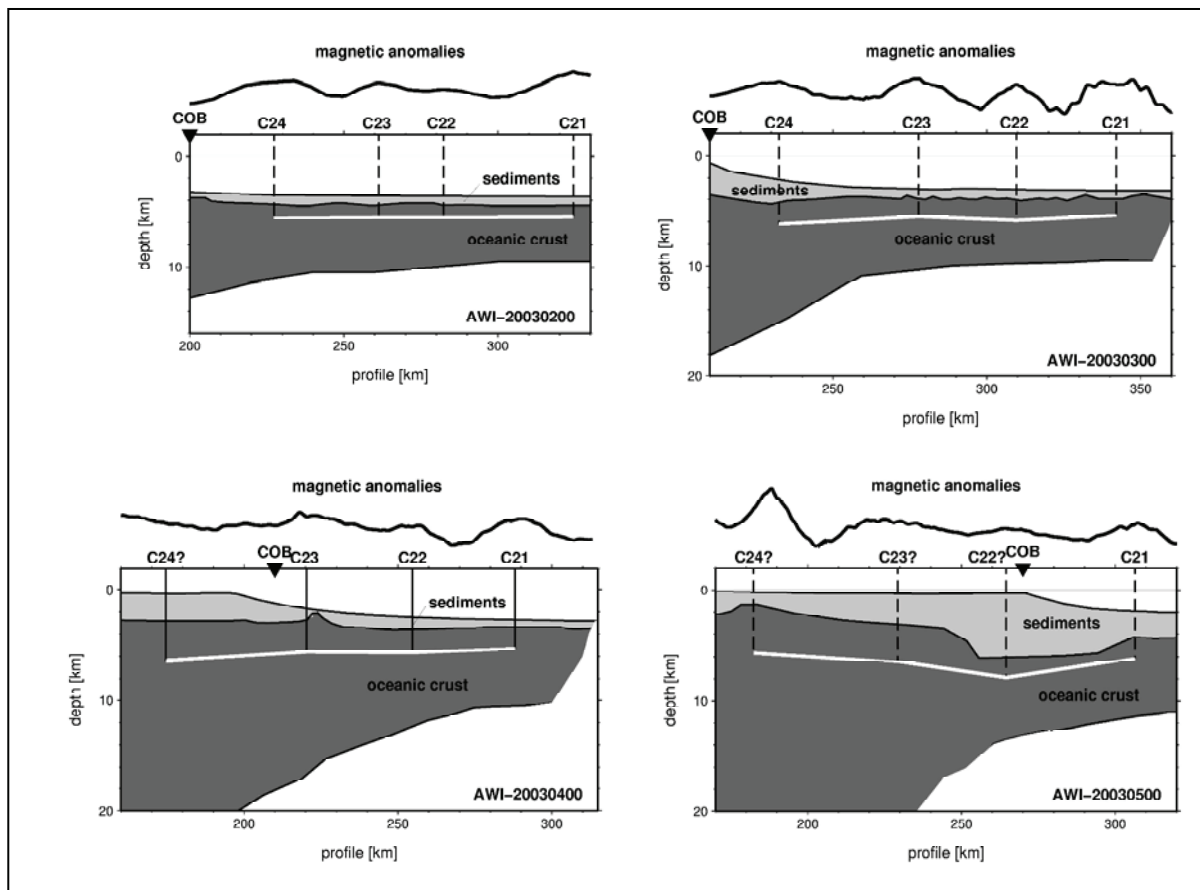


Figure 8.3: Simplified models show oceanic parts of the profiles. Magnetic anomaly data (Verhoef et al. 1996) are shown on top and peaks of spreading anomalies are marked. Bright grey colours show sedimentary layers and dark grey colours mark oceanic crust. White line mark depth of basement from thermal-tectonic subsidence and sediment load (Parson and Sclater model). Note that transitional crust of profile AWI-20030400 and AWI-20030500 is considered as oceanic crust only for classification purposes. Anomalies marked with question-mark were chosen from other publications (see text for details).

Variations of the depth to oceanic basement between the northeast and southeast Greenland margin is tested using the profiles SIGMA I – IV (Korenaga et al. 2000; Holbrook et al. 2001; Hopper et al. 2003) of the southeast Greenland margin. These profiles transect similar aged oceanic crust. Equivalent values for densities are used to keep consistency. The depth to

basement is determined from the interpreted velocity models (SIGMA I, III – IV) and along the 4 km s^{-1} – contour for SIGMA II (Figure. 8.4).

8.2.2 Discussion of predicted depths

The results of the calculations are summarized in Table 8.1 and illustrated in Figure 8.5. The differences between the predicted depths to oceanic basement of the Parson and Sclater model (PSM) to those derived from the seismic velocity models (VM) are shown in Figure 8.5 for the profiles AWI-20030200 – 500 and SIGMA I – IV. The larger the difference, the shallower is the basement depth derived from seismic modelling. The differences in basement depths are always larger (dashed lines) of the southeast Greenland margin than those of the northeast Greenland profiles (solid lines).

Chron	Age [Ma]	PSM [km]	20030200 [km]	20030300 [km]	20030400 [km]	20030500 [km]	S - I [km]	S - II [km]	S - III [km]	S - IV [km]
C21n	47.1	4.97	5.42	5.42	5.27	6.17	6.17	6.17	6.17	6.17
C22n	49.4	5.03	5.48	5.58	5.63	7.88	7.88	7.88	7.88	7.88
C23n	51.4	5.08	5.48	5.53	5.58	6.48	6.48	6.48	6.48	6.48
C24n	52.8	5.12	5.55	6.2	6.35	5.65	5.65	5.65	5.65	5.65

Table 8.1: Comparison of depths to oceanic basement. PSM: Time depending subsidence after Parson and Sclater (1977) and the additional effect of sediment load at the location of the magnetic chrons. The ages refer to the peak of normal polarities after (Cande and Kent 1995). Depth to basements for profiles 20030200 – 500 are taken from the velocity models (see Figure 8.3). S – I to S – IV refer to models of profiles SIGMA I – IV as shown in Figure 8.4.

The relative distances of the northeast and southeast Greenland profiles to the Iceland hotspot and plume location at the time of break-up (Figure 6.15) has been discussed before and is also remarkable here. Reliable constraints can be derived for the crustal parts between C21 and C23 of profiles AWI-20030200, 300 and 400 and SIGMA I - III. Uplift of the ocean basin occurs towards the hotspot location from 0.9 – 2 km from distal to proximal locations at C21 to 1.1 – 3.3 km at C23. Uplift increases also towards the oldest oceanic crust, C24, in similar manners with the distance to the hotspot location (1.2 – 4.5 km from distal to proximal locations) for profile AWI-20030500 (Figure 8.3). A reasonable explanation is the relation to the crustal thicknesses and the distance to a thermal anomaly. Initial crustal thicknesses of the distal profiles are smaller than of the proximal profiles. A closer location to a thermal anomaly, i.e. the Iceland hotspot, might have an effect on regional uplift. The model does not allow any conclusions about the source or reason of the difference. On the other hand, SIGMA II was proposed to have extremely thick initial oceanic crust (Korenaga et al. 2000, Figure 8.4). The crustal structure reveals a comparable style to profile AWI-20030400 (Figure 5.9). The magnetic data along profile SIGMA II shows a weak spreading anomaly pattern (Figure 8.4) but was used to support the interpretation as oceanic crust (Korenaga et al. 2000). The large difference of 3 – 4 km might be related to the fact that transitional crust was treated as oceanic for the profiles AWI-20030400 and 500. Crustal thickness increases significantly in these regions and a shallower basement depths was chosen according to the velocity models. The basement relief may also account for the large deviation between the two depths. This comparison outlines, that an interpretation as high thickened oceanic crust is debatable or that highly thickened initial oceanic crust does not match into a standard thermal subsidence model. On the other hand, such large deviations might suggest, that this part of the model has to be considered as transitional continental crust rather than oceanic, which fits the actual interpretation for profile AWI-20030400 and AWI-20030500.

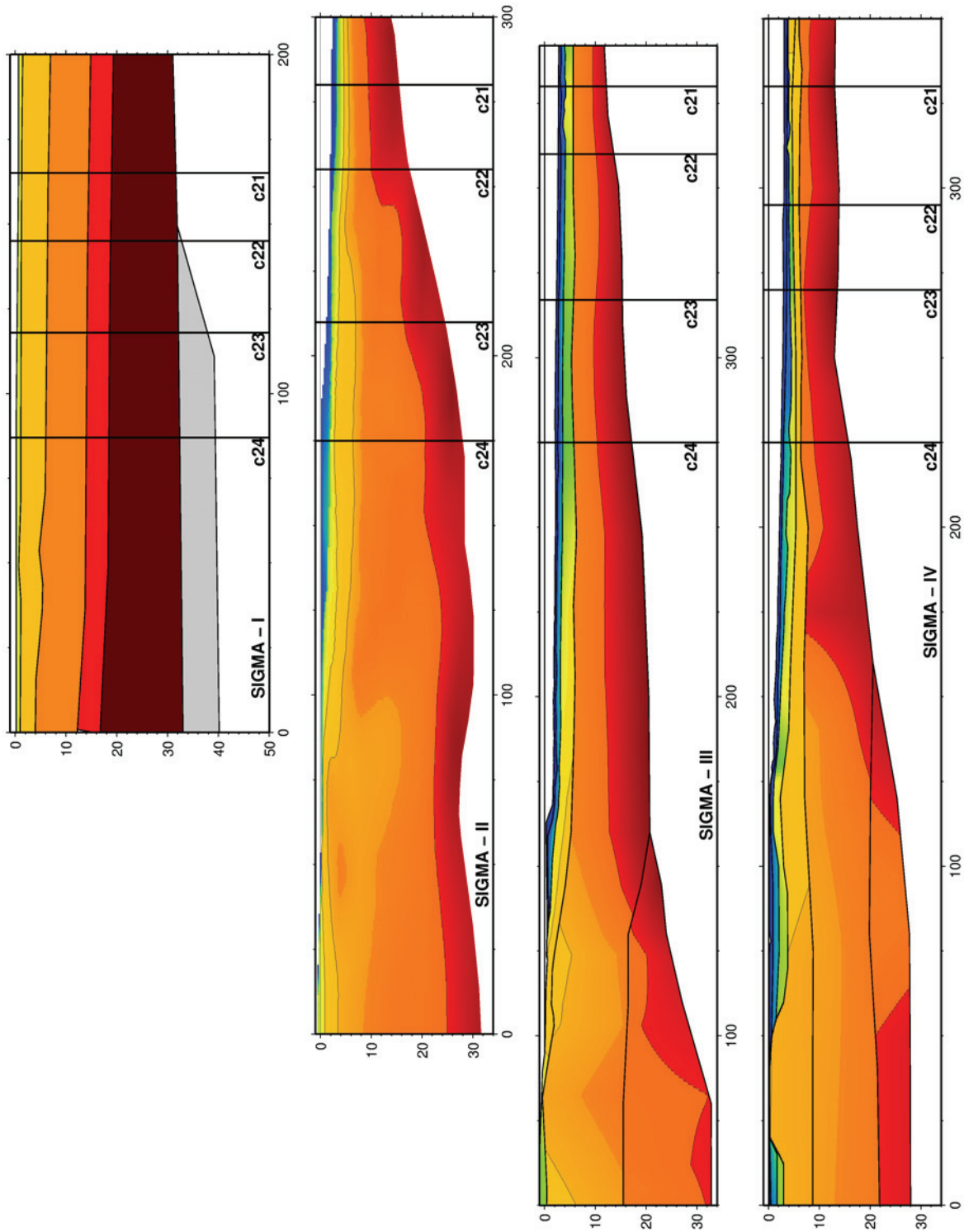


Figure 8.4 Southeast Greenland profiles SIGMA I – IV after (Korenaga et al. 2000; Holbrook et al. 2001; Hopper et al. 2003) shown as reference. Peaks of spreading anomalies are marked by vertical lines and labelled. Note that the red layer marks $>7.0 \text{ km s}^{-1}$. Orange and yellow colours mark crustal layers, green and blue colours sedimentary layers.

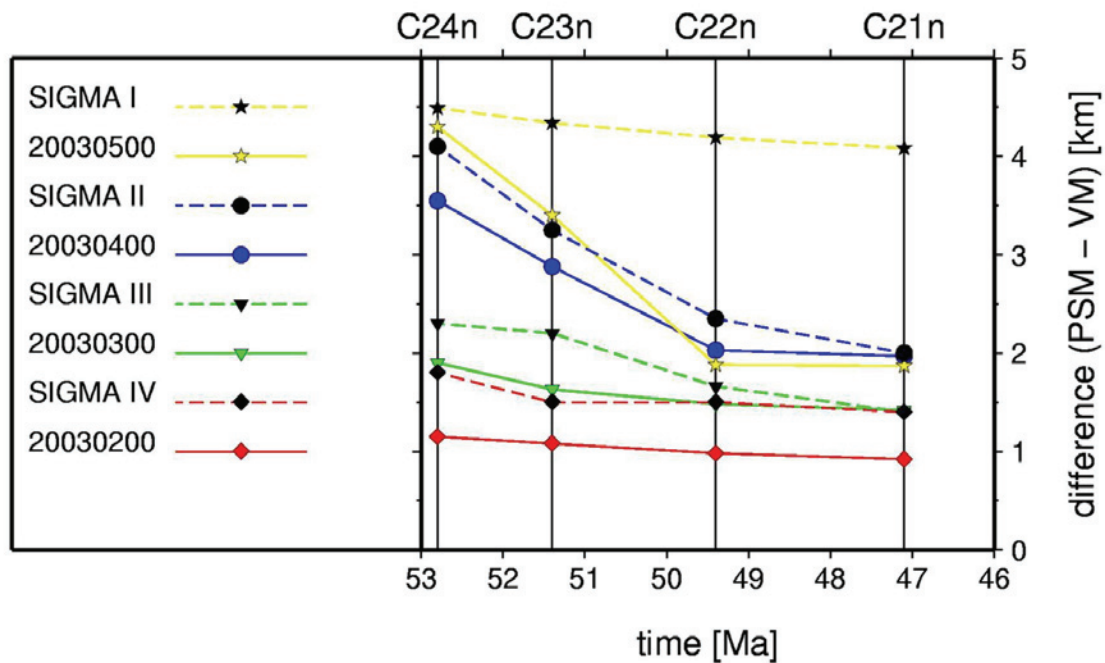


Figure 8.5: Differences between the subsidence model after Parson and Sclater (PSM) and the depth to oceanic basement along eight East Greenland transects with seismic velocity models (VM). See text for details.

But, if the hypothesis of oceanic rather than transitional crust is valid, this model implies a gradual uplift of the oceanic crust, from the younger ocean basin to the initial thicker than normal oceanic crust and also increasing from the distal to the proximal region of the possible Icelandic hotspot track. A similar observation can be outlined from the Møre Margin (Breivik et al. 2006). The depth to basement is identified along the locations of ocean spreading anomalies C10 to C24. The modelled basement depth fits a simple subsidence curve without the load of sediments, as illustrated in Figure 8.6. The difference between predicted and modelled basement increases from 0.5 to 1.7 km towards the COB with corrections for the load of the modelled sediments.

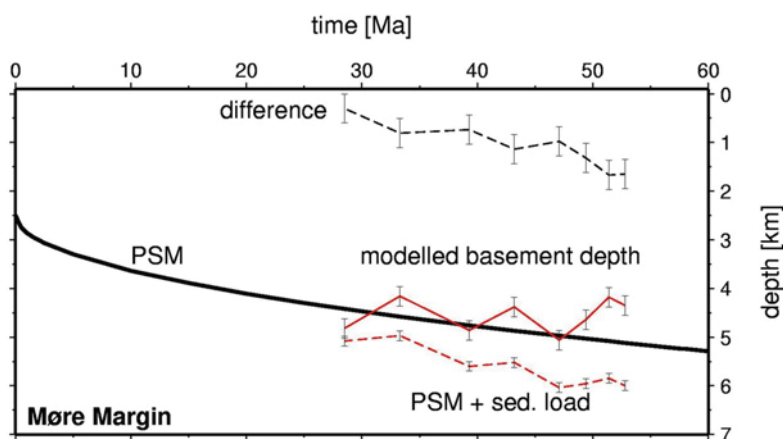


Figure 8.6: Differences between the subsidence model (solid black line) after Parson and Sclater (PSM) and the depth to oceanic basement from a velocity model along a seismic transect of the Møre Margin, Norway (Breivik et al. 2006). The solid red line marks the modelled depth to basement. Error bars result from the uncertainty of depth estimation. The dashed red line is the thermal-tectonic subsidence model (PSM) including the load of the modelled sediments with uncertainties in the thickness estimation. The black dashed line marks the difference between the predicted basement depth and the depth from velocity modelling.

8.3 Continental parts and COT

Thermal-tectonic subsidence is predicted for the continental parts using the McKenzie Model with modifications for the load of sediments, magmatic underplating and magmatic crustal intrusion. For this study, the COT is considered as rifted and stretched continental crust. Figure 8.7 illustrates schematically the validation of subsidence from the hinge zone to the seaward termination of the transition zone. Four possibilities are considered for the two southern profiles AWI-20030400 and AWI-20030500 in order to testify the amount of pure magmatic underplating and/or lower crustal magmatic intrusions of this body:

- a) 100 per cent magmatic underplating of thickness h_{up} and density ρ_{up} .
- b) 66 per cent pure magmatic underplating. 33 per cent of the high velocity layer is related to crustal thickness and is assumed to be intruded crust h_{intl} with density $\rho_{intl} = \rho_{up}$.
- c) 33 per cent pure magmatic underplating and equivalent to b).
- d) 100 per cent intruded lower crust with thickness $h_{intl} = h_{up}$ and density $\rho_{intl} = \rho_{up}$.

A conceptual model is established to evaluate the subsidence at discrete locations along the profiles (Figure 8.7). The following calculation routine is applied in order to estimate the subsidence at each selected point of the profiles:

- 1) Structural values are obtained along the modelled profiles (Tables 8.2, 8.3 and 8.5). The stretching factor β is derived from the relationship of the crustal thickness and the thickness of the hinge zone h_{hz} . An average density ρ_{sed} is calculated for the total sedimentary load. The sediment load contains the Cenozoic sedimentary layer and the continental and syn-rift sediments, where also basalts are included.
- 2) Thermal-tectonic subsidence S_{MK} is calculated using equation 8.4b.
- 3) Subsidence S_{Sed} due to the load of sediments is calculated using equation 8.5.
- 4) Uplift U_{up} due to magmatic underplating is calculated with equation 8.6.
- 5) Subsidence S_{intl} due to magmatic intrusions into lower crust rather than magmatic underplating is calculated with equation 8.7 and with the thickness h_{intl} as listed above. Unaffected lower crustal densities are assumed to be 2900 kg m^{-3} .
- 6) Subsidence S_{intu} due to intrusions in the upper crustal layer is calculated also with equation 8.7. Here unaffected upper crustal density is assumed to be $2700 - 2900 \text{ kg m}^{-3}$. Details are described for each subsidence model for the profiles.

The predicted depth to basement $D_{predict}$ at each location is the sum of the total subsidence and uplift (tables 8.2, 8.3 and 8.5) and the present day water depth h_w

$$D_{predict} = S_{MK} + S_{Sed} - U_{up} + S_{intl} + S_{intu} + h_w \quad (\text{Eq. 8.10})$$

Simplifications are necessary for this first-order prediction of the depth to the continental basement. 1D-predictions along profiles AWI-20030300 and 400 are performed in discrete steps between km 30 and km 210 for every 30 km, and up to km 270 for profile AWI-20030500, respectively. The thicknesses of the hinge zone is obtained from transects onshore (Schlindwein 1998; Schlindwein and Jokat 1999), which provide reasonable values of the unaffected crust. Isostasy of the rift system is assumed for the entire rift duration. Lithospheric flexure and lateral heatflows are neglected. Magmatic intrusions are considered as homogeneously distributed within the crustal layers. Erosion is not considered due to the unknown amount of replaced material. A comparison with onshore observations of rift related passive margin uplift and the ocean basin uplift provides constraints for the simplifications.

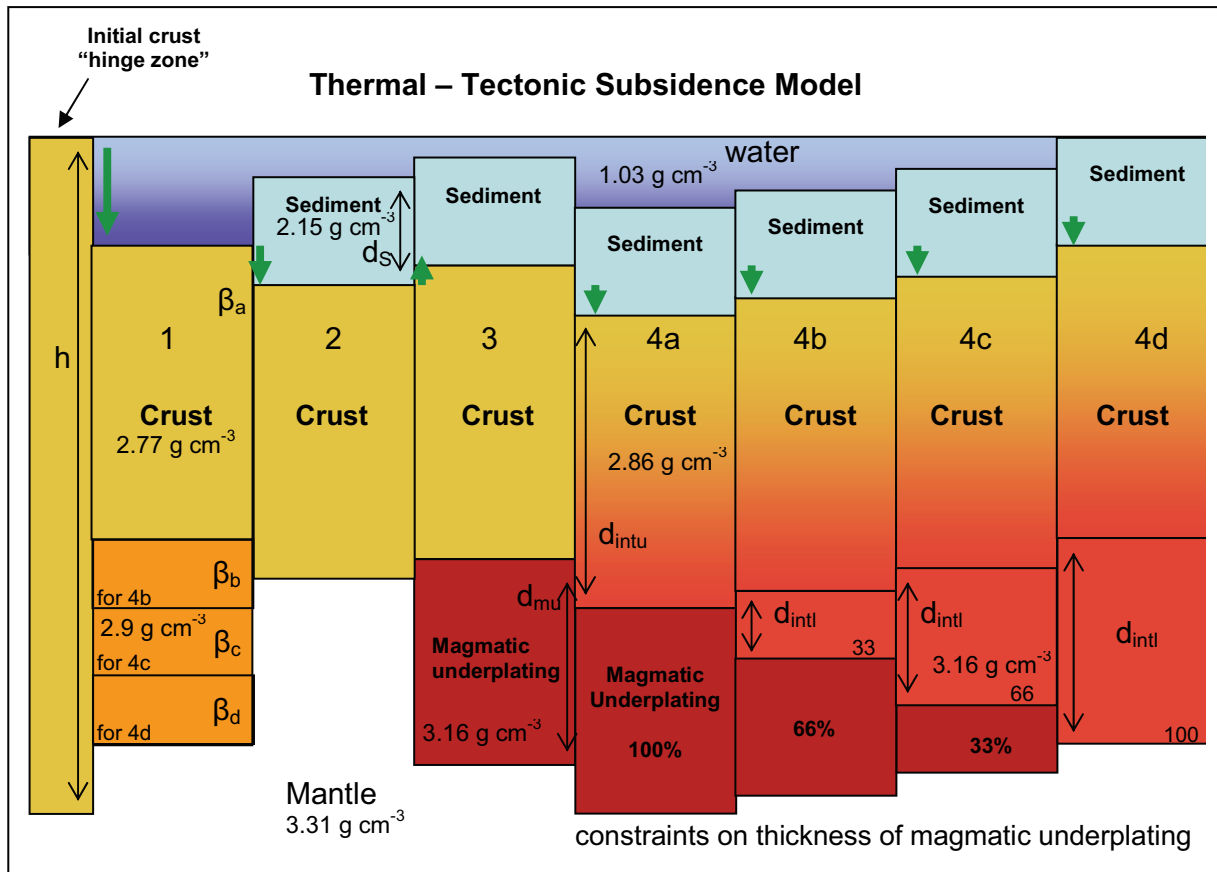


Figure 8.7: Thermal-tectonic subsidence model construction scheme. See text for detailed description. Stage 1 to 4 illustrate the four different effects of subsidence. Differentiations in a – b refer to different crustal thicknesses due to thicker continental crust (b – d) instead of magmatic underplating (a), and same for stretching factors β . If the rifted crust is thicker, the thermal tectonic subsidence is lower, and less thickness is used for magmatic underplating, and therefore for less uplift. Initial crust at hinge zone h is unaffected from any rifting. Crust of normal density (2.77 g cm^{-3}) is yellow; original lower crust of higher density (2.9 g cm^{-3}) is orange; sediments of density 2.15 g cm^{-3} and thickness d_s are light blue; magmatic underplating of density of 3.16 g cm^{-3} is dark red; crustal intrusions revealing subsidence are shown in red to yellow fading colours (stage 4a – 4d). Thickness of intruded upper crust d_{intu} is equivalent to case a) in stage 1. Thickness d_{intl} is either 1/3, 2/3 or the full thickness of the proposed magmatic underplating and having the density of it. Mantle density is taken to be 3.31 g cm^{-3} . Not that the density in g cm^{-3} is equivalent to 10^3 kg m^{-3} .

8.3.1 Predicted depth to basement of profile AWI-20030300

The thickness at the hinge zone is set to 30 km and the horst-structure beneath Shannon Island is considered as a simplified basement high. Initial crustal density $\rho_{c \text{ ini}}$ is assumed to be 2900 kg m^{-3} which allows a small amount of subsidence due to volcanic intrusions along the horst structure (Figure 6.7). The density (3030 kg m^{-3}) of the high velocity lower crust (ρ_{intl}), compared to the two southern profiles (3160 kg m^{-3}), and the missing top reflector (Figure 6.7) let assume, that totally intruded lower crust is rather the case than magmatic underplating. Up to 0.3 km subsidence occurred by the increase of density from 2900 to 3030 kg m^{-3} . The predicted basement depth D_{predict} (Table 8.2) differs gradually from zero up to 2.9 km from the basement depth of the seismic modelling (D_{model}). A leading factor of 5.73 for the thermal-tectonic subsidence S_{MK} (Eq. 8.4b) yields from the assumed initial crustal density $\rho_{c \text{ ini}}$ of 2900 kg m^{-3} and the modelled mantle density of 3310 kg m^{-3} as ρ_{c0} and ρ_{m0} in equation 8.4a, respectively. This still reveals a difference ΔD of more than 1.5 km at the COB (km 210). This comparison shows that the given thicknesses of the crust and densities reveal either weakly resolved parameters of sediment basin and/or under-estimated crustal thicknesses, or a

present state of gradual uplift from the hinge zone to the COB. Further discussions follow in combination with the two southern profiles.

P _{km}	h _w	h _{Sed}	h _c	h _{intl}	ρ _c	ρ _{c ini}	ρ _{intl}	ρ _{Sed-av}	S _{Sed}	β	S _{MK}	S _{intl}	S _{intu}	D _{predict}	D _{model}	ΔD
30	0.3	7.8	21.2	0	2.85	2.85	3.03	2.70	5.71	1.42	2.30	0.00	0.00	8.31	8.17	0.14
60	0.4	3.9	24.9	0	2.92	2.9	3.03	2.67	2.81	1.20	1.33	0.00	0.22	4.76	4.27	0.49
90	0.3	13.8	14.7	0	2.92	2.9	3.03	2.68	10.01	2.04	3.99	0.00	0.13	14.43	14.1	0.33
120	0.4	10.4	14.5	0	2.9	2.9	3.03	2.68	7.52	2.07	4.05	0.00	0.00	11.97	10.8	1.17
150	0.3	12.2	10.4	0	2.9	2.9	3.03	2.64	8.62	2.88	5.12	0.00	0.00	14.04	12.6	1.44
180	0.3	9.9	10.3	1.9	2.9	2.9	3.03	2.58	6.74	2.91	5.14	0.11	0.00	12.29	10.2	2.09
210	0.7	5.7	11.6	5.8	2.9	2.9	3.03	2.42	3.48	2.59	4.80	0.33	0.00	9.31	6.4	2.91

Table 8.2: Parameter of the subsidence calculations of profile AWI-20030300. Parameters are P_{km}, discrete profile locations [km]; h_w, present day water depth [km]; h_{Sed}, total thickness of sediments [km]; h_c, crustal thickness without LCB [km]; h_{intl}, thickness of intruded crustal layer [km]; ρ_c, mean crustal density [103 kg m⁻³]; ρ_{c ini}, initial crustal density [103 kg m⁻³]; ρ_{intl}, density of high velocity lower crust [103 kg m⁻³]; ρ_{Sed-av}, average density of sediments [103 kg m⁻³]; S_{Sed}, subsidence due to sediment load [km]; β, stretching factor; S_{MK}, thermal-tectonic subsidence [km]; S_{intl}, subsidence due to lower crustal volcanic intrusions [km]; S_{intu}, subsidence due to upper crustal volcanic intrusions [km]; D_{predict}, predicted depth to basement [km]; D_{model}, depth to basement from velocity modelling [km]; ΔD, difference between predicted and modelled basement depth [km].

8.3.2 Predicted depth to basement of profile AWI-20030400

A prediction of the basement depth can be performed equivalently along profile AWI-20030400. The crustal thickness at the hinge zone is set to 30 km, but the HVLC is considered in a first case as entirely magmatic underplated material. Initial crustal densities (ρ_{cini}) are set to between 2770 and 2800 kg m⁻³ (Table 8.3), which accounts for crustal intrusions within the transition zone. The transitional crust is thinned with a stretching factor up to 5.5 to a thickness of less than 5.5 km, which results in a large thermal-tectonic subsidence. On the other hand, magmatic underplating does not exceed 1 km of uplift at its thickest location (Table 8.3, km 120). The difference between modelled and predicted depth to basement increases from more than 0.3 km at km 30 to 4.2 km at the COB. The difference ΔD is still up to more than 3.5 km near the COB if crustal and mantle densities of 2800 and 3310 kg m⁻³ are used for the leading factor of S_{MK}, which yields 7.13.

P _{km}	h _w	h _{Sed}	h _c	h _{up}	ρ _c	ρ _{c-ini}	ρ _{up}	ρ _{Sed-av}	S _{Sed}	β	S _{MK}	U _{up}	S _{intu}	D _{predict}	D _{model}	ΔD
30	0.3	4.5	23	1.2	2.77	2.77	3.16	2.63	3.2	1.3	1.8	0.1	0	5.21	4.9	0.3
60	0.3	4.6	17	7.3	2.78	2.78	3.16	2.63	3.2	1.8	3.4	0.5	0	6.4	4.9	1.5
90	0.1	3.3	14.6	11.9	2.8	2.8	3.16	2.63	2.3	2.1	4.0	0.8	0	5.7	3.4	2.3
120	0.2	6.7	9.5	14.8	2.86	2.8	3.16	2.47	4.2	3.2	5.4	1.0	0.3	9.1	6.9	2.2
150	0.3	7.0	8.1	13.9	2.86	2.8	3.16	2.47	4.4	3.7	5.7	0.9	0.2	8.8	7.3	1.5
180	0.3	6.9	7.7	8.5	2.86	2.8	3.16	2.46	4.3	3.9	5.8	0.6	0.2	10.1	7.2	2.9
210	1.2	5.1	6.6	5.2	2.86	2.8	3.16	2.47	3.2	4.6	6.1	0.3	0.2	10.4	6.3	4.1

Table 8.3: Parameters for subsidence model for profile AWI-20030400. Parameters defined as in Table 8.2. Note that the high velocity lower crust is considered as magmatic underplating (h_{up} and ρ_{up}) and causes uplift U_{up}.

Assuming lower crustal magmatic intrusions rather than massive magmatic underplating, initial lower crustal density is expected to be increased from 2900 kg m⁻³ to 3160 kg m⁻³. The stretched crustal thickness is larger by the value of h_{up}, which reveals smaller stretching factors, and little thermal-tectonic subsidence S_{MK}. Subsidence S_{intl} occurs instead due to the lower crustal intrusions (Table 8.4). However, the predicted depth is up to 1.2 km shallower compared to the previous model considering uplift due to magmatic underplating (Tables 8.3 and 8.4; km 90). The influence of thermal-tectonic subsidence is stronger than the difference

between underplating and volcanic intrusions. Intermediate thicknesses of magmatic underplating (66% and 33% of h_{up}) are also determined and listed in Table 8.4.

P_{km}	D_{model}	D_{up}	$D_{66\%}$	$D_{33\%}$	$D_{0\%}$
30	4.89	5.21	5.17	5.14	5.11
60	4.87	6.44	6.24	6.05	5.85
90	3.48	5.92	5.33	5.01	4.69
120	6.97	8.39	8.66	8.26	7.86
150	7.23	8.62	9.35	8.97	8.59
180	7.30	9.52	9.87	9.64	9.41
210	6.34	10.56	10.22	10.08	9.94

Table 8.4: Depth to basement of profile AWI-20030400 for four different case of the amount of magmatic underplating. D_{model} shows depth from velocity model; D_{up} of total magmatic underplating (Table 8.3), $D_{66\%}$ of 66% underplating and crustal thickness of $h_c + 1/3 h_{up}$; $D_{33\%}$ of 33% magmatic underplating and $D_{0\%}$ of no magmatic underplating and a crustal thickness of $h_c + h_{up}$.

8.3.3 Predicted depth to basement of profile AWI-20030500

The crustal thickness at the hinge zone is assumed to be 33 km (Schlindwein and Jokat 1999) for profile AWI-20030500 and the high velocity lower crustal body as pure magmatic underplating (Table 8.5). The crustal density is assumed to be between 2800 – 2850 kg m⁻³ before magmatic intrusion took place.

The underplated magmatic body reveals uplift of less than 1 km and the predicted basement depth is up to 3.5 km deeper than derived from the velocity model (Table 8.5). The maximum of the difference ΔD reduces to less than 3 km at the COB, for a leading factor of 7.13 in the equation 8.4a of the thermal-tectonic subsidence. A similar approach by lower crustal intrusions rather than pure magmatic underplating reveals a up to 0.8 km shallower basement depth in the regions of the lower crustal body (Tables 8.5 and 8.6; km 150-180).

P_{km}	h_w	h_{Sed}	h_c	h_{up}	ρ_c	ρ_{c-ini}	ρ_{up}	ρ_{Sed-av}	S_{Sed}	β	S_{MK}	U_{up}	S_{intu}	$D_{predict}$	D_{model}	ΔD
30	0.5	4.6	27.8	0.0	2.85	2.85	3.16	2.63	3.2	1.2	1.3	0.0	0	5.0	5.0	0.0
60	0.4	5.9	15.5	9.6	2.8	2.8	3.16	2.63	4.1	2.1	4.2	0.6	0	7.5	6.4	1.1
90	0.4	6.8	11.1	8.2	2.8	2.8	3.16	2.58	4.6	3.0	5.2	0.5	0	9.2	7.2	2.0
120	0.1	6.2	9.3	10.4	2.86	2.8	3.16	2.52	4.1	3.6	5.6	0.7	0.4	8.9	6.3	2.6
150	0.2	5.6	9.1	13	2.86	2.8	3.16	2.49	3.6	3.6	5.7	0.9	0.4	8.5	5.8	2.7
180	0.2	6.5	7.9	13.5	2.86	2.8	3.16	2.55	4.3	4.2	6.0	0.9	0.3	9.4	6.7	2.7
210	0.3	5.6	11.3	9	2.86	2.8	3.16	2.42	3.4	2.9	5.2	0.6	0.5	8.4	5.9	2.5
240	0.4	5.6	11.1	5.2	2.86	2.8	3.16	2.37	3.3	3.0	5.2	0.3	0.4	8.8	6.0	2.8
270	0.3	5.7	7.2	0	2.86	2.8	3.16	2.15	2.8	4.6	6.1	0	0.3	9.5	6	3.50

Table 8.5: Parameters for subsidence modelling of profile AWI-20030500. See Table 8.2 for details.

8.3.4 Interpretation and Discussion

A uniform McKenzie-type subsidence model has shown large differences between the crustal depth based on velocity modelling and the predicted transitional crustal depth for the three margin spanning crustal models AWI-20030300, -400 and -500. All three models have shown consistently a shallower basement depth than predicted from the landward to the seaward boundary of the transition zones. The large discrepancy is could be related to errors of the simplifications of the subsidence model. The top basement of the profiles AWI-20030300, -400 and -500 is constrained by the change of the vertical velocity gradient and verified by density modelling. Therefore, an error of hundreds of metres is possible but would not correct for the differing basement depths. The ray-tracing technique does not resolve small scale horizontal variations, as can be assumed from horst and graben structures. Thus, the crustal

thickness and top basement are averaged over the real basement topography, which remains unknown in its details.

P_{km}	D_{model}	D_{up}	$D_{66\%}$	$D_{33\%}$	$D_{0\%}$
30	5.0	5.0	5.0	5.0	5.0
60	6.4	8.1	7.9	7.7	7.5
90	7.2	9.7	9.5	9.4	9.2
120	6.3	9.5	9.3	9.1	8.9
150	5.8	9.0	8.7	8.5	8.2
180	6.7	9.9	9.7	9.4	9.1
210	5.9	8.7	8.6	8.4	8.2
240	6.0	9.0	8.9	8.8	8.7
270	6	9.5	9.5	9.5	9.5

Table 8.6: Depth to basement for different crustal thicknesses for profile AWI-20030500.

The subsidence models are simplified by neglecting erosion of uplifted material above sea level and differences in ancient sea water levels. The predicted basement depths are evaluated by assuming the sequence of events happened all at or beneath the present day sea-level. But basin filling during rifting might have occurred subaerally and in a marine setting, which might have a large influence for these considerations. Erosion of the basin material would cause crustal uplift due to isostatic rebound. Thus, an error in the estimate of basin depth prior to erosion could be responsible for differences of the modelled and predicted basement depths.

Lithospheric changes, e.g. a lower mantle density due to a lithospheric thermal anomaly, have an affect of uplift of the margin. The subsidence analysis demonstrates clearly a stronger influence of thermal-tectonic subsidence, i.e. crustal thickness and lower stretching, than the difference between uplift by underplating and subsidence by lower crustal intrusions. A close fit of both, modelled and predicted basement depth, implies increasing lithospheric uplift from the continental part towards the seaward boundary of the transitional zone (COB). The maximum uplift is derived from the Parson and Sclater model for the oceanic parts. An increasing difference towards the COB of 1.4 – 1.9 km is shown between the predicted and the modelled oceanic basement depth of profile AWI-20030300 (Figure 8.3). An uplift of 1.5 - 2.9 km at the COB can be assumed from the McKenzie model, depending on the crustal and mantle densities used in equation 8.4a (Figure 8.8).

An equivalent range of lithospheric uplift is inferred for profile AWI-20030400. The thermal-tectonic models reveal differences of 3.7 to 4.2 km which fit, in a certain range, the differences at the COB (~ 3 km) derived from the Parson and Sclater model of the oceanic section (Figure 8.3). Without assuming lithospheric uplift, magmatic underplating seems to cause larger deviations from the velocity model. At least up to 33 per cent of magmatic underplating reveals a better approximation if a gradual uplift of 0.3 to 3 km is assumed from the hinge zone towards the COB (Table 8.7, Figure 8.9). This model contrasts previous interpretations (Figure 5.11) of the high velocity lower crust as pure magmatic underplating but predicts a large scale lower crustal intrusion combined with minor crustal stretching but lithospheric uplift. A minor portion of magmatic underplating can explain the depth of the Moho of about 31.3 km, while the hinge zone is assumed to be 30 km. This model does not contradict the interpretation of long-term magmatism, which intruded the rifted crustal region. The intrusions might be responsible for the magnetic anomalies within the transition zone (Figure 8.9). The top reflector of the high velocity lower crust could therefore be inferred as the difference of larger to lower amount of intrusions within the crustal section. However, a boundary between the intruded lower crust and magmatic underplated body is not resolved

from seismic data. This could be explained by a more gradual transition between the two lithologies due to the vertical increasing amount of intrusions.

The Parson and Sclater model reveals a difference of approximately 2 – 3 km between C22 and C23 for profile AWI-20030500 (Figure 8.5). The McKenzie model shows a difference of 2.4 – 3.5 km in this section, depending on either lower crustal intrusions or magmatic underplating. Table 8.8 and Figure 8.10 illustrate a model of lithospheric uplift and constraints on magmatic underplating for this profile. A steep increase of uplift from km 30 to km 120 is assumed which remains stable until km 270. Intruded lower crust is suggested for the majority of the high velocity lower crustal layer. A small amount of magmatic underplating accounts for the thickening of the transitional crust between km 120 and 210.

p_{km}	$U_{lithospheric}$	h_{up}	Ratio [%]	$D_{predict}$	D_{model}	ΔD
30	0.30	0.00	0	4.8	4.8	0.0
60	1.00	0.00	0	4.9	4.9	0.0
90	1.50	4.00	33	3.5	3.4	0.1
120	1.50	4.90	33	6.7	6.9	-0.2
150	1.50	4.60	33	7.5	7.3	0.2
180	2.00	0.00	0	7.4	7.2	0.2
210	3.00	0.00	0	6.9	6.3	0.6

Table 8.7: Transient lithospheric uplift $U_{lithospheric}$ for profile AWI-20030400. The proportional thickness of magmatic underplating h_{up} (and its ratio from the total thickness of high velocity lower crustal body) reveals closest fit to basement depth of the velocity model (Figure 8.12).

p_{km}	$U_{lithospheric}$	h_{up}	Ratio [%]	$D_{predict}$	D_{model}	ΔD
30	0.00	0.00	0	5.0	5.0	0.0
60	-1.00	0.00	0	6.5	6.4	0.1
90	-2.00	0.00	0	7.2	7.2	0.0
120	-2.50	0.00	0	6.4	6.3	0.1
150	-2.60	4.30	33	5.9	5.8	0.1
180	-2.70	4.50	33	6.7	6.7	0.0
210	-2.50	3.00	33	5.9	5.9	0.0
240	-2.00	1.60	0	6.7	6.0	0.7
270	-2.00	-	-	7.5	6	1.5

Table 8.8: Transient lithospheric uplift for profile AWI-20030500 and constraints on magmatic underplating.

8.4 Conclusion of the subsidence analysis

The subsidence analysis provides important constraints on the nature of the high velocity lower crust and the subsidence and uplift history of the northeast Greenland margin. Transient lithospheric uplift, from the COB land- and seawards, and intruded lower transitional crust and minor magmatic underplating, rather than pure magmatic underplating, seems a simplified but reasonable interpretation of this part of the margin. Tertiary uplift was proposed to explain flood basalts at 2 km above the present day sea-level (e.g. Larsen 1990) onshore of the East Greenland margin. Such an uplift event can be followed by erosion and additional isostatic rebound, preserving the rifted crust at shallower depths. Even if the presented models do not account for such a sequence of erosional uplift, they support the hypothesis of an uplift history. Uplift implies the erosion of deposited flood basalts which would consequently mean that the proposed production rates could be higher than previously proposed (Table 7.1). Therefore, I conclude that the continent – ocean transition zone off the northeast Greenland margin consist of either a voluminous magmatic underplating, or at least

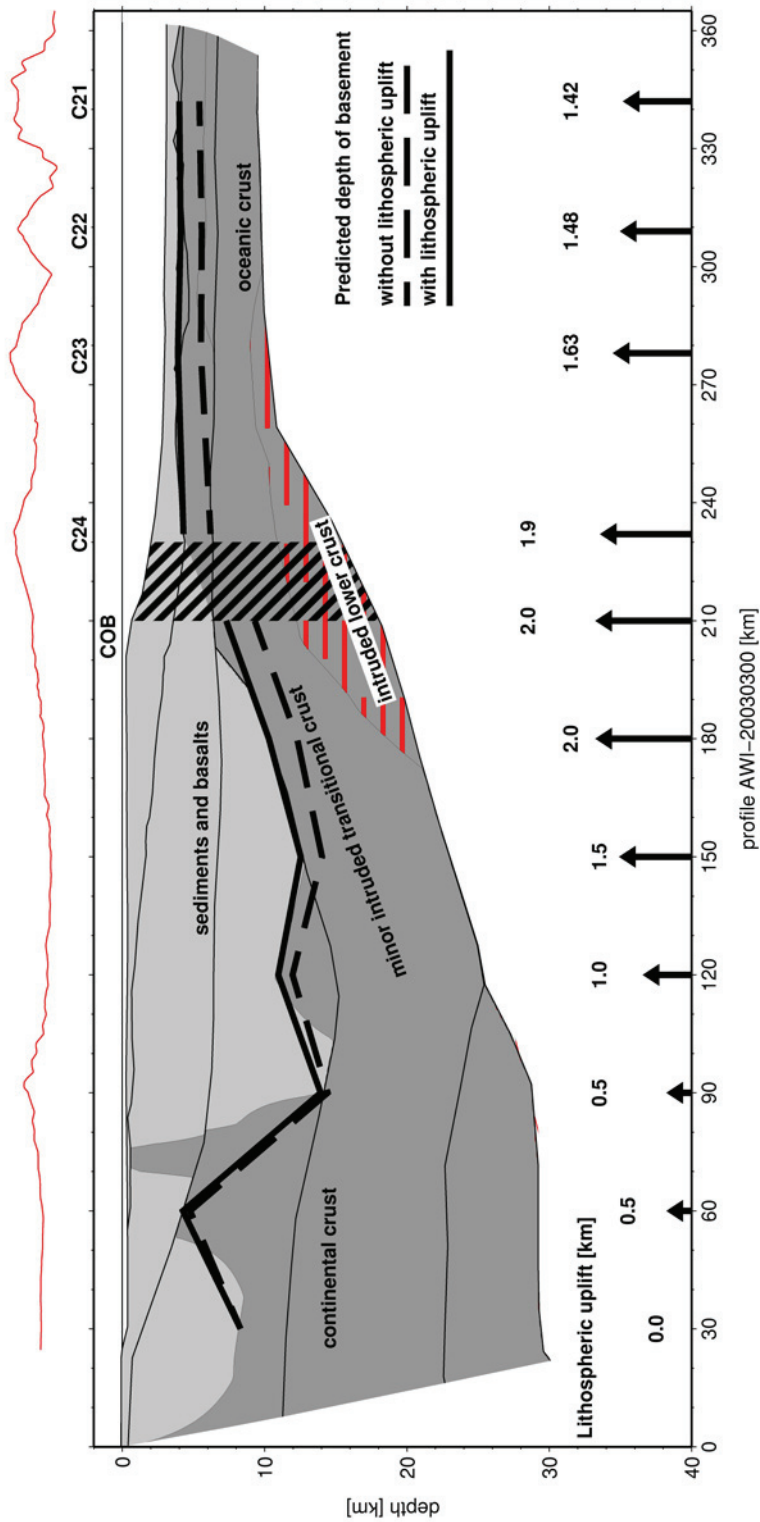


Figure 8.8: Lithospheric uplift of profile AWI-20030300 from the hinge zone to COB and oceanic basin. Light grey layers mark syn- and postrift sediments. Crustal layers are coloured in dark grey. Red stripes indicate lower crustal intrusions. Thick dashed line marks predicted basement depths of continental and oceanic crust from subsidence models. Thick solid line shows same but lithospheric uplift included. Amount of lithospheric uplift is shown as arrows and labelled. COB marks the seaward boundary of the continent – ocean transitional zone. Top: Magnetic line data and spreading anomalies.

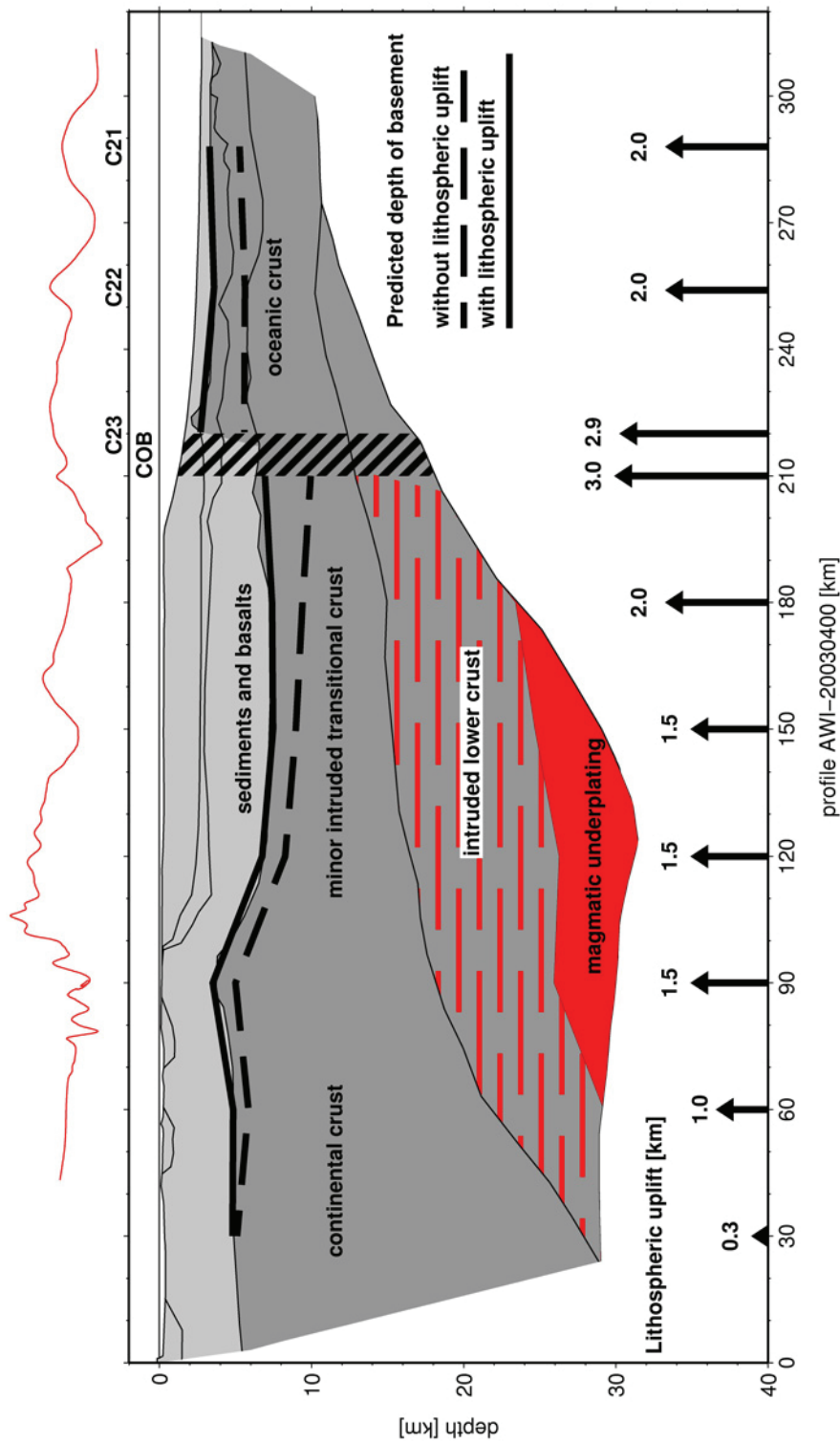


Figure 8.9: Lithospheric uplift of profile AWI-20030400 from the hinge zone to COB and oceanic basin. Light grey layers mark syn- and postrift sediments. Crustal layers are coloured in dark grey. Red stripes indicate lower crustal intrusions. Solid red region is constraint magmatic underplating based on subsidence analysis. Thick dashed lines mark predicted basement depths of continental and oceanic crust from subsidence models. Thick solid lines show same but lithospheric uplift included. Amount of lithospheric uplift shown as arrows and labelled. COB marks the seaward boundary of the continent – ocean transitional zone. Top: Magnetic line data and spreading anomalies.

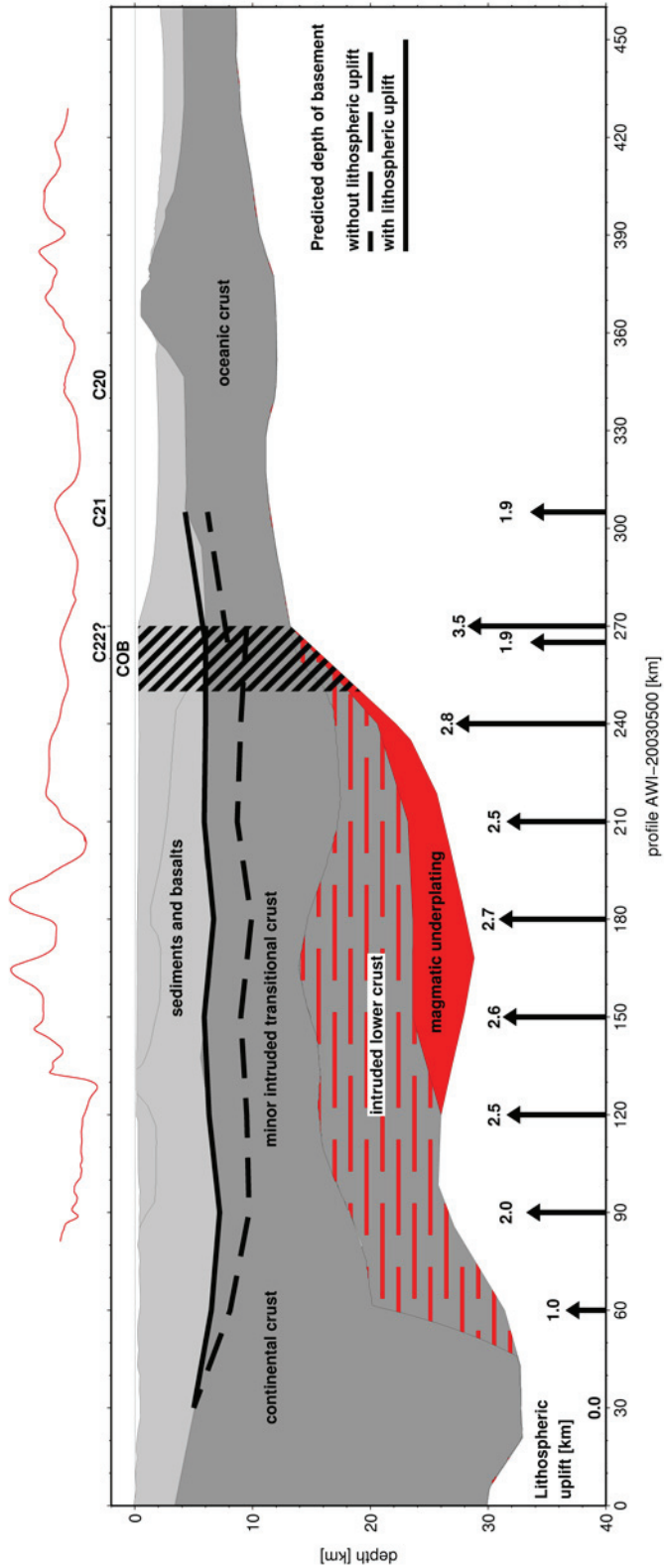


Figure 8.10: Lithospheric uplift of profile AWI-20030500 from the hinge zone to COB and oceanic basin. Light grey layers mark syn- and postrift sediments. Crustal layers are coloured in dark grey. Red stripes indicate lower crustal intrusions. Solid red region is constraint magmatic underplating based on subsidence analysis. Thick dashed lines mark predicted basement depths of continental and oceanic crust from subsidence models. Thick solid lines show same but lithospheric uplift included. Amount of lithospheric uplift shown as arrows and labelled. COB marks the seaward boundary of the continent – ocean transitional zone. Top: Magnetic line data and spreading anomalies.

of highly intruded lower crust and a minor proportion of additional magmatic underplating. It is likely, that lithospheric uplift initiated large scale erosion of sedimentary and basaltic strata, which has to be linked to a thermal anomaly lowering the mantle density.

Regional studies have considered lithospheric uplift due to the a thermal anomaly ($\Delta T \sim 100^\circ\text{C}$) in the vicinity of the plume head (Figure 8.11) at the time of break-up (Skogseid et al. 2000). An uplift of up to 1 km is illustrated, for the location of the plume at the time of break-up, extending up to the margin off Shannon Island in the north and also the very southern region of the location of the SIGMA IV profile.

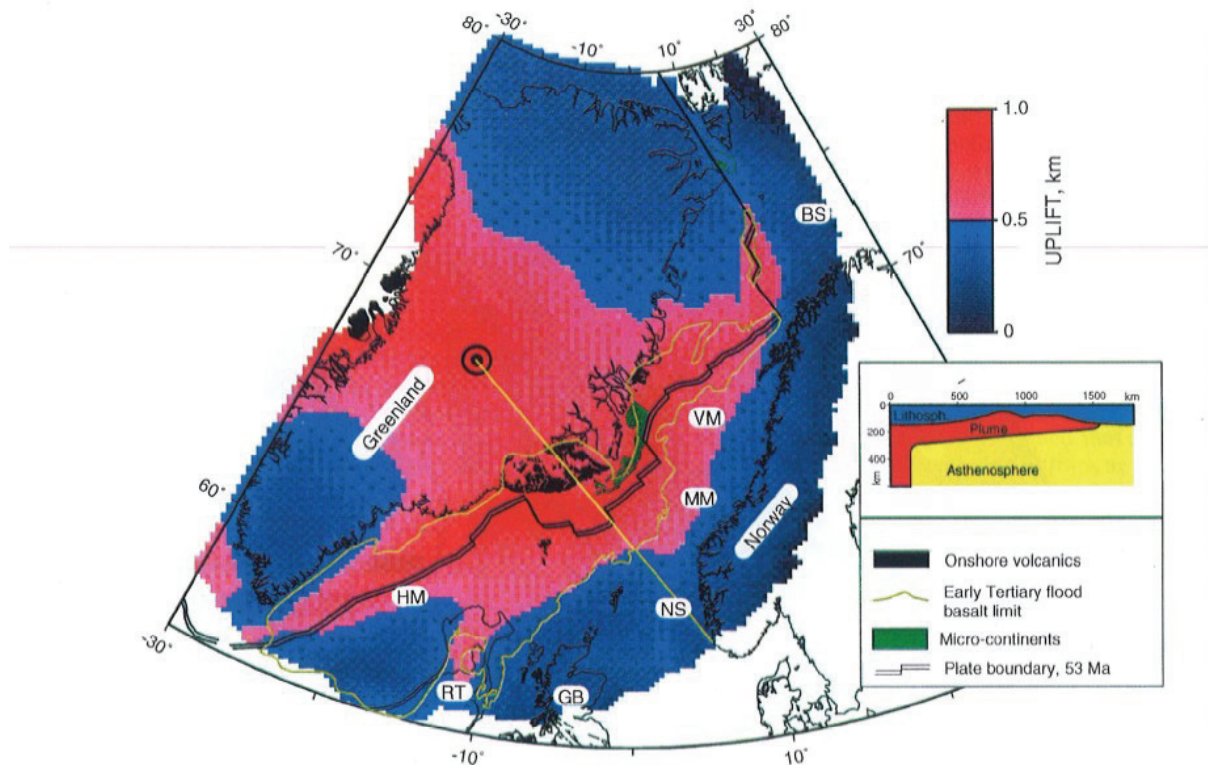


Figure 8.11: Theoretical lithospheric uplift related to an average temperature anomaly of 100°C in a plume head where the thickness distribution is a function of both the distance from the plume centre and the relief at the base of the overlying lithosphere (inset frame located along yellow line on map) (from Skogseid et al. 2000).

The lithospheric uplift due to the existence of a plume head beneath Greenland might have caused uplift upon sea-level and enabled subaerial erosion of upper material. Elongated uplift along the rift axis is suggested while inversion occurred in regions with thin lithosphere (Skogseid et al. 2000). These authors assume also a correlation of uplift and the subaerially emplaced flood basalt provinces in Greenland.

The presented subsidence analysis correlates with this model in terms of uplift during rifting and break-up and erosion of upper material. The elongated uplift around 53 Ma might have ceased and revealed the shallower basement as seen along the transects (Figures 5.8 – 5.10). If the observed uplift of the northeast Greenland margin is a relict of this event due to the erosion of material and/or the location of the present day Iceland hotspot or other thermal anomalies remains unresolved.

Reston and Morgan (2004) provide an explanation for the uplift break-up unconformity found on many margins (e.g. Braun and Beaumont 1989; Embry and Dixon 1990). The influx of hot asthenosphere from the global ridge system is assumed to initiate not only melting and the formation of oceanic crust but also cause simultaneous transient thermal uplift of the margin.

The hot material is replaced by the cooler mantle at the transition to seafloor spreading. Accelerated subsidence confused with a pulse of extension should mark such margins.

Neogene to Quaternary uplift of the European margins as an additional episode beside the Cenozoic/Paleocene uplift and the emplacement of lower crustal magma is considered by Japsen and Chalmers (2000). It postdates the North Atlantic break-up, which is conform with observations of uplift well after the main phase of Paleogene igneous activity (Chalmers 2000; Japsen and Chalmers 2000). It predates the onset of glaciation, which is an additional important cause of uplift (e.g. Rohrman and von der Beek 1996). It explains contrarily to the plume hypothesis accelerated subsidence of some basin centres of the European margins.

Similarities between the subsidence analysis and the uplifted regions near the continent ocean boundaries correlate with the regional studies of uplift and subsidence around the North Atlantic margin. There is no lack of explanations for uplift, subsidence and correlations between tectonic and magmatic episodes but controversies leave detailed inferences open. However, a break-up unconformity along the north-east Greenland margin is inferred from a simplified approach and forward model and correlates with the involved magmatism along the margin.

9 Conclusion and Outlook

This chapter summarizes the conclusions of the three publications incorporating the calculations of the subsidence and uplift history along the seismic profiles. A brief guideline for further research work is provided to address unresolved problems and investigations of new targets.

9.1 Conclusion

This study based on geophysical data acquired offshore northeast Greenland between the Jan Mayen Fracture Zone (70° N) and the Greenland Fracture Zone (77° N). The new data-set consists of four seismic refraction profiles containing 126 recording units, ship-borne gravity data along the transects and a high resolution helicopter-borne magnetic grid covering also the region of the two southern seismic lines off the Kejser Franz Joseph Fjord and Godthåb Gulf. A powerful tool for crustal architecture modelling is the integration of different geophysical methods and their combined interpretation with conjugate and adjacent margin models. Results of the northeast Greenland and Norwegian conjugate margins brought face to face and the adjacent margins of East Greenland were compared in order to quantify and qualify the variations and asymmetries of the North Atlantic margins. The major conclusions about the previously weakly imaged crustal architecture of the northeast Greenland continent – ocean transition zone provide important constraints for the tectonic and magmatic formation processes of the North Atlantic volcanic rifted margins.

The outlined objectives of this study, which are listed in the introduction, are addressed with the results of this study in three main categories; the crustal architecture of the continent – ocean transition zone, constraints for magmatic underplating, and the comparison of conjugate and adjacent margins.

9.1.1 Crustal architecture of the continent - ocean transition zone

The northeast Greenland margin shows a clear segmentation between the Greenland and Jan Mayen Fracture zones based on models of the crustal architecture from the continental to the oceanic basins. A fundamental observation of this study is a high velocity lower crustal body (HVLC), associated with seismic P-wave velocities in the range between 7.0 and 7.4 km s⁻¹, which extends for over ~200 km off the Kejser Franz Joseph Fjord and Godthåb Gulf to the onset of oceanic crust. The maximum thickness of this body is determined to up to 16 km, and a density of ~3.16 x 10³ kg m⁻³ is obtained from 2D gravity modelling. Strong reflections mark clearly the top and bottom (Moho) of this lower crustal body. A 120 – 130 km wide continent – ocean transition zone (COT) is proposed between the landward shallow basement highs correlating with crustal lateral velocity increases, and the first magnetic ocean spreading anomalies. The entire transitional crust exhibits of increased seismic velocities, which are associated with the presence of syn-rift magmatic intrusions that are suggested to be responsible for the complex magnetic anomaly pattern within the COT. High resolution magnetic data reveal new details of the complex magnetic pattern off the fjord region. High frequency variations within the large regional negative magnetic anomaly are suggested to have their source in shallow dyke intrusions. Longer wavelength variations are associated with deeper sources within the syn-rift basins and upper crustal layers. The almost unstructured sedimentary basins are proposed to consist of a mixture of syn-rift sediments and basalts, which yields a strong vertical velocity increase, and topped by Cenozoic sediments. A completely different crustal architecture is revealed off Shannon Island, just 100 km to the north, near the Greenland Fracture Zone. Sedimentary basins up to 15 km deep characterize

the margin, and exhibit evidence for a rough horst and graben structure. Increased lower crustal seismic velocities are absent within the transition zone, although the seaward termination gives hints for intrusions that may have been emplaced during break-up. A major finding is a local positive velocity anomaly beneath Shannon Island, and different to the weak basement highs in the south. An interpretation of this anomaly as formed over a major horst structure is favoured because it is associated with gravity data that are consistent with the presence of similar crustal architecture further north. The structure is also thought to have served as a magma conduit inferred from magnetic data and widespread extrusive rocks like those seen in outcrops on Shannon Island.

Based on these observations, excessive magmatism is inferred to have occurred in the region off Keiser Franz Joseph Fjord and The Godthåb Gulf during a long-lasting period of rifting. The part off Shannon Island and near the Greenland Fracture Zone is nevertheless classified as a magma-starved volcanic margin, due to the reduced syn-rift intrusions compared to the region further south.

The location of the continent – ocean boundary (COB) is depicted from the interpretations of the seismic velocity and density models. Therefore, I propose a delay in break-up in the zone north of the Jan Mayen Fracture Zone that was locked as a result of long term extension of the continental crust. Based on the location of the COB and its obliquity with respect to seafloor spreading anomalies, break-up is estimated to occur not earlier than 51.5 ± 0.2 Ma (C23) off Godthåb Gulf, and 50.1 ± 0.3 Ma (C22) off Keiser Franz Joseph Fjord, which is about 3.5 m.y. later than that further north, where break-up is estimated to occur at ~ 54 Ma. Age constraints for the time of break-up are derived from a re-evaluation of half spreading rates for the northeast Greenland margin.

9.1.2 Constraints for magmatic underplating

The dimension of the HVLC is mapped from the Kong Oscar Fjord, south of the Jan Mayen Fracture Zone, to near Shannon Island, and from below the fjords to the onset of oceanic crust. The thickness and extent varies significantly and encloses a maximum thickness of 15 – 16 km and a lateral extent of 190 – 225 km off Keiser Franz Joseph Fjord and Godthåb Gulf. A top crustal reflector is assumed to merge with the Moho in both directions. The possibility of a magmatic underplated body is discussed incorporating a history of multi-phase magmatism beginning at ~ 58 Ma and lasting until break-up at 50 Ma, based on estimates of magma production rates. The volume off Keiser Franz Joseph Fjord and Godthåb Gulf is estimated each to be ~ 2000 km³ for 1 km along-strike. The excess melt generation is for this case associated with a major feeder dyke and accordingly linked to the Iceland plume hypothesis. The strong decrease of this body to the north requires, however, a magmatic barrier between the Godthåb Gulf and Shannon Island. Direct evidences for a transfer zone or crustal-scale detachment fault are missing, but the segmentation along the northeast Greenland margin, as shown above, suggests the existence of such a structure.

In a comprehensive subsidence analysis it is demonstrated, that magmatic underplating does not provide sufficient uplift to the observed depth to basement of the thinned and subsided transitional crust. It seems more likely, that the high velocity lower crust consists of primary intruded pre-existing lower crust and incorporates only minor magmatic underplating. This assumption needs, however, an incorporation of a transient uplift from the COB to the transition zone and the ocean basin. Such a model is proposed in two attempts. Either Early Tertiary magmatism intruded the transitional crust solely, and/or additional magmatic underplating accreted during a second phase in Oligocene/Miocene, which is linked to the separation of the Jan Mayen microcontinent and onset of oceanization along the Kolbeinsey Ridge. Both models are quite similar and suggest that the Early Tertiary magmatism is quantitatively over-estimated. The latter could explain the possible small scale magmatic

underplating, which is inferred from the subsidence analysis, and relates it to the independent magmatic event postdating the Early Tertiary break-up by ~20 million years.

A clear preference for one of these models is not possible in this stage and leaves the question of the source and constitution of the high velocity lower crust off the northeast Greenland open.

9.1.3 Comparisons with the conjugate Norwegian and adjacent southeast Greenland margins

All crustal structural observations and geophysical interpretations of the northeast Greenland margin are compared with models of the southeast Greenland and conjugate Norwegian margin. Contrasting interpretations of the northeast Greenland (AWI-20030400) and the Norwegian Vøring margin reveal significant asymmetries of the crustal architecture. The major differences are a 10 km deeper Moho in the continental unit of the northeast Greenland margin, a wider COT, and a larger high velocity body. A line-to-line comparison with AWI-20030300 and a Lofoten margin reveals small-scale similarities in the structural styles but major asymmetries in large-scale tectonic structures and also interpretational differences, as the width of the COT or the domain of the HVLC (continental vs. oceanic), similar to the other compared marginal transects. In total, the differences in crustal thicknesses, dimensions of the HVLC, Moho depths and location of the COBs account to a clear asymmetric conjugate margin pair.

Regional maps are compiled and demonstrate the crustal variations along the East Greenland margins. The interpretations of the HVLC differ again from magmatic underplating and/or lower crustal intrusions in the north, and accretion of igneous crust in the south, and the distribution of the peak of the high velocity lower crust. The extent and thicknesses of the HVLC is in strong contrast with the thickness of the oceanic crust of both parts of the East Greenland margin. A distribution chart for the HVLC at North Atlantic margins demonstrates inverted emplacement of prominent landward and seaward HVLC thickness portions, which suggests a strong heterogeneity of the source of melts and the formation processes.

9.1.4 First utilization of the results

The US Geological Survey (USGS) is preparing a map of the Arctic region with sedimentary basins and main structural features. The Geological Survey of Denmark and Greenland (GEUS) was able to introduce the results of Voss and Jokat (2007) into the evaluation process concerning about the continent – ocean boundary off northeast Greenland. In early December 2007 I have received the confirmation that “ ... the USGS people will use a COB in the Arctic maps that is fully in accordance with the AWI data in northeast Greenland.”

9.2 Outlook

The vast amount of data used in this study did not allow the application of all possible modelling procedures and problem approaches. The study provides nevertheless important insights into the crustal architecture of the northeast Greenland margin and allows conclusions beside previous suggestions. On the other hand, the data coverage is still far behind of those like the Norwegian margin, which is in particular due to the hydrocarbon exploration purposes in Norway and the Greenland offshore ice conditions. The achievements of this study reveals just as much new questions and possible target areas for further scientific investigations. Several problems remained unanswered, which indeed, will probably only be solved with a deep sea drill hole, as everywhere in the world. The following suggestions should help to approach some of the problems and new questions:

Seismic shear-wave modelling

Most of the ocean bottom receivers and all land stations contained also 3-component seismometers, which recorded arrivals of shear-waves (S-waves), too. Arrivals of the S-waves were not considered yet although almost all OBS show clear S-waves. It has yet not been proved, if they penetrate also the high velocity lower crust. An equivalent velocity modelling and evaluation of the Poisson ration could reveal more constraints on the high velocity lower crust. Schmidt-Aursch and Jokat (2005a) performed an intensive reinterpretation of former profiles and calculated the Poisson ratios for the seismic models, but had not sufficient coverage for the lower crustal layers. The new data-set contains more ocean bottom recordings and might reveal new insights.

Revised 3D gravity modelling

The new crustal models should be implemented in the 3D-gravity modelling of (Schmidt-Aursch and Jokat 2005b) for the northeast Greenland margin. The details of the continent-ocean transition zone might have an influence in long wavelength Bouguer anomalies and would improve the fit of the observations. The different densities of the sub-continental and sub-oceanic mantle could either be approximated from a mantle thermal gradient model after Breivik et al. (1999) and/or variations in thicknesses of the lithosphere.

2D magnetic modelling

Magnetic modelling would need to incorporate observations from other margins as long as no thermal gradient is clear to estimate the depth of the Curie temperature. Additionally, paeleo-magnetic field parameters are needed to determine the orientation of the remanent magnetic field of crustal bodies. Onshore samples of rocks could help, which would also give estimates in susceptibilities and mineral content. Independent depth-to-basement estimates could be compared with the seismic models.

Further geophysical investigations

A proposal for further seismic investigations is shown in Figure 9.1. It should be noted, that the 5 km contour line of the high velocity lower crustal thickness is outlined and marked with triangles pointing to the increasing thickness.

The former profile 94310 (Schlindwein 1998) was planned to provide insights into the region along the large negative magnetic anomaly off the fjord region (Figure 9.1) of the northeast Greenland margin (Jokat et al. 1995). The data quality allowed no satisfying modelling (Schlindwein and Jokat, personal communication). One reason can be deduced from this study, showing many of high frequency magnetic anomalies for the region between Godthåb Gulf and Kejser Franz Joseph Fjord associated with shallow dyke intrusions scattering the seismic signals (Figure 5.3). The onset of the Cenozoic sediment basins seaward of line 94310 might also had an effect on the data quality. A further problem was the very large spacing of the recording units. I suggest to plan on a new seismic line along the central/northeast Greenland margin (P-CNEG), from Jameson Land across line 94340, the landward prolongation of the Jan Mayen Fracture Zone, AWI-20030500 (OBS 523), -400 (OBS 418) and -300 (OBH 319), which could reveal along-strike constraints of the high velocity lower crust and probably the existence of transform faults, separating the region off Shannon Island from the margin off Godthåb Gulf and Kejser Franz Joseph Fjord (Fig. 6.1). Table 6.1 shows key coordinates and the line lengths.

In order to investigate the extent of shallow lava flows, like observed off Shannon Island, I suggest to extent a seismic transect from near OBH 321 to OBH 215 (P-DHB) along the Danmarkshavn Basin. This line is located between the COB and the proposed deeper horst

block on line AWI-20030300 (Figure 6.7) and landward of the Greenland Escarpment on line AWI-20030200 (Figure 6.5).

Two further seismic lines in the prolongation of the Bessel Fjord (P-Bessel Fjord) and north of Store Koldewey (Fig. 9.1) across the Danmarkshavn Basin (P-Danmarkshavn) could help to model the basin structure with more details and develop a precise rifting model. Additional constraints on the location of the COB and the extent of shallow basalts would result.

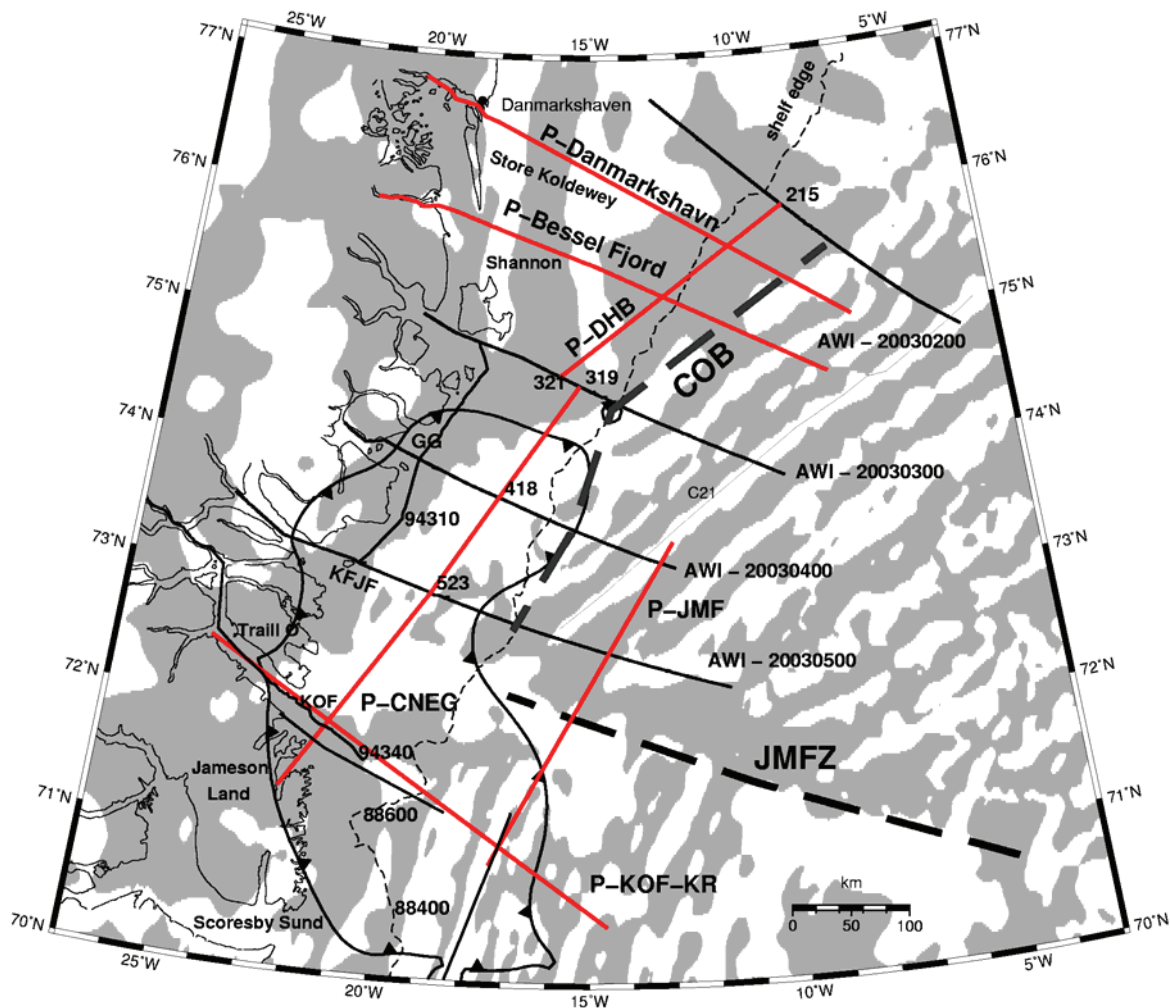


Figure 9.1: Proposal for future seismic investigations off the northeast Greenland margin. Background shows magnetic anomalies (white = positive) after Verhoef et al. (1996). Thick dashed lines mark Jan Mayen Fracture Zone and newly proposed continent – ocean boundary (this study). The 5 km contour-line of the high velocity lower crustal thickness is outlined and marked with triangles pointing towards the increase of thickness. Magnetic chron C21 is labelled as reference. Former seismic lines (thin black) are labelled. Suggestions for new seismic lines are marked in red and labelled with P-name. Numbers label ocean bottom recording units on former seismic lines. Abbreviations are: COB, continent – ocean boundary; CNEG, central-northeast Greenland; DHB, Danmarkshavn Basin; GG, Godthåb Gulf; JMFZ, Jan Mayen Fracture Zone; KFJF, Kejser Franz Joseph Fjord; KOF, Kong Oscar Fjord KR, Kolbeinsey Ridge.

A second set of lines should focus on the southern extent of the high velocity lower crust, the Jan Mayen Fracture Zone. One line (P-JMF) could cross the fracture zone and reveal constraints on its structural style and could be linked with lines 88400 (Weigel et al. 1995) and the profiles AWI-20030400 and -500. The former seismic lines 94340 and 88600 (Weigel et al. 1995; Schlindwein and Jokat 1999) should be extended in the prolongation of the Kong Oscar Fjord to the Kolbeinsey Ridge (P-KOF-KR) and test, if the observed magmatic

underplating and the Miocene to recent thick oceanic crust intervene, as suggested from the mapping (Figure 6.14). Supplementary seismic reflection data parallel to the OBS/OBH profiles would provide details on the basin structures, which are generally weakly resolved and simply outlined from raytracing. An integrated study, similar to this, incorporating 3D-gravity modelling, depth-to-basement calculations from new airborne magnetic data and multichannel seismic and seismic refraction data should sufficiently outline a 3D model of the high velocity body off the northeast Greenland margin. Finally, an appropriate located drill hole should be able to answer the question of timing and constitution of the lower crustal body, of the sedimentary basins and the potential for hydrocarbons.

Profile	Start		End		Lengths
P-CNEG	22.51 °W	71.37 °N	15.27 °W	74.58 °N	435 km
P-DHB	15.84 °W	74.65 °N	8.91°W	75.92 °N	242 km
P-Bessel Fjord	21.72 °W	75.97 °N	8.07 °W	74.6 °N	420 km
P-Danmarkshavn	20.55 °W	76.93 °N	7.16°W	75.02 °N	420 km
P-JMF	17.38 °W	70.89 °N	12.76 °W	73.37 °N	318 km
P-KOF-KR	24.65 °W	72.44 °N	14.59 °W	70.42 °N	422 km

Table 9.1: Key coordinates for proposed new seismic lines (Figure 9.1) and estimated lengths. See above figure notes for line labels.

Acknowledgements

The decision for writing a PhD was, personally for me, a decision to come back to Germany, to come back to my family and to my friends. Against all expectations, I also came to an extraordinary working group of an outstanding research institute. All these people made me feel that I decided right, and supported me were ever they could. Thank to all of you.

Doing something “special” does not mean, being someone “special”, but means knowing all the “specials”. My special thank is dedicated to ...

- ... Prof. Dr. Heinz Miller for the opportunity to write this thesis, and for the encouraging words after getting my first “major revisions”.
- ... Prof. Dr. Heinrich Villinger for his interest in this work, for the inspiring discussions and for the willingness to be the second referee.
- ... Dr. Wilfried Jokat for getting me into life of science, for supporting me for all three manuscripts, for taking me on vessels with RV Polarstern, ARK-XX/3 and ANT-XXIII/5, for the virtually never-ending discussions and the beautiful view on your “shed”.
- ... Dr. Mechita C. Schmidt-Aursch for being the co-author of the second manuscript and for the thousands of scripts, thoughts, discussions, phone calls, and for the encouraging words when it came to the end of the thesis. Many of my –O –K –V –: are dedicated to you.
- ... Dr. Vera Schlindwein for reading the third manuscript and for the many, many papers and discussions about East Greenland’s geology and magmatic underplating.
- ... Dr. Graeme Eagles for reading many of my manuscripts and improving them greatly, not only correct spelling. I miss him handing back my manuscript and saying “It’s not so bad!” and me seeing his comments, commas and arrows all over the text.
- ... Jan Grobys for sharing the office with me at AWI during bright and dark days. I hope I also could teach him something like – “Turn on the lights otherwise you will damage your eyes.”
- ... Daniela Berger, Bettina Bayer, Dr. Matthias König, Sven Riedel, Dr. Karsten Gohl, Dr. Gabriele Uenzemann-Neben, Tom Schmitz, Dr. Carsten Scheuer, Dr. Wolfram Geißler, Nicole Parsiegla, Birte Ehlers, Hartmut Martens and Norbert Lensch for sharing a great time at AWI, for discussions, and for many “pieces of cake”.

- ... Dr. Asbørn Breivik, Prof. Jan Inge Faleide and Dr. Filipos Tsikalas for giving me an exciting stay in Oslo and for the inspiring discussions about the conjugate margins.
- ... Bernhard Avril and his colleagues of the organization board of the European Science Foundation – EUROMARIGNS Project c/o the DFG for the financial support for conferences and workshops and for the support of young scientists.
- ... my parents and my brother for always taking me serious, for the unreserved love and for finding it exciting without really understanding what I was doing.

I want to thank my wife, Silvia, for being the greatest and most exciting finding of my life. Your patience and endurance during the last year is like a miracle to me.

References

- Allen, P. A. and J. R. Allen (1990). Basin Analysis. Oxford London Edinburgh Boston Melbourne, Blackwell Scientific Publications.
- Boillot, G., J. Girardeau and J. Kornprobst (1988). "The rifting of the Galicia margin: Crustal thinning and emplacement of mantle rocks on the seafloor." Proc. Ocean Drill. Program Sci. Results **103**: 741-756.
- Bown, J. W. and R. S. White (1995). "Effect of finite extension rate on melt generation at rifted continental margins." Journal of Geophysical Research **100**(B9): 18,011-18,029.
- Braun, J. and C. Beaumont (1989). "A physical explanation of the relation between flank uplifts and the breakup unconformity at rifted continental margins." Geology **17**: 760-764.
- Breivik, A. J., R. Mjelde, J. I. Faleide and Y. Murai (2006). "Rates of continental breakup magmatism and seafloor spreading in the Norway Basin-Iceland plume interaction." Journal of Geophysical Research **111**(B07102).
- Breivik, A. J., J. Verhoef and J. I. Faleide (1999). "Effect of thermal contrasts on gravity modeling at passive margins: Results from the western Barents Sea." Journal of Geophysical Research **104**(B7): 15293-15311.
- Brun, J. P. and M. O. Beslier (1996). "Mantle exhumation at passive margins." Earth and Planetary Science Letters **142**: 161-173.
- Cande, S. C. and G. M. Kent (1995). "Revised calibration of the geomagnetic polarity timescale for the Late Cretaceous and Cenozoic." Journal of Geophysical Research **100**(B7): 9761-9788.
- Chalmers, J. A. (2000). "Offshore evidence for Neogene uplift in central West Greenland." Global and Planetary Change **24**: 311-318.
- Chian, D., C. Keen, I. Reid and K. E. Loudon (1995). "Evolution of nonvolcanic rifted margins: New results from conjugate margins of the Labrador Sea." Geology **23**: 589-592.
- Christensen, N. I. and W. D. Mooney (1995). "Seismic velocity structure and composition of the continental crust: a global view." Journal of Geophysical Research **100**(B7): 9761-9788.
- Clift, P. D., J. Turner and O. D. P. L. S. Party (1995). "Dynamic support by the Iceland plume and vertical tectonics of the northeast Atlantic continental margins." Journal of Geophysical Research **100**(B12): 24473-24486.
- Coffin, M. F. and O. Eldholm (1994). "Large Igneous Provinces: Crustal structure, dimension, and external consequences." Reviews of Geophysics **32**(1): 1-36.
- Dahl-Jensen, T., T. B. Larsen, I. Woelbern, T. Bach, W. Hanka, R. Kind, S. Gregersen, K. Mosegaard, P. Voss and O. Gudmundsson (2003). "Depth to Moho in Greenland: receiver-

function analysis suggests two Proterozoic blocks in Greenland." Earth and Planetary Science Letters **205**: 379-393.

Eldholm, O. and K. Grue (1994). "North Atlantic volcanic margins: Dimensions and production rates." Journal of Geophysical Research **99**(B2): 2955-2968.

Eldholm, O., J. Thiede and E. Taylor (1987). "Evolution of the Norwegian continental margin: Background and objectives." Proc. Ocean Drill. Program Initial Rep., part A **104**: 5-25.

Embry, A. F. and J. Dixon (1990). "The breakup unconformity of the Amerasia Basin, Arctic Ocean; evidence from Arctic Canada." Geological Society America Bulletin **102**: 1526-1534.

Escher, A. and W. S. Watt (1976). Summary of the geology of Greenland, in A. Escher and W. S. Watt (ed.), Geology of Greenland, The Geological Survey of Greenland, Copenhagen: 10-16.

Escher, J. and T. Pulvertaft (1995). "Geological Map of Greenland, 1:2 500 000." Geological Survey of Greenland.

Fechner, N. and W. Jokat (1996). "Seismic refraction investigations on the crustal structure of the western Jameson Land basin, east Greenland." Journal of Geophysical Research **101**(B7): 15867-15881.

Foulger, G. R. and D. L. Anderson (2005). "A cool model for the Iceland hotspot." Journal of Volcanology and Geothermal Research **141**: 1-22.

Fowler, C. M. R. (2005). "The solid earth: an introduction to global geophysics." **2nd ed.**

Funck, T., J. R. Hopper, H. C. Larsen, K. E. Louden, B. E. Tucholke and W. S. Holbrook (2003). "Crustal structure of the ocean-continent transition at Flemish Cap: Seismic refraction results." Journal of Geophysical Research **108**: 2531-2551.

Funck, T., H. R. Jackson, K. E. Louden, S. A. Dehler and Y. Wu (2004). "Crustal structure of the northern Nova Scotia rifted continental margin (eastern Canada)." Journal of Geophysical Research **109**(B09102).

Grobys, J. (in press). Crustal evolution of the submarine plateaux of New Zealand and their tectonic reconstruction based on crustal balancing. Reports on Polar and Marine Research. Bremerhaven.

Haq, B. U., J. Hardenbol and P. R. Vail (1987). "Chronology of the fluctuating sea levels since the Triassic." Science **235**: 1156-1167.

Henriksen, N., A. Higgins, F. Kalsbeek and T. Pulvertaft (2000). "Greenland from Archaean to Quarternary; descriptive text to the geological map of Greenland, 1: 2 500 000." Geol. Greenland Surv. Bull. **185**: 1-93.

Hinz, K. (1981). "A hypothesis on terrestrial catastrophes wedges of very thick oceanward dipping layers beneath passive continental margins; their origin and palaeoenvironmental significance." Geologisches Jahrbuch **E2**: 3-28.

Hinz, K., O. Eldholm, M. Block and J. Skogseid (1993). "Evolution of North Atlantic volcanic continental margins." from Perol. Geol. of Northwest Europe: Proceedings of the 4th Conference: 901-913.

Hinz, K., J. C. Mutter, C. M. Zehnder and N. S. Group (1987). "Symmetric conjugation of continent-ocean boundary structures along the Norwegian and East Greenland margins." Mar. Petrol. Geol. **3**: 166-187.

Holbrook, W. S., H. C. Larsen, J. Korenaga, T. Dahl-Jensen, I. D. Reid, P. B. Kelemen, J. R. Hopper, G. M. Kent, D. Lizarralde, S. Bernstein and R. S. Detrick (2001). "Mantle thermal structure and active upwelling during continental breakup in the North Atlantic." Earth and Planetary Science Letters **190**: 251-266.

Holbrook, W. S., G. M. Purdy, R. E. Sheridan, L. Glover III, M. Talwani, J. Ewing and D. Hutchinson (1994b). "Seismic structure of the U.S. Mid-Atlantic continental margin." Journal of Geophysical Research **99**(B9): 17871-17891.

Holbrook, W. S., E. C. Reiter, G. M. Purdy, D. Sawyer, P. L. Stoffa and J. Makris (1994a). "Deep Structure of the U.S. Atlantic continental margin, offshore South Carolina, from coincident ocean bottom and multichannel seismic data." Journal of Geophysical Research **99**(B5): 9155 - 9178.

Hopper, J. R., T. Dahl-Jensen, W. S. Holbrook, H. C. Larsen, D. Lizarralde, J. Korenaga, G. M. Kent and P. B. Kelemen (2003). "Structure of the SE Greenland margin from seismic reflection and refraction data: Implications for nascent spreading center subsidence and asymmetric crustal accretion during North Atlantic opening." Journal of Geophysical Research **108**(B5): 2269.

Hopper, J. R., T. Funck, B. E. Tucholke, K. E. Loudon, W. S. Holbrook and H. C. Larsen (2006). "A deep seismic investigation of the Flemish Cap margin: Implications for the origin of deep reflectivity and evidence for asymmetric break-up between Newfoundland and Iberia." Geophysical Journal International **164**(3): 501.

Horsefield, S. J., R. B. Whitmarsh, R. S. White and J. C. Sibuet (1994). "Crustal structure of the Goban Spur rifted continental margin, NE Atlantic." Geophysical Journal International **119**(1): 1.

Japsen, P. and J. A. Chalmers (2000). "Neogene uplift and tectonics around the North Atlantic: overview." Global and Planetary Change **24**: 165-173.

Jokat, W., P. Alberts, H. GÖdde, N. Fechner, H. Fischbeck, C. Kopsch, B. Kunsch, N. Lensch, H. Martens, K. Moorfeld, V. Schlindwein, M. Studinger and D. Sylvester (1995). Seismic refraction, in H.-W. Hubberten (ed.), The expedition ARKTIS-X/2 of RV "Polarstern" in 1994, Reports on Polar Research, Alfred Wegener Institute for Polar and Marine Research, Bremerhaven. **174**.

Jokat, W., D. Berger, H. Bohlmann, V. Helm, M. Hensch, D. Jouselin, C. Klein, N. Lensch, P. Liersch, H. Martens, A. Medow, U. Micksch, L. Rabenstein, C. Salat, M. Schmidt-Aursch and A. Schwenk (2004). "Marine Geophysics." Reports on Polar and Marine Research **475**: 11-34.

- Kearey, P. and M. Brooks (1999). An Introduction to Geophysical Exploration. Oxford, Blackwell Science.
- Kertz, W. (1992). Einführung in die Gephysik I + II. Heidelberg, Berlin, Oxford, Spektrum Akad. Verlag.
- King, S. D. and D. L. Anderson (1995). "An alternative mechanism for flood basalt formation." Earth and Planetary Science Letters **136**: 269-279.
- King, S. D. and D. L. Anderson (1998). "Edge-driven convection." Earth and Planetary Science Letters **160**: 289-296.
- Korenaga, J. (2004). "Mantle mixing and continental breakup magamtism." Earth and Planetary Science Letters **218**: 463-473.
- Korenaga, J., W. S. Holbrook, G. M. Kent, P. B. Kelemen, R. S. Detrick, H. C. Larsen, J. R. Hopper and T. Dahl-Jensen (2000). "Crustal structure of the southeast Greenland margin from joint refraction and reflection seismic tomography." Journal of Geophysical Research **105**(B9): 21591-21614.
- Larsen, H. C. (1988). A multiple and propagating rift model for the NE Atlantic, in A. C. Morton and L. M. Parson (ed.), Early Tertiary volcanism and the opening of the NE Atlantic, Geological Society Special Publication. **39**: 157-158.
- Larsen, H. C. (1990). The East Greenland Shelf, (ed.), The Geology of North America, Geological Society of America, Boulder, Colo. **L**: 185-210.
- Lawver, L. A. and D. R. Müller (1994). "Iceland "hotspot" track." Geology **22**: 311-314.
- Le Pichon, X. and J. C. Sibuet (1981). "Passive margins: A model of formation." Journal of Geophysical Research **86**: 3708-3720.
- Louden, K. E. and D. Chian (1999). "The deep strucutre of nonvolcanic rifted continental margins." Phil. Trans. R. Soc. Lond. A. **357**: 767-804.
- Ludwig, W. J., J. E. Nafe and C. L. Drake (1970). Seismic refraction, in A. E. Maxwell (ed.), in: The Sea, Wiley-Interscience. **4**: 53-84.
- Mandler, H. and W. Jokat (1998). "The crustal structure of central east Greenland: results from combined land-sea seismic refraction experiments." Geophys. J. Int. **135**: 63-76.
- McKenzie, D. (1978). "Some remarks on the development of sedimentary basins." Earth and Planetary Science Letters **40**: 25 - 32.
- Menzies, M. A., S. L. Klemperer, C. J. Ebinger and J. Baker (2002). Characteristics of volcanic rifted margins, in M. A. Menzies, S. L. Klemperer, C. J. Ebinger and J. Baker (ed.), Volcanic Rifted Margins, Geological Society of America Special Paper, Boulder, Colorado. **362**: 1-14.

- Meyer, R., J. van Wijk and L. Gernigon (2007). The North Atlantic Igneous Province: A Review of the Models for its Formation, in G. R. Foulger and D. M. Jurdy (ed.), Plates, Plumes, and Planetary Processes, Geological Society of America Special Paper: 430 p.
- Mjelde, R., S. Kodaira, P. Digranes, H. Shimamura, T. Kananzawa, H. Shiobara, E. W. Berg and O. Riise (1997). "Comparison between a Regional and a Semi-regional Crustal OBS Model in the Vøring Basin, Mid-Norway Margin." Pure and Applied Geophysics **149**: 641-665.
- Mjelde, R., T. Raum, B. Myhren, H. Shimamura, Y. Murai, T. Takanami, R. Karpuz and U. Naess (2005). "Continent-ocean transition on the Voring Plateau, NE Atlantic, derived from densely spaced ocean bottom seismometer data." Journal of Geophysical Research **110**.
- Mjelde, R., H. Shimamura, T. Kananzawa, S. Kodaira, T. Raum and H. Shiobara (2003). "Crustal lineaments, distribution of lower crustal intrusives and structural evolution of the Voering Margin, NE Atlantic; new insights from wide-angle seismic models." Tectonophysics **369**: 199-218.
- Morgan, J. V., P. J. Barton and R. S. White (1989). "The Hatton Bank continental margin-III. Structure from wide-angle OBS and multichannel seismic refraction profiles." Geophys. J. Int. **98**: 367-384.
- Morgan, W. J. (1971). "Convection plumes in the lower mantle." Nature **230**: 42-43.
- Mosar, J., G. Lewis and T. H. Torsvik (2002b). "North Atlantic sea-floor spreading rates: implications for the Tertiary development of inversion structures of the Norwegian-Greenland Sea." Journal of Geological Society, London **159**: 503-515.
- Mutter, J. C. (1993). "Margins declassified." Nature **364**: 393-394.
- Mutter, J. C., W. R. Buck and C. M. Zehnder (1988). "Convective partial melting 1. A model for the firmation of thick basaltic sequences duirng the initiation of spreading." Journal of Geophysical Research **93**(B2): 1031-1048.
- Mutter, J. C., M. Talwani and P. L. Stoffa (1984). "Evidence for a thick oceanic crust off Norway." Journal of Geophysical Research **89**: 483-502.
- Mutter, J. C. and C. M. Zehnder (1988). "Deep crustal and magmatic processes: The inception of seafloor spreading in the Norwegian-Greenland Sea." Geol. Soc. Spec. Publ. London **39**: 35-48.
- Myhre, A. M. and J. Thiede (1995). "North Atlantic-Arctic Gateways." Proc. Ocean Drill. Program Initial Rep. **151**.
- Nadin, P. A., N. J. Kusznir and M. J. Cheadle (1997). "Early Tertiary plume uplift of the North Sea and Faeroe-Shetland basins." Earth and Planetary Science Letters **148**(109-127).
- Nafe, J. E. and C. L. Drake (1957). "Variations with depth in shallow and deep water marine sediments of porosity, density and the velocity of compresional and shear waves." Geophysics **22**: 523-552.

- Parson, B. and J. G. Sclater (1977). "An analysis of the variation of ocean floor bathymetry with heat flow and age." Journal of Geophysical Research **82**: 803-827.
- Raum, T., R. Mjelde, P. Digranes, H. Shimamura, H. Shiobara, S. Kodaira, G. Haatvedt, N. Sørenes and S. Thorbjørnsen (2002). "Crustal structure of the southern part of the Vøring Basin, mid-Norway margin, from wide-angle seismic and gravity data." Tectonophysics **355**: 99-126.
- Reid, I. (1994). "Crustal structure of a nonvolcanic rifted margin east of Newfoundland." Journal of Geophysical Research **99**(15): 15,161-15,180.
- Reston, T. J. and J. P. Morgan (2004). "Continental geotherm and the evolution of rifted margins." Geology **32**: 133-136.
- Rohrmann, M. and P. von der Beek (1996). "Cenozoic postrift domal uplift of North Atlantic margins: an asthenospheric diapirism model." Geology **24**: 901-904.
- Saunders, A. D., J. G. Fitton, A. C. Kerr, M. J. Norry and R. W. Kent (1997). The North Atlantic Igneous Province, in J. J. Mahoney and M. F. Coffin (ed.), Large Igneous Provinces, American Geophysical Union Monograph. **100**: 45-94.
- Saunders, A. D., H. C. Larsen and S. W. J. Wise (1998). Proceedings of the Ocean drilling Program, Scientific Results, (ed.), Ocean Drilling Program, College Station, TX. **152**.
- Schindwein, V. (1998). Architecture and evolution of the continental crust of east Greenland from integrated geophysical studies. Reports on Polar and Marine Research. Bremerhaven. **270**: 1-148.
- Schindwein, V. and W. Jokat (1999). "Structure and evolution of the continental crust of northern east Greenland from integrated geophysical studies." Journal of Geophysical Research **104**(B7): 15227-15245.
- Schindwein, V. and W. Meyer (1999). "Aeromagnetic study of the continental crust of northeast Greenland." Journal of Geophysical Research **104**(B4): 7527-7537.
- Schmidt-Aursch, M. C. and W. Jokat (2005a). "The crustal structure of central East Greenland-I: From the Caledonian orogen to the Tertiary igneous province." Geophys. J. Int. **160**: 736-752.
- Schmidt-Aursch, M. C. and W. Jokat (2005b). "The crustal structure of central East Greenland-II: From the Precambrian shield to the recent mid-oceanic ridges." Geophys. J. Int. **160**: 753-760.
- Scott, R. A. (2000). "Mesozoic-Cenozoic Evolution of East Greenland: Implications of a Reinterpreted Continent-Ocean Boundary location." Polarforschung **68**: 83-91.
- Skogseid, J., S. Planke, J. I. Faleide, T. Pedersen, O. Eldholm and F. Neverdal (2000). NE Atlantic continental rifting and volcanic margin formation, in A. Nøttvedt (ed.), Dynamics of the Norwegian Margin, Geological Society Special Publication, London. **167**: 295-326.

- Srivastava, S. P. and C. R. Tapscott (1986). Plate kinematics of the North Atlantic, in P. R. Vogt and B. E. Tucholke (ed.), The Western North Atlantic Region. The Geology of North America, Geological Society of America, Boulder. **M**: 379-404.
- Talwani, M. and O. Eldholm (1977). "Evolution of the Norwegian-Greenland Sea." Geological Society America Bulletin **88**(7): 969-999.
- Tsikalas, F., O. Eldholm and J. I. Faleide (2002). "Early Eocene sea floor spreading and continent-ocean boundary between Jan Mayen and Senja fracture zones in the Norwegian-Greenland Sea." Marine Geophysical Researches **23**: 247-270.
- Verhoef, J., W. R. Macnab, R. Arkani-Hamed and J. M. o. t. P. Team (1996). "Magnetic anomalies of the Arctic and North Atlantic Oceans and adjacent land areas; Open File 3125." Geological Survey of Canada.
- Vink, G. E. (1984). "A hotspot model for Iceland and the Vøring Plateau." Journal of Geophysical Research **89**: 9949-9959.
- Voss, M. and W. Jokat (2007). "Continent – ocean transition and voluminous magmatic underplating derived from P-wave velocity modelling of the East Greenland continental margin." Geophys. J. Int. **170**: 580-604.
- Weigel, W., E. R. Flüh, H. Miller, A. Butzke, G. A. Dehghani, V. Gebhardt, I. Harder, J. Hepper, W. Jokat, D. Kläschen, S. Kreymann, S. Schübler and Z. Zhao (1995). "Investigations of the east Greenland continental margin between 70° and 72°N by deep seismic sounding and gravity studies." Marine Geophysical Researches **17**: 167-199.
- Wernicke, B. P. (1985). "Uniform-sense normal simple shear of the continental lithosphere." Can. J. Earth Science **22**: 108-125.
- White, R. and D. McKenzie (1989). "Magmatism at rift zones: The generation of volcanic continental margins and flood basalts." Journal of Geophysical Research **94**(B6): 7685-7729.
- White, R. S. (1987). "When continents rift." Nature **327**: 191.
- White, R. S. (1992). Magmatism during and after continental break-up, in B. C. Storey, T. Alabaster and R. J. Pankhurst (ed.), Magmatism and the Causes of Continental Break-up, Geological Society Special Publication. **68**: 1-16.
- White, R. S., J. W. Bown and J. R. Smallwood (1995). "The temperature of the Iceland plume and origin of outward-propagating V-shaped ridges." Journal of Geological Society, London **152**: 1039-1045.
- White, R. S., D. McKenzie and R. K. O'Nions (1992). "Oceanic Crustal Thickness From Seismic Measurements and Rare Earth Element Inversions." Journal of Geophysical Research **97**(B13): 19683-19715.
- White, R. S., G. D. Spence, S. R. Fowler, D. McKenzie, G. K. Westbrook and A. N. Bowen (1987). "Magmatism at rifted continental margins." Nature **330**: 439 - 444.

Whitmarsh, R. B., R. S. White, S. J. Horsefield, J. C. Sibuet, M. Recq and V. Louvel (1996). "The ocean-continent boundary off the western continental margin of Iberia; crustal structure of Galicia Bank." Journal of Geophysical Research **101**(28291-28314).

Zelt, C. A. and R. B. Smith (1992). "Seismic Traveltime inversion for 2-D crustal velocity structure." Geophysical Journal International **108**: 16-34.

Curriculum Vitae

MAX VOSS

Birthname : Schroeder
Date of birth : 27. September 1973
Place of birth : Bielefeld
Status : Married
Nationality : German

Experiences

03/2007 – **RWE-Dea AG, Hamburg**
Geophysicist in Onshore Exploration Group (Central-West Europe)

02/2004 – 01/2007 **Alfred Wegener Institute (AWI), Bremerhaven**
c/o University of Bremen, Department of Geoscience
PhD Student in Marine Geophysics Group

04/2002 – 01/2004 **Sander Geophysics Ltd (SGL), Ottawa, Canada**
Employee in airborne geophysical survey company

Research Expeditions

04 – 06/2006 **South Atlantic**, Shona, Discovery and Walvish Ridge
08 – 10/2004 **Arctic**, Yermak Plateau, Spitzbergen and East Greenland
01 – 03/2000 **Antarctic**, Weddell Sea (as student)

Education

Studies
04/1997 – 02/2002 Geophysics, University of Cologne
Thesis: Properties of Directional Discontinuities in the solar wind
between 0.3 – 19 AU; Automated Identification and Analyses

10/1994 – 03/1997 Pre-degree in Physics, University of Aachen (RWTH)

Secondary school qualification
1993 Technical college, Mönchengladbach (Abitur: 2.2)

Scientific Publications and Presentations

- Scientific Publications**
- 09/2006 Voss M. and Jokat W. (GJI, 2007)
Continent – ocean transition and voluminous magmatic underplating derived from P-wave velocity modelling of the East Greenland continental margin
- 12/2007 Voss M., Schmidt-Aursch M.C. and Jokat W. (GJI, submitted)
Variations in magmatic processes along the East Greenland volcanic margin
- 12/2007 Voss M., Jokat W. (GJI, submitted)
From Devonian extensional collapse to Early Eocene continental break-up: an extended transect of the Kejsers Franz Joseph Fjord of the East Greenland margin
- Conference Presentations (Talks)**
- 12/2006 “Magmatism and a wide continent-ocean transition at the East Greenland volcanic rifted margin”
American Geophysical Union (AGU) Conference, San Francisco, USA
- 10/2006 “Magmatism and formation of a wide continent-ocean transition at the East Greenland margin, Euromargins 2003 OBS Experiment.”
European Science foundation (ESF) - Euromargins Conference, Bologna
- 04/2006 “Crustal Structure of the East Greenland Volcanic Margin - I: Voluminous Underplating North of the Jan Mayen Fracture Zone.”
European Geophysical Union (EGU) General Assembly, Vienna
- 02/2006 “The East Greenland continental margin: First interpretation results of deep seismic and potential field data between the Jan Mayen and Greenland fracture zones.”
Deutsche Geophysikalische Gesellschaft (DGG), Bremen
- 02/2005 „Crustal structure modelling and interpretation of the continent – ocean transition zone of the East Greenland margin between 72°N and 76°N“
Deutsche Geophysikalische Gesellschaft (DGG), Graz